

From the  
Walter-Brendel-Zentrum für Experimentelle Medizin  
of the Ludwig-Maximilians-Universität München  
Interim Director: Prof. Dr. med. Markus Sperandio



# Neural Regulation of Lymph Node Immune Responses

Dissertation  
zum Erwerb des Doctor of Philosophy (PhD)  
an der Medizinischen Fakultät der  
Ludwig-Maximilians-Universität

submitted by

陳建焮 Chien-Sin Chen

from

臺灣基隆 Keelung, Taiwan

On

07/08/2019

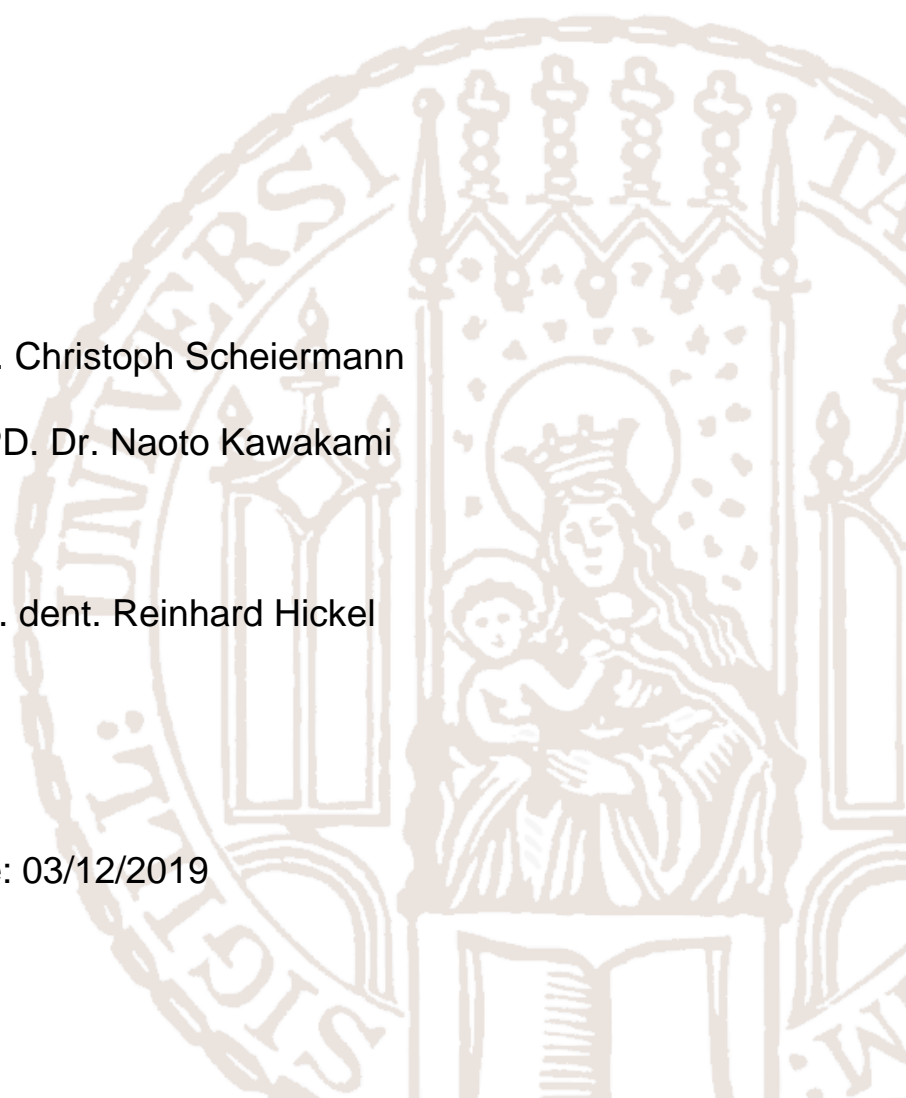


Supervisor: Prof. Dr. Christoph Scheiermann

Second evaluator: PD. Dr. Naoto Kawakami

Dean: Prof. Dr. med. dent. Reinhard Hickel

Date of oral defense: 03/12/2019





# Acknowledgement

We are trained to be independent scientists but I am sure I would not have been able to finish this work alone. I have gotten help from many people for my study and living in Germany. These are the three most important people to help me on this wonderful journey. My beloved parents, Cheng-Kuo Chen and Shu-Hua Chang keep supporting me and have encouraged me to study abroad since I was a kid. This tiny seed had been dormant for very long time until years ago. This dream came true when I met my supervisor Christoph Scheiermann. I thank him for offering me this fantastic opportunity to do my doctoral study in his lab. It is not just a scientific training but a great experience to broaden my vision and make many friends.

I am glad that my colleague Louise Ince and I got onboard the lab the same day. We have a lot of fun and explored many things together including science and issues for expats in Germany. She is such a nice and supportive friend. Notably, she also read, corrected the language and gave plenty of critical comments on this thesis. Alba de Juan, another very good friend, told me in two weeks after I started that I am always welcome to join her Spanish folks if I have not had friends to hang out, yet. That totally warmed my heart. Of course, she taught me very expressive Spanish terms, which I will never forget. It is absolutely enjoyable to work with my labmates Sophia Hergenhan, Stephan Holtkamp, Jasmin Weber and Robert Pick. They are reliable, relaxed and cool friends and of course very detailed and organized as they are Germans. I am so glad to have my lab life with these fun guys. My collaborators and TAC members, Susan Brain, Susanne Stutte, Rainer Haas and Naoto Kawakami supported me with invaluable resources and knowledge. Without them, I could not complete this study.

Outside of the lab, there are many friends enriching my life abroad. Alex Chen is not only my first landlord in Munich, but also a good friend who brought me into the Taiwanese network. I met Bai-Lee Liu, Hsin-Yi Chiu and Tsun-Ning Chung with whom we organized many events together and could talk a lot about ideas and dreams. Tim Kuo, Julie Su, Annie Lee, Jay Hsieh, Ava Feng and Julia Hsu are my favorite jetsetter-mates. We visited so many places together, although none of them lives in Munich. Atsuki, Maria, Ben and

Adrian were my best flatmates in the student housing, together with my beautiful tea-mate, Tanitas, who joined us from another flat. There were so many wonderful evenings we cooked, drank and talked together. In the same period, I met Annie Cheng and Jonathan Garcia. Years later, our friendship brought me to visit them in Mexico and had a fabulous trip together. Initially, I did not expect playing badminton in Munich. Luckily enough, I still found some rare racket geeks apart from excessive football fans. I enjoy playing with Olaf, Oliver, Sherry, Thomas, William and Katherine in our badminton club. That is to me the best way to balance my life from work. There are still many friends I cannot list them all here. These people do not directly support my study but they make my Munich life full of fun and really make this city another home of mine.

This is indeed a great journey. I do not mean there is no pressure at all, but I have gone through it with support. I did not expect so many travels for work or leisure on top of my study, but I like them so much because I see how much I benefit from them. I did not imagine of making so many friends but fortunately they have come into my life. I appreciate that I could do my doctoral study in this environment. I hope the findings of the project push the front of knowledge a bit forward.

# Abstract

Nerve-controlled immune homeostasis can be altered by infections or neural injuries and lead to local or systemic effects. However, immune outcomes of losing innervation in the lymph node, a critical organ for adaptive immunity development, are still unclear. In this study, surgeries were applied to locally manipulate neural tones in the popliteal lymph node (popLN) or its drainage area to study nerve-regulated immune functions and local immunity via innervating lymph node.

Sciatic denervation led to ipsilateral acute paw swelling and nodal expansion with increased leukocytes. In contrast, surgeries which denervate the drainage area but spare the popLN, such as femoral or ankle denervation, did not cause comparable expansion, suggesting that denervation sensitized the popLN. Nodal expansion was repressed after cetirizine treatment, indicating that histamine signaling is required. This nodal expansion consisted of an increase in every examined stromal and immune subset in company with upregulation of *Cxcl12*, *Cxcl13*, *Il1a*, *Il1b*, *Il6*, *Il10*, *Il17a* and *Il17f*, which accurately mirrored the microenvironment in denervated paws. Neutrophils, natural killer (NK) cells and migratory dendritic cells were early expanding, but depletion of neutrophils or NK cells did not prevent nodal expansion. Pertussis toxin treatment or neutralization of L-selectin,  $\alpha4$ - and  $\alpha L$ -integrin inhibited the nodal expansion. Denervation drove vigorous germinal center formation in the popLN as well as elevated serum immunoglobulin G (IgG) which was not auto-reactive to nuclear antigens. Nodal expansion was inhibited upon MHCII blockade, afferent lymphatics disconnection or conducting denervation in OT-II mice, suggesting a pathway of T cell-dependent B cell response with lymph-borne antigens. To simulate loss of neural tones, neural functions were ablated. However, sympathectomy or antagonism of neuropeptides, substance P (SP) and/or calcitonin gene-related peptides (CGRP), did not alter the nodal cellularity but systemic sympathectomy boosted *Il1a* and *Il4*. Restoration of SP and/or CGRP after denervation partially relieved nodal expansion. In conclusion, loss of innervation induced peripheral inflammation and reduced the popLN responding threshold, co-contributing to an excessive B cell response and IgG production which potentially causes long-term immune concerns to patients with neural injury.



# Table of Contents

<b>1 INTRODUCTION</b>	<b>1</b>
1.1 Importance and rationale	1
1.1.1 Overview	2
1.2 Effects of neural injury on the immune system	2
1.2.1 Stroke-induced immune modulation	3
1.2.2 Spinal cord injury-induced immune modulation	3
1.3 Neural physiology and immunology after traumatic injury	4
1.3.1 The distal end – Wallerian degeneration	4
1.3.1.1 Latency	6
1.3.1.2 Fragmentation of the axon	6
1.3.1.3 Demyelination and myelin clearance	7
1.3.2 The proximal side – sprouting tips for regeneration	8
1.3.3 Immune reactions to neural injury	8
1.3.3.1 Vessels and cytokines	9
1.3.3.2 Toll-like receptors	10
1.3.3.3 Antigen-specific immunity	10
1.4 Neurogenic inflammation	12
1.4.1 Calcitonin gene-related peptide	13
1.4.2 Substance P	14
1.5 Adaptive immunity	15
1.5.1 Cell-mediated immunity	16
1.5.2 Humoral immunity	17
1.5.2.1 T-cell-dependent response	17
1.5.2.2 T-cell-independent response	18
1.5.2.3 Somatic hypermutation and class switch recombination	19
1.6 Lymph node	20

1.6.1	Structure of lymph node	21
1.6.1.1	Vasculature	21
1.6.1.2	Nerves	22
1.6.1.3	Cell zones	22
1.6.2	Afferent lymphatics	23
1.6.2.1	From periphery to the lymph node	25
1.6.2.2	Conduits, filtration function and maintenance of lymph node physiology	25
1.6.3	Leukocyte trafficking to lymph nodes	26
1.6.3.1	Chemotaxis	27
1.6.3.2	Egress	29
1.6.3.3	Migration for functions	30
1.6.3.4	Leukocyte vessel interactions	30
<b>1.7</b>	<b>Structure of the peripheral nervous system</b>	<b>32</b>
1.7.1	Classification by neural substances	32
1.7.2	The sciatic nerve	33
<b>1.8</b>	<b>Immune regulatory functions of neural substances</b>	<b>33</b>
1.8.1	The autonomic nervous system	33
1.8.2	The sensory nervous system	34
1.8.3	Neural injury, autoimmunity and homeostasis	35
1.8.4	Infections	35
1.8.5	Allergic immunity	36
1.8.6	In spleen and lymph node	37
<b>1.9</b>	<b>Objectives</b>	<b>38</b>
<b>1.10</b>	<b>Model used</b>	<b>38</b>
<b>2</b>	<b>MATERIAL AND METHODS</b>	<b>41</b>
<b>2.1</b>	<b>Mice</b>	<b>41</b>
<b>2.2</b>	<b>Surgeries</b>	<b>41</b>

2.2.1	Sciatic denervation	42
2.2.2	Femoral denervation	43
2.2.3	Ankle denervation	43
2.2.4	Autologous transplantation of the sciatic nerve	43
2.2.5	Afferent lymphatic disconnection	44
2.2.6	Superior cervical ganglionectomy	44
<b>2.3</b>	<b>Histology – H&amp;E staining</b>	<b>45</b>
<b>2.4</b>	<b>Flow cytometry</b>	<b>46</b>
2.4.1	Tissue processing	46
2.4.1.1	Lymph nodes	47
2.4.1.2	Paws	47
2.4.1.3	Lymph node stromal cells	47
2.4.1.4	Spleen	48
2.4.1.5	Femoral bone marrow	48
2.4.1.6	Blood	48
2.4.2	Staining panels	49
2.4.2.1	General profiling of immune subsets in the LN	49
2.4.2.2	Dendritic cell subsets in the LN	49
2.4.2.3	Digestion-sensitive B cell differentiation markers on splenic and LN cells	50
2.4.2.4	Immune subsets in paws	50
2.4.2.5	Stromal cells in the LN	50
2.4.2.6	Verification of cell depletion efficacy	50
<b>2.5</b>	<b>Cell type-specific depletion</b>	<b>50</b>
2.5.1	Neutrophil	51
2.5.2	Natural killer cell	51
<b>2.6</b>	<b>Recruitment rate and dwell time</b>	<b>51</b>
2.6.1	Homing	51
2.6.2	Egress	52
<b>2.7</b>	<b>Treatment of drug or antibody</b>	<b>52</b>

2.7.1	Anti-histamine treatment	52
2.7.2	Homing blockade	53
2.7.2.1	Integrins	53
2.7.2.2	CD62L	53
2.7.2.3	Peripheral node addressin	53
2.7.3	Pertussis toxin treatment	53
2.7.4	Antigen presentation blockade	54
2.7.5	6-hydroxydopamine treatment	54
2.7.6	Treatment of neuropeptides or antagonist of neuropeptides	54
<b>2.8</b>	<b>Quantitative polymerase chain reaction</b>	<b>54</b>
<b>2.9</b>	<b>Immunofluorescence</b>	<b>55</b>
2.9.1	Whole-mount staining of the popliteal lymph node	57
2.9.2	Staining of popliteal lymph node section	57
2.9.3	Staining of the sciatic nerve section	58
<b>2.10</b>	<b>Serology</b>	<b>58</b>
2.10.1	Isotyping	58
2.10.2	Antibody titer determination	59
2.10.3	Autoantibody test	59
<b>2.11</b>	<b>Statistics</b>	<b>60</b>
<b>3</b>	<b>RESULTS</b>	<b>61</b>
<b>3.1</b>	<b>Denervation in the leg leads to acute swelling of the paw and enlargement of popliteal lymph node</b>	<b>61</b>
<b>3.2</b>	<b>Sciatic denervation contributes to nodal expansion</b>	<b>63</b>
<b>3.3</b>	<b>Denervated popliteal lymph nodes are more reactive</b>	<b>64</b>
<b>3.4</b>	<b>Sciatic denervation induces neutrophil infiltration and increases dendritic cell numbers in the draining area of the popliteal lymph node</b>	<b>68</b>

<b>3.5</b>	<b>Nodal expansion after denervation partially reflects the size of affected nervous branch and does not associate with degree of paw swelling</b>	<b>70</b>
<b>3.6</b>	<b>Infiltration of neutrophils and CD103 dendritic cells in the paw correlates to popliteal lymph node cellularity after denervation</b>	<b>75</b>
<b>3.7</b>	<b>Sciatic denervation affects immune and stromal cells in the local popliteal lymph node</b>	<b>78</b>
<b>3.8</b>	<b>Neutrophils and natural killer cells are bystanders to popliteal lymph node expansion after sciatic denervation</b>	<b>81</b>
<b>3.9</b>	<b>Nodal expansion after denervation is not due to degradation of dead terminal nerves but loss of innervation</b>	<b>84</b>
<b>3.10</b>	<b>Denervated popliteal lymph nodes exhibit increased leukocyte homing</b>	<b>86</b>
<b>3.11</b>	<b>Denervated popliteal lymph nodes exhibit unchanged egress rates</b>	<b>87</b>
<b>3.12</b>	<b>The microenvironment of the denervated popliteal lymph node is pro-inflammatory and supports a germinal center response</b>	<b>88</b>
<b>3.13</b>	<b>Sciatic denervation causes acute inflammation in the paw</b>	<b>91</b>
<b>3.14</b>	<b>Denervation shapes the microenvironment in paw and popliteal lymph node favoring germinal center formation and Th17 response</b>	<b>93</b>
<b>3.15</b>	<b>Sciatic denervation induces a B cell response in the denervated popliteal lymph node</b>	<b>94</b>
<b>3.16</b>	<b>Afferent lymphatic input is required for denervation-mediated nodal expansion</b>	<b>98</b>
<b>3.17</b>	<b>Sciatic denervation generates local and systemic effects</b>	<b>100</b>
<b>3.18</b>	<b>Sciatic denervation increases antibody titers</b>	<b>101</b>

<b>3.19</b>	<b>Antibodies induced by sciatic denervation are not reactive to antinuclear antigens</b>	<b>102</b>
<b>3.20</b>	<b>The sciatic nerve possesses sympathetic and sensory properties</b>	<b>103</b>
<b>3.21</b>	<b>Sympathectomy does not alter cell number and migratory dynamics in lymph nodes but modifies the local microenvironment</b>	<b>105</b>
<b>3.22</b>	<b>Antagonizing neuropeptide receptors is not sufficient to trigger nodal expansion</b>	<b>110</b>
<b>3.23</b>	<b>SP and CGRP agonism counteract the nodal expansion induced by sciatic denervation</b>	<b>112</b>
<b>4</b>	<b>DISCUSSION</b>	<b>117</b>
<b>4.1</b>	<b>Overview</b>	<b>117</b>
<b>4.2</b>	<b>Main phenotypes of sciatic denervation – popliteal lymph node expansion and paw swelling</b>	<b>118</b>
4.2.1	Direct innervation of the popliteal lymph node by the sciatic nerve	119
4.2.2	Dead nerve-induced immune responses	120
4.2.3	Causes of paw swelling	121
4.2.4	Dependence of phenotypes	124
4.2.4.1	Paw swelling quantification	125
4.2.4.2	Single and dual denervation	126
4.2.4.3	Paw swelling levels, denervation degrees and popliteal lymph node cellularity	126
4.2.4.4	A paw swelling resolution model	127
4.2.4.5	Targeting paw swelling	129
<b>4.3</b>	<b>Reactions in the popliteal lymph node</b>	<b>130</b>
4.3.1	Migratory momentum	131
4.3.2	B cell proliferation	132
4.3.3	Driver cells	133

4.3.3.1	Neutrophils	133
4.3.3.2	Natural killer cells	133
4.3.4	The microenvironment	134
4.3.4.1	Pro-inflammatory cytokines	134
4.3.4.2	Anti-inflammatory cytokines	135
4.3.4.3	Chemokines	135
4.3.4.4	Late expressed cytokines	136
<b>4.4</b>	<b>The immune response</b>	<b>136</b>
4.4.1	Upstream: T cell dependence, antigen presentation	137
4.4.2	Downstream: antibody production and antigen specificity	138
4.4.3	Remote responses	139
<b>4.5</b>	<b>Neural involvement</b>	<b>140</b>
4.5.1	Effects of sympathectomy	140
4.5.2	Targeting substance P and calcitonin gene-related peptide	141
4.5.2.1	Neuropeptide antagonism without sciatic denervation	142
4.5.2.2	Neuropeptide antagonism with sciatic denervation	144
4.5.2.3	Neuropeptide agonism with sciatic denervation	145
4.5.2.4	Summary of effects of neuropeptides on denervation-induced nodal expansion	147
<b>4.6</b>	<b>Conclusion</b>	<b>147</b>
<b>5</b>	<b>REFERENCES</b>	<b>151</b>
<b>6</b>	<b>APPENDICES</b>	<b>173</b>
6.1	Appendix 1 – flow cytometry configuration	173
6.2	Appendix 2 – antibody list	174
6.3	Appendix 3 – primer list	176



# List of Figures

FIGURE 1.1 PROCESS OF WALLERIAN DEGENERATION	5
FIGURE 1.2 THE MILIEU OF NEUROGENIC INFLAMMATION	13
FIGURE 1.3 VASCULATURE AND CELL ZONES OF THE LYMPH NODE	20
FIGURE 1.4 LYMPHATIC AND CONDUIT SYSTEMS OF THE LYMPH NODE	24
FIGURE 1.5 ANATOMY OF THE MODEL INVESTIGATED	39
FIGURE 1.6 THREE BRANCHES OF THE SCIATIC NERVE	40
FIGURE 2.1 ANATOMY OF DORSAL SIDE OF THIGH – MUSCLES, VESSELS AND THE SCIATIC NERVE	42
FIGURE 2.2 VENTRAL NECK ANATOMY – MUSCLES, VESSELS AND NERVES	45
FIGURE 3.1 MACROSCOPIC VIEWS OF MAIN DENERVATION PHENOTYPES	61
FIGURE 3.2 PROGRESSION OF FOOTPAD THICKNESS AND LYMPH NODE EXPANSION AFTER DENERVATION	62
FIGURE 3.3 CHANGE OF POPLN CELLULARITY AFTER CUTTING FEMORAL AND/OR SCIATIC NERVE(S)	63
FIGURE 3.4 SCHEME OF SCIATIC DENERVATION SURGERIES AT DIFFERENT LEVELS	64
FIGURE 3.5 EVALUATION OF CONDUCTIVITY OF AFFERENT LYMPHATICS AFTER ANKLE DENERVATION	65
FIGURE 3.6 HISTOLOGY OF PAW SKIN TISSUES	66
FIGURE 3.7 POPLN CELLULARITY ONE WEEK AFTER SCIATIC OR ANKLE DENERVATION	67
FIGURE 3.8 CELL DENSITY IN THE PAW AFTER SCIATIC DENERVATION	68
FIGURE 3.9 IMMUNE CELL SUBSETS IN THE PAW AFTER DENERVATION	69
FIGURE 3.10 FOOTPAD THICKNESS CHANGE AFTER CUTTING SCIATIC NERVE BRANCHES	70
FIGURE 3.11 QUANTIFICATION OF FOOTPAD THICKNESS OVER TIME	71
FIGURE 3.12 POPLN CELLULARITY AFTER DENERVATION OF DISTINCT BRANCHES	72
FIGURE 3.13 CORRELATIONS BETWEEN PAW AUC, LEUKOCYTES IN PAWS AND POPLNS AND DENERVATION DEGREE	74

FIGURE 3.14 DENERVATION-INDUCED PAW SWELLING UNDER CETIRIZINE TREATMENT	75
FIGURE 3.15 LEUKOCYTES IN PAW AFTER SCIATIC DENERVATION AND CETIRIZINE TREATMENT	76
FIGURE 3.16 LEUKOCYTES IN THE POPLN AFTER DENERVATION IN COMBINATION WITH CETIRIZINE TREATMENT	77
FIGURE 3.17 DYNAMICS OF IMMUNE SUBSETS IN POPLN AFTER SCIATIC DENERVATION	79
FIGURE 3.18 STROMAL COMPARTMENTS IN THE POPLN ONE WEEK AFTER SCIATIC DENERVATION	80
FIGURE 3.19 VERIFICATION OF EFFICACY OF NEUTROPHIL DEPLETION	81
FIGURE 3.20 EFFECTS OF NEUTROPHIL DEPLETION ON POPLN CELLULARITY AFTER UNILATERAL SCIATIC DENERVATION	82
FIGURE 3.21 EFFECTS OF NK CELL DEPLETION IN THE UNILATERAL SCIATIC DENERVATION MODEL	83
FIGURE 3.22 SCHEME OF AUTO-TRANSPLANTATION OF THE SCIATIC NERVE	84
FIGURE 3.23 CELLULARITY OF POPLN AFTER AUTO-TRANSPLANTATION AND TRANSECTION OF SCIATIC NERVE	85
FIGURE 3.24 ENHANCED HOMING TO DENERVATED POPLNS	86
FIGURE 3.25 UNCHANGED EGRESS RATE IN DENERVATED POPLNS	87
FIGURE 3.26 STABILITY OF THE HOUSEKEEPING GENE, <i>RPL32</i>	88
FIGURE 3.27 GENE EXPRESSION PROFILE OF CHEMOKINES AND CYTOKINES IN THE POPLNS	90
FIGURE 3.28 GENE EXPRESSION PROFILE OF CHEMOKINES AND CYTOKINES IN THE PAW	92
FIGURE 3.29 IDENTIFICATION OF B CELLS AS THE MAJOR PROLIFERATING CELLS IN THE DENERVATED POPLNS	94
FIGURE 3.30 IDENTIFICATION OF GERMINAL CENTERS IN THE DENERVATED POPLNS	95
FIGURE 3.31 POPLN CELLULARITY IN WILDTYPE AND OT-II MICE AFTER UNILATERAL SCIATIC DENERVATION	96

FIGURE 3.32 POPLN CELLULARITY CHANGE AFTER MHCII BLOCKADE AFTER UNILATERAL SCIATIC DENERVATION	97
FIGURE 3.33 VERIFICATION OF AFFERENT LYMPHATIC DISCONNECTION SURGERY	98
FIGURE 3.34 INFLUENCE OF AFFERENT LYMPHATIC DISCONNECTION SURGERY TO POPLN CELLULARITY AND PAW SWELLING AFTER THE UNILATERAL SCIATIC DENERVATION	99
FIGURE 3.35 SPLENIC NEUTROPHIL AND B CELL DYNAMIC AFTER UNILATERAL SCIATIC DENERVATION	100
FIGURE 3.36 PRODUCTION OF ANTIBODIES AFTER SCIATIC DENERVATION	101
FIGURE 3.37 REACTIVITY OF SERA FROM DENERVATED MICE TO ANTINUCLEAR ANTIGENS	102
FIGURE 3.38 NERVE FIBER PROPERTIES OF THE SCIATIC NERVE	103
FIGURE 3.39 SYMPATHETIC INNERVATION OF THE POPLN	104
FIGURE 3.40 CGRP <sup>+</sup> NERVES IN THE POPLN	104
FIGURE 3.41 LN CELLULARITY AFTER SYMPATHECTOMY	106
FIGURE 3.42 GENE EXPRESSION PROFILE IN POPLNS AFTER SYSTEMIC SYMPATHECTOMY	108
FIGURE 3.43 HOMING AND EGRESS RATES IN LOCAL SYMPATHECTOMIZED SPLNS	109
FIGURE 3.44 CELLULARITY OF BONE MARROW, SPLEEN, POPLN, ILN AND BLOOD AFTER CHRONIC NEUROPEPTIDE ANTAGONISM	110
FIGURE 3.45 IMMUNE SUBSETS IN THE POPLNS AFTER CHRONIC NEUROPEPTIDE ANTAGONISM	111
FIGURE 3.46 POPLN CELLULARITY AFTER UNILATERAL SCIATIC DENERVATION SURGERY IN COMBINATION WITH NEUROPEPTIDE ANTAGONISM	112
FIGURE 3.47 SPLENIC CELLULARITY AFTER UNILATERAL SCIATIC DENERVATION SURGERY IN COMBINATION WITH NEUROPEPTIDE ANTAGONISM	113

FIGURE 3.48 POPLN CELLULARITY AFTER THE UNILATERAL SCIATIC DENERVATION SURGERY IN COMBINATION WITH NEUROPEPTIDE AGONISM	114
FIGURE 3.49 SPLENIC CELLULARITY AFTER THE UNILATERAL SCIATIC DENERVATION SURGERY IN COMBINATION WITH NEUROPEPTIDE AGONISM	115
FIGURE 4.1 THE CASCADE OF NEURAL SUBSTANCE-DRIVEN LOCAL SWELLING AND LYMPH NODE ACTIVATION	124
FIGURE 4.2 MAGNITUDE OF PAW SWELLING AND NODAL EXPANSION DURING THE TIME AFTER DENERVATION	125
FIGURE 4.3 POSSIBLE MODELS OF DENERVATION-DRIVEN LYMPH NODE ENLARGEMENT	143
FIGURE 4.4 OVERLAY OF THE BIPHASIC MODEL AND NEUROPEPTIDE ANTAGONISM REGIMEN	145

## **List of Tables**

TABLE 1.1 CHEMOTACTIC COMPOUNDS FOR LEUKOCYTE TRAFFICKING TO THE LYMPH NODE	27
TABLE 1.2 ADHESION MOLECULES FOR LEUKOCYTE VESSEL INTERACTION	31
TABLE 3.1 COMPARISON OF GENE EXPRESSION PROFILES OF PAW AND POPLN AFTER DENERVATION	93
TABLE 3.2 SUMMARY OF EFFECTS OF NEUROPEPTIDE ANTAGONISM OR AGONISM ON CELL NUMBERS IN POPLNS AFTER DENERVATION	116
TABLE 4.1 HISTAMINE RECEPTORS: EXPRESSION, SIGNALING AND IMMUNE FUNCTIONS	122
TABLE 4.2 PROPOSED EFFECTS OF SCIATIC BRANCHES ON PAW SWELLING	128



# List of Abbreviations

<b>6-OHDA</b>	6-hydroxidopamine
<b><math>\alpha</math>7nAChR</b>	nicotinic acetylcholine receptor alpha 7
<b><math>\alpha/\beta</math>AR(s)</b>	alpha or beta adrenergic receptor(s)
<b>AAD</b>	acute axon degeneration
<b>ACh</b>	acetylcholine
<b>AChT</b>	acetylcholine transferase
<b>aDM, the</b>	the anterior belly of the digastric muscles
<b>AID</b>	activation-induced deaminase
<b>ANKx</b>	ankle denervation
<b>APC(s)</b>	antigen presenting cell(s)
<b>AUC</b>	area under curve
<b>BAFF-R</b>	B cell activatin factor receptor
<b>BALT(s)</b>	bronchus-associated lymphoid tissue(s)
<b>BCR(s)</b>	B cell receptor(s)
<b>BEC(s)</b>	blood endothelial cell(s)
<b>BF, the</b>	the biceps femoris muscle
<b>BIBN</b>	BIBN4096
<b>BLC</b>	B lymphocyte chemoattractant
<b>BM</b>	bone marrow
<b>cAMP</b>	cyclic adenosine monophosphate
<b>CCA, the</b>	the common carotid artery
<b>CCL</b>	C-C chemokine ligand
<b>CCR</b>	C-C chemokine receptor
<b>CD</b>	cluster of differentiation
<b>CD40L</b>	cluster of differentiation 40 ligand
<b>cDC(s)</b>	conventional dendritic cell(s)
<b>cDNA</b>	complementary DNA
<b>CFSE</b>	carboxyfluorescein succinimidyl ester
<b>CGRP</b>	carcitonin gene-related peptide
<b>CLR</b>	calcitonin receptor-like receptor
<b>CNS</b>	central nervous system
<b>Com</b>	combined treatment
<b>CPN(s), the</b>	the common peroneal nerves
<b>CRCs</b>	CXCL12-expressing population of reticular stroma
<b>CSR</b>	class switch recombination
<b>Ct</b>	cycle threshold
<b>CTZ</b>	cetirizine
<b>CXCL</b>	the chemokine (C-X-C motif) ligand
<b>DC(s)</b>	dendritic cell(s)

<b>dLN(s)</b>	draining lymph node(s)
<b>dn</b>	double negative (negative of EpCAM and CD103)
<b>DNA</b>	deoxyribonucleic acid
<b>DPBS</b>	Dulbecco's phosphate-buffered saline
<b>ECA, the</b>	the external carotid artery
<b>EDTA</b>	ethylenediaminetetraacetic acid
<b>EpCAM</b>	epithelial cell adhesion molecule
<b>FasL</b>	Fas ligand
<b>FBS</b>	fetal bovine serum
<b>FDC(s)</b>	follicular dendritic cell(s)
<b>FRC(s)</b>	fibroblastic reticular cell(s)
<b>FSx</b>	transection of the femoral and sciatic nerves
<b>Fx</b>	transection of the femoral nerve
<b>GABA</b>	$\gamma$ -aminobutyric acid
<b>GATA3</b>	GATA binding protein 3
<b>GC(s)</b>	germinal center(s)
<b>GCB(s)</b>	germinal center B cell(s)
<b><math>\gamma\delta</math>T</b>	gamma-delta T cells
<b>GvH</b>	graft-versus-host
<b>HEV(s)</b>	high endothelial venule(s)
<b>HN, the</b>	the hypoglossal nerve
<b>HPA axis</b>	hypothalamus-pituitary-adrenal axis
<b>HRP</b>	horseradish peroxidase
<b>HSC(s)</b>	hematopoietic stem cell(s)
<b>HvG</b>	host-versus-graft
<b>H<sub>x</sub>R</b>	histamine HX receptor
<b>IAP</b>	integrin-associated protein
<b>ICA, the</b>	the internal carotid artery
<b>ICAM(s)</b>	intercellular adhesion molecule(s)
<b>IF</b>	immunofluorescence
<b>IFN<math>\alpha</math></b>	interferon alpha
<b>IFN<math>\gamma</math></b>	interferon gamma
<b>IgM</b>	immunoglobulin M
<b>IJV, the</b>	the internal jugular vein
<b>IL</b>	interleukin
<b>ILC(s)</b>	innate lymphoid cell(s)
<b>iLN(s)</b>	inguinal lymph node(s)
<b>IM(s)</b>	inflammatory monocyte(s)
<b>iNKT</b>	invariant natural killer T (cells)
<b>ip</b>	intraperitoneal(ly)
<b>ipl</b>	intraplantar(ly)

<b>iv</b>	intravenous(ly)
<b>KLF4</b>	Krüppel-like factor 4
<b>LC(s)</b>	Langerhans cell(s)
<b>LEC(s)</b>	lymphatic endothelial cell(s)
<b>LN(s)</b>	lymph node(s)
<b>LPS</b>	lipopolysaccharide
<b>LT<math>\alpha/\beta</math></b>	lymphotoxin $\alpha/\beta$
<b>MAPK</b>	mitogen-activated protein kinase
<b>MBP</b>	myelin basic protein
<b>MCAO</b>	midcerebral artery occlusion
<b>MHCI</b>	major histocompatibility complex class I
<b>MHCII</b>	major histocompatibility complex class II
<b>MigDC(s)</b>	migratory dendritic cell(s)
<b>MRC(s)</b>	marginal reticular cell(s)
<b>Myd88</b>	myeloid differentiation primary response 88
<b>MZ(s)</b>	marginal zone(s)
<b>NE</b>	norepinephrine
<b>NF</b>	neurofilament
<b>NF<math>\kappa</math>B</b>	nuclear factor kappa B
<b>NGF</b>	neuron growth factor
<b>NIM(s)</b>	non-inflammatory monocyte(s)
<b>NK cells</b>	natural killer (cells)
<b>NK1R(s)</b>	neurokinin 1 receptor(s)
<b>NMU</b>	neuromedin U
<b>NPY</b>	neuropeptide Y
<b>OA, the</b>	the occipital artery
<b>OHM, the</b>	the omohyoid muscles
<b>OT-II</b>	*a mouse line whose majority of CD4 T cells react to OVA
<b>OVA</b>	ovalbumin
<b>PBS</b>	phosphate-buffered saline
<b>PC(s)</b>	plasma cell(s)
<b>pDM, the</b>	the posterior belly of the digastric muscles
<b>PFA</b>	paraformaldehyde
<b>plt mice</b>	paucity mice
<b>PNAd</b>	peripheral node addressin
<b>PNEC(s)</b>	pulmonary neuroendocrine cell(s)
<b>PNS</b>	peripheral nervous system
<b>popLN(s)</b>	popliteal lymph node(s)
<b>PSNS, the</b>	the parasympathetic nervous system
<b>QF, the</b>	the quadriceps femoris muscle
<b>qPCR</b>	quantitative (deoxyribonucleic acid) polymerase chain reaction
<b>RAMP1</b>	receptor activity modifying protein 1

<b>ResDC(s)</b>	resident dendritic cell(s)
<b>RNA</b>	ribonucleic acid
<b>S1P</b>	sphingosine-1-phosphate
<b>S1PR1</b>	sphingosine-1-phosphate receptor 1
<b>sc</b>	subcutaneous(ly)
<b>SCG, the</b>	the superior cervical ganglion
<b>SCGx</b>	superior cervical ganglionectomy
<b>SCI-(IDS)</b>	spinal cord injury-(induced immune depression syndrome)
<b>SCS</b>	subcapsular space
<b>SDF1</b>	stromal cell derived factor 1
<b>SHM</b>	somatic hypermutation
<b>SHM, the</b>	the sternohyoid muscles
<b>SIRP<math>\alpha</math></b>	signal-regulatory-protein- $\alpha$
<b>SMM, the</b>	the sternomastoid muscles
<b>SN(s), the</b>	the sural nerves
<b>SNI</b>	spared nerve injury
<b>SNS, the</b>	the sympathetic nervous system
<b>SP</b>	substance P
<b>spLN(s)</b>	superficial parotid LN(s)
<b>SR</b>	SR140333
<b>STAT6</b>	signal transducer and activator of transcription 6
<b>Sx</b>	transection of the sciatic nerve
<b>TBI</b>	traumatic brain injury
<b>TCR</b>	T cell receptor
<b>Td</b>	T cell-dependent
<b>Tfh(s)</b>	follicular T helper cell(s)
<b>TGF<math>\beta</math></b>	transforming growth factor beta
<b>TH</b>	tyrosine hydroxylase
<b>Th</b>	CD4 T helper
<b>Ti</b>	T cell-independent
<b>TLR(s)</b>	toll-like receptor(s)
<b>TMB</b>	3,3',5,5'-Tetramethylbenzidine
<b>TN(s), the</b>	the tibial nerves
<b>TNF<math>\alpha</math></b>	tumor necrosis factor alpha
<b>Treg(s)</b>	regulatory T cell(s)
<b>VCAM(s)</b>	vascular cell adhesion molecule(s)
<b>veh</b>	vehicle
<b>VIP</b>	vasoactive intestinal peptide
<b>VN, the</b>	the vagus nerve
<b>VSC(s)</b>	versatile stromal cell(s)
<b>VSV</b>	vesicular stomatitis virus
<b>WD</b>	Wallerian degeneration

# 1 Introduction

## 1.1 Importance and rationale

The nerve and the immune system are two distinct but mutually interacting units. Interactions between them can tune their functionalities and/or cause diseases. In one direction of the interactions, secreted neural substances modulate functions of the immune system; in the other direction, a misdirected immune system causes neural damage such as autoimmunity against neural components. A typical human autoimmune disorder in the nervous system is multiple sclerosis. Recently, neuro-reactive autoimmunity has been intensively studied using mouse experimental autoimmune encephalomyelitis models [1], and compared with clinical multiple sclerosis pathology [2]. However, the influence of nerves on the immune system in homeostatic and pathologic conditions and subsequent immune outcomes are overlooked. Studies of neurally injured patients have suggested that disturbed neural tones affect immunity at the regional and systemic levels [3-7]. Investigation of immune responses and the underlying mechanism in neural injury scenarios can not only help to understand molecular and cellular dialogs between the nervous and the immune systems but possibly predict long-term immune issues in neurally injured patients.

Brain, spinal cord and peripheral nerves are three sectors of the nervous system, which control bodily processes at different levels. Globally, traumatic brain injury (TBI) [8] and spinal cord injury (SCI) [9] affect millions of people, causing premature death and significant economic burden to the individual and to society. Neural modulation of immune organs is not as obvious and urgent as the issues of survival, mobility, pain and loss of senses to the patients, but can potentially cause long-term problems.

Lymph nodes (LN) are secondary lymphoid organs where adaptive immunity develops to create immune specificity and memory. Because LNs are territorial structures, every LN is in charge of immune responses in specific areas depending on its location. There are 28 to 36 LNs in mice [10] and the number of human LN has a wide range from 500 to 700 [11]. To fulfill their functions, lymph nodes possess a specialized network of blood and lymphatic vessels, stromal cells, leukocytes and, last but not least, nerves. This thesis

aims to study how nerves interact with the immune system in the LN and what the effects are, especially on adaptive immune responses.

### **1.1.1 Overview**

There are four parts in this introduction. The first one aims to provide a broad overview of neural injury or action-driven immune responses. It starts from immune alterations after different injuries of the central nervous system (CNS) (1.2), followed by the physiology and immunology due to injury of the peripheral nervous system (PNS) (1.3), and finishes with neurogenic inflammation which is derived from neural activities (1.4). The second part introduces the lymph node (1.6), the target organ investigated, following a section about adaptive immunity (1.5), which usually takes place in secondary lymphoid organs. The third part briefly gives a general overview of the PNS, points out the nerves studied in this project (1.7) and puts the spotlight on immune functions of multiple neural substances and actions (1.8). The last section highlights the potential impacts and the objectives (1.9) and then specifies the model used in this study to fill the knowledge gap (1.10).

## **1.2 Effects of neural injury on the immune system**

Brain and spinal cord injury (SCI) can suppress or activate the immune system but by different mechanisms. Neural injury-mediated immunosuppression mostly involves loss of neural substances, which directly or indirectly have immune functions. However, immune stimulating cases in experimental settings due to loss of neural substances are still absent. Excessive immunity induced by neural injuries is rather an autoimmune response which mainly results from exposure of leukocytes to massive amount of neural antigens during the injury [12]. Examples of brain and spinal cord injury affecting immune functions are provided below.

### **1.2.1 Stroke-induced immune modulation**

There are many clinical observations linking neural injuries to altered immune function. A multicenter study following stroke patients showed infection is one of the most common complications suggesting compromised immunity in these cases [3]. Most likely due to neural and humoral connections, the regional damage of the brain can cause systemic immunosuppressive effects [13, 14]. Systemic ablation of sympathetic tone by administration of the neurotoxin, 6-hydroxydopamine shows protective effects against infections in a mouse stroke model – midcerebral artery occlusion (MCAO) - via preventing conversion of hepatic invariant natural killer T (iNKT) cells into immunosuppressive status [14]. This study identifies the sympathetic tone to be the key messenger connecting the brain and functional iNKT cells in the liver.

### **1.2.2 Spinal cord injury-induced immune modulation**

Brain and spinal cord injuries (SCI) are damages at different levels in the central nervous system with outcomes depending on innervation territories. Effects of SCI are normally determined by the level of damage, and unlike to some brain injuries compromise global immunity. Although differences exist, SCI still shares commonality with brain-damaged cases in the sense that infection is the leading cause of death of SCI patients, mainly by septicemia and pneumonia [6, 7], indicating there are multiple mechanisms leading to a convergent immunosuppressive outcome. These patients show reduced immunity possibly because of less proliferation of progenitor cells [5] and lower levels of leukocyte adhesion molecules that impairs migratory capacity [15]. Interestingly, lesion to the spinal cord at higher thoracic level causes higher susceptibility to pneumonia in a mouse pneumonia model [16]. This level of dependence of susceptibility is not due to denervation of solely the spleen [16], but dysregulation of the sympathetic-neuroendocrine adrenal reflex [17].

Classical understanding of high level SCI-induced immune suppression involves excess neurogenic local norepinephrine (NE) in the spleen and humoral glucocorticoids via hypothalamus-pituitary-adrenal (HPA) axis [18, 19]. A recent study introduces a new concept called the sympathetic-neuroendocrine adrenal reflex in the SCI scenario [17]. In

this reflex, loss of sympathetic innervation to adrenal gland after SCI leads to repressed NE and increased cortisol in plasma resulting in leukocyte depletion and lymphoid atrophy [17]. Unlike the classical model stimulating the adrenal gland via a humoral pathway, this alternative mechanism does not involve the HPA axis activation but works by direct sympathetic innervation [17]. Because of dependence on direct innervation, the reflex shows level dependence of SCI as well [17]. However, mouse hepatitis virus exhibits higher infectivity to SCI mice but it does not exhibit level dependence of SCI [20], rendering the level dependence a pathogen-specific feature.

### **1.3 Neural physiology and immunology after traumatic injury**

Neural injury causes long-term immune effects due to an imbalance of functional substances as discussed, but the injury itself can also result in drastic physiological change and transiently activated immune responses. Complete break of a nerve separates the nervous fiber into proximal and distal ends. The latter is segregated from the rest of the nervous system, while the former remains connected. Within the first few minutes after trauma of the mouse spinal nerve, the proximal and distal ends undergo an acute axon degeneration (AAD) which occurs as they die back 200 to 300 micrometers to reach a stable distance from the lesion [21]. After AAD, divergent fates of two ends exhibit multi-phasic processes for either regeneration or degeneration.

#### **1.3.1 The distal end – Wallerian degeneration**

Wallerian degeneration (WD) is the process that when an axon is cut describes how the distal end of the nerve gradually loses its integrity (**Figure 1.1**). It involves multiple functional steps and occurs in both central and peripheral nervous systems (CNS and PNS, respectively) after axotomy to avert further damage to intact nerves and shape the microenvironment for repair [22]. Although WD can occur in both CNS and PNS, different types of cells are involved in the process, for example, Schwann cells and macrophages in the PNS and oligodendrocytes and microglia in the CNS [22]. The progression rate of WD shows a great range of variation based on species, as well as on the types and

thickness of the injured nerve [22]. Discovery of the “Slow Wallerian degeneration” (Wld<sup>S</sup>) mouse line exhibiting extremely slow development of WD stirs understandings of mechanistic details of WD [23]. Using this mouse line and advanced microscopic techniques, WD has been shown to occur in several stages from latency, fragmentation to clearance.

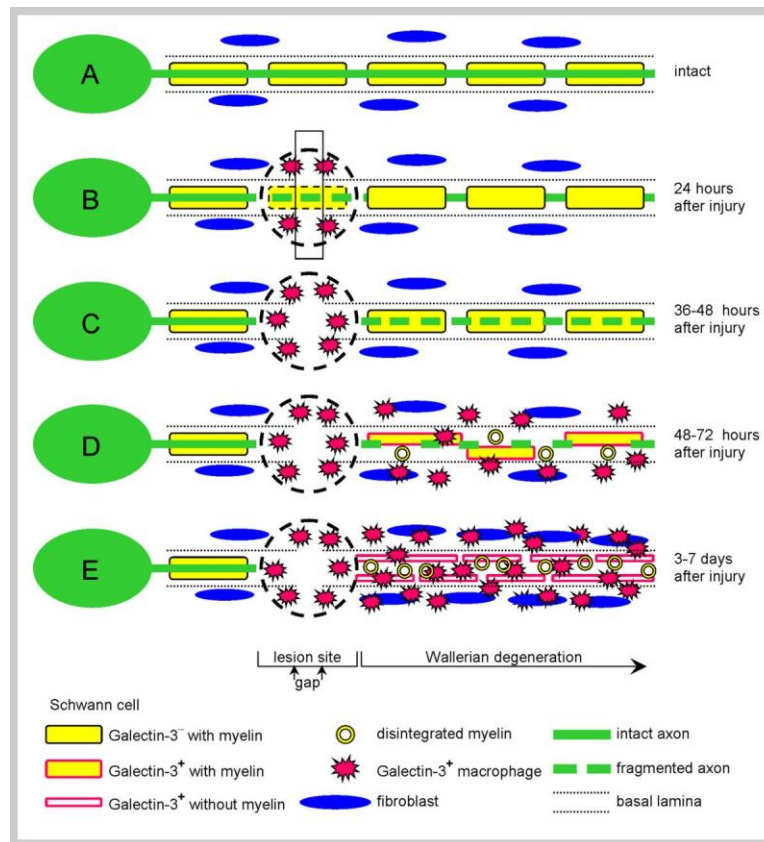


**Figure 1.1 Process of Wallerian degeneration**

This figure is originally in Rotshenker’s review article [22]. It shows development of Wallerian degeneration in several stages with their signature events. Stage A is the uninjured state, a normal intact axon. Stage B is the latency marked by undisrupted structure of the distal end (1.3.1.1). Stage C involves onset of axon fragmentation but still maintains the myelin sheath (1.3.1.2). Stage D and E are most immunological stages in which large amount of hematogenic (bone marrow-derived) macrophages, neutrophils and T cells are recruited for clearance of ejected myelin (1.3.1.3). Lengths of stages are different between experimental settings and systems. Galectin-3<sup>+</sup> macrophages are believed to be hematogenic and galectin-3 is important for their phagocytosis because loss of galectin-3 compromises clearance of antibody-opsonized apoptotic cells [24].

#### 1.3.1.1 Latency

Shortly after AAD, there is a latent phase lasting from hours to days in which the distal end of the nerve retains its morphology and conductivity so that it is still excitable [25]. It is about 1-3 day(s) in wild-type mice [26, 27], albeit with progressively losing membrane potential [28]. By the time of complete loss of conductivity, more than half of nerves appear still to be morphologically normal, indicating that the electrophysiological integrity degrades quicker than the cytoskeleton in the case of axotomy [26]. In this phase, the content of calcium ions in the distal end of the nerve rises and increased calcium then activates calpain, a protease for cytoskeletal dissolution, to potentiate the degeneration [29]. This pathway strongly relies on the influx of calcium, which is increased by dysregulation of voltage-gated ion channels and sodium/calcium exchangers [30, 31]. This spreads imbalanced calcium along the distal axon rather than confined at the injured site [32] so that it primes the following axon fragmentation.

#### 1.3.1.2 Fragmentation of the axon

Activation of the protease starts to drive fragmentation of the axon in the distal end. This is characterized by dissolution of structural proteins, destruction of mitochondria and destabilization of cytoplasmic vesicles. Axon fragmentation is observed even in an *in vitro* culture of explanted sciatic nerves, indicating it is an intrinsic process depending on only the axon itself and the associated Schwann cells [33]. Schwann cells associated with the axon are stimulated and result in axon fragmentation, which is a local granular breakdown of axons with decreasing length of each fragment over time [34]. In fact, Schwann cells seem to be very important in this process because inhibition of their dedifferentiation (via endoneurial injection of PD0325901), transcription (via endoneurial injection of actinomycin D) or actin polymerization (via endoneurial injection of Cytochalasin-D) dampens axon fragmentation [34]. Mouse sciatic nerve transection latency is about 37-42 hours [35]. Sciatic axotomy in YFP-H mice, whose motor and sensory nerves in the PNS are labeled with yellow fluorescent protein in the whole axon, reveals that axons start to fragment in an anterograde manner between 36-44 hours after lesion in mice and rats [22,

33]. It exhibits strong correspondence temporally and spatially with formation of myelin ovoid, which is a hallmark of myelin disintegration [33, 34].

#### *1.3.1.3 Demyelination and myelin clearance*

In WD, demyelination of nerves involves Schwann cells unwrapping from the axon and ejecting myelin. A classical study using electron microscopy to analyze intramembranous particles in Schwann cells and the distal axon revealed that the pattern of intramembranous particles in Schwann cells changes 12 hours after transection of the sciatic nerve in mice, which is even faster than the axon which reacts in 24 hours, suggesting that Schwann cells are the initiators of the process [36]. In addition to induction of axonal fragmentation, Schwann cells begin dedifferentiation which stops synthesizing myelin [37] and converts the cells to the unmyelinated glial cells (Remak cells) in a repair-specialized mode [38]. Schwann cells then proliferate and form a structure termed “Bünger bands” to keep and concentrate the regenerative factors for guiding neural regrowth [39]. Mitosis in Schwann cells was initially thought to rely on recruited myelomonocytic cells – macrophages [40]. However, other studies show the proliferative feature without presence of macrophages [41], and depletion of macrophages by clodronate does not alter Schwann cell number in a neural compression injury model [42].

Myelin debris contains myelin-associated glycoprotein and oligodendrocyte-myelin glycoprotein, which are inhibitory substances against axonal growth [43]. Therefore, elimination of myelin debris as soon as possible is essential. Interestingly, endogenous antibodies against myelin are preexisting to quickly neutralize and opsonize the released myelin [44]. Detached Schwann cells play a role in phagocytosis of myelin debris at the early stage and macrophages from monocytes or resident macrophage actively remove the majority of myelin at the late stage [45, 46]. Between these two stages, neutrophils, as the first responders from blood, infiltrate to the injured site within 8 hours and reach their peak in a day to clean myelin debris [47]. Endoneurial resident macrophages are then reactivated within 2 days after injury and begin to clean myelin debris [46, 48]. Then large amount of monocytes are recruited to the lesion in 4 days and differentiate into macrophages [49]. These C-C chemokine receptor 2 (CCR2)<sup>+</sup> monocyte-derived

macrophages are the major myelin cleaners [40], and they secrete interleukin-1 (IL1) to reactivate Schwann cells [50] and neuron growth factor (NGF) to facilitate neural regrowth [51]. However, CCR2-deficient mice show the same rate of WD in which the myelin cleaner role of macrophages is compensated by another phagocyte: neutrophils [52]. Phagocyte recruitment is critical for myelin ejection and removal. The mouse mutant with *Ube4b* fused with *Nmnat1* (the slow WD, *Wld<sup>S</sup>* mouse line) [23] or pharmacological blockade of type 3 complement receptor [53] does not exhibit recruitment of macrophages and WD demyelination is efficiently delayed.

### **1.3.2 The proximal side – sprouting tips for regeneration**

In contrast to undergoing WD on the distal side, the proximal end is in a healing-regrowth program. Normally on the proximal side of the nerve, the nerve sprouts from the tip of transection and nodes of Ranvier for potential reconnection. In a mouse spinal nerve injury model, the earliest sprouting begins between 6-24 hours and 30% of nerves sprout within 2 days after axotomy [21]. The rate of regeneration largely depends on the type of nerve. Independent to the speed of regrowth, extended regrown nerves are unlikely to return to the lesion site and rejoin the distal end because diffusion-driven travel of growth factors lacks precise directionality [21].

Proximal ends are not always on the safe side. Retrograde degeneration of axons features in neurodegenerative disorders such as amyotrophic lateral sclerosis (ALS), Alzheimer's disease and Parkinson's disease. It is considered as a proximal stump undergoing WD, and therefore defined as "Wallerian-like degeneration" because of high similarity, albeit opposite directionality [54]. This renders studying WD a useful proxy to assess mechanistic details of neurodegenerative disorders.

### **1.3.3 Immune reactions to neural injury**

While regeneration or degeneration takes place in the proximal or distal end respectively, immune components are activated to assist the processes, especially for the myelin clearance on the distal side. Severance of nerves activates Schwann cells and so initiates

reactions for myelin clearance and neural recovery. These processes require a responsive network consisting of cells, vessels and soluble compounds.

#### *1.3.3.1 Vessels and cytokines*

Plasma leakage from blood to nerves is defined as perineural permeability, which shows a bimodal pattern in WD. Soluble factors rely on enhanced permeabilization to reach the nerve, likely used to be for repair. Early breakdown of this barrier (within 48 hours) enables infiltration of monocytes to the injured site [46]. The first peak in perineural permeability occurs 4-7 days after sciatic nerve transection in rat, and matches the dynamics of acute inflammation [55]. Perineural permeability then declines from the first peak, reaches the trough in 2 weeks and bounces back in 4 weeks for recovery of homeostasis after WD [56]. T cells, as the last arriving cells, are recruited after 3 days and keep increasing until week 2-3 when they reach their peak [57].

Cytokines produced by these T cells are important for regeneration. CNS injury skews the systemic cytokines towards a cluster of differentiation 4 (CD4) T helper cells type 2 (Th2) profile which involves increased IL4, IL5 and IL13 cytokine levels, normally associated with eosinophilic responses and allergy. This Th2 shift is associated with higher susceptibility to infection, better neuroprotection against experimental autoimmune encephalomyelitis (EAE) and pro-regeneration in CNS injury models [58]. Th2 cytokines and some anti-inflammatory cytokines such as IL10 and transforming growth factor beta (TGF $\beta$ ) promote neural healing [59], but controversially, only adoptively transferred Th1 but not Th2 and Th17 – conditioned cells promote the neural recovery program via activation of M2 macrophages in the SCI model [60]. Nowadays, it seems that Th1 cytokines such as interferon gamma (IFN $\gamma$ ), IL1 and IL12 are beneficial for WD but inhibitory to recovery, which relies more on Th2 cytokines. Further studies on the temporal and spatial profile of cytokines and the status of macrophages during the transition between WD and recovery phases are required for further clarification of the role of cytokines.

In the nerve sheath after unilateral sciatic nerve transection, the allergic cytokine histamine increases in the proximal end and the contralateral intact nerve but decreases

in the distal stump [61], suggesting protective or healing functions of infiltrating mast cells in nerves which are still alive after injury. Histamine seems to play a role in neural pathology driven by microglia, whose activation and infiltration are signs of neurodegenerative diseases. Histamine in the brain activates microglial migration, but inhibits their lipopolysaccharide (LPS)–driven migration and IL1 $\beta$  release by the same histamine receptor, histamine H4 receptor (H<sub>4</sub>R) [62]. However, treating neuron-microglia co-culture with histamine and LPS reduces the survival rate of dopaminergic neurons (tyrosine hydroxylase, TH<sup>+</sup>) by 30%, and this effect requires the presence of microglia [63]. This highlights the importance of histamine receptors and phagocytes in neuroinflammation in CNS.

#### *1.3.3.2 Toll-like receptors*

Mouse sciatic nerve transection activates Schwann cells to produce interleukin 6 (IL6) within 3 hours [64], tumor necrosis factor alpha (TNF $\alpha$ ) and IL1 alpha (IL1 $\alpha$ ) within 5 hours and IL1 beta (IL1 $\beta$ ) within 24 hours [65]. Secretion of these pro-inflammatory cytokines might link to activation of Schwann cells via toll-like receptors (TLRs). Schwann cells express TLR3 (senses double-stranded RNA), TLR4 (senses lipopolysaccharide (LPS), heat shock proteins, heparan sulfate and hyaluronic acid fragments) and TLR7 (senses single-stranded RNA) continuously and express TLR1 (senses bacterial lipoproteins) after axotomy [66]. Deficiency of the key adaptor protein Myeloid differentiation primary response 88 (Myd88), TLR2 (senses bacterial peptidoglycans and heat shock protein 70), or TLR4 reduces the pro-inflammatory cytokines and macrophage infiltration and thus delays WD [67], suggesting the existence of endogenous ligands of TLRs during WD. Whether these endogenous ligands are recognized as antigens for induction of more specific responses is unclear.

#### *1.3.3.3 Antigen-specific immunity*

Given that the induction of autoimmune responses requires the ingestion, processing and the presentation of self-antigens, are the macrophages and Schwann cells, which

phagocytose myelin debris able to induce autoimmunity against myelin after peripheral neural injury?

A facial nerve injury has shown that injury of myelinated nerves induces autoreactive T cells recognizing myelin basic protein (MBP) and secreting IFN $\gamma$  in superficial cervical LNs [68]. This autoimmunity seems to be beneficial, as counteracting post-injury autoimmunity by injection of CD4<sup>+</sup>CD25<sup>+</sup> regulatory T cells (Tregs) is detrimental for neuronal survival after injury [69]. *Rag1* deficiency compromises neither WD (also true in *Prkdc*<sup>-/-</sup> and *Foxn1*<sup>-/-</sup>) [70] nor recovery of motor function [71]. Interestingly, boosting immunity by adoptively transferring activated wild-type lymphocytes to wild-type or *Rag1*<sup>-/-</sup> recipients accelerates the motor recovery [71]. These evidences point to that mild activation of adaptive immune responses is neuro-protective and beneficial for regeneration on the post-injury stage. Afterwards, this induced immunity is eventually restricted and terminated by Schwann cells via expression of Fas ligand (FasL) [72].

Adaptive immune responses are driven by antigen presentation, which relies on the presentation machinery, major histocompatibility complex class II (MHCII). Hematogenous macrophages, endoneurial macrophages [48], and Schwann cells [73] express MHCII, phagocytose and present myelin. The former two are the professional antigen presenting cells (APCs) and the latter, Schwann cell, is the facultative APCs, expressing low level of MHCI (a protein complex on the surface of all nucleated cells for presenting intracellular peptides to cytotoxic lymphocytes) but no MHCII until they are activated by IFN $\gamma$  and TNF $\alpha$  [72, 74]. After the antigen acquisition and presentation, adaptive immunity is commenced (explained in **1.5**).

Peripheral neural autoimmune disorders are usually caused by molecular mimicry of pathogens [75]. Prevention of being harmed by autoimmunity to healthy myelin depends on a molecular insulation mechanism. This inhibitory mechanism relies on the signaling pathway of signal-regulatory-protein- $\alpha$  (SIRP $\alpha$ , also known as CD172 $\alpha$  and SHPS1) expressed on phagocytes. CD47 (also known as integrin-associated protein, IAP) is expressed on various cell types and binds to SIRP $\alpha$  to inhibit phagocytosis [76]. Under normal conditions, the myelin sheath presents CD47 to prevent itself from being phagocytosed [77].

## 1.4 Neurogenic inflammation

In addition to neural injury-induced immune reactions, stimulation of some nerves can lead to inflammation too. This process is called neurogenic inflammation because the response is triggered by an activation of the nerve, which drives the secretion of neuropeptides and subsequent inflammation (**Figure 1.2**). The cascade is initiated by activation of noxious signal receptors, and the sensory neural substances are important mediators which have effects on immune, endothelial, epithelial or smooth muscle cells to initiate inflammation [78]. A symptom of this phenomenon was first described in the late 19 century as skin vasodilation after electric stimulation to the dorsal roots. Recently, increasing studies revealed that these substances have not only effects on the blood vessel but directly modulate the activation status of both resident and circulating immune cells including macrophages [79], dendritic cells [80], Langerhans cells [81, 82], mast cells [83], neutrophils [84, 85], and T cells [80, 86]. As calcitonin gene-related peptide (CGRP) and substance P (SP) from nociceptors are now recognized to be the major neurogenic inflammatory mediators, neurogenic inflammation is viewed as neural substance-mediated vaso-immune responses to various environmental cues sensed by sensory nerves (reviewed in [78]). Unlike sympathetic and parasympathetic nerves with relatively simple profiles of secretory neural substances, sensory nerves produce a variety of neuropeptides (database: <http://www.neuropeptides.nl/>). Two of the most studied ones, CGRP and SP, are introduced below.

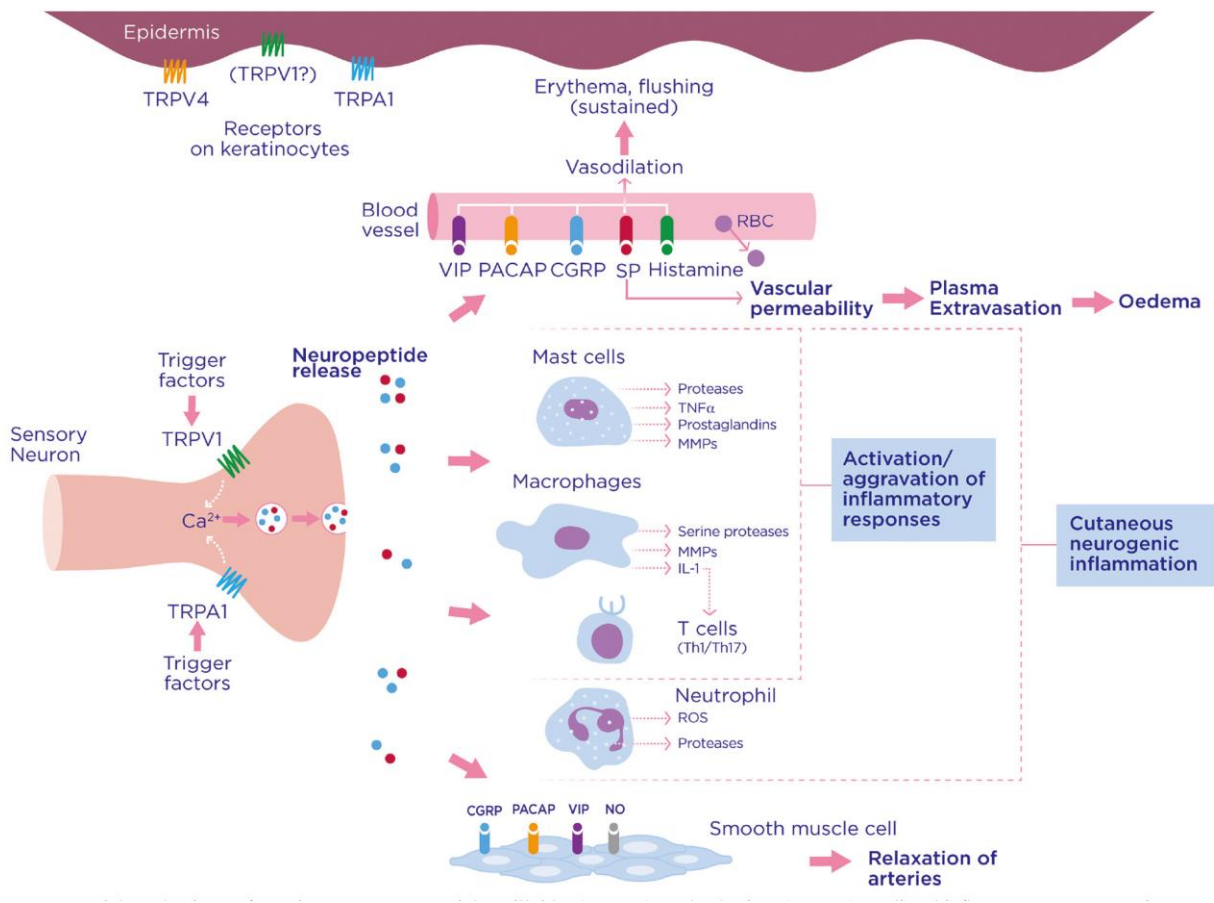


**Figure 1.2 The milieu of neurogenic inflammation**

This figure is originally in the review article from Steinhoff et al [87]. It clearly illustrates the key players in a neurogenic inflammation including the receptors of noxious signals, functional neuropeptides and target cells. After stimulation of those receptors, the sensory nerve releases neuropeptides, which are the critical mediators for driving inflammation. These substances vasodilation, leakage of plasma and activation of immune cells such as mast cells and macrophages. The most characterized neuropeptides are CGRP (1.4.1) and SP (1.4.2).

### 1.4.1 Calcitonin gene-related peptide

CGRP is one of the most investigated secreted peptidyl neural substances. It consists of 37 amino acids (the full length peptide) and has two forms ( $\alpha$  and  $\beta$ ) via alternative RNA processing [88]. This peptide is widely expressed in the CNS and PNS and closely relates to pain sensation, vasodilation and immune modulation. It is mainly synthesized in and

secreted by C and A $\delta$  fibers in the PNS [88]. The receptors of CGRP consist of a main receptor, calcitonin receptor-like receptor (CLR), and an auxiliary unit, receptor activity modifying protein 1 (RAMP1), for full functionality [89]. These two proteins form a functional dimer complex with CLR capable to bind CGRP and adrenomedullin and RAMP1 providing ligand selectivity.

Neural damage such as peripheral axotomy [90], activation of nociceptive receptor such as transient receptor potential cation channel subfamily V member 1 (TRPV1) [91] or reception of NGF [92] can stimulate release of CGRP from nociceptors (sensory neurons specialized in sensing noxious environmental signals) to drive neurogenic inflammation. This CGRP secretion can be inhibited by NE due to  $\alpha_2$ -adrenoreceptor signaling [93], pointing out a dialog between the SNS and nociceptors.

A part of CGRP's pro-inflammatory activity is attributed to its vasodilation function, which locally induces edema and leukocyte infiltration. CGRP is by far the most potent vasodilator and has relatively high acting duration of 5 hours even at picomole level in skin [94, 95]. The CGRP-mediated vasodilation has endothelium-dependent and independent (via acting on smooth muscle cells directly) pathways depending on whether nitric oxide from the endothelial cells is required [96, 97]. However, CGRP is not always pro-inflammatory. There are actually many cases showing its anti-inflammatory functions (this will be mentioned below). Therefore, in the scheme of neurogenic inflammation, CGRP acts on the vessels and facilitates inflammation but it negatively regulates local immunity in other scenarios (reviewed in [98]).

#### **1.4.2 Substance P**

Substance P (SP) is a neurotransmitter, neuromodulator and immune modulator, containing 11 amino acids. It is synthesized in the soma of neurons and released either at the neuronal soma or the axon terminal after transported [99]. Its bioactivity is mediated by a G-protein-coupled receptor, neurokinin 1 receptor (NK1R) signaling. Therefore, the presence of membrane-bound NK1R and the stability of SP determines the duration and sensitivity of SP reactivity. The NK1R is expressed in the CNS and PNS, endothelial cells, smooth muscle cells, mucosal tissues including gastrointestinal and genitourinary tracts

and pulmonary tissues. The NK1R signaling is regulated by  $\beta$ -arrestin which uncouples the receptor with the associated G-protein followed by receptor internalization [100] and the level of soluble SP is controlled by endothelin-converting enzyme 1 mediating SP degradation [101].

SP resembles CGRP in many ways – for example, they are both involved in pain sensing and are widely present in the CNS and PNS. They are often co-localized in the same nerves and are released together upon capsaicin treatment [102]. The activity of SP on vessels is closely associated with induction of nitric oxide which then controls vascular smooth muscle cell relaxation [103]. In addition to vasodilation, the SP-nitric oxide axis promotes migration and proliferation of endothelial cells [104] and mobilization of CD29+ stromal cells in an alkali burn model [105], highlighting SP's role in wound healing [106] and cancer metastasis [107].

In the neurogenic inflammatory scenario, compared with CGRP, SP is about 10,000-fold less potent in vasodilation activity [103] but it strongly increases vessel permeability, promoting plasma leakage and leukocyte extravasation [108]. These two concurrently secreted neural substances thus differentially facilitate distinct processes acutely on the vessel while neurogenic inflammation occurs. SP then induces secondary effects in late phase by binding to mast cells and other leukocytes to trigger release of pro-inflammatory cytokines such as histamine, prostaglandins and leukotrienes [108]. Notably, SP-treated mast cells balance the effect of CGRP by producing proteases which degrade CGRP and thus control the duration of vasodilation [109]. On the other hand, mast cells are induced to degranulate when treated with SP [110]. These compose a well-regulated network of neurogenic inflammation.

## **1.5 Adaptive immunity**

The main organ investigated in this project is the lymph node, which is a secondary lymphoid organ important for the development of adaptive immunity. Adaptive immunity, initially called “acquired immunity”, was found to be the mechanism conferring protection against smallpox by cowpox vaccination. In 1890s, discussion of acquired immunity highlighted its two important features – specificity and memory [111]. Unlike innate

immunity which recognizes common elements of pathogens by pattern recognition receptors and reacts quickly, adaptive immunity requires a longer time to produce effector cells or antibodies which are highly specific and long-lasting [112]. T and B cells are the major effectors, which differentiate after priming and activation by APCs and helper cells. This process mainly takes place in secondary lymphoid organs and involves antigen presentation, clonal selection and expansion of lymphocytes.

Adaptive immunity eventually results in generation of either CD8 cytotoxic T cells or antibody-producing plasma cells (PCs), depending on the types of antigen exposed. These two pathways are not mutually exclusive but are usually negatively correlated [113]. In fact, priming rats with higher antigenic activity of *Salmonella Adelaide* flagellin skews the recall immune reaction toward antibody production rather than cell-mediated responses [113]. The balance between types of immunity is determined and supported by different types of immunogens and CD4 T helper (Th) cells [114, 115]. Naïve CD4 T helper cells have plasticity to differentiate into activated subsets such as Th1, Th2, Th17 and regulatory T (Treg) cells upon cytokine stimulation [114, 115]. Th cell polarization in adaptive immunity affects the direction of responses so that it carries out either cell-mediated or humoral immunity via shaping the favored microenvironment.

### **1.5.1 Cell-mediated immunity**

Cell-mediated immunity involves elimination of pathogen-infected cells by the cytotoxic function of CD8 T cells. To fully activate CD8 T cells, engagement of the T cell receptor (TCR) and the co-stimulatory molecule CD28 [116, 117] is required, along with the presence of inflammatory cytokines such as IL12 and IFN $\gamma$  [118]. During infection, CD8 T cells are recruited to the LN to acquire antigen-specific TCR activation and co-stimulation of CD28 [119]. These signals are normally provided by APCs when the pathogen comes in the form of a whole pathogen; however, these APCs are less likely to be fully activated by epitopes of pathogens (for example, viral infection) so that this process then requires additional help from CD4 T helper cells – so called “licensing” [120]. In a type I immune response, Th1 cells release IL12 and IFN $\gamma$  to maximize the activation of CD8 T cells via licensing of APCs [120]. Outside of the LN, CD4 T cells can direct armed CD8 T cells to

the infected tissue for elimination of infected cells [121]. T-box transcription factor (T-bet) is the key factor for Th1 differentiation from naïve CD4 T cells because T-bet expression counteracts GATA3 (GATA binding protein 3), the core transcription factor of Th2 so that it channels the fate decision of naïve helper cells toward Th1 [122]. T-bet is important for not only Th1 development but also CD8 cytotoxic and memory T cell differentiation in type I immunity [123, 124]. IL2 was considered as a growth factor of CD8 T cells but is recently viewed as a differentiation factor relating to the cytotoxic function [125] and capability of secondary expansion of CD8 memory T cells via autocrine signaling [126, 127].

## **1.5.2 Humoral immunity**

Humoral immunity results in production of antibody from plasma cells (PCs). PCs and memory B cells are terminal subsets in the B cell differentiation pathway [128, 129]. There are T-cell-dependent (TD) and T-cell-independent (TI) B cell responses depending on whether Th2 cells are required [130].

### *1.5.2.1 T-cell-dependent response*

In TD response, binding of protein antigens to B cell receptors (BCR) leads B cells to endocytose, process and present the digested peptide on their MHCII [131, 132]. Antigen-primed B cells need three signals from Th2 cells for full activation: MHCII-TCR cognate engagement [133], CD40-CD40L co-stimulation [134] and IL4 reception [135]. After interaction with cognate B cells, antigen-experienced follicular helper T (Tfh) cells together with activated B cells form germinal centers (GCs) in B cell follicles [136, 137]. Activated B cells enter GC in secondary or tertiary lymphoid organs to undergo affinity maturation and class switching, which diversifies antibody classes and improves antibody affinity [138]. Interestingly, in germ-free animals, although the number of GC is lower in homeostasis [139], substantial quantities of antibodies are produced after challenge, and class switching still occurs, indicating that these animals are still capable to form GCs [140, 141]. The extent of GC B cell (GCB) expansion is proportional to the amount of antigen presented by GCBs to Tfh cells and positively relates to antibody affinity [142]. However,

overloading antigen generates bystander GCBs and Tfh cells causing the formation of auto-antibodies [143]. High affinity antibody-bearing B cells surviving from clonal selection in the GCs differentiate into either PCs or memory B cells. Memory B cell development in the lymph node requires (1) B cells expressing IL9 receptor (IL9R) with intrinsic responsiveness to IL9 and (2) IL9 secreted by Tfh cells [144]. Long-lived PCs residing in bone marrow and spleen secrete antibody persistently for more than 120 days or longer to maintain humoral immunity independent of antigen re-boost [145, 146].

Th2 cells typically secrete IL4, IL5, IL9 and IL13 and are associated with TD B cell responses and allergy [147]. They can be activated by dendritic cells (DCs), basophils, epithelial cells and innate lymphoid cells (ILCs) [147, 148]. To classify Th2-promoting DCs by transcription factors, they express interferon regulatory factor 4 (IRF4) and Krüppel-like factor 4 (KLF4) [149-151]. To categorize these DCs by surface marker, CD301b<sup>+</sup>DC seems important for Th2 responses. In a model using ovalbumin and different adjuvants to elicit immune responses in the draining LN (dLN), depletion of CD301b<sup>+</sup>DCs prevents the Th2 response and reduces the Th1 response [152]. However, although depletion of CD301b<sup>+</sup>DCs abolishes the Th2 response, it does not affect frequencies of Tfh cells and GCBs or production of IgG and IgE [152]. TCR signaling together with IL4 reception drives Th2 polarization by inducing GATA3 expression, which further promotes Th2 cytokines [147, 153, 154]. Unlike the canonical Th polarization, which requires IL4 reception initially, a low dose of cognate peptide triggers GATA3 expression and IL2 production, which then induces production of IL4 for type 2 immune response [155].

#### *1.5.2.2 T-cell-independent response*

The TI B cell response, can be subdivided into two subtypes depending on the antigen. Antigens that trigger BCR and Toll-like receptors (TLRs) signaling activate the type 1 response while the type 2 reaction is driven by antigens capable of cross-linking multiple BCRs [156-158]. TLR signaling is still required for initial B cell proliferation and survival in type 2 TI response, and is essential for antibody secretion [157]. TI responses predominantly involve production of immunoglobulin M (IgM) by B1 cells in the peritoneal cavity or by marginal zone (MZ) B cells in the spleen [159, 160]. TI responses were

thought of only producing short-lived PCs, but this has been proven wrong by observing the presence of *Streptococcus pneumoniae*-induced PCs for 180 days after B cell depletion [161]. In T cell-deficient mice, albeit GC formation fails, generation of long-lived PC is not affected [162]. These studies show long-lived PC differentiation is not an exclusive outcome of TI or TD responses and is independent of GC formation.

### 1.5.2.3 Somatic hypermutation and class switch recombination

The goal of somatic hypermutation (SHM) is to diversify antibody specification for broad coverage of antigens or affinity maturation. This process requires activation-induced deaminase (AID), which converts cytosine to uracil by deamination in the Ig loci [163, 164]. Normally this reaction is lymphocyte specific and occurs the first time during lymphocytogenesis in order to have a wide spectrum of clones. The second time it happens after activation by epitope exposure. Activated clones of B cells then express AID and undergo SHM in GCs to further diversify the variation region of the antibody (B cell receptor) [164]. After that, these B cells survey again the epitopes presented by follicular dendritic cells (FDCs) in the LN [165]. A parabiosis study revealed that FDCs do not have characteristics of the parabiosis partner, suggesting local progenitor replenishment [166]. FDCs interact with B cells by antigen-antibody or antigen-complement immune complexes in the GC [165, 167]. B cells with high affinity receptors then survive while the others undergo apoptosis because insufficient survival factors were received. This process can run repetitively to obtain the clones with extremely high affinity to presented epitopes.

Class switch recombination (CSR) aims to generate multiple subtypes of antibody, which are specialized, to work with different immune cells and molecules and protect different body compartments. It also requires AID [164]. The CSR program of B cell is turned on with engagement of CD40 to CD40L and ligation of TLR4 (by LPS, for example). IL4 synergistically enhances CD40 signaling for CSR via nuclear factor kappa B (NF $\kappa$ B) and signal transducer and activator of transcription 6 (STAT6) activation [168]. B cell CSR mainly takes place in GC in the LN [164, 169]. In extrafollicular B cells, transmembrane activator and calcium-modulator and cytophilin ligand interactor and B cell activating factor

receptor (BAFF-R) mediate class switching [170] due to Myd88 signaling [171]. In Myd88-deficient B cells, IgG1 and IgM production is impaired after TD immunization [172], indicating Myd88 plays a role in both TI and TD responses. Taken together, SHM and CSR are two major events activated B cells experience in GCs in order to refine antibody affinity and diversify subtypes of antibody.

## 1.6 Lymph node

In order to form quality responses, the lymph node (LN) requires structural, cellular and molecular components. It is composed by (1) structural components such as blood and lymphatic vessels, stromal cells and conduits, (2) resident cells such as resident DCs and subcapsular macrophages, (3) motile cells such as B and T cells, migratory DCs, and many other leukocytes and (4) nerves (**Figure 1.3**). These components reside in different areas of the LNs for their functionality. The majority of cells in LNs are dynamic and maintained in a steady state. Its local environment can be dramatically changed after receiving immune stimulation, which quickly turns on events in the LN such as leukocyte recruitment, proliferation and nodal remodeling.

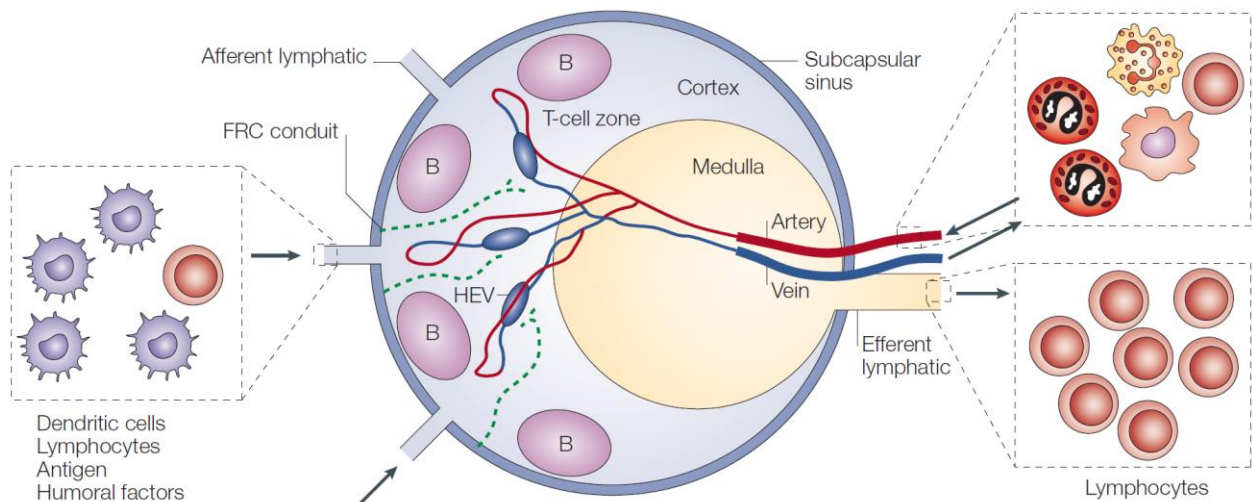


**Figure 1.3 Vasculature and cell zones of the lymph node**

This figure is originally in the review article from Miyasaka and Tanaka [173]. It presents a concise view of vessels and compartments of the lymph node. The LN associated vasculature consists of lymphatic vessels

and blood vessels (1.6.1.1). Afferent lymphatics bring cells and soluble factors from the drainage area to the LN. These cells or substances arriving at the subcapsular space (SCS) either enter the LN parenchyma via fibroblastic reticular cell conduits or flow to efferent lymphatics and leave from the LN medulla. The other route for cellular trafficking is entry via high endothelial venules (HEVs), which are specialized hubs for immune cells to transmigrate. This route enables recruitment of cells from blood. The LN has very organized compartments including the SCS layer, the cortex (containing B cell follicles nearby the SCS and T cell area between follicles) the medulla (1.6.1.3). Although nerves are missing in this figure, they should be associated and innervate the capsule and enter the LN along blood vessels (1.6.1.2).

## 1.6.1 Structure of lymph node

LNs are associated with lymphatic vessels, blood vessels, and nerves. They geographically access LNs differently and connect LNs with their drainage area, circulation and the nervous system.

### 1.6.1.1 Vasculature

Cell trafficking from/to the lymph node occurs via vasculatures including blood and lymphatic vessels. Arterioles enter lymph nodes at the hilum, which is a slightly sunken area on the LN surface. They branch into smaller hierarchal vessels inside LNs including high endothelial venules (HEVs) where circulating leukocytes infiltrate from blood [174, 175]. After HEVs, blood vessels converge and exit LNs as a single vein. Lymphatic vessels attached to LNs are either efferent or afferent, depending on the direction of lymph flow. A LN has only one or two efferent lymphatic vessel(s) bringing lymph from the medulla of one LN to the next LN. The last efferent lymphatic vessel of this chain leads to the thoracic and right lymphatic ducts and rejoins the blood stream. Afferent lymphatic vessels bring LNs “soluble immune factors” from the drainage area and serve as fast tracks to get immune cells in. The subcapsular space (SCS) of LNs is the first stop for soluble antigens and pathogens transported from afferent lymphatics. Soluble factors there either diffuse further along the conduits in LNs or are phagocytosed by macrophages lining the wall of the SCS (included in 1.6.2).

### 1.6.1.2 Nerves

Nerves ramify the vessels and capsule as well as the parenchyma of LNs [176]. Early findings of LN innervation largely focused on the sympathetic nervous system (SNS). Sympathetic nerves are found associated with the capsule, blood vessels, internodular regions and the border of B cell follicles in rodents [177, 178]. Sympathetic nerves in human LNs have a very similar distribution pattern which densely touches the hilar region and goes in mainly along blood vessels and is absent in follicles [179]. Co-localization of an anterograde tracking dye injected via superior cervical ganglion (SCG) and S100 staining reveals sympathetic innervation of S100<sup>+</sup> cells, a DC subset in the LN [180]. Beside classical catecholamines, neuropeptide Y (NPY) immunoreactive fibers co-localized with sympathetic nerves in the LN [181]. Neuropeptides SP and CGRP, usually found in sensory nerves, are also present and overlap with each other in the LN. These nerves are closely associated with vessels [181, 182]. Although innervation of lymphoid tissues has been characterized [183], high definition systemic scans of neural anatomy in LNs have not been performed.

### 1.6.1.3 Cell zones

Lymph nodes contain many types of immune cells, which locate in distinct areas. Structurally from the outer layer to its core, there are capsule, SCS, cortex, paracortex and medulla. CD169<sup>+</sup> macrophages are not present in the parenchyma but cover the SCS and internodular lymphatic vessels. They form a network, which functions as a filter and presents antigens taken from the lymph to B cells [184]. In the cortex, there are multiple B cell follicles located close to the SCS. Another major cell type, T cells, resides in the paracortical area and the regions between B cell follicles. T and B cell areas and functions are tightly regulated by chemokine expression of stromal cells, which is dictated by TNF $\alpha$  and lymphotoxin  $\alpha/\beta$  (LT $\alpha/\beta$ ) [185]. Fibroblastic reticular cells (FRCs) expressing C-X-C motif ligand 12 (CXCL12) form a network for T cell migration and FDCs expressing CXCL13 populate B cell follicles, position B cells and define B cell areas [186]. The medulla is a complex area in LN. There are dense blood and lymphatic vessels, covered by CD169<sup>+</sup> macrophages, along with PCs, DCs, mast cells and lymph [187].

### 1.6.2 Afferent lymphatics

Each LN has its specific drainage area it is responsible for, facilitating immune surveillance of that region. Afferent lymphatics, which direct cells and soluble factors into the LN as well as conduits channeling soluble factors inside the LN, are critical for fulfillment of this function. Cytokines, chemokines, immune cells, viruses and free soluble antigens can be brought by lymphatics from the drainage area to the draining LN and induce immune responses (**Figure 1.4**). In addition to lymph-based leukocyte trafficking, circulating leukocytes can also migrate to the LN via blood vessels. These facts depict LNs as an interface between resident cells, regional migratory leukocytes and circulating immune cells to achieve and optimize immune responses.

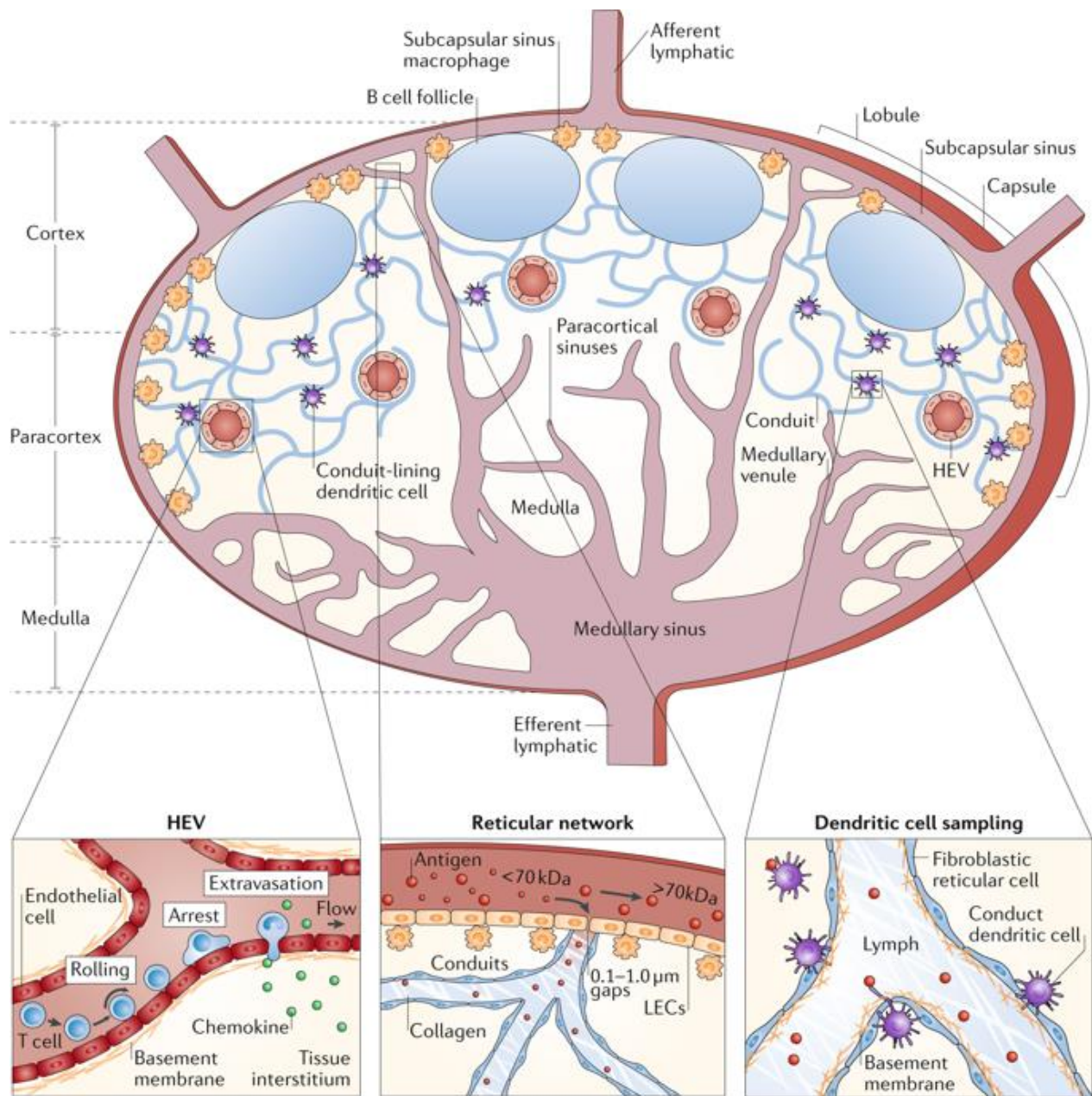


**Figure 1.4 Lymphatic and conduit systems of the lymph node**

This figure is originally in the review article from Schudel et al [188]. This figure focuses on lymphatic vessels and conduits. The LN can collect lymph from its drainage area (1.6.2.1). This process enables entry of immune cells and soluble factors into the LN and induce immune responses. The first place they arrive at is the subcapsular space (SCS), which is covered by a CD169<sup>+</sup> macrophage network serving as a filter. SCS is also the interface between the lymphatic and the conduit systems. The latter can be viewed as an intra-nodal lymphatic network in which soluble factors are strictly controlled by physical properties such as molecular size and cellular factors, for example, macrophages and B cells (1.6.2.2).

### *1.6.2.1 From periphery to the lymph node*

Afferent lymphatics bring cells, pathogens and free molecules to LNs, and the region they cover defines the LN's drainage area. Molecules can enter LNs via passive diffusion. This route is mainly determined by the molecule size. Molecules less than 10 nm can freely diffuse into blood or lymph but they are predominantly transported via blood because of higher fluid velocity which maintains a concentration gradient, driving diffusion [189]. Substances with increasing size can no longer pass barriers freely and so preferentially leave through lymphatics which is more permeable structurally [189]. Alternatively, instead of crossing the vascular wall, they can alternatively enter lymphatic vessels with interstitial fluid via the terminal of lymph capillaries [190]. These transportation routes to LNs have been intensively studied from angles of immunology and drug delivery. Once the substance enters the lymphatic vessel, muscle contraction-driven lymph flow carries it toward the LN [191]. Similar to blood vessels, lymphatics have hierarchy so small lymph capillaries eventually converge to a few collective lymphatics before reaching LNs.

### *1.6.2.2 Conduits, filtration function and maintenance of lymph node physiology*

After arrival at the SCS in LNs, small molecules less than 4 nm can easily diffuse in the conduit system in the lymph node to reach local DCs and this way is much quicker than entering LNs via antigen carrier DCs [192], but larger molecules rely on phagocytosis or other processes. Molecules larger than 70-80 kDa are endocytosed by CD169<sup>+</sup> macrophages and the smaller molecules (less than 70-80 kDa) can reach resident DCs in T cell area via conduits [192], or enter B cell follicles via conduits [193] or via diffusion across SCS. Additionally, while substances travel from afferent to efferent lymphatics in SCS, only these smaller molecules can be channeled to the lumen of HEVs via conduits [194]. By contrast, molecules larger than 70-80 kDa, if they do not flow through SCS directly to efferent lymphatics [194], are trapped by CD169<sup>+</sup> macrophage mesh lining the SCS for antigen acquisition by B cells [184, 195, 196]. SCS CD169<sup>+</sup> macrophages, acting as gatekeepers, screen soluble substances in afferent lymph at the SCS to set a

reasonable threshold of immune activation [197] and prevent systemic dissemination of pathogens [198].

Afferent lymphatic flow not only has immune surveillance functions but is also required for LN maintenance. Occlusion of afferent lymphatics of popliteal lymph nodes changes LN cell composition and HEV morphology, wipes out CD169<sup>+</sup> macrophages and reduces the number of interdigitating DCs [199]. In longer term experiments of over 15 weeks, surgical blockade of afferent lymphatic flow eliminates GCs [200]. This evidence highlights the importance of lymphatic flow to LNs in homeostasis and during immune perturbation, suggesting mechanisms of functional circulation of immune cells or molecules between LNs and their drainage area.

### **1.6.3 Leukocyte trafficking to lymph nodes**

Leukocyte trafficking to LNs via HEVs relies firstly on chemotaxis, and then interaction with the vessel walls. In addition to migration through blood, leukocytes can also migrate to the lymph node via afferent lymphatics. In general, it is believed that DCs are the commanders which infiltrate the lymph node and initiate the immune cascades [201], such as lymph node remodeling and further leukocyte recruitment. In general, C-C chemokine ligand 19 (CCL19) and CCL21 attract leukocytes from the periphery or circulation to the LN, and CXCL12 and CXCL13 position these cells at specific sites inside the LN. In contrast to having multiple chemoattractants to achieve recruitment, egress is mainly mediated by sphingosine-1-phosphate (S1P). Receptors, producers, responders and functions of them are discussed below and summarized in **Table 1.1**.

**Table 1.1 Chemotactic compounds for leukocyte trafficking to the lymph node**

Compound	A.k.a.	Producers	Major location	Receptors	Responding cells	Fucntions
<b>CCL19</b>	ELC	FDCs, FRCs and LECs	widely presence in the LN	CCR7	lymphocytes and migratory DCs	lymphocytes and migratory DCs trafficking to the LN
<b>CCL21</b>	SLC	FDCs, FRCs and LECs	widely presence in the LN	CCR7	lymphocytes and migratory DCs	lymphocytes and migratory DCs trafficking to the LN
<b>CXCL12</b>	SDF1	CRCs	T cell zones and dark zones of B cell follicles	CXCR4, CXCR7	widely expressed	leukocyte homing to the LN and positioning
<b>CXCL13</b>	BLC	FDCs, MRCs and VSCs	B cell follicles	CXCR5	B, Tfh	B cell and Tfh positioning
<b>S1P</b>		many	blood and lymph	S1PR1	lymphocytes	lymphocyte egress from the LN

**Table 1.1 Chemotactic compounds for leukocyte trafficking to the lymph node**

Centering on the soluble compounds mediating chemotaxis, their respective producers, receptors responders and main functions are summarized. These mediators are the most investigated chemokines involving in leukocyte trafficking to/from the LN. Details are included in the text below. ELC: EB11 ligand chemokine; SLC: secondary lymphoid-tissue chemokine; SDF1: The stromal cell-derived factor 1; BLC: B lymphocyte chemoattractant.

### 1.6.3.1 Chemotaxis

Chemokines CXCL12, CXCL13, CCL19 and CCL21 are critical for leukocyte homing to LNs and are produced by lymphatic endothelial cells (LECs), FDCs and other stromal cells [202]. FDCs and fibroblastic reticular cells (FRCs) can secrete CCL19, CCL21 [203], and CXCL13 [204]. CXCL13, also known as B lymphocyte chemoattractant (BLC), is essential for B cell homing and responses and is highly expressed by FDCs [205, 206]. In addition to CXCL13, FDCs express B cell survival factors as well [205]. However, although depletion of FDCs abolishes B cell responses, this does not dramatically deplete CXCL13 in the LN, suggesting contribution from other cell types. Marginal reticular cells (MRCs) express CXCL13 and B cell survival ligands too, but they cannot rescue the failure of B cell responses after FDC ablation [207]. A newly characterized cell type versatile stromal cells (VSCs) also produce CXCL13 for directing B cells [208]. Initially, CXCL13 via binding to its receptor CXCR5 was described as a chemotaxis driver selectively for B cells [206],

but not for other circulating leukocytes such as T cells, neutrophils and monocytes [209]. Nowadays, it is well accepted that a specific subset of T cell, Tfh cells, also express CXCR5 [210] and this activation-driven expression and the recruitment of Tfh cells are closely tied to B cell responses in the GCs [143, 205].

CXCL12, also known as stromal cell derived factor 1 (SDF1), is expressed by stromal cells and mediates B and T cell homing to LNs and Peyer's patches [211], as well as bronchus-associated lymphoid tissue (BALT) in the lung [212]. However, the identity of the cells producing CXCL12 there is still not clearly defined. They are only vaguely known as stromal cell types inducibly expressing podoplanin [212]. The CXCL12-expressing population of reticular stroma (CRCs) is described closely associated with the T cell area and in the dark zone of GCs [213]. The canonical receptor of CXCL12 is CXCR4 [214, 215], which is widely expressed on many leukocyte subsets and together with other adhesion molecules shapes leukocyte trafficking behavior to different tissues [216-218]. Recently, CXCR7 was identified as an alternative receptor of CXCL12 [219], and is expressed by T and B cells and DCs [220, 221]. In an EAE model, IL17 stimulates brain endothelial cells to greatly express CXCR7 to scavenge abluminal CXCL12 so that it further promotes EAE via facilitating lymphocyte extravasation to brain parenchyma [222].

Although FRCs express both CCL19 and CCL21, they preferentially make more CCL21 [203]. Together with FDCs, these LN stromal cells generate a gradient of mixed chemoattractants centered at the LN. In the periphery, LECs in afferent lymphatics produce chemokine CCL19 and CCL21 that serve as key drivers to draw DCs to the LN from the drainage area [223]. They present CCL21 on heparan-sulfate (a linear polysaccharide abundant on surface proteins and extracellular matrix that binds a wide range of ligands) and mice lacking heparan-sulfate have reduced numbers of lymphocytes and DCs homing to LNs [224]. CCL19 and CCL21 both bind to CCR7 with similar affinity [225] and direct DC migration to the LN [226, 227]. CCL21 in FRCs is found to be produced in the membrane-bound form, which triggers integrin-mediated adhesion of DCs and cleavage of CCL21 after engagement of CCR7 on DCs [227]. Released free CCL21, together with CCL19, drives gradient-based DC swarming [227]. This observation suggests afferent lymphatics, another CCL21 producing unit, might exploit the same mechanism to attract DCs in the periphery. In contrast to CCL21, CCL19 does not have a

membrane anchoring domain so it is freely diffused [228]. CCL19 can be placed in the HEV lumen by “transcytosis” to attract lymphocytes in the circulation [229]. A spontaneous mutation causing loss of CCL19 and CCL21-ser occurs in ‘paucity of lymph node T cells’ (*plt*) mice [230, 231]. In *plt* mice, the T cell response is shifted from the LN to the spleen, and is delayed but enhanced [232]. These mice have much fewer DCs in most subtypes but the monocyte-derived lineage in LNs during inflammation [233]. In *plt* mice, monocytes are still recruited to LNs and become inflammatory dendritic cells with capability of Th1 response induction, relying on CCR2 (but not CCL2 or CCR7) [233]. In contrast, CCR7-deficient mice, losing the receptor of CCL19 and CCL21, have impaired B cell, T cell, and DC migration, disorganized B and T cell zones in LNs, spontaneously activated B cells, and impaired humoral response [226]. These findings suggest that (1) CCL19/CCL21-CCR7 signaling is at the very upstream of adaptive immune response, which broadly affect the structure, or the responding kinetics of naïve or inflammatory LNs respectively, (2) Ablation of this axis (via losing ligand or receptor) greatly compromises LN sensation of immune stimulation at periphery via disabling recruitment of activated mature DCs and (3) Dissolving this axis skews the type of responses towards Th1 responses (via only allowing LN infiltration of monocyte-derived DCs but not the other type of DCs).

### 1.6.3.2 Egress

Lymphocyte egress from lymphoid organs depends on the surface receptor sphingosine-1-phosphate receptor 1 (S1PR1) controlling the transit time of lymphocytes [234, 235]. S1PR1 signaling is G $\alpha$ i-dependent so it can be inhibited by pertussis toxin [235, 236]. The egress process is basically an ordinary chemotactic response but directed from the lymphoid tissues to blood and lymph, directly controlling the dwell time [237]. This is achieved by the fact that the concentration of the ligand of S1PR1, sphingosine-1-phosphate (S1P), exists at high levels (100-300 nM) in blood and lymph driving lymphocyte egress from LNs via efferent lymphatics [238]. Egress can be inhibited by fingolimod (FTY720) treatment, preventing lymphocytes from migrating to medullary sinusoids in the LN [239]. Sustained blockade of egress is immunosuppressive, and Fingolimod has been developed as a drug to combat multiple sclerosis, effectively reducing the rate of relapses in relapsing-remitting MS over a two-year period [240, 241].

Cell residence time in the LN relies on the net effect of recruitment/retention signals and egress forces. After PCs mature in the LN, the domination of CCR7 and CXCR4 as retention signals or S1PR1 as an egress driver determines whether cells remain in the LN or migrate out into the circulation [242, 243].

#### *1.6.3.3 Migration for functions*

After immune challenge, the egress force is inhibited [244], suggesting lymphocytes stay longer in secondary lymphoid organs for mounting immune responses. This egress restriction mechanism depends on interference of S1PR1 functions by direct inhibitory interaction with the activation marker CD69 [245], or CD69-mediated type I interferon signaling [246], suggesting activation-driven mechanisms temporally restrain egress for providing enough time for leukocytes to get sufficient immune cues. Some cells migrate to the LN for functional optimization. For example, during inflammation, circulating Treg cells infiltrate the inflamed site, migrate to the draining LN and reenter the inflamed skin to exert their functions [247]. Lymphocyte numbers in LNs can affect the amplitude of adaptive immunity with the evidence that immunization given at the time LNs have more lymphocytes generates higher antibody titer [248]. Immunization is not the only case of LN cellularity-dependent responsiveness, which seems to be a ubiquitous phenomenon. Similar observation was found in EAE disease progression [249]. These evidences tie functions and trafficking behavior together, indicating the importance to position specific immune cells at certain sites and timing for maximizing their functionality.

#### *1.6.3.4 Leukocyte vessel interactions*

Leukocyte recruitment to LNs requires transmigration through the vessel walls at HEVs [174, 175, 250]. This process is known as the adhesion cascade, which involves many adhesion molecules including integrins, selectins, and intercellular adhesion molecules (ICAMs). Different immune subsets exploit different sets of adhesion molecules for vascular adhesion and transmigration, indicating a cell type-specific adhesion mechanism (reviewed in [251, 252]). The expression of these molecules on vessel walls of different organs at different times of day, along with the interacting partners on leukocytes, shapes

the global chrono-migratory profile of immune cells [217, 252]. Major adhesion molecules mediating leukocyte homing to LNs are summarized below (**Table 1.2**) [217, 250]. Blockade of CD11a in combination with CD49d [249] or L-selectin or ICAM1 alone [217] efficiently interferes with homing and causes lymph node atrophy due to targeting T and B cell homing pathways to LNs. Except from these major cell types, pre-conventional dendritic cells (pre-cDCs) [253] and natural killer (NK) cells [254] also migrate into LNs via L-selectin mediated recruitment.

**Table 1.2 Adhesion molecules for leukocyte vessel wall interaction**

<b>Endothelial cells</b>	<b>Leukocytes</b>			
common name	common name	CD name	integrin name	Blocking Ab
ICAM1	LFA1	CD11a/CD18	$\alpha$ L $\beta$ 2	M17/4
	Mac1	CD11b/CD18	$\alpha$ M $\beta$ 2	
VCAM1	VLA4	CD49d/CD29	$\alpha$ 4 $\beta$ 1	PS/2
P-selectin (CD62P) E-selectin (CD62E)	PSGL1			
CD34 GlyCAM1 MadCAM1	L-selectin	CD62L		MEL-14

**Table 1.2 Adhesion molecules for leukocyte vessel interaction**

Multiple steps are required for leukocytes to migrate from circulation to the LN via HEVs. This table lists some critical molecules on the endothelial cell side as well as their interaction partners on leukocytes. Blockade of these molecules on leukocytes can effectively interfere with this migration cascade and prevent leukocyte recruitment to the LN.

HEVs are ports for immune cells to migrate into the LN, so their morphology and integrity are essential for functionality. During an immune response, large numbers of leukocytes transmigrate through HEVs and cause physical disruption of the junctions between endothelial cells. In a physiological setting, this damage is normally rescued by podoplanin-Clec2 engagement with platelets, which then release S1P to promote endothelial junction repair [255]. Unlike this passive mechanism accompanying leukocyte infiltration, DCs actively control the HEV phenotype to gate lymphocyte entry via LT $\beta$  signaling [175].

## **1.7 Structure of the peripheral nervous system**

Peripheral tissues are innervated by three kinds of nerves – motor, sensory and autonomic nerves [256]. The autonomic nerves can be further subdivided into sympathetic and parasympathetic nerves [257]. The SNS has short preganglionic nerves which go to three sites (1) the paravertebral sympathetic trunk [258], (2) celiac ganglion [259] or (3) mesenteric ganglia [260]. Those preganglionic nerves originate in the brain, and end up at those three sites via the spinal cord; the postganglionic neuronal soma of the SNS reside in these compartments and project their fibers to target organs [258]. Parasympathetic innervation of the periphery is mainly contributed by the 10<sup>th</sup> cranial nerve, the vagus nerve [257, 261, 262]. Additionally, the pelvic nerve from the sacral spinal cord also delivers parasympathetic tone to bladder and gonads [263-265]. The organization of sensory nerves is very similar to the SNS but instead of transit via ganglia in the sympathetic trunk, sensory postganglionic neurons are located in dorsal root ganglia by the spinal cord [266]. Motor nerves innervate muscles and have little immune functions identified so far.

### **1.7.1 Classification by neural substances**

The unique feature of sensory nerves is their afferent functions, which transmit peripheral stimuli to the brain. However, they also conduct efferent functions using neural substances such as SP, CGRP, NGF and vasoactive intestinal peptide (VIP) to exert immune modulation. Sympathetic nerves are mostly using norepinephrine (NE) as a functional molecule, but there is also a minor population of cholinergic sympathetic nerves, meaning they secrete acetylcholine (ACh) [267]. Parasympathetic nerves widely innervate visceral organs and release ACh as the major compound and VIP and nitric oxide as minor messengers. A subset of these nerves is reported to be catecholaminergic [268]. Some examples about how these neural substances regulate immune functions are presented in **1.8** and details are reviewed in [269-272] for sensory neuropeptides, [273-275] for the SNS substances, and [275-277] for the general neural-controlled immunity.

### **1.7.2 The sciatic nerve**

The mouse leg is innervated by the femoral and sciatic nerves. Both nerves are myelinated, but the latter is thicker and controls most parts of the leg. The sciatic nerve is a mixed nerve, with sensory fibers as the most abundant and sympathetic nerves as the second largest population [278]. These sensory and sympathetic fibers are derived from lumbar dorsal root ganglia and sympathetic ganglia in the sympathetic trunk, respectively. Although it controls many muscles, it only contains 6% of motor nerves [279].

## **1.8 Immune regulatory functions of neural substances**

Neural substances were initially identified as neurotransmitters to convey messages between nerves. Immune cells express receptors of neural substances from the autonomic nervous system [275, 280] and sensory fibers [271, 272]. In addition to that, increasing studies have shown that some immune cells even produce neural substances, such as ACh and SP [281, 282]. This fact enables cooperation between the nervous and immune systems for immune functions. Neural substances have divergent regulatory functions depending on the targeting cell types, receptors and local context.

### **1.8.1 The autonomic nervous system**

The majority of studies of immune and sympathetic crosstalk have found that beta adrenergic receptors ( $\beta$ ARs), especially the  $\beta$ 2AR, are controlling immune functions [283].  $\beta$ 2AR is widely expressed on immune cells such as B cells, T cells, and macrophages. Its activation mostly inhibits T cell proliferation but affects B cell proliferation differently depending on co-stimulatory mitogens [273, 284].  $\beta$ 2AR signaling is usually immunosuppressive due to activation of the cyclic adenosine monophosphate (cAMP) – protein kinase A (PKA) pathway, but it can alternatively trigger the mitogen-activated protein kinase (MAPK) pathway for stimulatory functions [283]. Following activation, Th1, but not Th2, cells express  $\beta$ 2AR enabling negative modulation of IL2 production by  $\beta$ 2AR

agonists, suggesting that different polarizations of T cells have distinct sensitivity to NE due to differences in  $\beta$ 2AR expression level [285]. Activation of  $\beta$ 2AR on NK cells reduces their frequency [286] and suppresses tumor-killing functions [287]. In addition to  $\beta$ ARs, alpha adrenergic receptors ( $\alpha$ ARs) also exert immune modulation [178], but have been less investigated. Their activation on NK cells e.g. enhances their cytotoxic activity [288]. These studies show examples that sympathetic nerves can differentially modulate immune functions depending on cell type and receptor expression. In fact, sympathetic nerves and the immune system form a functionally interwoven and anatomically complicated network at levels of cell development, trafficking and activation (reviewed in [274]). Compared with the SNS, the parasympathetic nervous system (PSNS) is less explored at the point of immune regulation. Most findings of immune modulation by the PSNS focus on a well-defined mechanism called the “anti-inflammatory reflex” described in **1.8.4**.

## **1.8.2 The sensory nervous system**

Although sensory nerves convey messages back to the CNS, they also have efferent functions involving the secretion of several neuropeptides. The two most studied neuropeptides in the context of immune modulation are CGRP and SP whose neurogenic inflammation functions were discussed in section **1.4**. To simulate the release of CGRP in skin, endothelial cells were treated with CGRP followed by co-cultured with Langerhans cells and CD4 T cells. In this setting, IL6 production from endothelial cells is induced and bias the outcome of antigen presentation by Langerhans cells to T cells [289]. However, in general it is immune inhibitory because RAMP1 (a subunit of the receptor of CGRP)-deficient mice exhibit higher levels of inflammatory cytokines and hypertension [290]. From the cell migration perspective, CGRP can facilitate the adhesion of neutrophils to the vessel wall [291, 292]. Moreover, it inhibits the production of the chemokines CXCL1, CXCL8 and CCL2 from LPS-treated human endothelial cells [293]. CGRP also changes fundamental cell functions. For example, it turns on the anti-inflammatory program of macrophages during *Staphylococcus aureus* infection [79], inhibits TNF $\alpha$  production from peritoneal macrophages after LPS stimulation [294], and dampens the bacteria-killing

capability of neutrophils [84]. Cutting corneal nerves in corneal transplant surgery results in the release of SP and causes immune rejection due to suppression of Treg cell functions [295]. Further discussion of the immune functions of sensory neural substances is included in **1.8.4** and **1.8.5** below.

### **1.8.3 Neural injury, autoimmunity and homeostasis**

Neural injuries in the CNS usually compromise the systemic immune system. Release of NE in liver triggered by experimental stroke programs the iNKT cells for global immune tolerance [14]. Similarly, spinal cord injury causes activation of sympathetic nerves, which directly facilitate glucocorticoid production in the adrenal gland and results in overall immune suppression [17]. In addition to regulating immune cell activity, the neuromuscular reflex can control the access of myelin autoreactive T cells to the CNS. By suspending mice by their tails, which impairs gravity-induced activation of sensory neurons, mice are protected from CNS infiltration of pathogenic T cells via restricting CCL20 on dorsal blood vessels at particularly the fifth lumbar spinal cord [296]. Apart from models of trauma and pathology, sympathetic nerves also control cell migratory behavior in homeostasis. During activation of sympathetic nerves, noradrenergic tone mobilizes hematopoietic stem cells (HSCs) by controlling  $\beta$ 3AR signaling in bone marrow stromal cells [297], and cholinergic cues reduces adhesion and homing to support HSCs mobilization [298]. These examples clearly demonstrate how a neural event at one site affects immune cells remotely and controls systemic immune sensitivity or chemotaxis.

### **1.8.4 Infections**

Immune regulatory effects of nerves have been shown to be beneficial, preventing excessive or inappropriate inflammatory responses. To avoid the cytokine storm generated by macrophages during infection, the vagus nerve can be activated by bacterial endotoxin and secretes ACh to attenuate inflammatory cytokines in the serum [299]. This process requires the splenic nerve to convey the message from the vagus-innervated celiac ganglion to the spleen by releasing NE [300]. Splenic nerve-derived NE engages

$\beta$ 2AR on T cells expressing acetylcholine transferase (AChT) to stimulate ACh production [281]. Released ACh then binds to nicotinic acetylcholine receptor alpha 7 ( $\alpha$ 7nAChR) on the splenic macrophages and inhibits their secretion of inflammatory cytokines [301, 302]. This cascade has been recognized as an anti-inflammatory reflex. This reflex has been tested clinically to reduce elevated pathogenic TNF $\alpha$  in rheumatoid arthritis patients [303]. Nerve-mediated immune modulation is not always systemic, though. Gut infected by *Spib* (a *Salmonella Typhimurium* mutant whose proliferation is impaired) activates local sympathetic nerves, which stimulates the macrophages in the muscularis layer of the gut to reinforce their tissue protective functions via  $\beta$ 2AR signaling [304]. In this case, the nerves only affect the area nearby.

However, pathogens can leverage these regulatory mechanisms. During *Staphylococcus aureus* infection, bacterial components can stimulate nociceptors for pain perception and in parallel CGRP release, which represses the pro-inflammatory activity of macrophages [79]. In the skin, *Streptococcus pyogenes* infection-mediated local release of CGRP attenuates the bacteria killing function of neutrophils and leads to more severe tissue damage by the bacteria [84]. Blocking the nociceptors by Botulinum Neurotoxin A or a CGRP receptor antagonist rescues defensive functions of neutrophils [84]. A similar nociceptor-CGRP-immunosuppression mechanism was discovered in the lung with neutrophils and  $\gamma\delta$ T cells in the context of *Staphylococcus aureus* pneumonia [85]. These findings imply that neural substances are likely fine tuning immune responses, and this function sometimes get hijacked by pathogens.

### **1.8.5 Allergic immunity**

Inflammation with type 2 cytokines results in allergic responses in mucosal tissues. ILC2s are important producers of type 2 cytokines, and can react to NE [305], neuromedin U (NMU) [306, 307] and CGRP [308] belonging to adrenergic, cholinergic and nociceptive neural substances respectively. Stimulation of  $\beta$ 2ARs on ILC2s represses type 2 inflammation and ILC2s lacking  $\beta$ 2ARs exhibit higher allergic responses in lung and gut [305], suggesting negative regulation of ILC2 responses by sympathetic nerves. In contrast to sympathetic nerves, CGRP, a nociceptive neural substance, enhances ILC2

responses in lungs in a ovalbumin/alum inhalation model [308]. The CGRP-ILC2-mediated immune responses, together with  $\gamma$ -aminobutyric acid (GABA)-induced goblet cell hyperplasia in lungs, are coordinated by an innervated cell type – pulmonary neuroendocrine cells (PNECs) [308, 309]. Complete depletion of PNECs in mice, using *Shh*-driven *Ascl1*-knockout mice which eliminate PNEC precursors during the developmental stage, greatly compromises the mucosal type 2 immune response [308]. Single cell RNA expression profiles of ILC2s in lungs identifies expression of neuromedin U receptor 1 (NMUR1) at the unstimulated state and after IL25 stimulation whereas after stimulation of IL33, another ILC2 activator, ILC2s reduces NMUR1 [307]. Ligation of NMUR1 maintains division and functions of ILC2s and enhances allergic responses after IL25 stimulation [307]. A similar mechanism exists in the gut, where ILC2s intrinsically expressing NMUR1 were found co-localized with cholinergic nerves [306]. These studies mark the importance of neural regulation of immunity centering on ILC2 and PNEC in mucosal barriers.

### **1.8.6 In spleen and lymph node**

Secondary lymphoid organs are important for generating cellular immunity and antibodies. How nerves affect immune functions particularly in secondary lymphoid organs are still unclear. A study in rhesus macaques showed that social stress causes sympathetic hyper-innervation of LNs via NGF signaling and further interferes with the type I interferon response [310]. Chemical ablation of sympathetic nerves compromises primary antibody responses, and is particularly effective in C3H and BALB/c mice [177]. This evidence points toward local sympathetic innervation of LNs inhibiting inflammation. However, sympathetic tone can also be associated with inflammatory diseases. In arthritis, LN-associated adipose tissues were found to have greater sympathetic innervation which promotes lipolysis via stimulating  $\beta$ 3-adrenoreceptor on adipocytes, [311], suggesting indirect effects on LN via metabolically controlling surrounding fat.

The humoral immune response in capsaicin-pretreated rats is compromised but can be restored by subcutaneous SP infusion [312]. Moreover, contact hypersensitivity is dampened when the skin or its draining LN is locally blocked of SP but not CGRP signaling

[313]. These examples indicate the importance of neural substances in secondary lymphoid organs. However, the concrete functional connection between these secondary lymphoid organs and associated nerves are still unknown.

## **1.9 Objectives**

Ample examples from patients or animal studies show that immune functions can be affected by neural perturbations including injury responses, hyper-activation of nerves or loss of functional neural substances. These cases have highly various profiles due to tissue diversity and models used. A lymph node exhibits only local immune surveillance but as a secondary lymphoid organ capable of forming adaptive immunity it can have global and long-term immune effects. This relies on sophisticated vascular networks and organized nodal structure. However, immune regulatory effects of lymph node-associated nerves on adaptive immunity has yet to be explored even though lymph nodes are innervated and some hints showing neural substances might modulate adaptive immunity via affecting secondary lymphoid organs. This project is designed to study lymph node and the local immunity of its drainage area in the context of losing local neural tones. The results shed light on the mechanistic details of neural immune interactions and provide insights into the management of potential undesired immune responses in patients suffering from neural injuries.

### **1.10 Model used**

To investigate whether peripheral neural inputs affect physiology of LNs and their drainage area, an *in vivo* system with clear lymphatic drainage and an uncomplicated innervation pattern is desired. The mouse hind limb at hip level has a relative simple neural structure, which mainly consists of the sciatic and femoral nerves. This renders manipulation of neural tones locally in the hind limb surgically feasible. The popliteal lymph node (popLN), located in the popliteal fossa behind the knee, drains the lower leg and paw [314], and is innervated by the sciatic nerve [198]. With the advantage of accessibility, simplicity and defined drainage area, the mouse hind limb was selected to be an ideal

model to study the dialog between the immune and nervous systems (**Figure 1.5**). By cutting the sciatic and femoral nerves unilaterally, neural tones can be removed from one leg, but remain in the other. This enables paired comparisons between the denervated and innervated legs in the same animal.

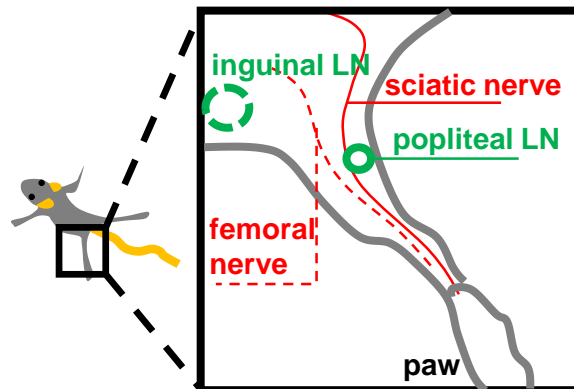


**Figure 1.5 Anatomy of the model investigated**

Mouse hind limb was selected as the working model due to being innervated by two main nerves and possessing one distal LN. The femoral nerve runs on the ventral side and the sciatic nerve ramifies to the dorsal and lateral sides. Popliteal LNs drain the paw area and are innervated by sciatic nerves [198, 314]. Clear drainage and innervation provide advantages for studying the interactions between the nervous and immune systems.

The mouse sciatic nerve divides above the popliteal fossa into three branches in order of descending size, the common peroneal nerve (CPN), the tibial nerve (TN) and the sural nerve (SN) (**Figure 1.6**). To understand the relationship between LN enlargement, paw swelling and degree of denervation, systematic cutting of sciatic nervous branches can be performed and the paw thickness and cellularity of popLNs can be assessed.

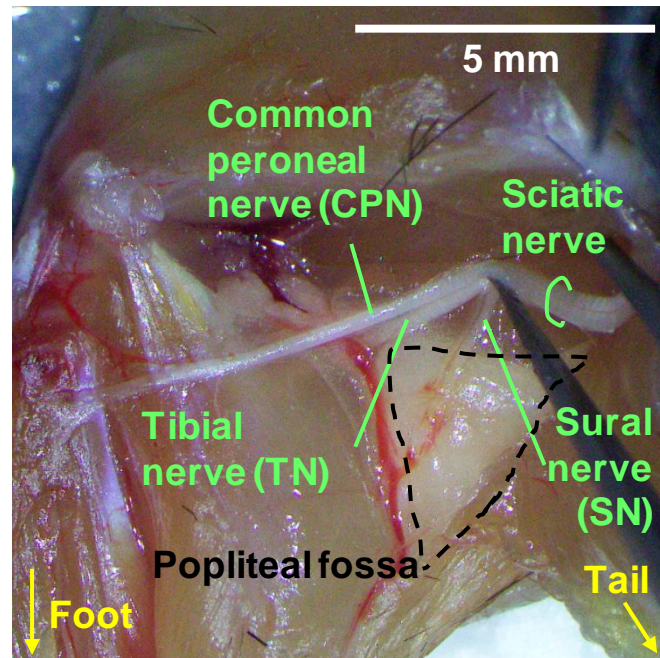


**Figure 1.6 Three branches of the sciatic nerve**

In this dorsal view of the mouse leg, the sciatic nerve diverges into, from thickest to thinnest, the common peroneal nerve, the tibial nerve and the sural nerve. They divide above the popliteal fossa and innervate different parts of the leg.

## **2 Material and methods**

### **2.1 Mice**

8-12 week-old male wild-type C57BL6/N mice were purchased from Charles River for denervation experiments. 9-20 week-old OT-II (Thy1.1) mice were kindly provided by Dr. Susanne Stutte, LMU Munich. Mice were housed under a 12 hours light:12 hours dark illumination cycle with unlimited access to food and water. Cervical dislocation under isoflurane was applied at indicated end points for animal euthanized. All experimental procedures have been approved by the Regierung of Oberbayern in accordance with German legislation.

### **2.2 Surgeries**

All surgical procedures were performed as recovery surgeries using a stereo microscope (SZX7, Olympus). All denervation surgeries were done unilaterally to enable comparison with the contralateral, intact, side in the same animal. In all sham surgeries, the target structure was exposed but not cut. Afferent lymphatic disconnection was done bilaterally serving as a manipulation on lymphatic input in combination with unilateral sciatic denervation.

Mice were anesthetized by intraperitoneal (ip) injection of ketamine (100 mg/kg, Medistar) and Xylazine (20 mg/kg, Rompun, Bayer vital GmbH). Prior to surgical procedures, mice were regionally shaved at indicated sites using the veterinarian clipper (Aesculap, GT415, BRAUN) and depilation cream (Haarentfernungs-Crème, Veet). Hair removal and incision site of each surgery was described individually below. It was performed on a heat pad to reduce heat loss under anesthesia, and cleaning the incision area with ethanol.

After surgical procedures, surgical wounds were running sutured with sterile vicryl-coated 6-0 suture (V991H Ethicon, Johnson & Johnson Medical Ltd). From the surgical day (D0), mice received buprenorphine (0.1 mg/kg, Temgesic, Indivior UK Limited) analgesic subcutaneously (sc) twice a day for 4 consecutive days.

## 2.2.1 Sciatic denervation

For sciatic denervation and transplantation, hairs on the dorsal (lateral) side of the thighs were shaved along the line of the femur. After opening the skin on the dorsal side along the femur (about 1 cm incision) (**Figure 2.1A**), connective tissues between the biceps femoris muscle (BF) and the quadriceps femoris muscle (QF) in the thigh were carefully torn to expose the sciatic nerve. The sciatic nerve was then cut twice, 3 mm apart, and the section between incisions removed to leave a clear gap close to hip level (**Figure 2.1B**). After the surgery, the wound was closed using the absorbable suture (Ethicon, 6-0, V991H) stated before. The popliteal lymph node (popLN) and/or paw skin were harvested at indicated times for examination.

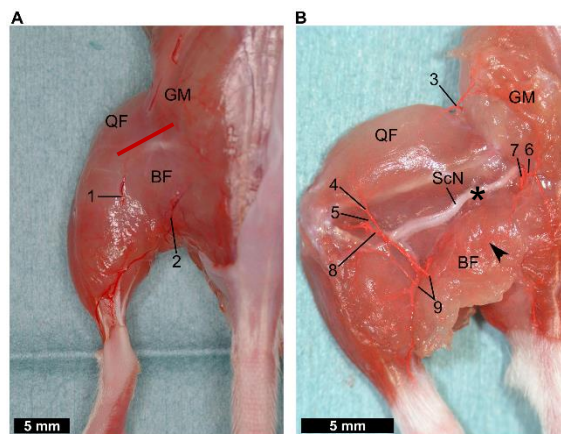


**Figure 2.1 Anatomy of dorsal side of thigh – muscles, vessels and the sciatic nerve**

(A) After removal of the skin. (B) Distal and cranial ends of the biceps femoris muscle are divided. The vascular network in the biceps femoris muscle can be seen in A and B (arrowheads). (1) lateral saphenous vein, (2) ischial vein, (3) iliacofemoral artery, (4) lateral proximal genicular artery, (5) popliteal artery, (6) cranial gluteal artery, (7) caudal gluteal artery, (8) distal caudal femoral artery, (9) branches to distal part of the biceps femoris muscle, (10) terminal branches of the deep femoral artery, (BF) biceps femoris muscle, (GM) gluteal muscles, (MH) medial hamstring muscles, (QF) quadriceps femoris muscle, (ScN) sciatic nerve. Modified from Kochi et al. PLoS ONE 2013 [315].

Red line in (A): the site of incision on the skin. The sciatic nerve was seen after separating the junction between BF and QF. (B) 3 mm resection was made close to hip level (asterisk) to disconnect the distal end of the nerve.

### **2.2.2 Femoral denervation**

The femoral nerve is superficial and runs along the femoral artery and vein. For femoral denervation, skin on the ventral (inward) side of the thighs was depilated. The vessels and the femoral nerve were seen after 1 cm incision of the skin along the vessel bundle seen through skin and the nerve was carefully separated from the vessel bundle of femoral artery and vein, and cut to leave a 3 mm gap in the nerve fiber. After the surgery, the wound was closed using the absorbable suture (Ethicon, 6-0, V991H) stated before. 7 days later, the popLN was analyzed.

### **2.2.3 Ankle denervation**

For ankle denervation, skin surrounding the ankle area was depilated. Three major branches of the sciatic nerve enter the paw from posterior and bilateral sides of the ankle. Incision of the skin was made slightly higher than the joint, and these branches were resected for 2 mm individually. Surface tissues on both lateral sides were disrupted to access the nerves. After the surgery, the wound was closed using the absorbable suture (Ethicon, 6-0, V991H) stated before. 7 days later, the popliteal LN and paw skin were analyzed.

### **2.2.4 Autologous transplantation of the sciatic nerve**

For autologous sciatic transplantation, hair on the dorsal (lateral) side of the thighs was removed along the line of the femur. After sciatic denervation (**2.2.1**), the excised piece of the sciatic nerve was transplanted into the space between the BF and QF of the contralateral leg (receiving sham surgery). After the surgery, the wound was closed using the absorbable suture (Ethicon, 6-0, V991H) stated before. 7 days later, the popLN and paw skin were analyzed.

### **2.2.5 Afferent lymphatic disconnection**

For afferent lymphatic disconnection, skin above the popliteal fossa was depilated. Afferent lymphatics reaching the popLN can be cut and heat-sealed as described [316]. Briefly, popLNs were carefully disconnected from surrounding tissues except the hilar region to leave blood connection and the efferent lymphatic(s) intact. An electrocauter (GEM-5917, BiosebLab) was then used to coagulate the surface of surrounding tissues to prevent them from re-connecting. Afterwards, the popLN was pulled slightly out and secured by tying to surrounding connective tissue. To do this, a small loop of fine suture thread (T04A10Q07-13, AROSurgical) was made to lasso the popLN from the remaining blood vessel connections. After the surgery, the wound was closed using the absorbable suture (Ethicon, 6-0, V991H) stated before. The popLN was examined after 7 days.

On the day of popLN analysis, the connection of the popLN to afferent lymphatics needed to be examined right before taking out the popLN. To confirm if afferent lymphatics remained disconnected from the popLN, 1% Evans Blue (E2129, Sigma-Aldrich Chemie GmbH) in saline was injected intraplantarly (ipl) to mice under anesthesia (by ketamine and xylazine, see 2.2). Mice were placed on a 37°C heating pad and remained anaesthetized for 20 minutes to allow the dye to be transported to the lymph nodes through afferent lymphatics. The mice were then killed via cervical dislocation and the popLNs visualized to check lymphatic integrity. PopLNs turning blue could be witnessed if the surgery was not successful or re-connection took place. PopLNs receiving lymph-borne dye were excluded from experiments.

### **2.2.6 Superior cervical ganglionectomy**

For superior cervical ganglionectomy (SCGx), skin on the ventral neck area was depilated. A standardized method of superior cervical ganglionectomy in rats has been clearly shown [317]. Briefly, ventral incision of skin from the anterior tip of the sternum to the chin was made to expose two mandibular glands. They were separated by gently tearing the connective tissues in the middle and pulled apart. After separation of connective tissues at the trigeminal point of the sternohyoid muscles (SHM), the sternomastoid muscles (SMM) and the omohyoid muscles (OHM), the carotid bifurcation of the internal and

external carotid arteries (ICA and ECA) was exposed (**Figure 2.2**). The superior cervical ganglion (SCG) is located beneath this bifurcation from the ventral view. The bifurcation was flipped outwards to the side to expose the SCG and then the ganglion was carefully removed by dissection with forceps. After the surgery, the wound was closed using the absorbable suture (Ethicon, 6-0, V991H) stated before. The popLN was analyzed after 7 days.

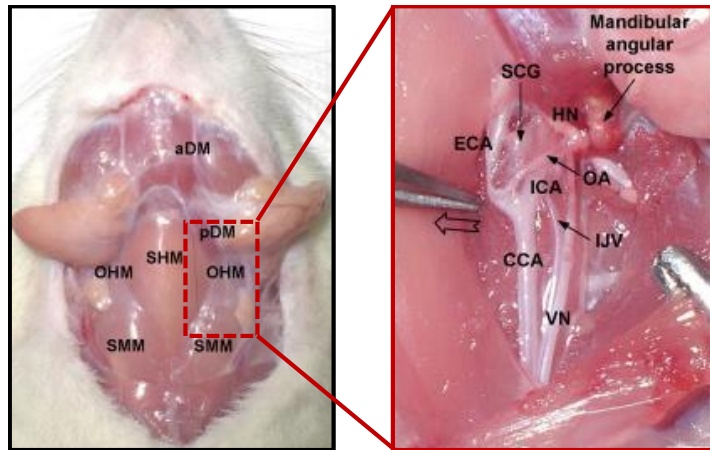


**Figure 2.2 Ventral neck anatomy – muscles, vessels and nerves**

The carotid bifurcation and the SCG were found beneath the trigeminal point of the SHM, SMM and OHM. (aDM/pDM) the anterior/posterior belly of the digastric muscles; (CCA) the common carotid artery; (VN) the vagus nerve; (IJV) the internal jugular vein; (OA) the occipital artery; (HN) the hypoglossal nerve. Modified from Savastano et al. J Neurosci Method 2010 [317].

## 2.3 Histology – H&E staining

All steps were carried out at room temperature. Paw samples were harvested by cutting at the ankles and fixing the entire foot in 4% paraformaldehyde (PFA, 12777847 Affymetrix) for 2 hours. Afterwards, paws were immersed in 0.5 M neutral Ethylenediaminetetraacetic acid (EDTA, 20301 VWR Chemicals) solution (pH = 7) and incubated at room temperature with gentle agitation for 10 days for decalcification. Decalcified samples were then placed in Cryomolds (4557, Tissue-Tek®, Sakura) with OCT™ compound (4583, Tissue-Tek®, Sakura) followed by snap-freezing on dry ice.

These samples were cut using a cryostat (CM3050 S, Leica) into coronal sections 20 microns thick. Before staining, sections were treated with ice-cold acetone for 10 minutes, air-dried and rehydrated by adding phosphate-buffered saline (PBS) to samples for 10 minutes. Samples were then bathed in Harris hematoxylin solution (HHS32, Sigma-Aldrich Chemie GmbH) for 7 minutes. Before eosin staining, hematoxylin-stained samples were rinsed under running water for 15 minutes. Samples were then placed in 0.1% acidified eosin solution (0.1 g eosin Y (230251, Sigma-Aldrich Chemie GmbH) and 15  $\mu$ L glacial acetic acid (537020, Sigma-Aldrich Chemie GmbH) in 100 mL water) for 3 minutes. Afterwards, samples were washed under running water for 20 minutes, and then quickly dipped into absolute ethanol (A3678, Pan Reac AppliChem ITW Reagents) and then into xylenes (108633, Merck Chemicals GmbH). Finally, samples were air-dried and imaged under a Leica DM2500 bright field upright microscope (Zernike, Bioimaging core facility, Biomedical center, Ludwig-Maximilians-Universität München).

## **2.4 Flow cytometry**

To quantify and identify cell subsets, primary cells were isolated from fresh tissues. Samples were processed differently to obtain single cell suspensions for identity marker labeling by fluorescence-conjugated antibodies. Total cell number was assessed using a Coulter counter (Z2 Analyzer, Beckman Coulter). Cell identities were read by flow cytometry (Gallios, Beckman Coulter, see **Appendix 6.1** for its configuration) and the data were analyzed using FlowJo software (FlowJo LLC, Becton Dickinson). Based on different tissue nature and cell types of interest, different tissue handlings and staining panels are described below individually.

### **2.4.1 Tissue processing**

To optimize staining, this step aimed to remove red blood cells and release structurally bound populations to obtain high quality single cell suspensions.

#### 2.4.1.1 *Lymph nodes*

To include identification of dendritic cells (DCs) and macrophages, lymph nodes (LNs) were chopped with scissors in calcium and magnesium extra-supplied Dulbecco's PBS (DPBS) (14040-083, Gibco) with DNase I (200 µg/mL, 11284932001 Roche) and collagenase IV (1 mg/mL, C5138, Sigma-Aldrich Chemie GmbH). Digestion units were slowly rotated and incubated in 37°C for 30 minutes. Afterwards, the digested sample was gently ground against a 70-micron cell strainer (22362648, Fisher Scientific) and rinsed with cold PEB (2 mM EDTA and 2% fetal bovine serum (FBS, 10500-064 Gibco) in PBS). After centrifugation (300 g, 4 °C, 5 minutes), the single cell suspension was obtained by re-suspending cells in the desired volume which was then proceeded to staining in 100 µL PEB with mixed antibodies.

For certain panels (**2.4.2.3**), the chopping and digestion steps were skipped in order to avoid loss of collagenase-sensitive surface markers such as cluster of differentiation 138 (CD138). Harvested samples were instead placed in PEB and ground against 70-micron cell strainers directly for single cell suspensions and then stained as described in the previous paragraph.

#### 2.4.1.2 *Paws*

Paws were separated from legs by cutting at ankles. Toes were then cut, leaving only the footpads. Soft tissues and skin were separated from bones in the footpads by scraping them against the bone using a scalpel. After weighing, soft tissues and skin were then chopped and digested in calcium and magnesium-added DPBS with DNase I (40 µg/mL), collagenase IV (1 mg/mL) and dispase II (2 U/mL, 17105-041, Gibco) with slow agitation at 37°C for 1 hour. Single cell suspensions were obtained after grinding digested samples against 70-micron cell strainers and washed with cold PEB.

#### 2.4.1.3 *Lymph node stromal cells*

LNs were chopped and then digested in calcium and magnesium-added DPBS with DNase I (40 µg/mL), collagenase IV (1 mg/mL) and collagenase D (3.5 mg/mL,

11088858001, Roche) with slow agitation at 37°C for 1 hour. Samples were then allowed to settle vertically for 3 minutes, and the supernatant carefully removed by pipette to leave the cell pellet. Fresh enzyme mix was then added to the remaining pellets which were mechanically disaggregated by pipetting. The enzymatic reaction was terminated by pipetting 7.5  $\mu$ L 0.5 M EDTA (AM9261, Invitrogen) to every milliliter to reach the final EDTA concentration of 3.75 mM, followed by flushing samples with PEB through 70-micron cell strainers to obtain a single cell suspension.

#### *2.4.1.4 Spleen*

Spleens were ground directly against 70-micron cell strainers without digestion. After cell pellets were obtained by centrifugation, red blood cells (RBCs) were eliminated by re-suspending samples in RBC lysis buffer (0.154 M  $\text{NH}_4\text{Cl}$ , 0.05 mM EDTA, 10 mM  $\text{KHCO}_3$ , pH 7.25) at room temperature for 5 minutes. This reaction was stopped by adding an equal amount of PBS. Single cell suspensions of the remaining splenic cells were ready for staining following centrifugation and re-suspension in PBS.

#### *2.4.1.5 Femoral bone marrow*

Crude femoral bone marrow was flushed out and disaggregated by pipetting. Samples were centrifuged and re-suspended in RBC lysis buffer at room temperature for 5 minutes. RBC lysis was then stopped by adding PBS. After another centrifugation, cell pellets were re-suspended for single cell suspension.

#### *2.4.1.6 Blood*

Approximately 400  $\mu$ L of blood was harvested from the retro-orbital sinus into a collection tube with 5  $\mu$ L 0.5 M EDTA using microhematocrit tubes (749311, Brand GmbH + CO KG). The concentration of white blood cells was quantified using a ProCyte Dx™ (IDEXX Laboratories). The rest of the blood sample was then subjected to RBC lysis twice, neutralization and re-suspension for single cell suspension allowing further staining.

## 2.4.2 Staining panels

Single cell suspensions were stained by different antibody combinations for distinct purposes described individually below. All antibodies were recognizing mouse antigens, purchased from Biolegend and used at a dilution of 1:200 in PEB unless otherwise specified (**Appendix 6.2**). After the staining process, samples were re-suspended in 100  $\mu$ L PEB following washing and centrifugation. Right before reading by the flow cytometer, 50  $\mu$ L of 3  $\mu$ M 4',6-diamidino-2-phenylindole (DAPI, 422801, Biolegend) was spiked into samples.

### 2.4.2.1 General profiling of immune subsets in the LN

Anti-CD8-PE (53-6.7), anti-CD3-PE/Dazzle™ 594 (17A2), anti-Gr-1-PerCP/Cy5.5 (RB6-8C5), anti-B220-PE/Cy7 (RA3-6B2), anti-CD169-Alexa 647 (3D6.112), anti-NK1.1-Alexa 700 (PK136, 56-5941-82, eBioscience), anti-CD11c-APC/Cy7 (N418) and anti-CD4-BV570 (RM4-5) antibodies were mixed well with single cell suspensions of samples and incubated at 4°C for 30 minutes.

### 2.4.2.2 Dendritic cell subsets in the LN

Samples were blocked with anti-CD16/CD32 (93, 1:50) antibodies at 4°C for 20 minutes before proceeding to staining. Anti-Gr-1-FITC (RB6-8C5, 1:400), anti-CD11b-PE (M1/70, 1:400), anti-CD45-PE/Dazzle™ 594 (17A2), anti-major histocompatibility complex class II (MHCII, I-A/I-E, 1:1000)-PE/Cy5 (M5/114.15.2), anti-CD8-PE/Cy7 (53-6.7, 1:400), anti-CD4-APC (GK1.5, 1:400) and anti-CD11c-APC/Cy7 (N418) antibodies were mixed well with single cell suspensions of samples at 4°C for 30 minutes.

#### *2.4.2.3 Digestion-sensitive B cell differentiation markers on splenic and LN cells*

Anti-Gr-1-FITC (RB6-8C5, 1:400), anti-CD138-PE (281-2), anti-FAS-PE-CF594 (Jo2, 562499, BD Bioscience), anti-B220-PE/Cy7 (RA3-6B2) and anti-GL7-Alexa 647 (GL7) antibodies were mixed well with single cell suspensions of samples at 4°C for 30 minutes.

#### *2.4.2.4 Immune subsets in paws*

Samples were blocked with anti-CD16/CD32 (93, 1:50) antibodies at 4°C for 20 minutes before proceeding to staining. Anti-CD103-FITC (2E7), anti-Ly6C-PE (HK1.4), anti-CD45-PE/Dazzle™ 594 (30-F11), anti-Ly6G-PerCP/Cy5.5 (1A8), anti-MHCII-PE/Cy7 (M5/114.15.2), anti-epithelial cell adhesion molecule (EpCAM)-Alexa 647 (G8.8), anti-CD11b-Alexa 700 (M1/70) and anti-CD11c-APC/Cy7 (N418) antibodies were mixed well with single cell suspensions of samples at 4°C for 30 minutes.

#### *2.4.2.5 Stromal cells in the LN*

Anti-CD45-FITC (30-F11), anti-podoplanin-PE (8.1.1.), and anti-CD31-APC (MEC13.3) antibodies were mixed well with single cell suspensions of samples at 4°C for 30 minutes.

#### *2.4.2.6 Verification of cell depletion efficacy*

To verify successful depletion of neutrophils, blood and spleen were examined. Gr-1-PerCP/Cy5.5 (at 4°C for 30 minutes) staining was used in combination with forward and side scatter profiles to determine depletion efficacy.

To verify successful depletion of natural killer (NK) cells, circulating cells were stained with anti-CD49b-PE/Cy7 (DX5) at 4°C for 30 minutes.

## **2.5 Cell type-specific depletion**

Cell type identity markers were targeted to remove certain cell types specifically using neutralizing antibodies. These were injected ip to target cells systemically.

### **2.5.1 Neutrophil**

To deplete neutrophils, each mouse was injected with 200 µg of either isotype control antibody (LTF-2, BE0090, BioXCell) or anti-Ly6G antibody (1A8, BE0075, BioXCell) at D0 and D4. When organs were harvested at D7, spleen and blood were taken to verify the depletion efficacy (see **2.4.2.6**). Leukocytes in popLNs were analyzed by flow cytometry at D7.

### **2.5.2 Natural killer cell**

To eliminate NK cells, each mouse was injected with 200 µg either isotype control antibody (C1.18.4, BE0085, BioXCell) or anti-NK1.1 antibody (PK136, BE0036, BioXCell) at D-1 and D4. When organs were harvested at D7, blood was taken to verify the depletion efficacy (see **2.4.2.6**). Leukocytes in popLNs were analyzed by flow cytometry at D7.

## **2.6 Recruitment rate and dwell time**

Labeled exogenous cells were used to monitor migratory behaviors of leukocytes in a unilaterally denervated system. Splenic and LN single cell suspensions were obtained via pushing them against 70-micron cell strainers without digestion. Splenic and LN cells were mixed in the ratio of 50:50 and incubated with 1.5 µM carboxyfluorescein succinimidyl ester (**CFSE, 65-0850-84, Thermo Fisher Scientific**) in PBS at 37°C for 20 minutes. Afterwards, labeled cells were washed 3 times with 37°C PEB. On D7 post-surgery, each mouse received  $2 \times 10^7$  donor cells via iv injection. Remaining donor cells were subjected to cell identity staining (**2.4.2.1**) and flow cytometry to examine the labeling efficacy and donor composition.

### **2.6.1 Homing**

2 hours after labeled donor cells were transferred to unilaterally denervated mice, their popLNs were harvested and processed. Cells were analyzed by flow cytometry.

## **2.6.2 Egress**

Denervated mice were divided into 2 groups, with both groups receiving donor cells. 2 hours later one group was killed and immune subsets in popLNs were quantified and served as the basal level. Meanwhile, the other group received homing blockers (anti-integrin  $\alpha 4$  and anti-integrin  $\alpha L$ , 100  $\mu$ g each/mouse, PS/2 and M17/4, BE0071 and BE0006, BioXCell) and kept for another 12 hours. Afterwards, their immune subsets in popLNs were quantified by flow cytometry and compared with the other group's (basal level) to obtain the egress rate.

## **2.7 Treatment of drug or antibody**

In unilateral sciatic denervated (Sx) mice, leukocyte adhesion to the vascular bed, chemotaxis, and antigen presentation were inhibited using neutralizing antibodies or a bacterial toxin. Leukocytes in popLNs were analyzed by flow-cytometry at D7.

To target neural substances, neurotoxin or neural substance receptor antagonists were administered.

### **2.7.1 Anti-histamine treatment**

Cetirizine dihydrochloride (20 mg/kg, 2577 Tocris Bioscience) was administered daily from the surgery day (D0) to the harvest day (D7). The compound was dissolved in PBS and injected ip except at D0 when it was injected sc. Immediately before the surgery, one dose was divided equally into 4 portions which were injected to hocks and surgery sites in both legs. Leukocytes in popLNs were analyzed by flow cytometry at D7.

## **2.7.2 Homing blockade**

Mice undergoing denervation surgery were treated with different antibodies against different adhesion molecules. All blockades were conducted by ip injection at D1 and D4. All antibodies used here were diluted in PBS to the working concentration.

### **2.7.2.1 Integrins**

Either combined anti-integrin  $\alpha4/\alphaL$  (100  $\mu\text{g}$  each/mouse, PS/2 and M17/4, BE0071 and BE0006, BioXCell) antibodies or their isotype control antibodies (100  $\mu\text{g}$  each/mouse, LTF-2 and 2A3, BE0090 and BE0089, BioXCell) was injected. Antibodies were diluted in PBS to the working concentration.

### **2.7.2.2 CD62L**

Either anti-CD62L antibody (200  $\mu\text{g}$ /mouse, Mel-14, BE0021, BioXCell) or its isotype control antibody (200  $\mu\text{g}$ /mouse, 2A3, BE0089, BioXCell) was injected.

### **2.7.2.3 *Peripheral node addressin***

To target Peripheral node addressin (PNAd) on high endothelial venules (HEVs), either anti-PNAd antibody (200  $\mu\text{g}$ /mouse, MECA-79, 120802, Biolegend) or its isotype control antibody (200  $\mu\text{g}$ /mouse, RTK2118, 400802, Biolegend) was injected.

## **2.7.3 Pertussis toxin treatment**

Pertussis toxin (PTX, 1  $\mu\text{g}$ /mouse, 516560, Merck) was dissolved in PBS and injected ip to the denervated mice at D0 and D4. The control group received only PBS.

#### **2.7.4 Antigen presentation blockade**

Either anti-MHCII antibody (500 µg/mouse, Y3P, BE0178, BioXCell) or its isotype control antibody (500 µg/mouse, C1.18.4, BE0085, BioXCell) was injected ip at D0 and D4. The antibody was diluted in PBS to the working concentration.

#### **2.7.5 6-hydroxydopamine treatment**

To ablate sympathetic tones in the periphery, a chemical method using 6-hydroxydopamine (6-OHDA) has been described [318]. Mice were treated ip with 6-OHDA 100 mg/kg (with ascorbate 20 mg/mL in saline) on D0, 250 mg/kg on D2. Chemically sympathectomized mice were ready to be analyzed from D5.

#### **2.7.6 Treatment of neuropeptides or antagonist of neuropeptides**

Calcitonin gene-related peptide (CGRP, 1 µg/mouse/day, 1161, Tocris) and substance P (SP, 250 µg/kg/day, 1156, Tocris) were dissolved in PBS and injected ip separately or together to mice. For antagonism of CGRP and SP, their antagonists BIBN4096 (4561, Tocris) and SR140333 (4012, Tocris) were dissolved in dimethyl sulfoxide (DMSO, D8418, Sigma-Aldrich Chemie GmbH) in 25 mg/mL and 50 mg/mL respectively as stocks and stored at -20°C. Working solutions were prepared by diluting the stocks in PBS. BIBN4096 and SR140333 were treated separately or together at 1 mg/kg/day per compound. The treatment was given daily by ip injection. When treatment was applied on the surgery or harvest day, it was delivered 4 hours before the operation on D0 and 2 hours before harvesting on the last day to fully cover the experimental period.

### **2.8 Quantitative polymerase chain reaction**

LN or paw samples were immersed in 200 µL QIAzol lysis reagent (79306, QIAGEN) in innuSPEED Lysis Tubes (845-CS-1020050, AJ Innuscreen GmbH) and homogenized using SpeedMill PLUS (Analytik Jena AG). Ribonucleic acid (RNA) was separated from

deoxyribonucleic acid (DNA) and protein by mixing QIAzol lysate with 40  $\mu$ L chloroform (C2432, Sigma-Aldrich Chemie GmbH). RNA from the aqueous layer was then precipitated in isopropanol (A3928, Reac AppliChem ITW Reagents), washed with 75% ethanol and dissolved in water. Potential residual DNA in the extract was digested by recombinant DNase I (04716728001, Roche) and the remaining RNA was later further purified using RNeasy MiniElute Cleanup Kit (74204, QIAGEN). Conversion of RNA to complimentary DNA (cDNA) was carried out using High-Capacity RNA-to-cDNA™ Kit (4387406, Applied Biosystems™). Reverse transcription program: 25°C 10 minutes, 37°C 2 hours, 85°C 5 minutes and 4°C hold. 400 ng RNA from each sample was reverse-transcribed in a 20  $\mu$ L reaction. Samples were then diluted with water to make 1 ng RNA/ $\mu$ L working cDNA solution. Rest of cDNA samples has been stored at -20°C, and Rest of RNA samples has been stored at -80°C.

19 mouse genes were quantified by quantitative polymerase chain reaction (qPCR) using these cDNAs and Fast SYBR™ Green Master Mix (4385614, Applied Biosystems™). Reaction solution contained 1  $\mu$ L working cDNA solution from each sample, primers of target genes, water and Fast SYBR™ Green Master Mix. Target genes were: *Rpl32*, *Ccl19*, *Ccl21*, *Cxcl12*, *Cxcl13*, *Tnfa*, *Tgfb*, *Ifng*, *Il1a*, *Il1b*, *Il2*, *Il4*, *Il6*, *Il7*, *Il10*, *Il12*, *Il13*, *Il17a* and *Il17f*. Primer sequences are listed in **Appendix 6.3**. qPCR program: 95°C 10 minutes, 40 cycles of 95°C 15 seconds and 60-62°C 1 minute depending on the primer set (indicated in **Appendix 6.3**). Melting curve was measured using the machine's built-in setting.

Data were analyzed using  $\Delta\Delta$ Ct. Briefly, Ct of target gene minus Ct of *Rpl32* (the reference gene) to obtain  $\Delta$ Ct. Each  $\Delta$ Ct was subtracted by  $\Delta$ Ct of samples from D0 to have  $\Delta\Delta$ Ct. The relative expression was then calculated as  $2^{-\Delta\Delta$ Ct} with the assumption that the amplification of each PCR cycle is 2.

## 2.9 Immunofluorescence

PopLN samples were subjected to whole-mount or section staining and the sciatic nerve was processed as cross-sectioned slices. To prepare on-slide staining of tissue sections,

samples of the sciatic nerve and the popLN were harvested and placed in Cryomolds (4557, Tissue-Tek®, Sakura) with OCT™ compound (4583, Tissue-Tek®, Sakura) followed by snap-freezing on dry ice. The embedded samples were then sliced using Leica CM3050 S. All steps in the staining procedures were done at room temperature except primary antibody staining which was performed at 4°C.

Primary antibodies: rabbit anti-mouse tyrosine hydroxylase (TH, 1:1000, polyclonal, AB152, Merck Millipore), rat anti-mouse CD31-Alexa 647 (1:100, MEC13.3, 102516, Biolegend), rat anti-mouse CD4-APC (1:100, GK1.5, 100412, Biolegend), rat anti-mouse CD8-Alexa 647 (1:100, 53-6.7, 100724, Biolegend), rat anti-mouse B220-Alexa 488 (1:100, RA3-6B2, 103225, Biolegend), rat anti-mouse Ki67-PE (1:100, SolA15, 12-5698-92, eBioscience), rat anti-mouse GL7-Alexa 647 (1:100, GL7, 144606, Biolegend), rabbit anti-mouse calcitonin gene-related peptide (CGRP, 1:1000, 24112, Immunostar), rabbit anti-mouse substance P (SP, 1:1000, 20064, Immunostar), mouse anti-mouse beta 3 tubulin ( $\beta$ 3-tubulin)-Alexa 488 (1:200, 2G10-TB3, 54-451082, eBioscience), chicken anti-mouse neurofilament (NF)-H (1:200, AB5539, Merck Millipore) and chicken anti-mouse NF-M (1:200, AB5735, Merck Millipore) were used as primary antibodies.

Secondary antibodies and streptavidin-conjugated fluorochrome: goat anti-rabbit IgG-biotin (1:500, polyclonal, BP-9100, Vector Laboratories), goat anti-chicken IgY-Alexa 488 (1:500, polyclonal, A-11039, Thermo Fisher Scientific) and streptavidin-Cy3 (1:200, 405215, Biolegend). Details of antibodies are summarized in **Appendix 6.2**.

Images were acquired using SlideBook 6 software (3i, Intelligent Imaging Innovation) coupled with the spinning-disk confocal microscope (built on Zeiss Axio Examiner Z.1, organized by 3i, Intelligent Imaging Innovation). Scans of LN sections and whole mounts were taken with 100x magnification (10x ocular and 10x objective). Cross-sections of sciatic nerves were imaged with 640x magnification (10x ocular and 64x objective). All images were reconstructed using auto-alignment tools of SlideBook 6. Rebuilt volumetric scans were flattened by maximum projection method. Brightness, contrast, colors and overlay of images were adjusted using Fiji software (ImageJ).

### **2.9.1 Whole-mount staining of the popliteal lymph node**

For whole-mount imaging of sympathetic nerves in the popLN, the popLN was harvested and cut in half using a scalpel blade. Samples were placed in 4% PFA for 30 minutes. After this fixation step, samples were immersed in the blocking cocktail containing 20% goat serum (31872, Invitrogen), 0.5% Triton X100 (M143, Amresco) and 20% (v/v) streptavidin solution (SP-2002, Vector Laboratories) in PBS for 2 hours. For primary antibody staining, anti-TH and anti-CD31-Alexa 647 antibodies, 2% goat serum and 20% (v/v) biotin solution (SP-2002, Vector Laboratories) in PBS were applied on samples for staining overnight. The following day, the primary antibody solution was washed off with PBS and replaced with goat anti-rabbit-biotin secondary antibody in PBS with 2% goat serum. Samples were stained with this secondary antibody solution for 2 hours and washed off with PBS prior to incubation with streptavidin-Cy3 in PBS for 30 minutes. All the staining procedure were done in dark.

### **2.9.2 Staining of popliteal lymph node section**

To identify functional processes of cell types in the popLN, 10  $\mu$ m sections were made. Samples were fixed with 4% PFA for 10 minutes and then blocked with 20% goat serum and 0.5% Triton X100 in PBS for 30 minutes. Fluorescence-conjugated primary antibodies recognizing mouse CD4, CD8, B220, Ki67 and GL7 were used in PBS containing 2% goat serum to stain samples overnight.

To map CGRP<sup>+</sup> nerves in the popLN, 20  $\mu$ m popLN sections were generated. Samples were blocked with 20% goat serum, 0.5% Triton X100 and 20% (v/v) streptavidin solution in PBS for 2 hours. For primary antibody staining, antibodies binding to CGRP, CD31 and  $\beta$ 3-tubulin were used in 2% goat serum and 20% (v/v) biotin solution in PBS to stain samples overnight. The following day, the primary antibody mix was replaced with biotinylated goat anti-rabbit secondary antibody in PBS with 2% goat serum. Samples were stained with the secondary antibody for 2 hours and washed off with PBS prior to incubation with streptavidin-Cy3 in PBS for 30 minutes.

### **2.9.3 Staining of the sciatic nerve section**

For imaging the sciatic nerve, 20  $\mu\text{m}$  cross-section slices were made. Samples were fixed with 4% PFA for 10 minutes and then blocked with 20% goat serum, 0.5% Triton X100 and 20% (v/v) streptavidin solution in PBS for 2 hours. Primary antibodies reacting to CD31, CGRP, SP, NF-H, NF-M and TH were used in PBS containing 2% goat serum and 20% (v/v) biotin solution to staining overnight. The following day, primary antibody solution was washed off and secondary antibodies (biotinylated goat anti-rabbit and goat anti-chicken-Alexa 488) in PBS with 2% goat serum were applied for 2 hours and washed off with PBS prior to incubation with streptavidin-Cy3 in PBS for 30 minutes.

## **2.10 Serology**

To obtain serum, blood samples were incubated at room temperature for 30 minutes to coagulate and then spun at 1,500 g. The transparent supernatant (serum) was then collected, aliquoted and diluted before use. Practices followed the manufacturer's instructions for each kit. All the buffers, antibodies and solutions are provided with the kits.

### **2.10.1 Isotyping**

For isotyping, sera were diluted (1:10,000) and applied on the Pierce Rapid ELISA Mouse mAb Isotyping Kit (37503, Invitrogen). Briefly, 50  $\mu\text{L}$  samples were mixed with 50  $\mu\text{L}$  anti-mouse antibodies-horseradish peroxidase (HRP) solution and transferred to pre-coated flat-bottom wells. After 1-hour incubation, sample-antibody solution was discarded and washed off with Tris-buffered saline with 0.05% Tween 20. 75  $\mu\text{L}$  3,3',5,5'-Tetramethylbenzidine (TMB) substrate solution was added and stood in the wells in room temperature for 5 minutes, followed by adding 75  $\mu\text{L}$  stop solution. Absorbance of 450 and 570 (reference wavelength) nm was measured by TECAN plate reader (SPARK 10M, TECAN)

### **2.10.2 Antibody titer determination**

For quantification of total circulating Immunoglobulin G (IgG), Mouse IgG total Ready-SET-Go!<sup>®</sup> (88-50400-86, Invitrogen) was used with diluted sera (1:10,000 or 1:20,000). Briefly, flat-bottom 96-well plates were coated with capture antibody by adding diluted capture antibody (250x) to the plates and incubating at 4°C overnight. Next day, the coating solution was discarded and the plates were washed with PBS with 0.05% Tween 20. 250 µL blocking solution was added to the plates and left for 2 hours at room temperature. The blocking solution was discarded and the plates were washed with PBS with 0.05% Tween 20. Prior to applying standards and samples, the standards were prepared based on 2-fold serial dilution. 200 µL standards or samples as well as 50 µL of detection antibody were added to the plate and incubated in room temperature for 3 hours. Following the wash steps using PBS with 0.05% Tween 20, TMB substrate solution was added and stood in the wells in room temperature for 15 minutes, followed by adding 100 µL stop solution. Absorbance of 450 and 570 (reference wavelength) nm was measured by TECAN plate reader (SPARK 10M, TECAN).

### **2.10.3 Autoantibody test**

Sera were diluted to 10 µg/mL and tested on HEp-2 slides (ORG870, Orgentec) for anti-nuclear antibodies. Samples of 25 µL were added on the pre-coated slides and stood in a moisture chamber at 4°C for 30 minutes. After the incubation, the slides were rinsed and immersed with PBS for 5 minutes. After drying excessive PBS, the detection antibodies were applied on the slides and incubated for 30 minutes. The slides were carefully washed with PBS and dried off, followed by being covered by cover-slides. The slides were imaged using SlideBook 6 software coupled with the spinning-disk confocal microscope and the images were processed with Fiji as described in **2.9**.

## 2.11 Statistics

Data from the same experimental setting were pooled and analyzed as a collective dataset. Data were analyzed using Prism 7 (GraphPad). Outliers of each data set were detected and eliminated using a built-in function of outlier detection in Prism 7 with false discovery rate = 1%. After clearance of outliers, data was presented in mean  $\pm$  standard error.

Data comparison between control and experimental group(s): Paired student's t test was applied to compare effects of individual treatments between sham and denervated popLNs in the same mouse. To compare effects between two groups, unpaired student's t test was used. To compare effects across multiple groups (more than two), for example, different surgeries or antibody titer at different time points, one-way ANOVA and optionally Tukey's post-test was used for further comparison between each two group. Two-way ANOVA was used to analyze the effects of multiple independent variables on outcomes of the surgery. Šídák's or Tukey's post-test was taken depending on the number of subgroups compared within the same variable. The former was used for comparison between two groups, whereas the latter was used to compare between more than two groups. To analyze the correlation between two data sets, Pearson's correlation was used. Correlation coefficient ( $r$ , -1 to 1) presented the strength and direction of correlation. Determination of correlation ( $r^2$ ) was used to examine how well all data points fit the linear regression line of two variables. For example, when  $r^2$  is 0.9, it means 90% of data points can be explained by the linear regression line.

The calculated probability of false rejection of the null hypothesis is presented as  $p$  – the probability of type I error. In a simpler sentence,  $p$  shows the probability of recognizing datasets as different when they are actually the same due to observation of extreme values. When the probability is lower than a common threshold 5% ( $p < 0.05$ ), the difference across datasets is recognized as statistically significant. In this study, as the same threshold was taken, once  $p < 0.05$ , difference between groups was taken as significant. Higher confidence levels of difference were taken when the calculated probability was even lower ( $p < 0.01$ , 0.001 or 0.0001). These levels were used as determinant of significance at different levels.

### 3 Results

#### 3.1 Denervation in the leg leads to acute swelling of the paw and enlargement of popliteal lymph node

In the first experiment, the sciatic and femoral nerves were cut to deprive the lymph node of neural inputs. Cutting the sciatic and femoral nerves led to two major phenotypes – swelling of the popLN itself and of its draining area, the paw (**Figure 3.1**). Paw swelling was an acute and transient phenotype, peaking after a day and returning to baseline within a week (**Figure 3.2A**). Swelling of the lymph node, however, persisted over the whole investigated timeframe of four weeks. Quantification of cellularity in popLNs after denervation clearly showed that the LN phenotype was due to a dramatic increase in cellularity, reaching peak levels after two weeks and remaining high four weeks post-surgery (**Figure 3.2B**). This result implied that loss of neural tones in the leg leads to substantial alterations in lymph node cellularity, potentially due to changes in cell migration, proliferation and/or egress dynamics.

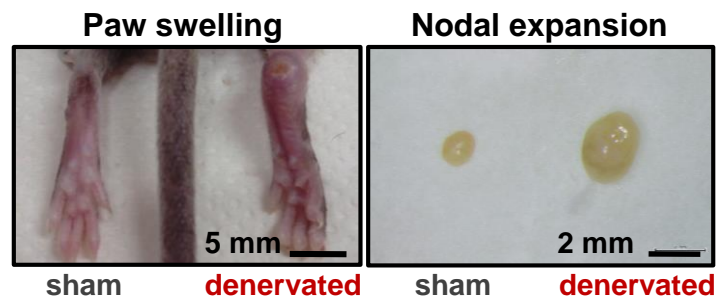


**Figure 3.1 Macroscopic views of main denervation phenotypes**

Denervation led to paw swelling and enlargement of its draining popLN after a week.

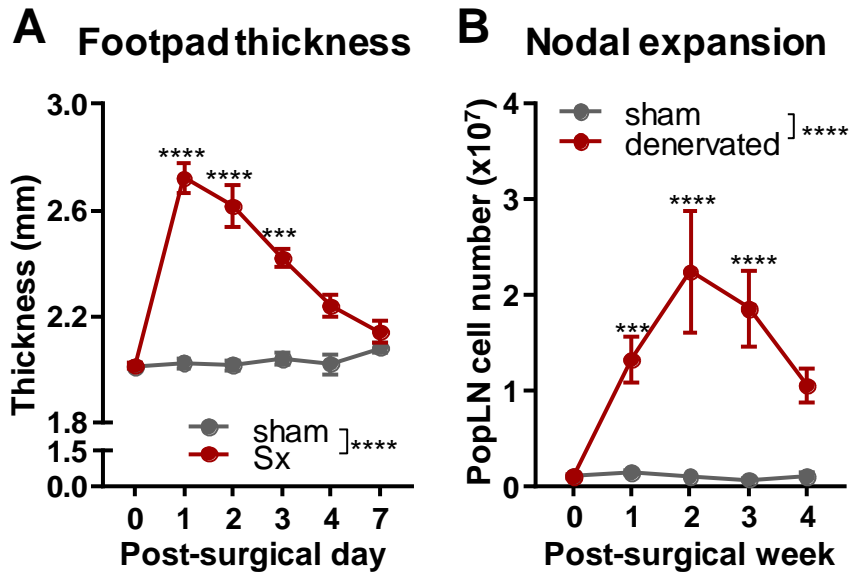


**Figure 3.2 Progression of footpad thickness and lymph node expansion after denervation**

**(A)** Denervation induced a thickened footpad within a day, returning to the basal level within a week.  $n = 5-20$ . Two-way ANOVA, Šídák's post-test. **(B)** Denervation raised popLN cellularity in a week which lasted at least 4 weeks.  $n = 4-7$ . Two-way ANOVA, Šídák's post-test. \*\*\* $p < 0.001$ , \*\*\*\* $p < 0.0001$ .

### 3.2 Sciatic denervation contributes to nodal expansion

Overall deprivation of neural tone by cutting both femoral and sciatic nerves in the leg expanded the popLN. Resection of the sciatic nerve prevents viral dissemination from the popLN, so indicating that the sciatic nerve is the only nerve directly innervating the popLN [198]. In contrast, the femoral nerve does not directly innervate the popLN but rather its draining area, whereas the sciatic nerve projects to both [198]. This feature allowed testing whether loss of direct innervation by the sciatic nerve or indirect innervation via the femoral nerve caused the phenotypes observed. Analysis of popLN cellularity showed that sciatic denervation (Sx) alone produced a LN phenotype equivalent to that of cutting both femoral and sciatic nerves whereas femoral denervation by itself did not (**Figure 3.3**). This indicated that direct innervation was important in regulating the cellular dynamics of popLNs.

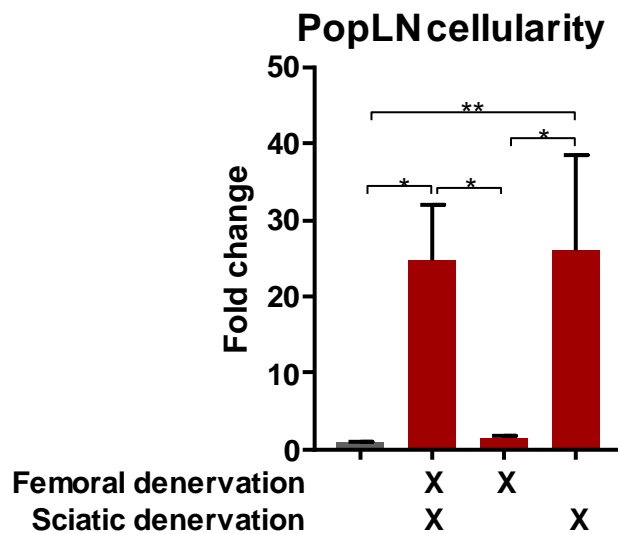


**Figure 3.3 Change of popLN cellularity after cutting femoral and/or sciatic nerve(s)**

Cutting the sciatic nerve alone reproduced the phenotype of cutting both femoral and sciatic nerves. This phenomenon attributed denervation-induced nodal expansion to loss of direct innervation via the sciatic nerve. n = 3-9. One-way ANOVA, Tukey's post-test. \*p < 0.05, \*\*p < 0.01.

### 3.3 Denervated popliteal lymph nodes are more reactive

Denervation-induced nodal expansion could reflect the primary response of losing innervation or a secondary reaction to the paw swelling. To tease apart a direct neural effect on the popLN from indirect, peripheral influences, a denervation model targeting the draining area of the popLN but bypassing the popLN itself was developed to address this point. Unilateral surgical ankle denervation (ANKx) was used to remove neural input to the paw but retain intact innervation of the popLN by cutting the three main branches of the sciatic nerve at ankle level (**Figure 3.4**).

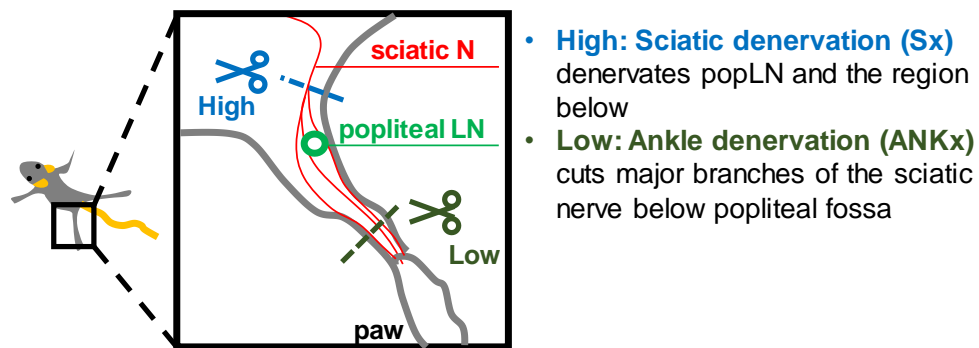


**Figure 3.4 Scheme of sciatic denervation surgeries at different levels**

Two sciatic denervation procedures were designed to study the functions of direct innervation in popLNs by doing one denervation affecting popLN and the other one bypassing it.

With ANKx there could be a concern of cutting lymphatic vessels, which could block the recycling of interstitial fluid and leukocyte homing to the popLN via afferent lymphatics. Evans Blue was therefore injected intraplantarly to test this. Straight after ANKx, Evans Blue solution was injected and was observed reaching the popLN, demonstrating that the surgery did not disrupt lymphatic flow from the paw to the popLNs (**Figure 3.5**).

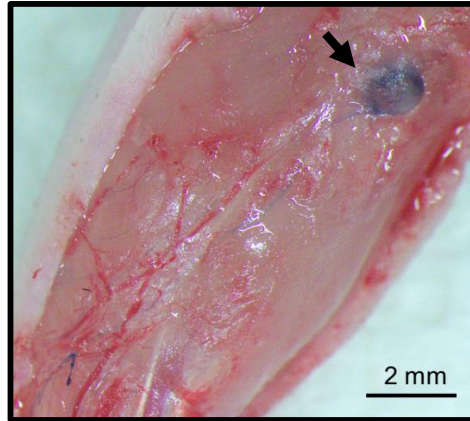


**Figure 3.5 Evaluation of conductivity of afferent lymphatics after ankle denervation**

Right after the surgery, Evans Blue solution was injected intraplantarly into the footpad. The popliteal fossa was exposed surgically 10 minutes after the ankle denervation and the popLN was found taking up the dye (arrow).

The surgical wound was large and proximal to the paw, so ANKx generated some local swelling of paw regardless of whether the mice received nerve resection or a sham surgery. H&E staining revealed increased hair follicle-like structure in the swollen paws on either side (**Figure 3.6**).

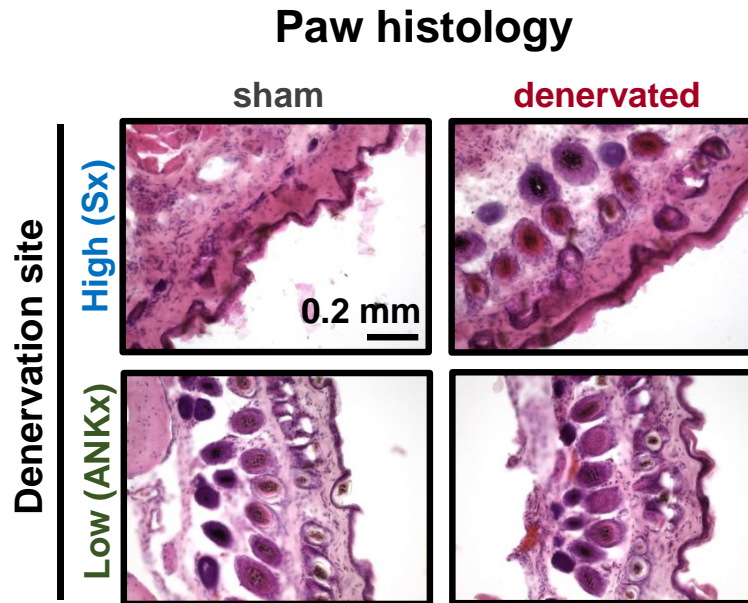


**Figure 3.6 Histology of paw skin tissues**

Paw tissues were harvested, followed by snap freezing in OCT. Sliced specimens went through H&E staining and were imaged under a bright-field microscope.

In comparison to the popLN cellularity on the sham side, ankle operation brought the cellularity to about 2.5-fold to the level reached after Sx surgery, reflecting a higher degree of general surgery-induced inflammation due to ANKx (**Figure 3.7A**). To account for such variation in the sham-operated control groups, cell counts in popLNs on the denervated side were normalized to the sham side within the same surgical group (Sx or ANKx) and plotted as 'fold change'. Although sham ankle operation caused slight nodal expansion even without cutting nerves, cutting sciatic nervous branches at ankle level did not drive the popLN cellularity to a comparable level to the Sx surgery (**Figure 3.7B**). Thus, cutting sciatic nervous branches below popLNs clearly did not cause nodal expansion to the same extent as cutting it above, suggesting a direct regulatory role of the nerve on the popLN. Another possible explanation was that ANKx had a lesser degree of effect on the significantly smaller draining area.

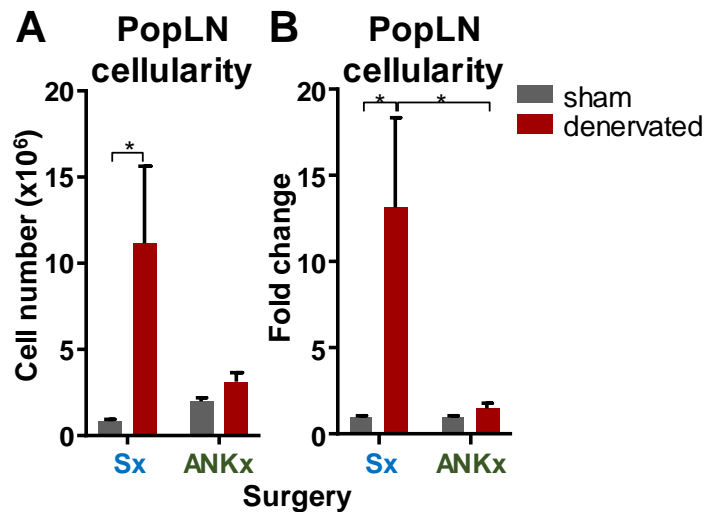


**Figure 3.7 PopLN cellularity one week after sciatic or ankle denervation**

**(A)** PopLN cellularity showed different basal levels in the sham popLN. **(B)** To be able to compare two groups on the same basis, counts were normalized to the counts of sham popLN, and cellularity was presented as fold change. n = 5-6. Two-way ANOVA, Šídák's post-test. \*p < 0.05.

### 3.4 Sciatic denervation induces neutrophil infiltration and increases dendritic cell numbers in the draining area of the popliteal lymph node

Paw pathology after denervation seemed to be an acute event and shared the macroscopic features of edema driven by an increase in interstitial fluid [319]. Indeed, the denervated paws exhibited lower cell numbers per milligram of tissue (**Figure 3.8**), indicating that fluid diluted cell density in the swollen paw. However, this dilution of cellularity was not recovered when paw thickness came back to baseline in a week (**Figure 3.2** and **Figure 3.8**).

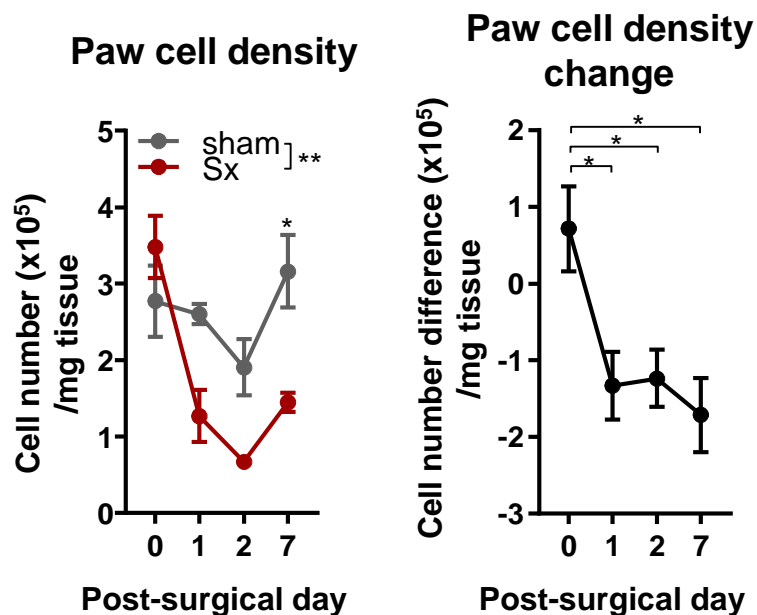


**Figure 3.8 Cell density in the paw after sciatic denervation**

Denervation decreased cell density in the paw, indicating tissue swelling due to fluid uptake.  $n = 5-10$ . Two-way ANOVA, Šídák's post-test for paw cell density and one-way ANOVA, Tukey's post-test for paw cell density change. \* $p < 0.05$ , \*\* $p < 0.01$ .

Leukocytes were found to infiltrate into denervated paw tissue, with neutrophils being the major population (accounting for half of the leukocytes in the first two days after denervation) (**Figure 3.9**). Seven days after Sx, DC populations constituted a quarter of leukocytes, which were mainly EpCAM<sup>-</sup>CD103<sup>-</sup> (double negative, dn) DCs (**Figure 3.9**). Langerhans cells (LCs) were the second largest DCs subset, initially decreasing but recovering by days 2 and 7 (**Figure 3.9**). EpCAM<sup>-</sup>CD103<sup>+</sup> DC were the smallest population, which quickly increased and reached a plateau two days after denervation (**Figure 3.9**). Ly6C<sup>+</sup> monocyte counts also increased from 0.05% to about 0.24% of total cells after denervation (**Figure 3.9**).

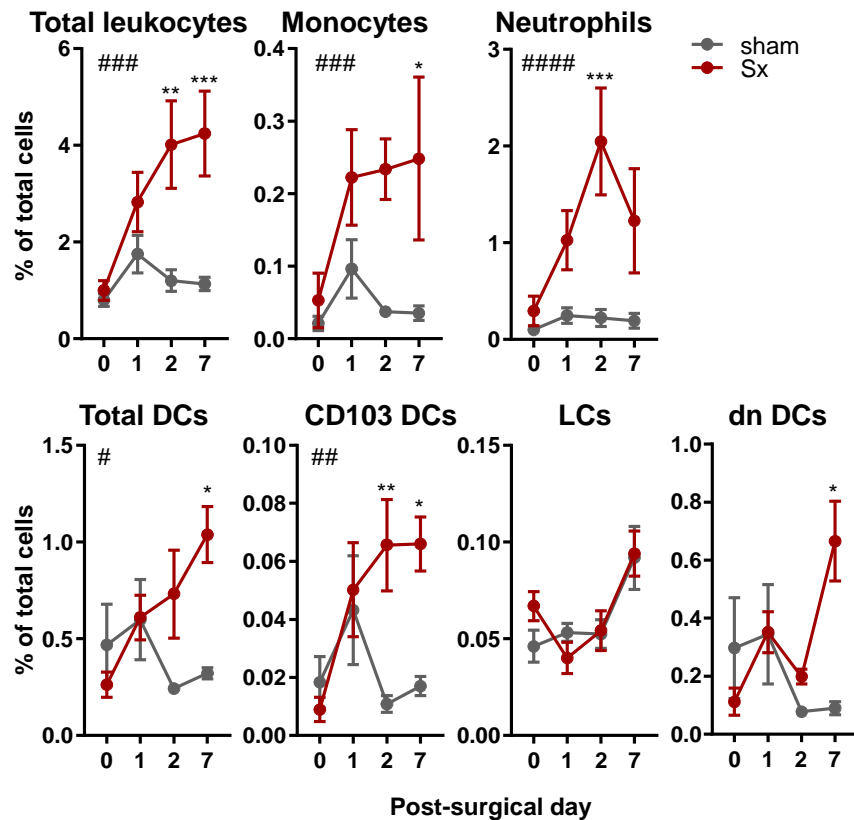


**Figure 3.9 Immune cell subsets in the paw after denervation**

Leukocytes were quantified and sub-divided into monocytes, neutrophils and three DC subsets. Most of them except LCs were found to be increased after denervation. n = 5-10. Two-way ANOVA, Šídák's post-test. \*p < 0.05, \*\*p < 0.01, \*\*\*p < 0.001. #: statistical difference between "sham" and "Sx".

### 3.5 Nodal expansion after denervation partially reflects the size of affected nervous branch and does not associate with degree of paw swelling

To understand the relations between nodal expansion, paw thickening and degree of denervation of the draining area, mice were divided into seven groups whose sciatic nerves received single, dual or complete transection by cutting one, two or all branch(es) respectively. Sizes of denervated branches were used as a proxy of degree of denervation. The three branches in order of descending size were the common peroneal nerve (CPN), the tibial nerve (TN) and the sural nerve (SN) (**Figure 1.6**).

Paw swelling was depicted as a curve to show the progress of the phenotype within a week after denervation. In terms of maximal paw swelling, every group but SN reached the peak one or two days after denervation (**Figure 3.10**). Cutting the SN alone did not cause paw thickening (**Figure 3.10**). Groups with the SN left intact (CPN, TN and CPN+TN) had denervated paw thickness returning to the level of the sham side at day 4 after denervation (**Figure 3.10**), indicating a quicker resolution of paw swelling.

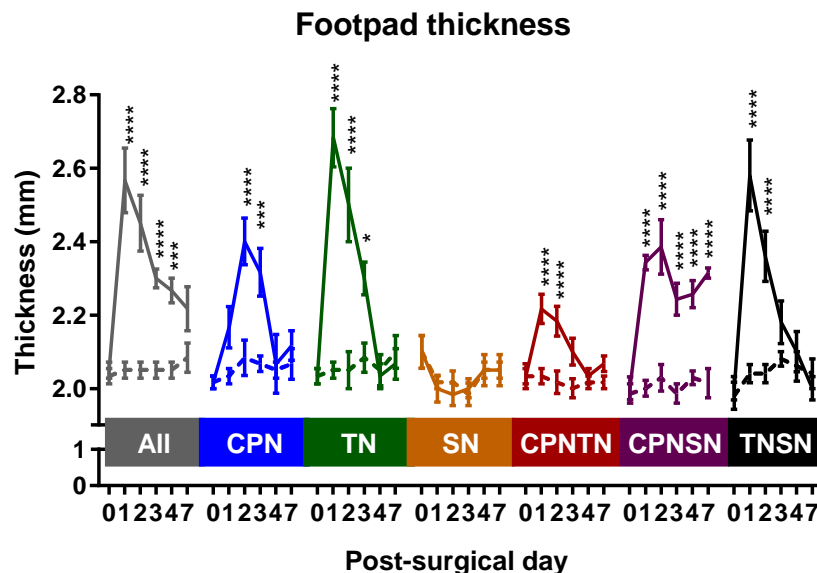


**Figure 3.10** Footpad thickness change after cutting sciatic nerve branches

Distance between ventral and dorsal sides of the paw was measured. The solid and dashed lines represent the thickness of the denervated and sham paws respectively.  $n = 5-7$ . Separated Two-way ANOVA was applied to each group, Šídák's post-test. \* $p < 0.05$ , \*\*\* $p < 0.001$ , \*\*\*\* $p < 0.0001$ .

The integral of the net thickening during this time (area under the curve, AUC) was calculated as a comprehensive indicator of net paw thickness change. From the lowest to the highest AUC, cutting the SN caused no swelling; leaving the SN intact (CPN+TN) resulted in an AUC of 0.5; the CPN, TN and TN+SN denervation resulted in an AUC around 1.0; cutting all the branches or the CPN+SN resulted in the highest AUC, over 1.5 (**Figure 3.11**). These two groups had similar AUCs (about 1.8) but different degrees of denervation (**Figure 3.11**).

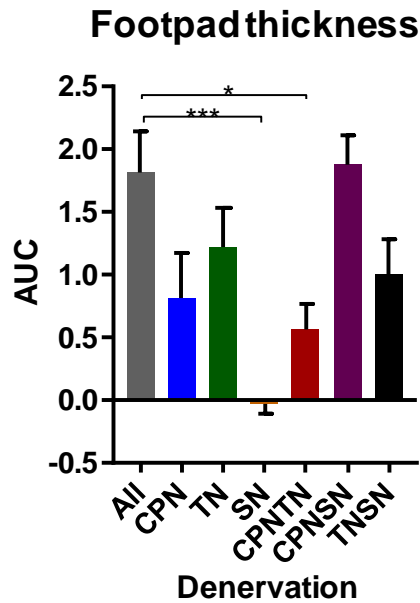


**Figure 3.11 Quantification of footpad thickness over time**

Footpad thickness data from the curve plot was transformed into a bar graph for easier comparison. The integral of difference between denervated and sham curves over time was calculated as area under the curve (AUC) to represent severity of paw swelling. n = 5-7. One-way ANOVA, Tukey's post-test. \*p < 0.05, \*\*\*p < 0.005.

Next, the interaction between the level of nodal expansion and the degree of denervation was analyzed. Comparing denervation of single branches with cutting all branches, the degrees of nodal expansion positively correlated with the size of the nervous branch denervated, reflecting the degree of denervation (**Figure 3.12**). However, dual branch denervations did not follow this principle. Cutting both CPN and SN exhibited the largest nodal expansion, showing about 1.5-fold higher than complete denervation (**Figure 3.12**). This may be due to interplay of different nerve interactions that are currently not clear.

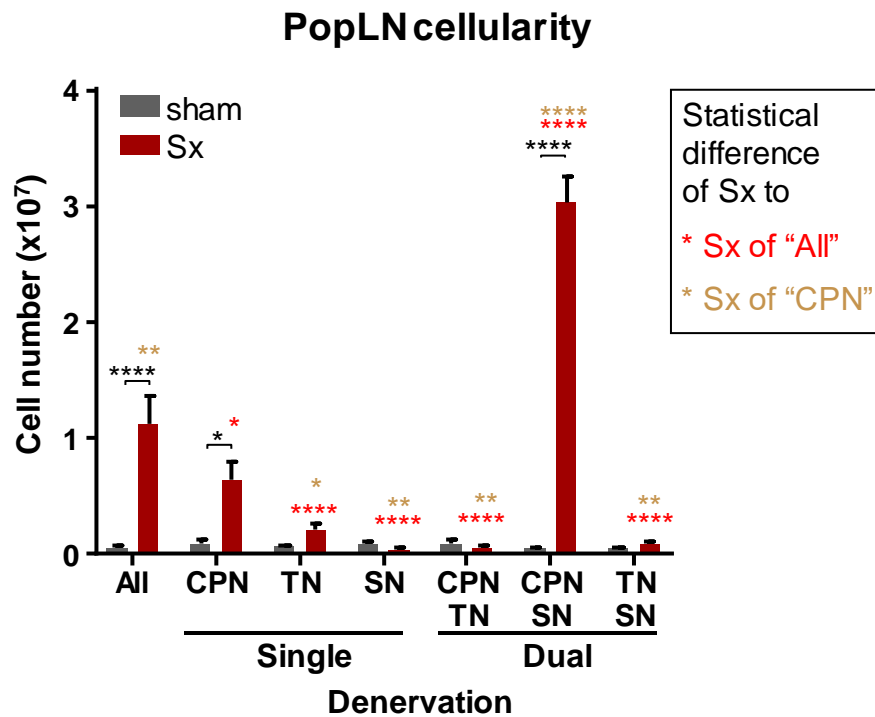


**Figure 3.12 PopLN cellularity after denervation of distinct branches**

PopLN cellularity after a set of seven surgeries were quantified. The surgical set covered cutting all branches, two branches or individual ones.  $n = 5-7$ . Two-way ANOVA, Tukey's post-test. \* $p < 0.05$ , \*\* $p < 0.01$ , \*\*\* $p < 0.001$ , \*\*\*\* $p < 0.0001$ .

We next addressed whether paw swelling and LN expansion were correlated. In single denervation, nodal expansion was proportional to the size of the denervated branch, but this was not observed in paw swelling (**Figure 3.11** and **Figure 3.12**). In addition, cutting all branches as well as cutting the CPN+SN caused the same level of paw swelling but not nodal expansion (**Figure 3.11** and **Figure 3.12**). Lastly, groups of SN, CPN+TN and TN+SN had nearly no increase in popLN cellularity after denervation but only the two dual denervation groups caused paw swelling (**Figure 3.11** and **Figure 3.12**). According to these results, nodal expansion was likely not directly correlated with the severity of paw swelling.

Denervation degrees, paw AUC and cell numbers of leukocytes in paws and popLNs under sham and denervated conditions in the sciatic branch denervation dataset were compared for correlation analyses. Denervation degree is an arbitrary unit representing the innervation area. The actual innervation area of each branch is hard to quantify but this unit offers a rough estimation according to the order of thickness of sciatic branches. CPN is the thickest one so its denervation was assigned a score of 3, TN a score of 2 and SN a score of 1. For multiple denervation these scores were added. For example, cutting CPN and TN ends up in the denervation degree of 5 due to 3+2. Paw AUC in general positively correlated with all the leukocytes studied but Langerhans cells (**Figure 3.13A**). Although positively related, all the correlation coefficients ( $r$ ) were less than 0.7, so that none of them had the determination of correlation ( $r^2$ ) more than 0.5, indicating limited correlations between leukocyte subsets in popLNs and paws and paw swelling degree (**Figure 3.13**). The same conclusion of lacking a strong correlations was made between leukocyte subsets and denervation degrees (**Figure 3.13B**). These comparisons confirmed that nodal expansion did not reflect degree of paw swelling and denervation. However, denervation degrees were loosely linked to paw swelling levels with  $r^2$  slightly more than 0.5 (**Figure 3.13C**), but, according to correlation analysis, these factors did not transfer to nodal expansion.

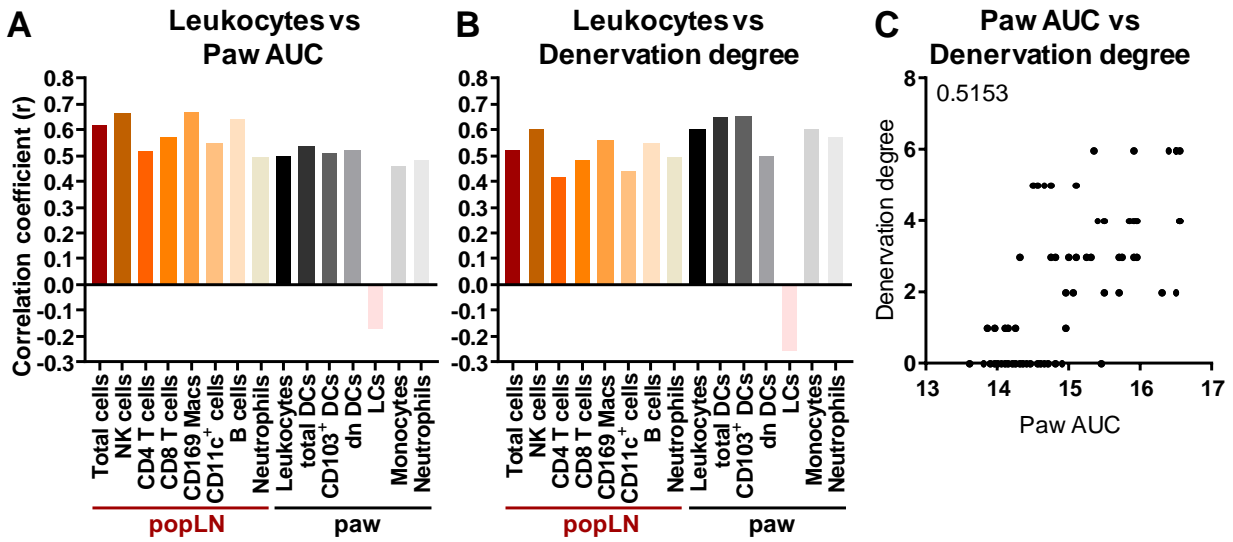


**Figure 3.13 correlations between paw AUC, leukocytes in paws and popLNs and denervation degree**

(A) Paw AUC and leukocyte counts were put together and estimated the correlation degree using correlation coefficient (r) of Pearson's correlation. (B) Correlation coefficient of Pearson's correlation of denervation degree and leukocyte counts were calculated. (C) Determination of correlation (r<sup>2</sup>) of Pearson's correlation was used as a correlation indicator. It is shown in the graph.

These findings clarified the associations of three different aspects: the level of nodal expansion, paw swelling and thickness of the nerve(s) represented by the size and combination of branch(es) cut in the sciatic nerve. The thickness effect was only correlated in LN cellularity in the case of single branch cutting.

### 3.6 Infiltration of neutrophils and CD103 dendritic cells in the paw correlates to popliteal lymph node cellularity after denervation

To further define the relation between paw swelling, paw leukocytes and nodal expansion, one of the most common and blood-brain-barrier impermeable anti-histamine drugs – Cetirizine (CTZ) – was selected to inhibit paw swelling in the denervation model without affecting histaminergic signaling in the central nervous system. CTZ was given intraperitoneally at the same time as sciatic denervation surgery and heel width was included as another parameter in addition to footpad thickness for evaluating the amount of swelling. Denervation-induced footpad thickening and heel width were subtly ameliorated after CTZ treatment but the effect was not significant (**Figure 3.14**). Despite lack of significant repression of swelling, CTZ substantially and specifically prevented the rise of neutrophils and CD103 DCs in the paw after denervation (**Figure 3.15**). Moreover, CTZ treatment blocked Sx-induced nodal expansion (**Figure 3.16**). These results positively correlated the popLN cellularity with the numbers of neutrophils and CD103 DCs in the paws.

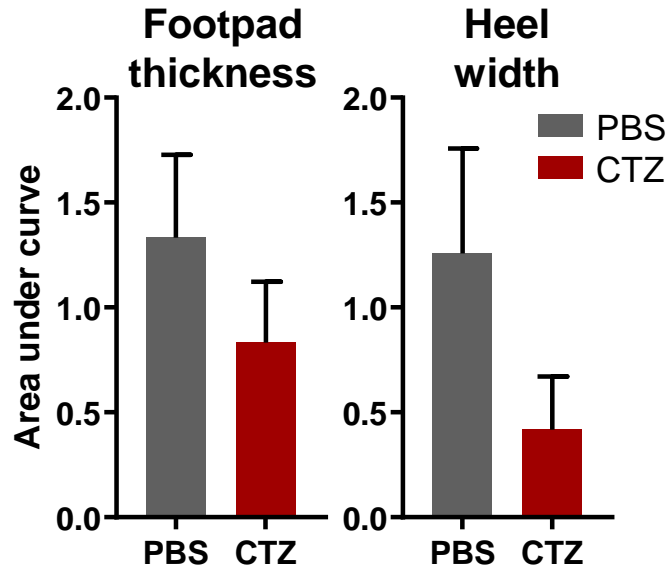


**Figure 3.14 Denervation-induced paw swelling under cetirizine treatment**

Footpad thickness and heel width were measured during a week and their pathology curves were converted to AUC. n = 6. Unpaired Student's t-test.

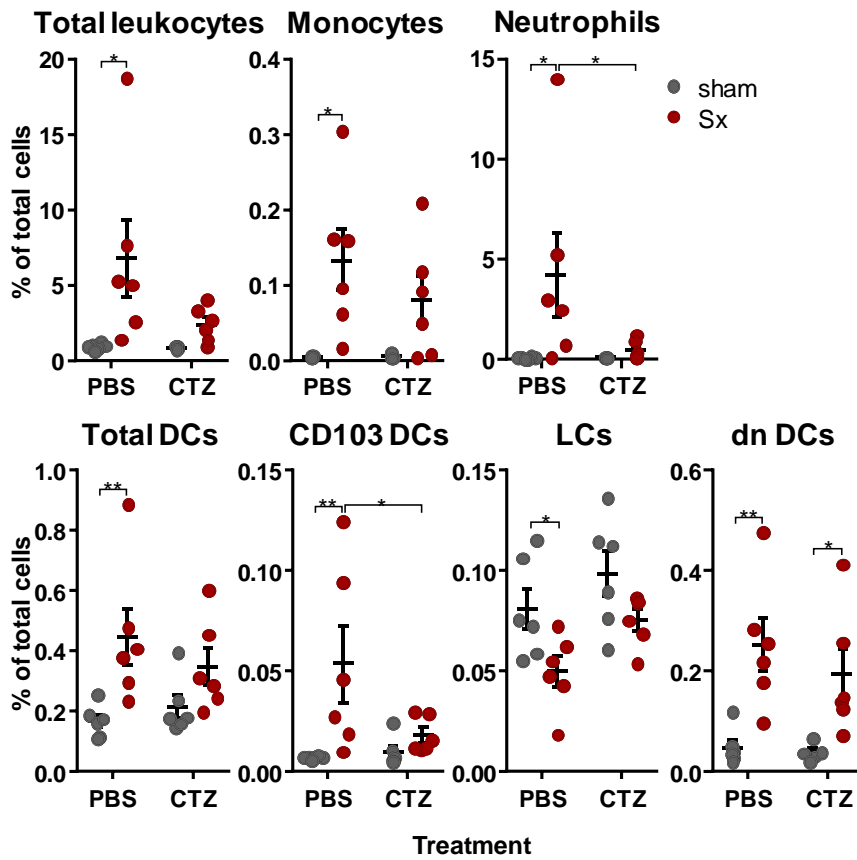


**Figure 3.15 Leukocytes in paw after sciatic denervation and cetirizine treatment**

Mice were treated with cetirizine daily for a week from the surgery day after which immune cells in the paw were analyzed. n = 6. Two-way ANOVA, Šídák's post-test. \*p < 0.05, \*\*p < 0.01.

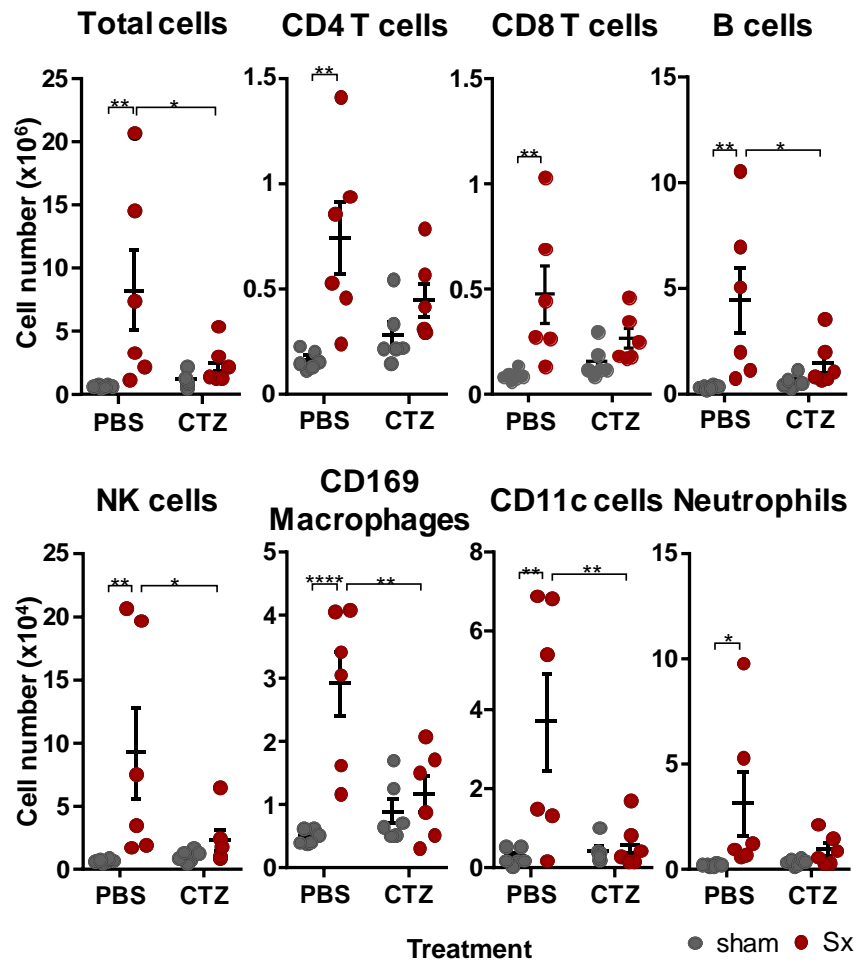


**Figure 3.16 Leukocytes in the popLN after denervation in combination with cetirizine treatment**

Effects of cetirizine treatment on denervation-induced nodal expansion were assayed by quantifying total cellularity and immune subsets in the popLNs.  $n = 6$ . Two-way ANOVA, Šídák's post-test. \* $p < 0.05$ , \*\* $p < 0.01$ , \*\*\* $p < 0.0001$ .

### **3.7 Sciatic denervation affects immune and stromal cells in the local popliteal lymph node**

LNs are hubs for immune cells that in combination with vascular and stromal cells mount adaptive immune responses. Denervation-induced LN expansion might dramatically alter LN function and its cellular composition. To characterize the nodal immune cell subsets, flow cytometry was used to quantify both mobile and resident populations such as CD4 T, CD8 T, B, NK, CD169+ and CD11c+ cells, neutrophils, as well as migratory and resident DCs within a week after unilateral Sx. In the period of 4 weeks, overall cell number increased after denervation as shown (**Figure 3.2B**), and so did all studied subsets which generally reached their peaks at week 2 and/or 3 (**Figure 3.17A**). There was barely cell type-specific expansion pattern in this scale. To look at each subset closer in shorter time frame, cell numbers of the immune subsets were monitored after 1, 2 and 7 days after sciatic denervation. In denervated popLNs, all of the investigated immune cell types were increased (**Figure 3.17B**). Moreover, distinct cell types exhibited different dynamics. One of the early peaking cell types, migratory DCs, had a unique dynamics curve which leveled at the second post-surgical day while most of the other subsets were still increasing (**Figure 3.17B**). These dynamics aligned well with the typical adaptive immune response, in which DCs are the cell type of initiation. Therefore, it strongly suggested an adaptive immune response taking place after Sx.

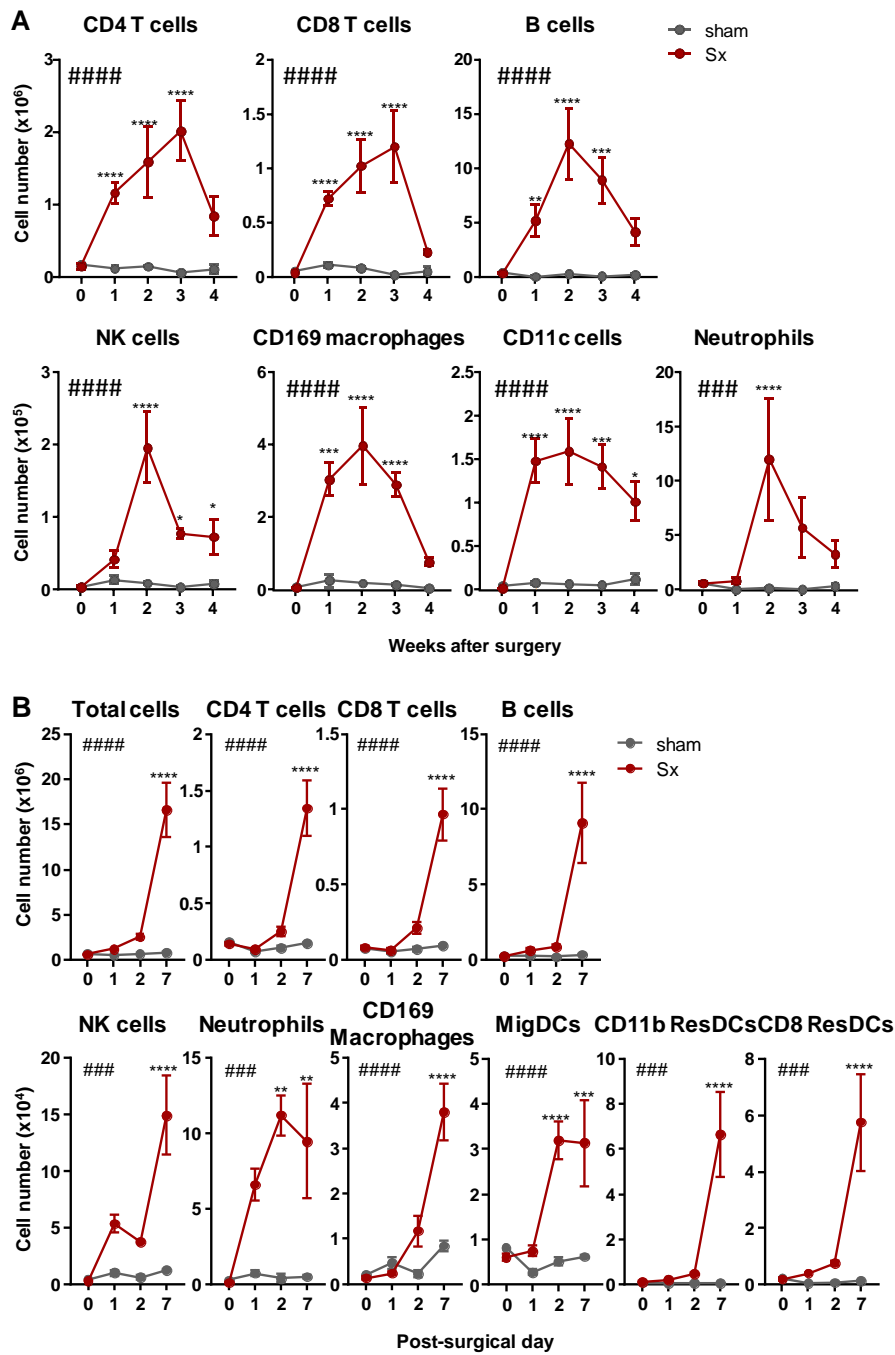


**Figure 3.17 Dynamics of immune subsets in popLN after sciatic denervation**

(A) Cell numbers of subsets in the popLNs in the sham and denervated sides were quantified and compared on different weeks.  $n = 2-8$ . (B) Cell numbers of subsets in the popLNs in the sham and denervated sides were monitored on different days.  $n = 3-5$ . Two-way ANOVA, Šídák's post-test.  $**p < 0.01$ ,  $***p < 0.001$ ,  $****p < 0.0001$ . #: statistical difference between "sham" and "Sx."

Propagation of immune responses in the lymph node requires a conducive microenvironment. Therefore, also the stromal components were analyzed after denervation. Fibroblastic reticular cells (FRCs), blood endothelial cells (BECs) and lymphatic endothelial cells (LECs) also increased (**Figure 3.18A**). Although the absolute number of high endothelial venules (HEVs) increased, vascular density decreased, indicating that stromal cells did not expand proportionately with leukocytes (**Figure 3.18B**). These results demonstrated that denervation has a broad effect on various cell types and might be involved in initiation of an immune program.

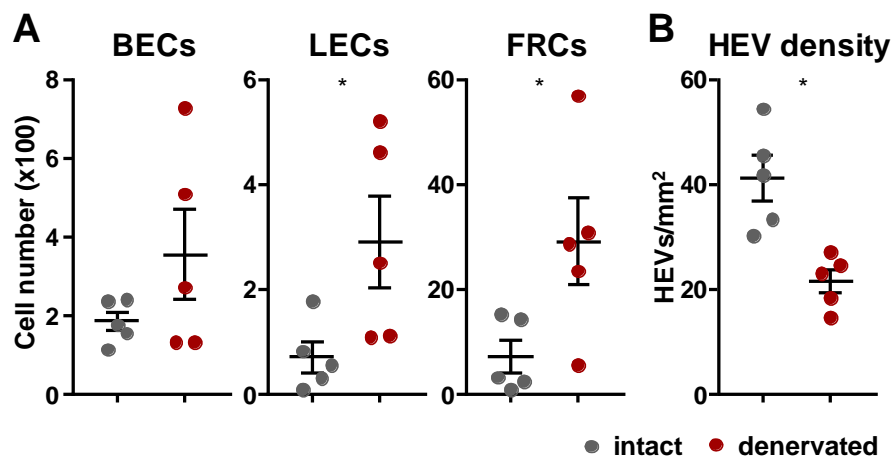


**Figure 3.18 Stromal compartments in the popLN one week after sciatic denervation**

(A) Blood and lymphatic endothelial cells and fibroblastic reticular cells were isolated and quantified. (B) HEVs in the middle of the popLNs were imaged and HEV density was calculated as HEV count per square millimeter. n = 5. Unpaired Student's t-test. \*p < 0.05.

In summary, Sx led to overall expansion of cells in the popLN including leukocytes and stromal cells but only altered numbers of CD8 T cells and eosinophils in the blood. In the popLN, the three earliest responders – neutrophils, NK cells and migratory DCs, were possibly the initiators for the enlargement of popLN after denervation.

### 3.8 Neutrophils and natural killer cells are bystanders to popliteal lymph node expansion after sciatic denervation

Among all the investigated immune cells in the LNs, neutrophils, NK cells and migratory DCs were three populations peaking earlier than the others (**Figure 3.17B**). They were thus likely to be the pioneer cells initiating the response in the LN. To test the requirement of neutrophils for nodal expansion after denervation, an experiment including neutrophil depletion and sciatic denervation was conducted. Using an anti-Ly6G antibody, neutrophil counts were substantially decreased in spleen and blood, indicating an overall reduction of neutrophils in the system (**Figure 3.19**). However, neutrophil depletion via this treatment did not block nodal expansion after the denervation surgery (**Figure 3.20**).

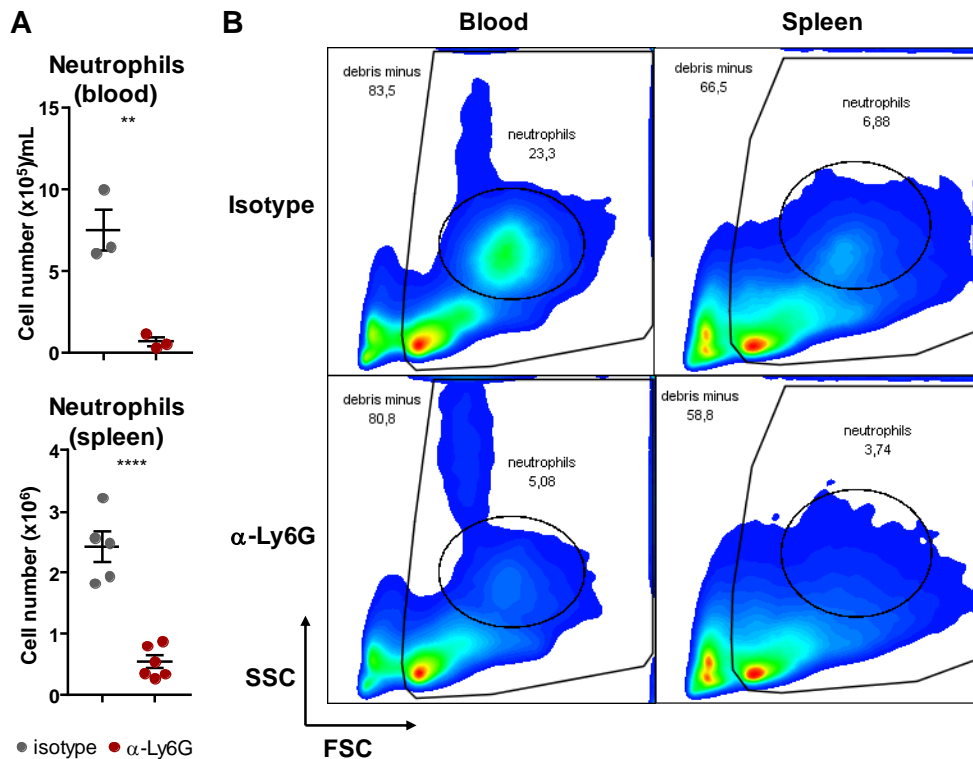


**Figure 3.19** Verification of efficacy of neutrophil depletion

Anti-Ly6G (1A8) antibody was injected intraperitoneally (ip) on the day of surgery and the fourth day after. **(A)** Circulating and splenic neutrophils were quantified.  $n = 3-6$ . Student's t-test. \*\* $p < 0.01$ , \*\*\*\* $p < 0.0001$ . **(B)** Neutrophil scatter profiles of blood and splenic samples were checked.

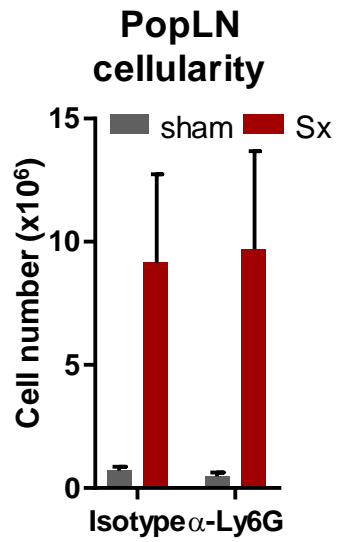


**Figure 3.20 Effects of neutrophil depletion on popLN cellularity after unilateral sciatic denervation**

PopLN cellularity was assessed one week after denervation. In this period, mice received two doses (day 0 and 4) of anti-Ly6G or isotype antibody. n = 6. Two-way ANOVA, Šídák's post-test.

Using the same experimental design, an anti-NK1.1 antibody was used to eliminate NK cells, and nodal expansion was assessed. As the NK cell identity marker was targeted by the depletion antibody, CD49b was used as an alternative marker for NK cell detection. NK cell count dropped strongly after depletion (**Figure 3.21A**). However, lower NK cell numbers did not attenuate nodal expansion compared to the isotype-treated group (**Figure 3.21B**). Taken together, although the treatment did not induce a complete lack in these cell types, neutrophils and NK cells were likely redundant to nodal expansion after sciatic denervation due to lack of influence after depletion.

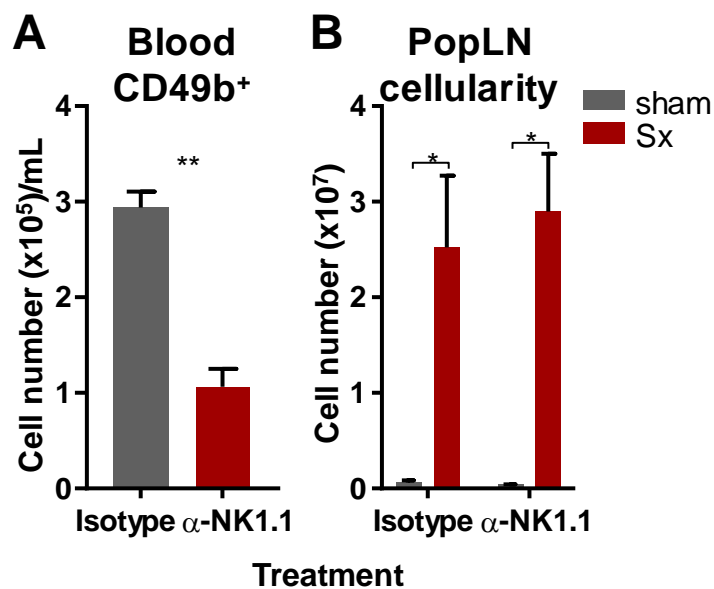


**Figure 3.21 Effects of NK cell depletion in the unilateral sciatic denervation model**

**(A)** Mice received two doses of antibody treatment on one and three day(s) after the surgery. Efficacy of NK cell depletion was evaluated by checking CD49b<sup>+</sup> cells in the blood. n = 2-3. Unpaired Student's t-test. \*\*p < 0.01 **(B)** PopLN cellularity was counted a week after the unilateral sciatic denervation. n = 2-3. Two-way ANOVA, Šídák's post-test. \*p < 0.05.

### 3.9 Nodal expansion after denervation is not due to degradation of dead terminal nerves but loss of innervation

Complete neural resection separates terminal nerves from their central connection and thus the rest of the nervous system. These “dead” nerves enter Wallerian degeneration, which involves a macrophage response due to traumatic nerve injury [22, 40, 46, 48, 49]. Whether this immune reaction triggers the LN phenotype was tested by transplanting a small piece of sciatic nerve dissected from the denervated leg into the innervated leg of the same mouse (**Figure 3.22**).

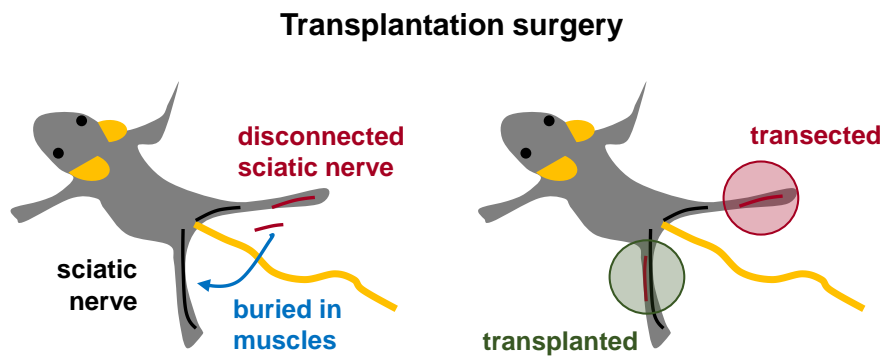


**Figure 3.22** Scheme of auto-transplantation of the sciatic nerve

A piece of sciatic nerve was transplanted into the other leg of the same mouse. The fragment of the nerve was buried between muscle bundles.

In this setting, one leg was innervated and the other was not, but both legs contained a segment of isolated nerve which could induce Wallerian degeneration on both sides and possibly drive a response in the LN. However, popLNs on the innervated side did not exhibit an increased LN cellularity despite the presence of an implanted nerve piece. PopLNs on the denervated side, on the other hand, enlarged (**Figure 3.23**). This result demonstrated that the denervation-induced LN expansion was likely not due to degradation of a dead nerve *per se* but due to loss of functional innervation.

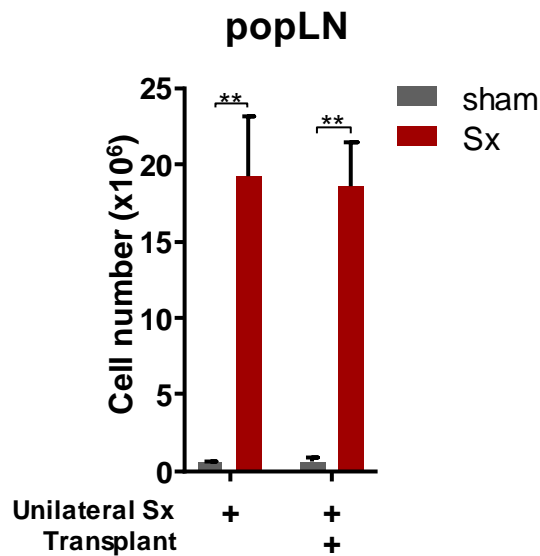


**Figure 3.23 Cellularity of popLN after auto-transplantation and transection of sciatic nerve**

Transplantation of a piece of the sciatic nerve was performed. A week after the surgery, popLN cellularity was assessed. The grey bar in the transplant group represents the cellularity of intact popLN with a transplanted piece of sciatic nerve. n = 3. Two-way ANOVA, Šídák's post-test. \*\*p < 0.01.

### 3.10 Denervated popliteal lymph nodes exhibit increased leukocyte homing

Since Sx dramatically altered cellularity in the popLN, we next investigated its effect on homing to and egress from the LN, along with local proliferation. Tracing donor cells isolated from spleen and LNs, which were adoptively transferred via intravenous injection, unveiled a preference of homing to LNs on the denervated side. In the same recipient, a 4-fold increase of homed cells was observed in the denervated LN compared to the innervated contralateral LN. (**Figure 3.24A**). Treating mice with antibodies directed against integrins or L-selectin prevented denervation-induced expansion of LNs (**Figure 3.24B**), highlighting the requirement of cell recruitment from the blood in the denervation model.

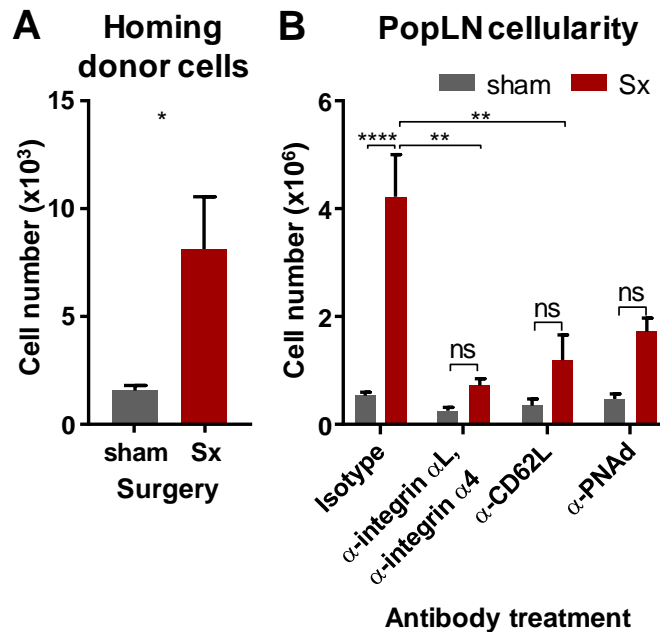


**Figure 3.24 Enhanced homing to denervated popLNs**

**(A)** Donor cells were labeled and adoptively transferred i.v. to unilateral denervated recipients. Two hours afterwards, labeled cells in the popLNs were quantified.  $n = 8$ . Paired Student's t-test.  $*p < 0.05$ . **(B)** Different antibodies to block homing were injected on the first and fourth day after the surgery and the popLN cellularity was analyzed on the seventh day.  $n=4$  for groups with blocking antibodies, isotype groups behaved similarly and were pooled to give  $n=15$ . Two-way ANOVA, Tukey's post-test.  $**p < 0.01$ ,  $****p < 0.0001$ .

### 3.11 Denervated popliteal lymph nodes exhibit unchanged egress rates

To estimate the egress rate from the lymph node, we blocked homing and investigated how LN cellularity declined afterwards. Homing blockers were injected 2 hours after donor cell transfer to prevent more donor cells from infiltration. Donor cell numbers were quantified at 0 and 12 hours after homing blockade. Egress rate was calculated by dividing donor cell fraction at 12 hours from its counterpart at 0 hour (no block) and plotted as the remaining fraction in this 12-hour time window. This procedure was performed on mice one week after unilateral Sx. Comparison of remaining donor cell number revealed no differences between intact and denervated popLNs (**Figure 3.25**). This result, together with observation on homing dynamics (**Figure 3.25**), indicated that Sx at this stage of the response selectively enhanced LN homing but had no effect on egress to drive nodal expansion.

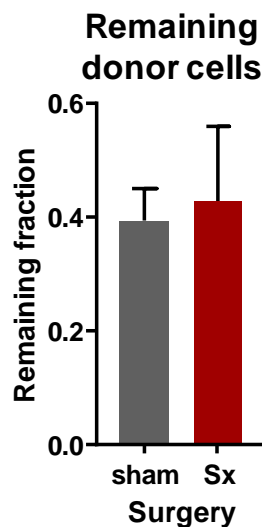


**Figure 3.25 Unchanged egress rate in denervated popLNs**

Remaining donor cells in the popLNs were quantified 12 hours after homing blockade following 2 hours homing of labeled donor cells. Prior to donor cell transfer, mice received unilateral sciatic denervation a week beforehand. n = 8. Unpaired Student's t-test.

### 3.12 The microenvironment of the denervated popliteal lymph node is pro-inflammatory and supports a germinal center response

Microenvironmental changes in the popLN after denervation were investigated by the quantification of transcripts of messenger RNA (mRNA). Whole tissue quantitative polymerase chain reaction (qPCR) was performed to monitor the change of selected genes. *Rpl32* was selected as the internal housekeeping gene control because of its high stability between sham and Sx groups (**Figure 3.26**).

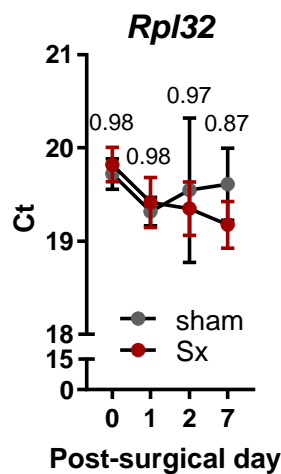


**Figure 3.26 Stability of the housekeeping gene, *Rpl32***

Expression of *Rpl32* in sham and denervated popLNs was investigated one week after the surgery. Cycle thresholds (Cts, the minimal number of cycle sufficient to generate fluorescence over the detection limit) were compared between the popLNs from sham and denervated sides and the p value at each time point was shown above the data point in the graph acting as an indicator of stability across two parameters, surgery and time. n = 5. Two-way ANOVA, Tukey's post-test.

The chemokines *Ccl19*, *Ccl21*, *Cxcl12* and *Cxcl13* and the cytokines *Tnfa*, *Tgfb*, *Ifng*, *Il1a*, *Il1b*, *Il2*, *Il4*, *Il6*, *Il7*, *Il10*, *Il12*, *Il13*, *Il17a* and *Il17f* were chosen for accessing chemotactic strength and T helper responses. PopLNs were harvested on 0, 1, 2, 7 days after unilateral Sx and their mRNAs were quantified by quantitative PCR.

*Ccl21* had no significant change and *Ccl19* only showed an increase at D2 but on the sham side (**Figure 3.27**). *Cxcl12* and *Cxcl13* are related to germinal center (GC) responses. These chemokines peaked at D2, implying the formation of GCs (**Figure 3.27**).

With respect to inflammatory cytokines in denervated popLNs, *Tnfa* did not change, but *Il1a*, *Il1b* and *Il6* significantly rose within 24 hours and reached a peak at D1 (**Figure 3.27**). Type 1 immunity-related cytokines *Ifng* and *Il12* exhibited contradictory trends after denervation. The former went down and the latter went up (**Figure 3.27**). *Il2*, exhibited no changes in denervated popLNs (**Figure 3.27**). The type 2 immunity-related cytokine *Il4* did not change but *Il13* went down after denervation (**Figure 3.27**). With respect to anti-inflammatory cytokines, *Tgfb* did not change but *Il10* went up at D2 after denervation (**Figure 3.27**). *Il1*, *Il6*, *Il10*, *Il17a* and *Il17f* are related to a Th17 response and all increased after denervation but in different phases (**Figure 3.27**). By far the strongest response was seen in *Il1b* (~70-fold increase in the Sx side), demonstrating that a strong inflammatory response was taking place after surgical denervation. In this denervation model, *Il1*, *Il6* peaked at D1, *Il10* at D2 and *Il17a* and *Il17f* at D7 (**Figure 3.27**).

This profile revealed several waves of chemokines and cytokines altered after denervation. These were strongly pro-inflammatory, and mainly related to Th17 and GC responses.

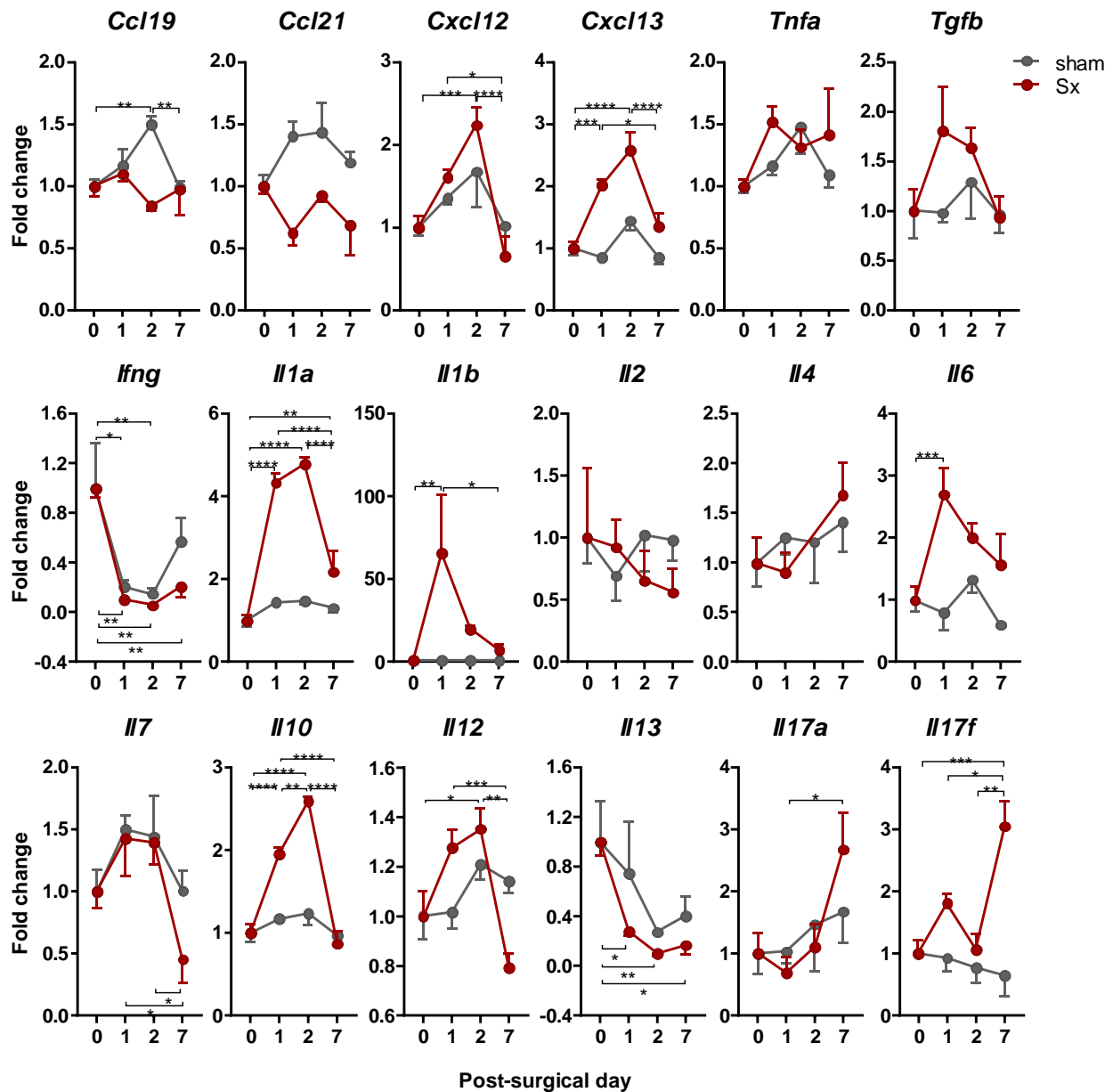


**Figure 3.27 Gene expression profile of chemokines and cytokines in the popLNs**

PopLNs were harvested before the surgery, on the first, second and seventh day after the surgery. Total RNA was extracted and converted to cDNA. Using the  $\Delta\Delta C_t$  method, 18 genes were profiled. Data were presented as fold of expression of indicated genes compared with the expression at day 0. n = 5. Two-way ANOVA, Tukey's post-test. \*p < 0.05, \*\*p < 0.01, \*\*\*p < 0.001, \*\*\*\*p < 0.0001.

### 3.13 Sciatic denervation causes acute inflammation in the paw

In addition to the popLN, whole tissue qPCR was also performed on paw tissue in the same time window after denervation. The same set of chemokines and cytokines were investigated.

*Ccl19* and *Ccl21* did not show significant changes but *Cxcl12* and *Cxcl13* both were upregulated after denervation (**Figure 3.28**). The inflammatory cytokines, *Tnfa*, *Il1a*, *Il1b* and *Il6*, significantly rose at D2 after denervation with *Il1b* up ~>500-fold but also the anti-inflammatory cytokine, *Il10*, rose and reached 6.5-fold a week after denervation (**Figure 3.28**). Unlike *Il10*, *Tgfb* did not change (**Figure 3.28**). The peak timing of inflammatory cytokines and *Il10* illustrated a biphasic profile of the microenvironment in the paws (**Figure 3.28**). With respect to type 1 and 2 immunity-related cytokines, *Ifng*, *Il4*, *Il12* and *Il13* did not exhibit significant changes (**Figure 3.28**), neither did *Il2* or *Il7* (**Figure 3.28**). *Il17a* and *Il17f* expression significantly increased after denervation but with different dynamics and amplitudes (**Figure 3.28**).

This data set showed a two-wave profile of cytokine after denervation. The first wave was dominated by inflammatory cytokines at D1, particularly *Il1b*. After that, the second wave, *Il10*, *Il17a* and *Il17f* kept rising to higher levels. *Cxcl12* and *Cxcl13* were also induced by denervation.

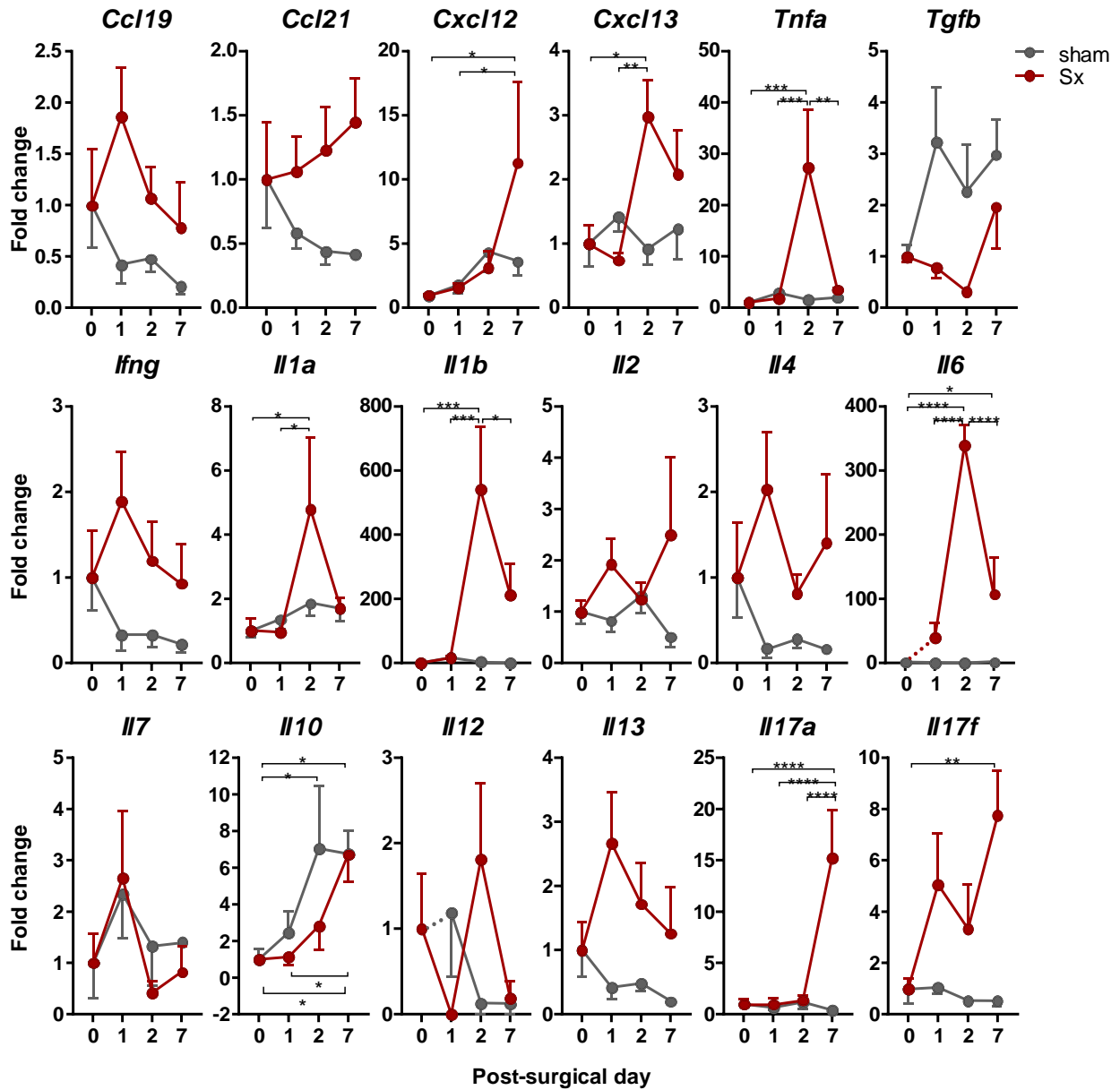


**Figure 3.28 Gene expression profile of chemokines and cytokines in the paw**

Paws were harvested before and on the first, second and seventh day(s) after the surgery. Bones were then removed from soft tissues and skin. Total RNA was extracted and converted to cDNA. Using the  $\Delta\Delta C_t$  method, 18 genes were profiled. Data were presented as fold of expression of indicated gene compared with the expression at day 0. n = 5. Two-way ANOVA, Tukey's post-test. \*p < 0.05, \*\*p < 0.01, \*\*\*p < 0.001, \*\*\*\*p < 0.0001.

### 3.14 Denervation shapes the microenvironment in paw and popliteal lymph node favoring germinal center formation and Th17 response

Gene expression profiles of denervated paw and popLN were taken to compare the microenvironment in the popLN and its draining area. Their profiles showed strong overlap. Specifically, both exhibited upregulation of *Cxcl12*, *Cxcl13*, *Il1a*, *Il1b*, *Il6*, *Il10*, *Il17a* and *Il17f* (**Table 3.1**), suggesting a pro-GC formation and pro-Th17 microenvironment.

There were still differences between denervated popLNs and paws. Upregulation of *Tnfa* was found in the paw but this was absent in popLN (**Table 3.1**). *Ifng*, *Il7* and *Il13* were repressed in denervated popLNs but this was not the case in denervated paws (**Table 3.1**).

PopLN should reflect the immunity of its draining area. Therefore, it is considered as the place where the ensuing immune reaction occurs. However, looking at the highest/lowest point of genes altered after denervation, popLN seemed to reach the point earlier than paw (**Table 3.1**), indicating that denervation might have effects on the popLN preceding peripheral inflammation.

	<i>Ccl</i>		<i>Cxcl</i>		<i>Tnfa</i>	<i>Tgfb</i>	<i>Ifng</i>	<i>Il</i>										
	19	21	12	13				1a	1b	2	4	6	7	10	12	13	17a	17f
Paw			<u>7</u> 11.3	<u>2</u> 3.0	<u>2</u> 27.4			<u>2</u> 4.8	<u>2</u> 541.6			<u>2</u> 340.1		<u>7</u> 6.7			<u>7</u> 15.2	<u>7</u> 7.8
popLN			<u>2</u> 2.2	<u>2</u> 2.6			<u>127</u> 0.06	<u>12</u> 4.8	<u>1</u> 65.8			<u>1</u> 2.7		<u>2</u> 2.6		<u>127</u> 0.1		<u>7</u> 3.1

**Table 3.1 Comparison of gene expression profiles of paw and popLN after denervation**

Gene expression profiles after denervation were summarized by the direction of change (up or down) and the highest/lowest timing in the progression. Only changes above 2-fold or below 0.5-fold from day 0 were included. Red box: upregulation. Grey box: downregulation. Underlined number in the box: the day after denervation having highest or lowest expression of indicated gene. Italics: fold-change to sham-operated side



A common B cell reaction in LNs is the formation of germinal centers (GCs) and the production of high affinity antibodies, which can be identified by the activation molecule GL7. Immunofluorescence imaging showed GL7 co-located with the proliferating B cell clusters in the denervated LN (**Figure 3.30**), indicating that B cells were proliferating to form germinal centers in LNs on the denervated side.

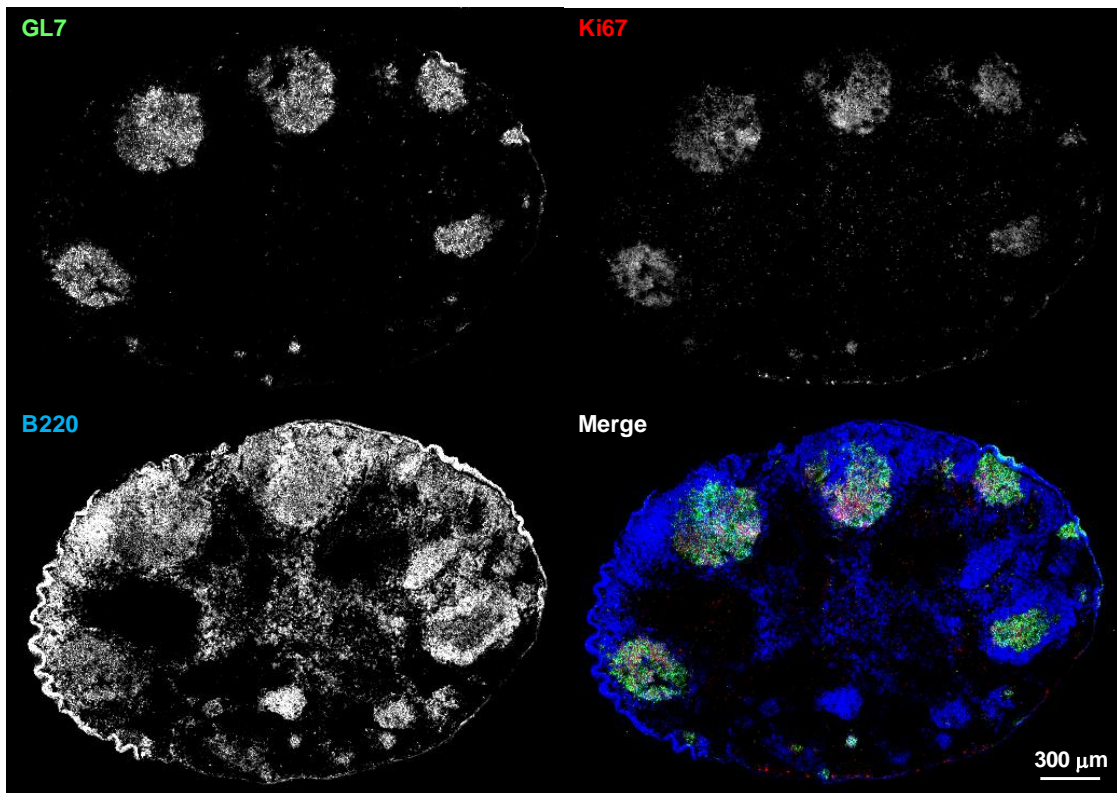


**Figure 3.30 Identification of germinal centers in the denervated popLNs**

Sections from the middle of popLNs were stained with anti-B220 (blue), anti-GL7 (green) and Ki67 (red). GL7 is a germinal center marker.

Because formation of germinal centers requires interactions of antigen-reactive B cells with cognate T helper cells via MHCII-TCR and CD40-CD40L engagement [133, 134], antigen specific T helper cells are essential. Whether impaired MHCII-TCR interaction prevent the denervation-mediated LN phenotype was tested by doing denervation surgery in OT-II mice which exhibit mostly monoclonal T helper cells [320]. Unilateral Sx induced nodal expansion of popLNs in both WT and OT-II mice, however, to a markedly different degree, at 18.6 and 6.3-fold, respectively (**Figure 3.31**). This implied that loss of antigen specific CD4 T cells reduced the degree of nodal expansion after denervation.

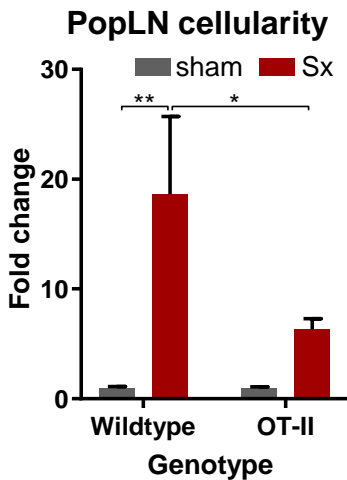


**Figure 3.31 PopLN cellularity in wildtype and OT-II mice after unilateral sciatic denervation**

Age-matched OT-II and WT mice were denervated and their popLNs cellularity was analyzed a week after the surgery. n = 7 - 9. Two-way ANOVA, Šídák's post-test. \*p < 0.05, \*\*p < 0.01.

Before cognate T cells can interact with B cells, T cells themselves need to be activated by antigen presenting cells (APCs) [321]. We tested the relevance of antigen presentation by injecting an MHCII-neutralizing antibody. MHCII blockade substantially dampened expansion of popLNs after denervation (**Figure 3.32**).

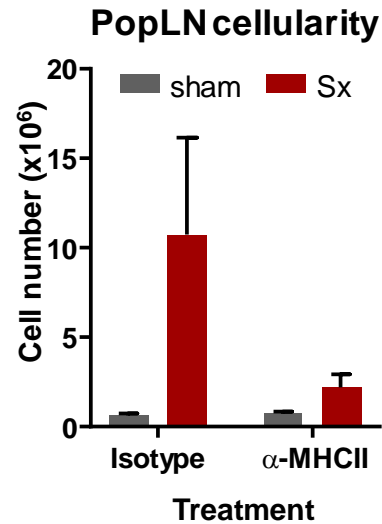


**Figure 3.32 PopLN cellularity change after MHCII blockade after unilateral sciatic denervation**

Mice received an anti-MHCII (Y3P) or isotype control antibody on the day of surgery and 4 days after the surgery. PopLN cellularity was assessed one after the surgery. n = 6. Two-way ANOVA, Šídák's post-test.

### **3.16 Afferent lymphatic input is required for denervation-mediated nodal expansion**

Afferent lymphatics channel immune cells and soluble molecules from peripheral tissues to draining LNs [191, 192, 223, 227]. Whether afferent lymphatic input was required for the development of denervation-mediated LN expansion was examined by combining Sx with a surgery that severed LNs from afferent lymphatics. Mice receiving unilateral Sx were divided into two groups. One group's afferent lymphatics leading to popLNs were cut and those in the other group were left intact. The success of the afferent lymphatic disconnection surgery was verified right before sacrificing animals by inability of Evans Blue solution to reach popLN given via ipl injection (**Figure 3.33**).

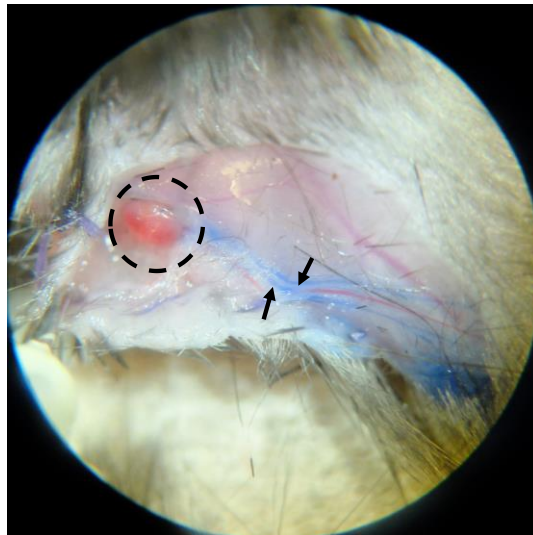


**Figure 3.33 Verification of afferent lymphatic disconnection surgery**

Afferent lymphatics entering the popLN were surgically cut and sealed using a hot coagulation needle. A week after the surgery, the popLN was shown disconnected from the paw due to the inaccessibility of Evan's Blue solution delivered via ipl injection.

Disconnection of afferent lymphatics to popLNs prevented the denervation-induced nodal expansion but did not reduce the paw swelling (**Figure 3.34**). This finding implied, in addition to the prerequisite of a LN homing process from blood that afferent lymphatic input is essential for the proliferation phenotype of denervated LNs.

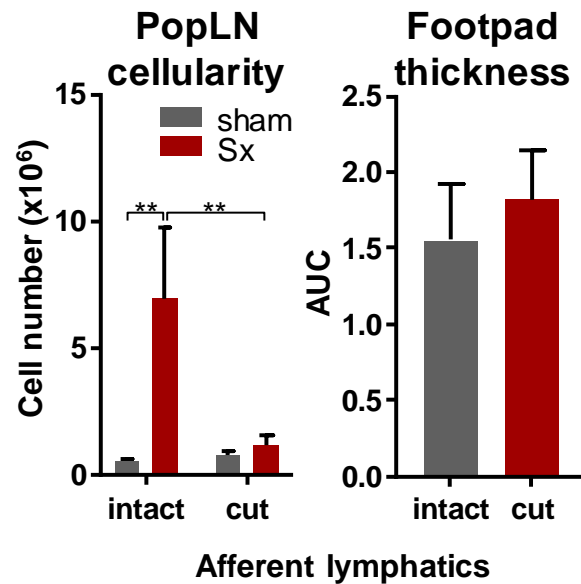


**Figure 3.34 Influence of afferent lymphatic disconnection surgery to PopLN cellularity and Paw swelling after the unilateral sciatic denervation**

Sx and afferent lymphatic disconnection surgeries were performed on the same day. Paw thickness was recorded during the time and popLNs were harvested and analyzed a week after the surgeries.  $n = 6-13$ , inaccessibility of Evan's Blue to the popLN was confirmed before sample harvest. Two-way ANOVA, Šídák's post-test for popLN cellularity. Unpaired Student's t-test for footpad thickness.  $**p < 0.01$ .

### 3.17 Sciatic denervation generates local and systemic effects

Sciatic denervation caused a dramatic increase in cellularity of the affected popLNs (**Figure 3.17**). This response reflected a radical change of the local environment after denervation. In addition to producing local influences, whether sciatic denervation could further generate systemic responses was examined by investigating cells in the spleen, as the secondary lymphoid organ reflecting more systemic responses. The overall splenic cellularity increased slightly a week after unilateral denervation albeit being not statistically significant (**Figure 3.35**). At that time, more B cells were found in the spleen and there appeared to be a B cell response, aligned with the response in the popLNs, with expansion of germinal center B cells (GCBs) and plasma cells (PCs) (**Figure 3.35**). Higher splenic PC numbers can come from more circulating PCs or local *de novo* PCs generated in the spleen. However, the spleen contained not only more PCs, but GCBs (**Figure 3.35**). GCBs normally develop in the local LN whose draining area experiences immune challenges, or directly in the spleen in response to circulating antigens [138]. Therefore, increase of GCBs suggested an *in situ* B cell response in the spleen, which was remotely activated by sciatic denervation.

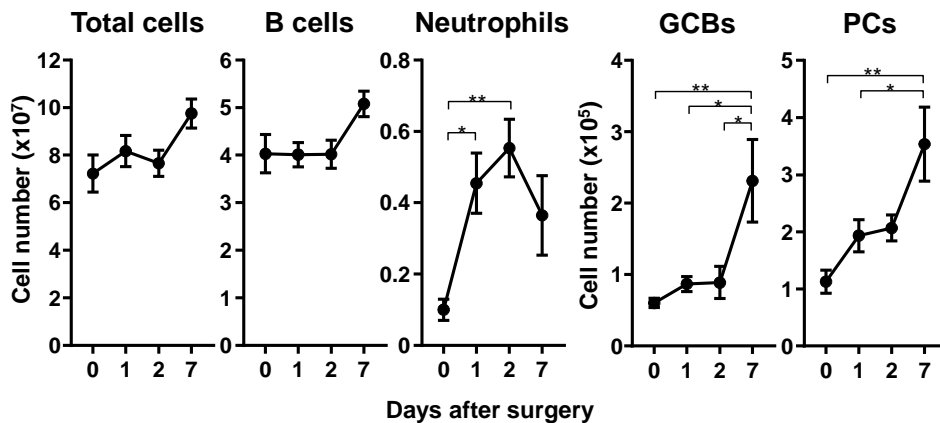


**Figure 3.35 Splenic neutrophil and B cell dynamic after unilateral sciatic denervation**

After the surgery, splenic cells were followed during the week afterwards. Neutrophils and B cells including total B cells, GCBs and PCs were quantified. GCBs and PCs represent the intermediate and final stage, respectively, in B cell activation and differentiation. n = 5. One-way ANOVA, Tukey's post-test. \*p < 0.05, \*\*p < 0.01.

### 3.18 Sciatic denervation increases antibody titers

Given that sciatic denervation led to the formation of GCs and an increase of GCBs and PCs in spleen, we investigated whether systemic antibody titers were affected. Sera were isolated and isotyped from the denervated mice at different times after the surgery. 3 weeks after sciatic denervation immunoglobulin (Ig) G<sub>1</sub> and IgG<sub>2b</sub> were the major isotypes (**Figure 3.36A**). Therefore, total IgG titers in the blood were assayed and found to increase 2-3-fold 3 weeks after denervation (**Figure 3.36B**), indicating that denervation not only caused local GC responses but also promoted systemic antibody generation.

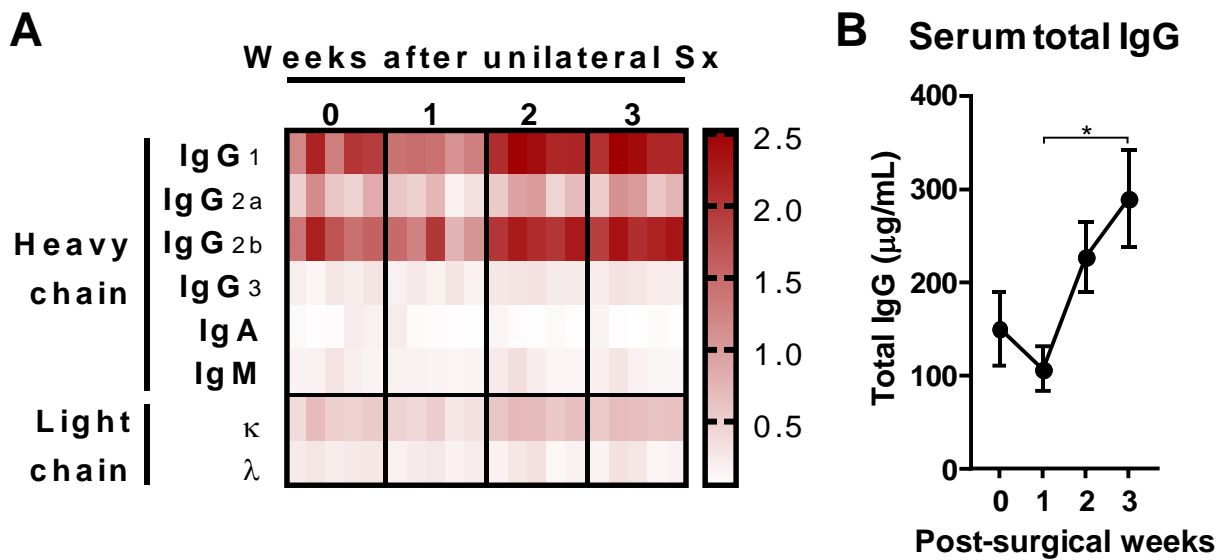


**Figure 3.36 Production of antibodies after sciatic denervation**

**(A)** Sera taken from denervated mice at distinct times was isotyped. Heat-map value: absorbance of 450 nm light. **(B)** Total IgG levels in the sera were quantified. n = 5. One-way ANOVA, Tukey's post-test. \*p < 0.05.

### 3.19 Antibodies induced by sciatic denervation are not reactive to antinuclear antigens

To investigate whether the antibodies generated were autoreactive, sera from denervated mice were harvested at different times and incubated on HEp2 slides. These slides contain lysed HEp2 cells, which are engineered to display a broad spectrum of nuclear antigens such as double stranded DNA, histones and centromeric antigens [322]. The antibodies induced after sciatic denervation did not bind to nuclear antigens on the slide (**Figure 3.37**). This result suggested that antibodies elicited by the denervation process were likely not autoreactive.

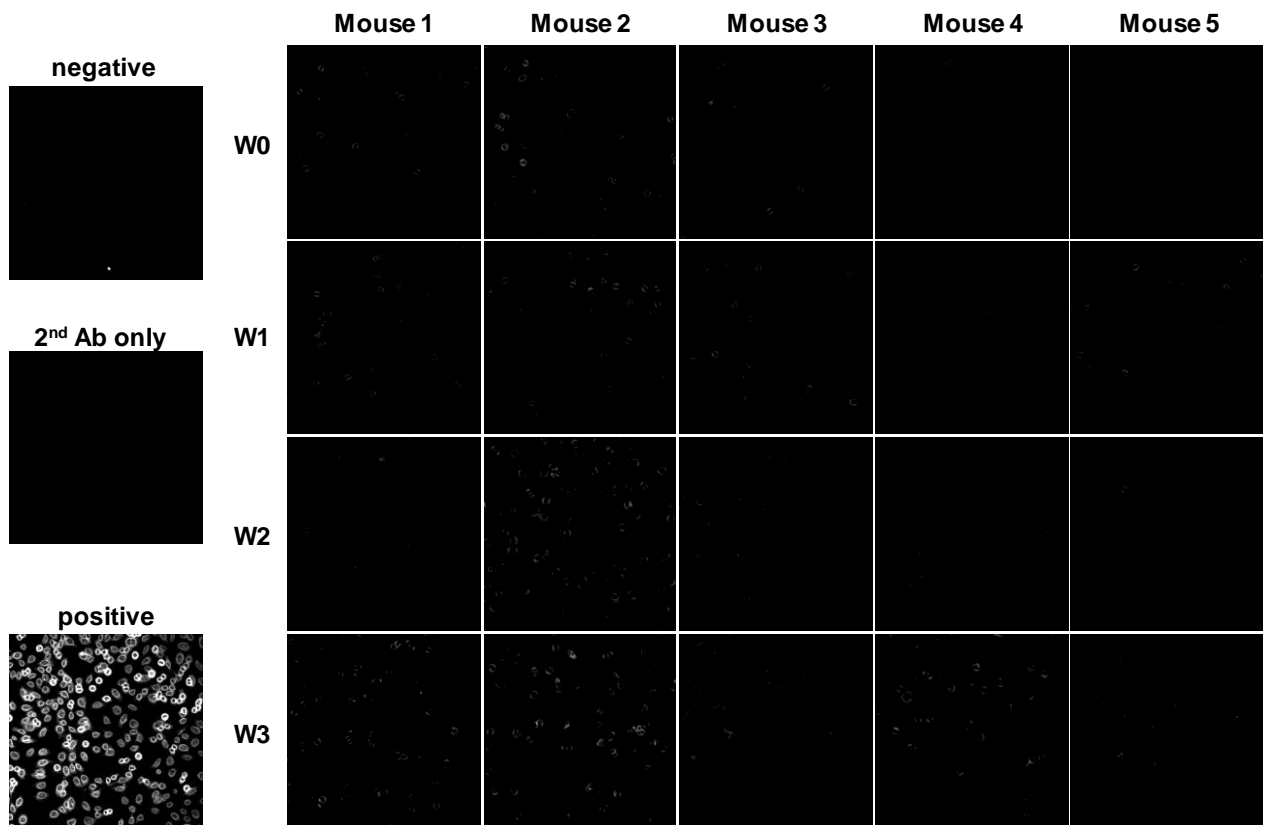


**Figure 3.37** Reactivity of sera from denervated mice to antinuclear antigens

Serum from each mouse was adjusted to 10  $\mu\text{g/mL}$  of total IgG. 25  $\mu\text{L}$  of adjusted sera were incubated with HEp2 slides overnight. The reactivity was imaged by immunofluorescence.

### 3.20 The sciatic nerve possesses sympathetic and sensory properties

Denervation leads to death and degradation of neural fibers, their separation from the neuronal body and loss of neural input in respective ramified areas [22]. The sciatic nerve consists predominantly of sensory fibers (70-80%), sympathetic fibers (about 20%) and motor fibers (5%) [278, 279]. Using immunofluorescence analyses for tyrosine hydroxylase (TH), substance P (SP) and calcitonin gene-related peptide (CGRP), bundles of different subsets in terms of compounds secreted were identified in the sciatic neural projections (**Figure 3.38**). This confirmed the sensory and sympathetic majority of nerves in the sciatic nerve.

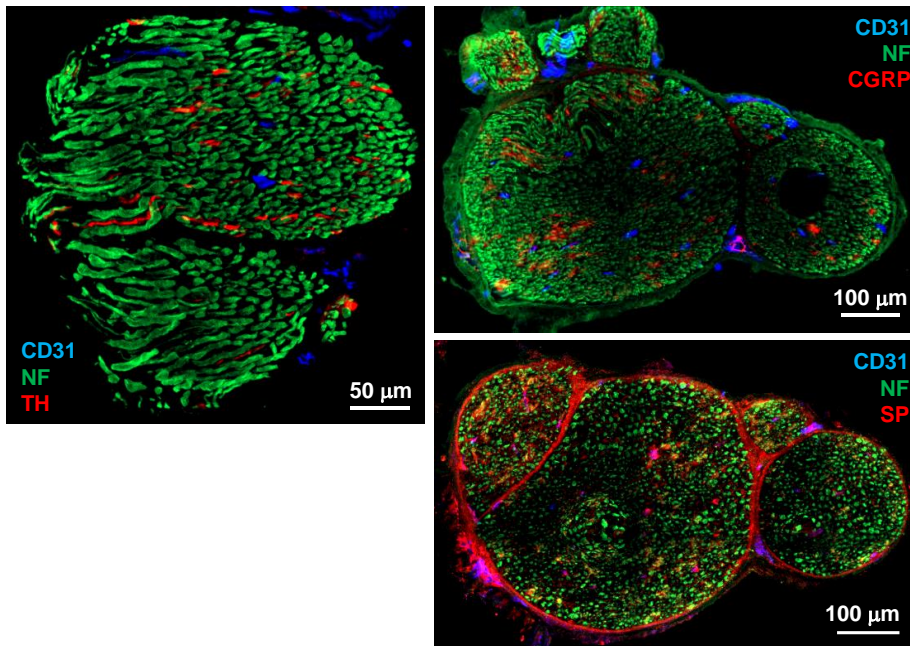


**Figure 3.38** Nerve fiber properties of the sciatic nerve

Cross sections of sciatic nerves were stained with vasculature markers (CD31, blue), neural structural markers (NF, green) and functional neural substance markers (TH, CGRP and SP, red). TH is the rate-limiting enzyme in the catecholamine biosynthesis pathway, marking sympathetic nerves (left). CGRP (top right) and SP (bottom right) are secretory neuropeptides from sensory nerves.

Additionally, popLNs were imaged for sympathetic nerves, which were mainly found on the capsule and associated with vessels (**Figure 3.39**). CGRP<sup>+</sup> peptidergic sensory nerves were observed in the popLN hilum region and along central vessels but not much on the capsule (**Figure 3.40**). This indicated that nerves might have functions in LN physiology, such as controlling the circulation and communication with immune cells.

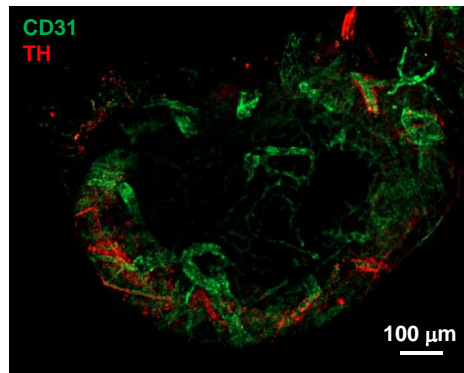


**Figure 3.39 Sympathetic innervation of the popLN**

TH and CD31 labeled sympathetic nerves and endothelial cells, respectively. Sympathetic nerves were shown along the capsule and vessels in the hilum region of the popLN.

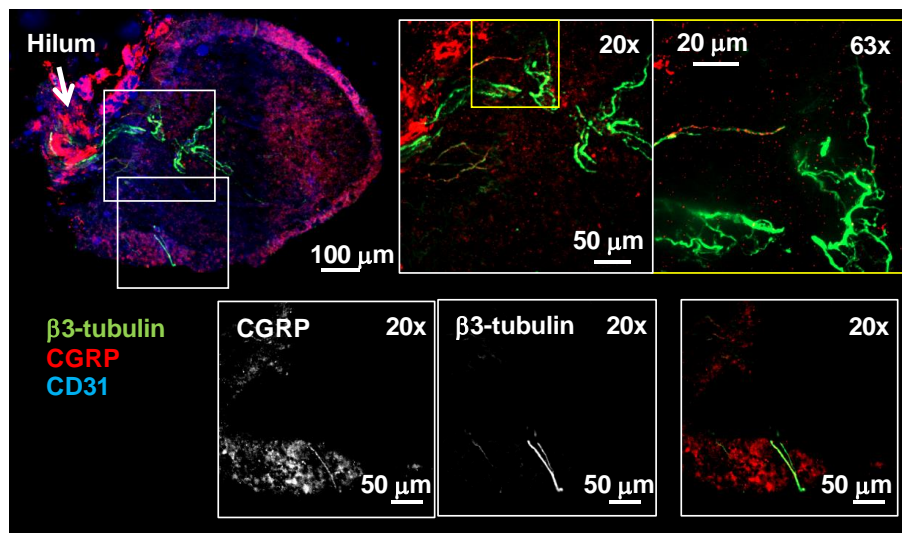


**Figure 3.40 CGRP<sup>+</sup> nerves in the popLN**

Vessels, CGRP<sup>+</sup> nerves and neural fibers were labeled by CD31, CGRP and β3-tubulin, respectively. CGRP signal was found on the LN capsule (bottom squares) and associated with hilum vessels (top squares).

### **3.21 Sympathectomy does not alter cell number and migratory dynamics in lymph nodes but modifies the local microenvironment**

Given that the sciatic nerve possesses multiple and different nerve fibres, additional models were needed to ascertain whether sensory or sympathetic signaling was the main driver of the phenotype observed. To investigate functions of the sympathetic nervous system (SNS) in LN cellularity, two methods were used to manipulate sympathetic tone. Chemical sympathectomy by ip injection of 6-hydroxydopamine (6-OHDA) systemically abolishes sympathetic nervous functions in the periphery [323]. On the other hand, superior cervical ganglionectomy (SCGx) is a local surgical approach depriving sympathetic tone in the cervical area [317]. After 6-OHDA treatment, cellularity in popLNs was found to be similar to vehicle-treated groups (**Figure 3.41A**). To focus more on local effects, SCGx was performed. However, this did not cause changes in steady cellularity in superficial parotid lymph nodes (spLN), the LN directly innervated by the superior cervical ganglion (SCG) (**Figure 3.41B**). These findings indicated sympathetic nerves by themselves to exert minimal effects on LN cellularity.

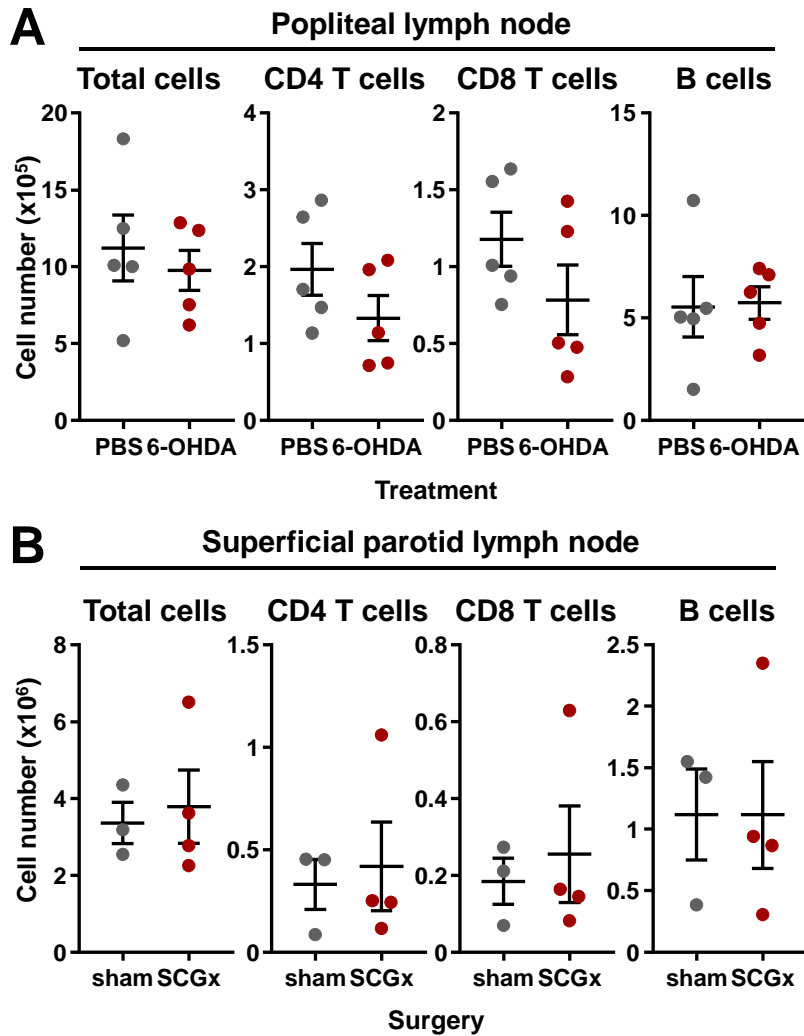


**Figure 3.41 LN cellularity after sympathectomy**

**(A)** Mice were treated by 6-OHDA to chemically and systemically ablate sympathetic nerve functions and popLN cellularity was assessed.  $n = 5$ . Unpaired Student's t-test. **(B)** Superior cervical ganglionectomy was performed as local sympathectomy and the cellularity of superficial parotid LNs was quantified afterwards.  $n = 3-4$ . Paired Student's t-test.

However, since the microenvironment might be modified by sympathectomy we profiled the same set of genes as analyzed previously.

With respect to chemokines no significant changes were observed (**Figure 3.42**). With respect to cytokines *Il1a* and *Il4* were altered (**Figure 3.42**). These results identified *Il1a* and *Il4* as two significantly upregulated genes in sympathectomized popLNs (**Figure 3.42**), indicating that loss of sympathetic tone might create an inflammation and type 2 immunity-favored microenvironment.

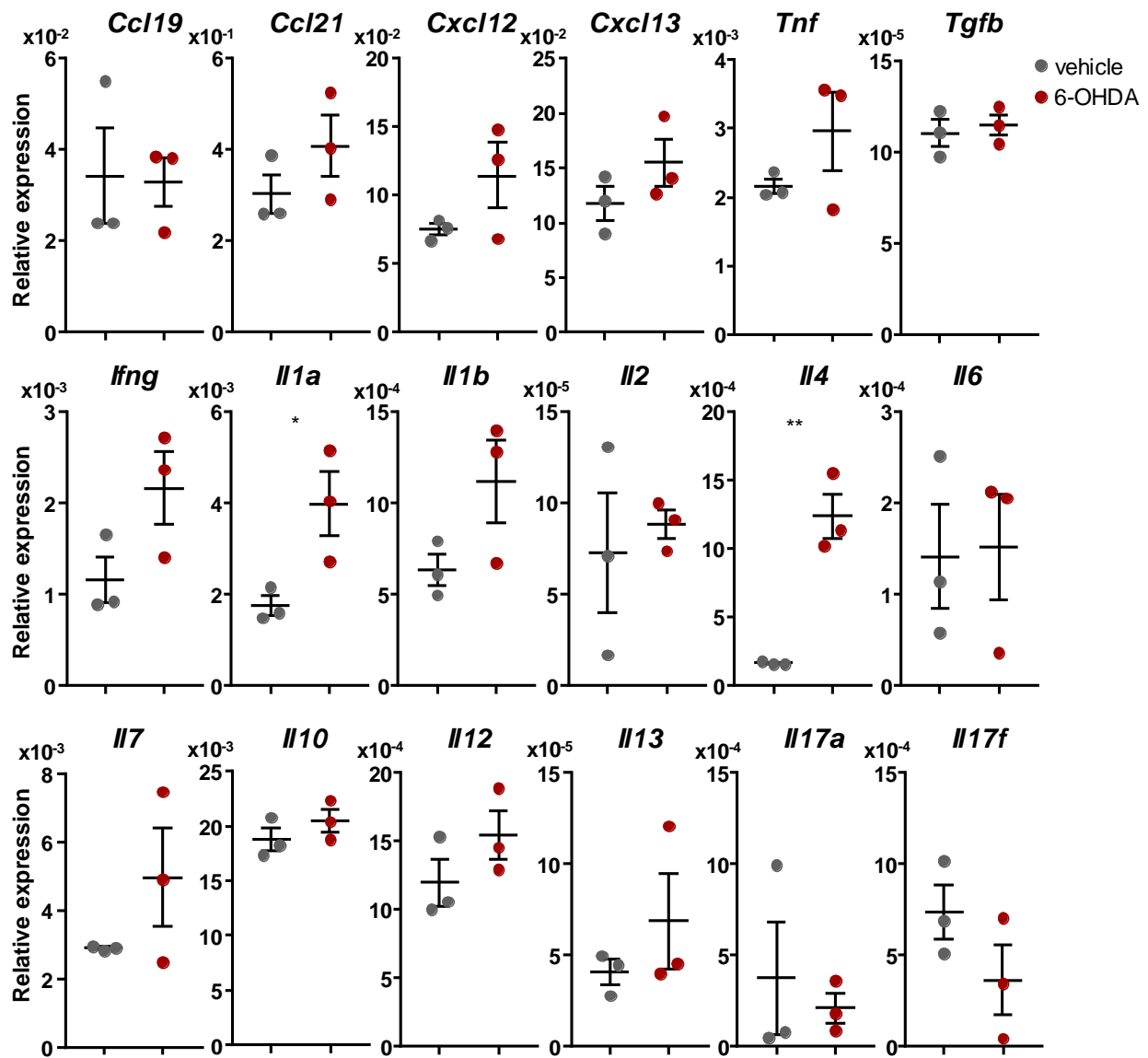


**Figure 3.42 Gene expression profile in popLNs after systemic sympathectomy**

After chemical sympathectomy, popLNs were harvested and gene expression was profiled based on quantitative PCR. n = 3. Unpaired Student's t-test. \*p < 0.05, \*\*p < 0.01.

In the SCGx model, homing and egress rates were tested to answer whether sympathetic innervation altered cell migration to the LN. SCGx did not affect homing or egress of CFSE-labeled to LNs (**Figure 3.43AB**). These results showed that the homing capacity and dwell time were not altered by local sympathectomy alone. In summary, sympathectomy did not change migration pattern or cellularity in steady state.

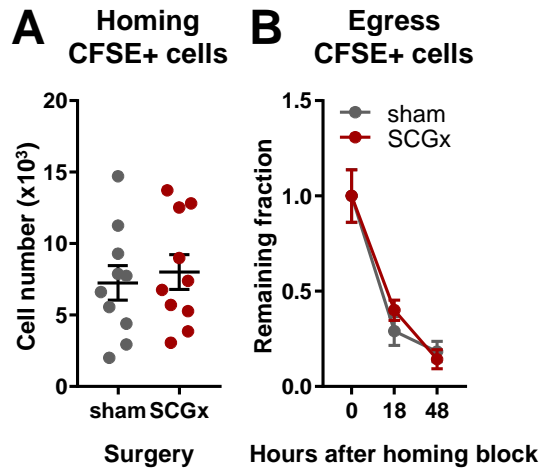


**Figure 3.43 Homing and egress rates in local sympathectomized spLNs**

**(A)** Labeled donor cells were transferred and homed to sham or SCGx spLNs in a 2-hour window. Homing cells were then quantified.  $n = 10$ . Paired Student's t-test. **(B)** After 2 hours of homing, homing blockers were applied. Remaining cells were then quantified after indicated periods.  $n = 6$ . Paired Student's t-test.

### 3.2.2 Antagonizing neuropeptide receptors is not sufficient to trigger nodal expansion

Sensory nerves compose the biggest portion of the sciatic nerve [278, 279]. Among the substances sensory nerves secrete, SP and CGRP are the major neuropeptides with immune regulatory effects [78, 98, 106]. Given that loss of innervation caused nodal expansion, we assessed whether blockade of sensory neuropeptide signaling generated the same phenotype. To mimic conditions of loss of sensory neural tone, antagonists of receptors of SP and CGRP, SR140333 (a SP receptor antagonist) and BIBN4096 (a CGRP receptor antagonist) were i.p. injected in mice. No obvious effects on cellularity in hematopoietic compartments including blood, BM, spleen, popLN and iLN were observed (Figure 3.44).

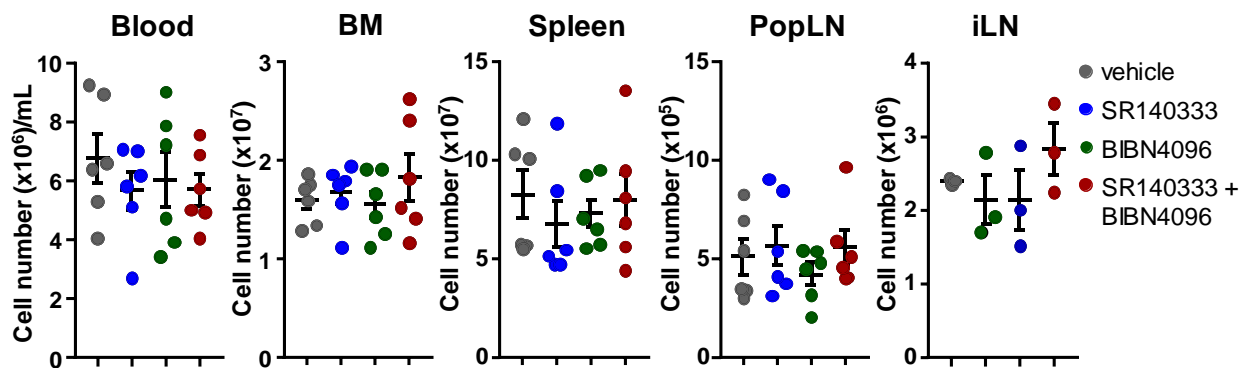


**Figure 3.44** Cellularity of bone marrow, spleen, popLN, iLN and blood after chronic neuropeptide antagonism

SR140333 and BIBN4096 were given daily individually or in combination for a week. Cellularity in 4 organs and circulating leukocyte counts were monitored. n = 3-6. One-way ANOVA, Tukey's post-test.

The only studied population, which changed after neuropeptide antagonism, were neutrophils in the popLN (**Figure 3.45**). However, neutrophils were previously shown to be bystanders to the LN phenotype after denervation. This finding showed that sensory neuropeptide antagonism did not change popLN cellularity

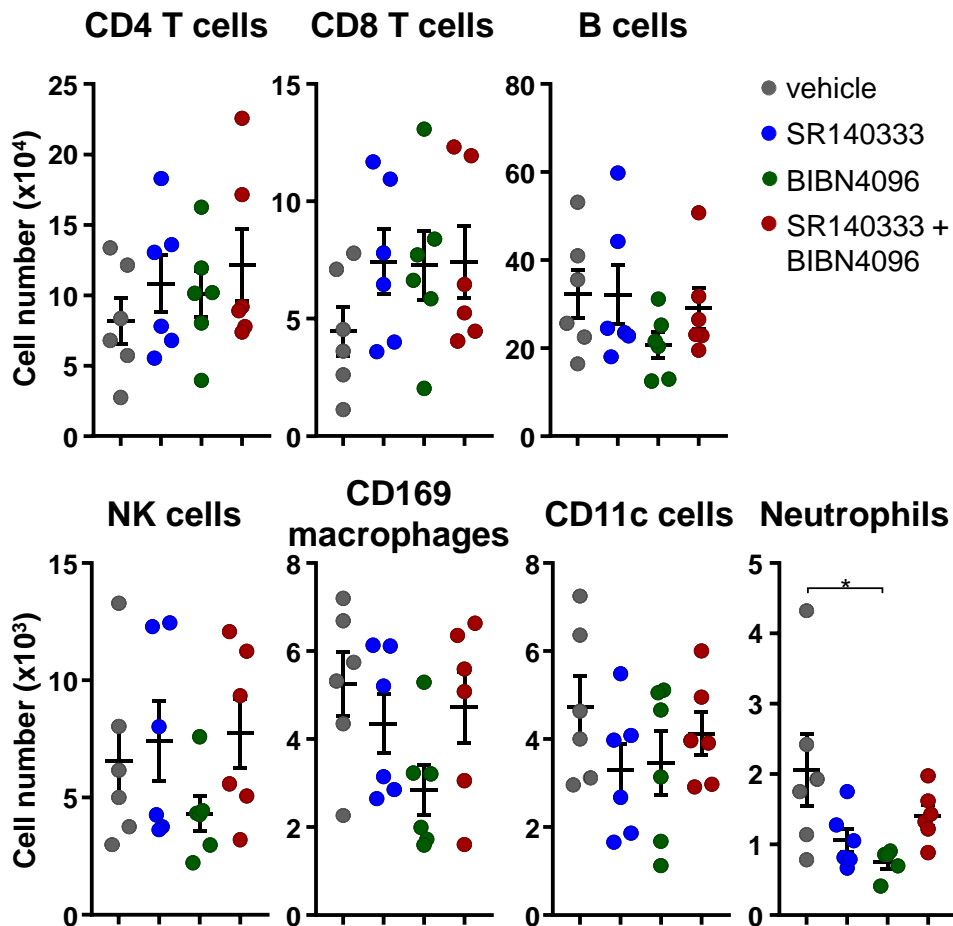


**Figure 3.45 Immune subsets in the popLNs after chronic neuropeptide antagonism**

SR140333 and BIBN4096 were given daily individually or in combination for a week. PopLN cellularity was analyzed by flow-cytometry.  $n = 6$ . One-way ANOVA, Tukey's post-test.  $*p < 0.05$ .

### 3.23 SP and CGRP agonism counteract the nodal expansion induced by sciatic denervation

Sciatic denervation leads to loss of neural substance secretion in the leg. However, inhibition of SP and CGRP by themselves did not reproduce the phenotype of nodal expansion (**Figure 3.45**). It was next investigated whether antagonizing or adding SP and CGRP could enhance or attenuate denervation-induced nodal expansion. Treatment of animals with neither SR140333 or BIBN4096 separately nor combined inhibited denervation-induced nodal expansion (**Figure 3.46**) or spleen cellularity (**Figure 3.47**).

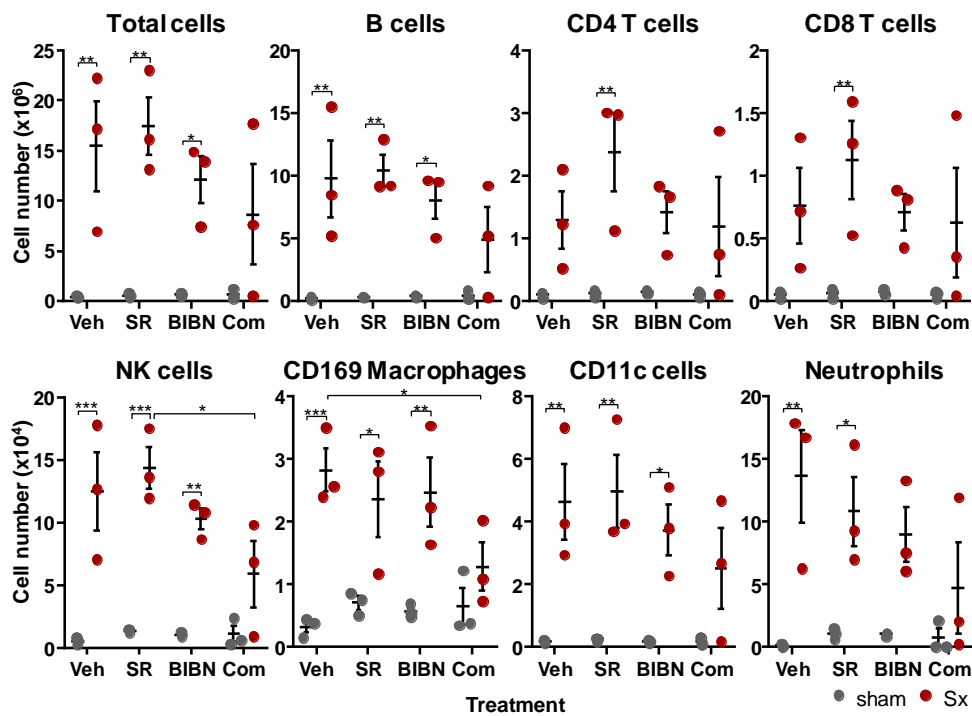


**Figure 3.46 PopLN cellularity after unilateral sciatic denervation surgery in combination with neuropeptide antagonism**

Mice were treated with SR140333 and/or BIBN4096 daily until the mice were sacrificed. PopLN cellularity was assessed one week after denervation. n = 3. Two-way ANOVA, Tukey's post-test. \*p < 0.05, \*\*p < 0.01, \*\*\*p < 0.001.

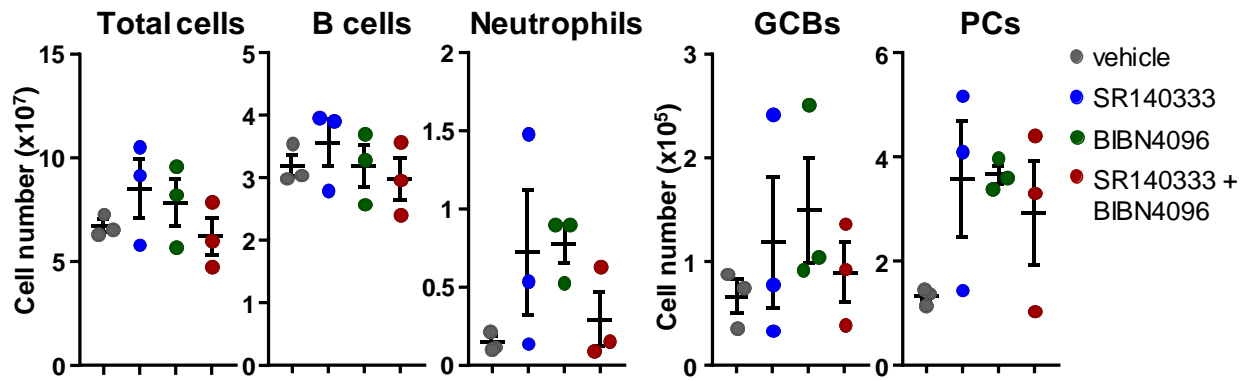


**Figure 3.47 Splenic cellularity after unilateral sciatic denervation surgery in combination with neuropeptide antagonism**

Mice were treated with SR140333 and/or BIBN4096 daily until mice were sacrificed. Splenic cellularity was checked one week after denervation. n = 3. One-way ANOVA, Tukey's post-test.

On the other hand, giving neuropeptides as agonists together with denervation suppressed the amplitude of denervation-induced cellularity, specifically of CD11c cells, T cells and neutrophils (**Figure 3.48**). The smaller increase in CD11c and T cell numbers indicated a weaker activation of adaptive immunity which was reflected by inferior expansion of B cells in the groups receiving SP and/or CGRP, although not statistically significant (**Figure 3.48**).

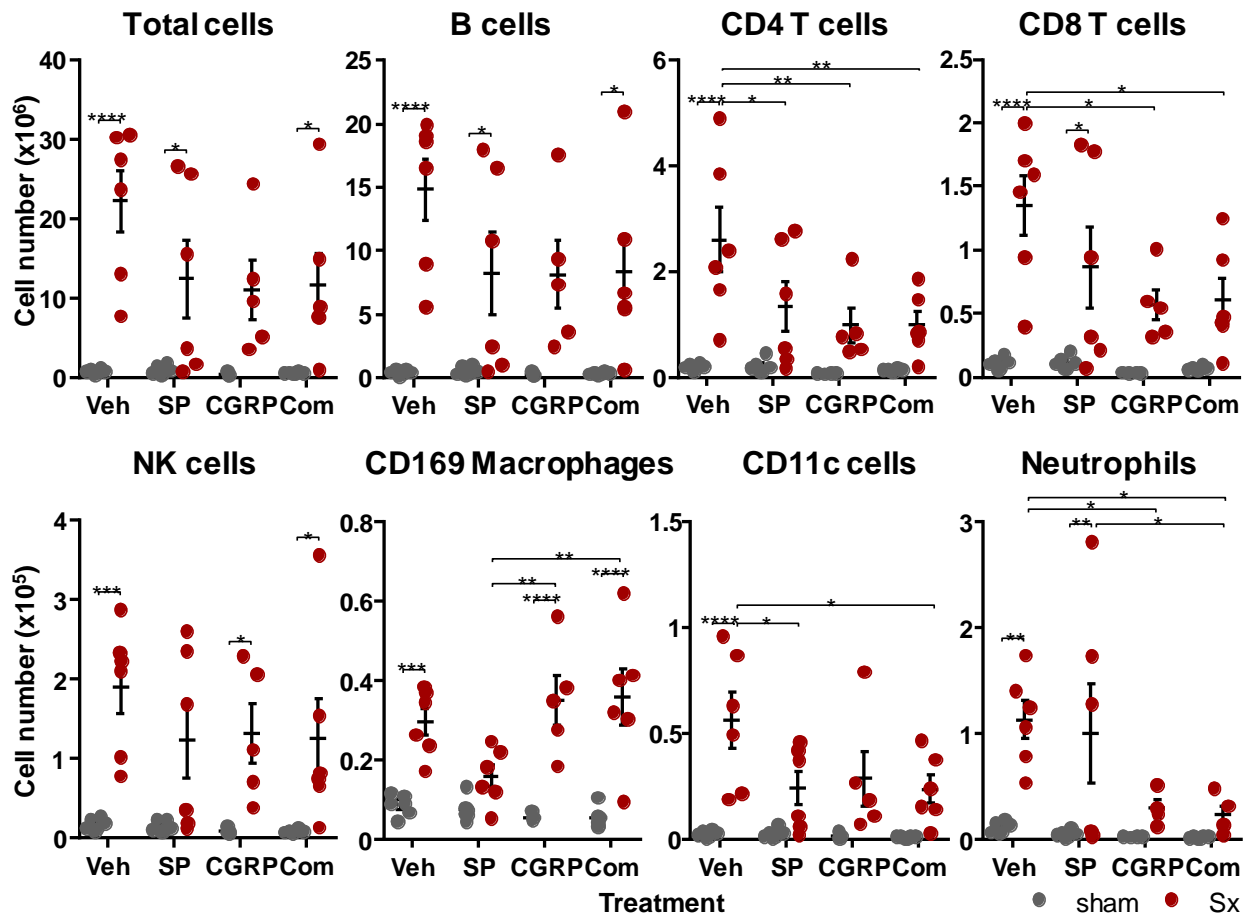


**Figure 3.48 PopLN cellularity after the unilateral sciatic denervation surgery in combination with neuropeptide agonism**

Mice were treated daily with SP and/or CGRP until mice were sacrificed. PopLN cellularity was assessed a week after denervation.  $n = 5-6$ . Two-way ANOVA, Tukey's post-test. \* $p < 0.05$ , \*\* $p < 0.01$ , \*\*\* $p < 0.001$ , \*\*\*\* $p < 0.0001$ .

Repressed activation by neuropeptide treatment did not only occur in the popLNs but also in the spleen. Mice treated with neuropeptide, despite receiving the same unilateral sciatic denervation, exhibited lower numbers of GCBs and PCs in the spleen compared with the vehicle-treated group (**Figure 3.49**).

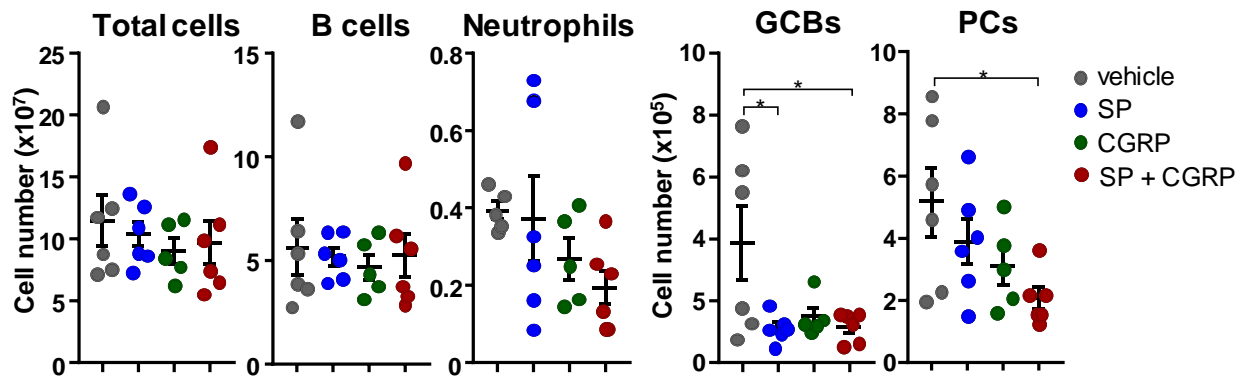


**Figure 3.49 Splenic cellularity after the unilateral sciatic denervation surgery in combination with neuropeptide agonism**

Mice were treated daily with SP and/or CGRP until mice were sacrificed. Splenic cellularity was assessed one week after denervation. n = 6. One-way ANOVA, Tukey's post-test. \*p < 0.05.

To conclude, antagonism of SP and CGRP receptors alone did not reproduce nodal expansion (**Table 3.2**), the phenotype after sciatic denervation, indicating the existence of contributing factors. However, combining denervation surgery with neuropeptide agonism showed an abrogated increase in numbers of key lymphocytes and CD11c cells, pointing out the inhibitory effects of neuropeptides in this system (**Table 3.2**).

Organ	Cell type	Antagonism			Agonism		
		SP	CGRP	SP+CGRP	SP	CGRP	SP+CGRP
popLN	Total cells						
	B cells						
	CD4 T cells				—	—	—
	CD8 T cells					—	—
	NK cells						
	CD169 Macrophages				—*		
	CD11c cells				—	—*	—
	Neutrophils					—	—
spleen	Total cells						
	Neutrophils						
	B cells						
	GCBs				—		—
	PCs						—

**Table 3.2 Summary of effects of neuropeptide antagonism or agonism on cell numbers in popLNs after denervation**

Mice underwent unilateral Sx and were treated by either agonist(s) or antagonist(s) of neuropeptide(s) for a week. Numbers of total cells and subsets of popLNs and spleens after denervation are summarized. The comparisons were made between vehicle treated and experimental groups. In the original figures, difference between groups were evaluated by One-way (spleen) or Two-way ANOVA (popLN) and then Tukey's post-test. n = 3-6. Minus symbol (—) notes inhibition of expansion of indicated cell type under particular treatment. —p < 0.05, — —p < 0.01. \*showing trend, but not statistically significant.

## 4 Discussion

### 4.1 Overview

Interactions between the nervous and immune systems are bidirectional communications. Actions from the immune system such as cytokines engagement or pathogenic T cell infiltration of the brain, spinal cord and peripheral nerves create sensory perceptions or autoimmune responses [324]. Nerves can actively influence immune responses by releasing functional neural substances [78, 272, 274, 280, 282]. The latter has been observed in the cases of infections [84, 85, 299, 304] and neural injuries [14, 17], in which the nervous system takes actions to combat infectious or traumatic perturbations. However, whether and how nerve-driven immunomodulation is controlled in a regional manner in homeostasis and pathology has not yet been made clear. Furthermore, whether neural injury causes long-term immune outcomes has not been assessed. To understand the mechanistic details is challenging because there are functionally diverse neural substances from different nervous subsets, and various physiological functions controlled by nerves, such as muscle contraction, which might in turn affect lymph flow and ensuing immune responses.

In this project, the popliteal lymph node (popLN) was chosen as the research object because it can facilitate adaptive immunity (which ties to immune memory), has a clear drainage area and is innervated by the sciatic nerve, which can be accessed by surgical approaches. This enabled studying the regional immune responses in the popLN and its drainage area under local manipulation of neural tones. Immune cell numbers, chemokines and cytokines were assessed and quantified after surgical operations. To tackle the problem of high complexity of neural substances, nerves were grouped by their functional properties, such as sympathetic and sensory nerves, and examined individually by surgical or pharmacological methods.

Paw swelling and popLN expansion were observed after sciatic denervation (Sx) due to an increase in leukocyte numbers (**Figure 3.1, Figure 3.2, Figure 3.9 and Figure 3.17**). At the cellular level, different immune subsets exhibited different dynamics of popLN infiltration and resulted in vigorous formation of germinal centers (GCs), which leads to

increased circulating immunoglobulin G (IgG) levels (**Figure 3.24**, **Figure 3.30** and **Figure 3.36**). These antibodies did not recognize general self-nuclear antigens as some autoreactive antibodies do (**Figure 3.37**). Given that blockade of major histocompatibility complex class II (MHCII) suppressed nodal expansion after denervation, the reaction was likely antigen-dependent (**Figure 3.32**). To identify causative neural tones, subset-specific depletion of nerves was conducted. None of the neural subtype ablations studied drove popLN cellularity higher (**Figure 3.31**, **Figure 3.34** and **Figure 3.35**). However, Sx led to lesser nodal expansion once substance P (SP) and calcitonin gene-related peptide (CGRP) were given systemically (**Figure 3.48** and **Figure 3.49**). These results suggest that denervation causes an antigen-dependent response with excessive serum IgG, which can be tuned down by administration of SP and CGRP.

## **4.2 Main phenotypes of sciatic denervation – popliteal lymph node expansion and paw swelling**

To shut down the neural tones in the leg, both femoral and sciatic nerves were resected. In this condition, ipsilateral popLNs and paws were found to be expanded (**Figure 3.1**). Paw leukocyte populations and popLN cellularity strongly increased in the denervated condition, indicating the steady state was shifted toward inflammation in denervated popLNs and paws (**Figure 3.2**, **Figure 3.9** and **Figure 3.17**). However, a report from Kubera et al. studying how nerves influence the host-versus-graft (HvG) and graft-versus-host (GvH) reactions obtained different results. In that paper, unilateral Sx itself did not increase the size of denervated popLNs after a week to 10 days, but additional transference of splenic cells elicited stronger responses in the denervated popLN of both HvG and GvH groups [325]. This observation suggests that denervation alone does not change popLN cellularity but rather increases its reactivity to further stimulation. Compared to the system in this project, the paper applies the same surgical approach but uses a different mouse line. The recipient mice in the GvH group are the F1 of C57BLxCBA which do not exhibit autonomous denervation-induced nodal expansion, whereas the C57BL6/N mice used in this project do. The real reason for differing results between the two studies remains unclear but may be mouse-strain dependent.

#### 4.2.1 Direct innervation of the popliteal lymph node by the sciatic nerve

To examine which nerve causes nodal expansion, individual denervation of the sciatic or femoral nerve was performed and the Sx successfully reproduced the nodal expansion phenotype of double denervation (**Figure 3.3**). This result shows that sciatic but not femoral denervation is required for the nodal expansion phenotype, prompting the next question: What makes the sciatic nerve special for the popLN responses? Iannacone et al. injected vesicular stomatitis virus (VSV) into the footpad of CD169 macrophage-deficient mice and found the lethality due to viral dissemination to the central nervous system was prevented by sciatic nerve resection [198]. They focused on the antiviral role of CD169 macrophages in the popLN but also showed the direct innervation of popLN by the sciatic nerve. Based on this study, the direct innervation of popLN by the sciatic nerve may be the key to explain why only cutting the sciatic but not femoral nerve contributes comparable nodal expansion. A hypothesis that direct innervation is critical for popLN responsiveness or sensitivity was therefore proposed. A surgical method – ankle denervation (ANKx) – bypassing the popLN but denervating its drainage area was then developed to test this hypothesis (**Figure 3.4**).

Histology analysis revealed that Sx generated paw inflammation on the denervated side but not the sham side whereas ANKx elicited paw inflammation even on the sham side (**Figure 3.6**). ANKx requires opening of skin encircling the ankle to expose three major branches of the sciatic nerve and the operation itself causes a certain degree of tissue disruption. This resulted in the paw skin thickening regardless of denervation. The popLN drains the paw so it in fact responded to this perturbation by having more cells (**Figure 3.7A**). This effect was stronger on the denervated side but neither ANKx nor sham of ANKx produced comparable nodal expansion to Sx (**Figure 3.7A**). Given that the ANKx-sham operation itself generated an inflammatory background, which was substantially higher than the Sx-sham group, the denervation data were normalized to their respective sham controls for comprehensive comparisons. Sciatic denervation at hip level expanded popLN cellularity to about 13-fold but denervation at the ankle level had less than doubled (**Figure 3.7B**). This result, together with individual denervation of the femoral or sciatic nerve, highlights the importance of direct innervation of the popLN by the sciatic nerve.

However, there is an argument that the limited arousal effects of ANKx on popLN cellularity is due to being the relative small portion of popLN's drainage area. Another concern was whether afferent lymphatics were concurrently cut in ANKx, but this was later proven wrong (**Figure 3.5**). To elucidate the relationships between size of denervation portion, degree of paw swelling and popLN cellularity, surgeries creating distinct degrees of denervation were designed to understand the dependence of these phenotypes (discussed in **4.2.4**).

#### **4.2.2 Dead nerve-induced immune responses**

Axotomy triggers WD involving demyelination and immune reactions to the distal stump [22], indicating that the distal fragment of the nerve activates immune responses. Whether the nodal expansion phenotype observed after Sx is a coherent event driven by degradation of dead nerves was examined using autologous transplantation of the sciatic nerve (**Figure 3.22**). In that case, both legs contained a separated nervous segment, but one leg was intact and the other was denervated. PopLNs receiving both transplant and sham surgery of denervation did not develop nodal expansion a week after the surgeries (**Figure 3.23**). This result almost rules out the dead nerve-induced immune response to be the key contributor for denervation-induced nodal expansion. The only concern is whether the transplant segment has immunogenic competence even if it is not connected to recipient vasculature. This might interfere with recruitment of immune cells to the lesion via circulation. However, this issue of having isolated vasculature is unlikely to be the decisive factor, which prevents nodal expansion because dead nerves left by femoral, and ankle denervation with connected vessels did not induce nodal expansion (**Figure 3.3** and **Figure 3.7**). Together with previous findings, nodal expansion after denervation is more likely to be driven by loss of innervation, and partially associated with peripheral inflammatory responses in the drainage area.

### 4.2.3 Causes of paw swelling

Apart from the nodal expansion, Sx also led to paw swelling which was associated with increased leukocyte content (**Figure 3.9**), but even so, denervation was found to reduce cell density in paws (**Figure 3.8**), meaning that an increase of either cell size or interstitial fluid occurred. The former cause of swelling is supported by many clinical cases in which patients suffering from trauma-caused muscle denervation develop muscle hypertrophy (enlargement of muscle fibers) or pseudohypertrophy (due to an increase of fat tissues within muscle bundles) [319]. However, the forward scatter of denervated samples was not higher than the forward scatter of sham-operated samples in flow cytometry (data not shown), indicating that paw swelling was not driven by alternation of cell size. The latter cause can be examined by Evans Blue permeability assay. This assay was conducted but unfortunately the photon absorbance levels from such tiny pieces of tissue were below the detection limit. Besides, the harvesting method was too disruptive to retain the interstitial fluid as bone removal was necessary. However, during harvesting, it was noted that denervated paws had less tissue resilience against mechanical pressure and more fluid escaped, suggesting the latter reason is more likely.

Histamine is recognized to associate with allergy and inflammation, creating local edema and leukocyte infiltration [326, 327]. Typical histamine-releasing cells are mast cells, basophils, enterochromaffin-like cells and neurons. However, histidine decarboxylase, which synthesizes histamine, is widely expressed in immune cells such as neutrophils, macrophages, dendritic cells (DCs) and T cells [328]. The functions of histamine are diverse, and vary according to the receptors stimulated, their coupled G-proteins, and the recipient cell types [326-328]. Histamine can bind to 4 receptors with different histamine affinities and functions: in general histamine H1 to 4 receptors (H1R, H2R, H3R and H4R) fulfill allergic responses, gastric reactions, neurotransmitter's roles and immune modulations respectively [326-328]. These diverse effects are linked to the G protein coupled to each receptor – Gq (H1R), Gs (H2R), and Gi (H3R and H4R) (**Table 4.1**). Paw swelling could potentially be a response of the skin due to release of histamine. Using the model of *Potamotrygon motoro* stingray venom (PmV) injection in mouse paws, Kimura et al. found H1R, H3R and H4R antagonism and cromolyn – a mast cell granule stabilizer – can reduce PmV-induced edema and leukocyte infiltration [329]. Cetirizine (CTZ),

initially known as H1R antagonist but later found to have inhibitory functions at H4R as well [328], elicited a reduction of paw swelling by roughly 40% (**Figure 3.14**) and a lower paw leukocyte content (particularly of neutrophils) (**Figure 3.15**), agreeing with the findings of Kimura et al. [329]. Therefore, denervation-induced paw swelling is likely due to histamine release and H1R and/or H4R signaling.

**Table 4.1 Histamine receptors: expression, signaling and immune functions**

Receptor	GPCR $\alpha$ -subunit	Expression	Intracellular signals	Immunological activity
H1R	$G\alpha_q$	Smooth muscle cells, endothelial cells, nerve cells, epithelial cells, neutrophils, eosinophils, monocytes, macrophages, DCs, T and B cells	PLC, PIP2, DAG, IP3, $Ca^{2+}$ , PKC	Allergic reactions and inflammation, histamine release, eosinophil and neutrophil chemotaxis, antigen presentation ability, Th1/IFN- $\gamma$ activity, and recruitment of Th2 cells; decreases humoral immunity and IgE production
H2R	$G\alpha_s$	Smooth muscle cells, endothelial cells, nerve cells, epithelial cells, neutrophils, eosinophils, monocytes, macrophages, DCs, T and B cells	Adenylate cyclase, cAMP, PKA, CREB, EPAC	Increases IL-10 production and humoral immunity; decreases cellular immunity; inhibits Th2 cells and cytokines, chemotaxis of eosinophils, and neutrophils; suppresses IL-12p70 of MoDCs
H3R	$G\alpha_{i/o}$	Histaminergic neurons, monocytes, eosinophils	Inhibits adenylate cyclase and cAMP, increases $Ca^{2+}$ levels	Control of neurogenic inflammation, increased proinflammatory activity, and antigen presentation capacity
H4R	$G\alpha_{i/o}$	Eosinophils, DCs, Langerhans cells, neutrophils, T cells, basophils, mast cells	Inhibits adenylate cyclase and cAMP, increases $Ca^{2+}$ levels	Affects pDC and mDC functions, Th1/Th2 differentiation, eosinophil and mast cell chemotaxis, IL-6 production, leukotriene B4, and migration of $T\gamma/\delta$ cells; increases IL-17 secretion by Th17 cells, and regulatory T recruitment; suppresses IL-12p70 of MoDCs

**Table 4.1 Histamine receptors: expression, signaling and immune functions**

The original tables are published in [330] and [331]. This table combined the information from those reviews to provide an overview of immunological functions of histamine signaling.

In neurogenic inflammation, SP and CGRP released by nerves drive mast cell degranulation and histamine secretion which, in return, positively stimulates nerves to release SP and CGRP [332]. The sensory events generated by this axis are hypersensitivity and itching, which can be blocked by inhibiting H1R and H4R [333]. Loss of neural vesicular regulation by cutting nerves results in the release of neural substances at distal nervous ends. This mechanism involving the neuropeptide-histamine axis can explain the observations of denervation-induced swelling and increase of leukocytes in paws.

Natural killer (NK) cells, B and T cells, neutrophils, macrophages and dendritic cells express H1R and/or H4R [326]. Among all the immune subsets investigated in this project, CTZ treatment significantly reduced the number of neutrophils and a particular DC subset – CD103<sup>+</sup> DCs – in the paw after denervation (**Figure 3.15**). Even so, reduction of total leukocytes in denervated paws after CTZ treatment were mild and did not reach significant levels (**Figure 3.15**), indicating that there are other pathways controlling leukocyte infiltration in addition to H1R and H4R signaling. Moreover, the vasodilation activity of histamine can account for the increased interstitial fluid in denervated paws. These findings suggest that histamine, either mast cell-derived or neurogenic, is one of the contributors of denervation-induced paw swelling and leukocyte infiltration (**Figure 4.1**). The role of another mast cell mediator, tumor necrosis factor alpha (TNF $\alpha$ ), in the LN is discussed in **4.2.4.5**.

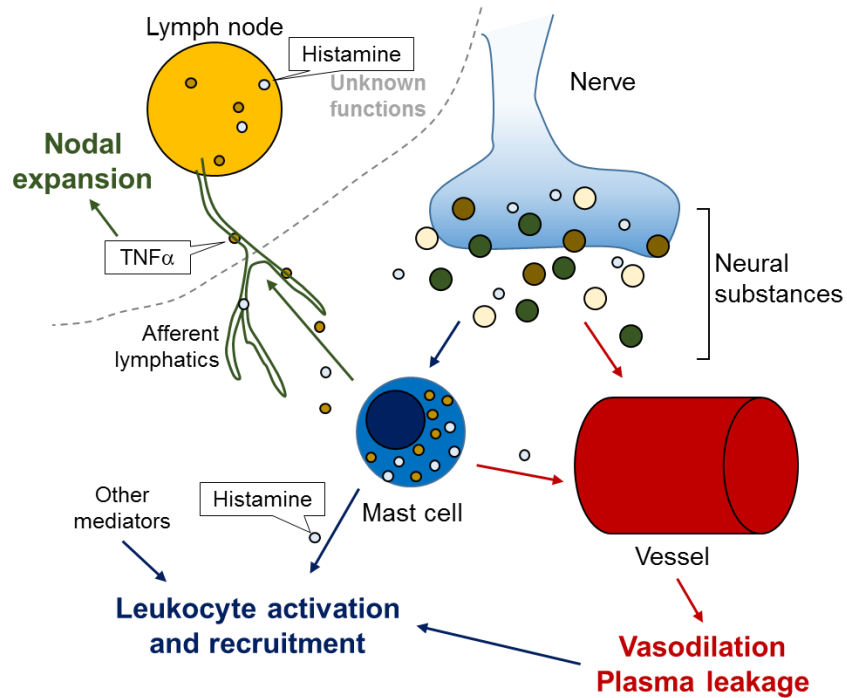


**Figure 4.1 The cascade of neural substance-driven local swelling and lymph node activation**

The neural substances induce vasodilation and plasma leakage directly or indirectly via stimulating mast cell-derived histamine. Increased vessel permeability as well as direct actions of histamine on immune cells facilitates leukocyte activation and recruitment. TNF $\alpha$  and histamine are released concurrently during mast cell degranulation. Interestingly, nodal hypertrophy during infection is selectively enhanced by TNF $\alpha$  but not histamine [314]. However, CTZ treatment blocked denervation-induced nodal expansion (**Figure 3.16**), differentiating the role of histamine between infection and neural injury models.

#### 4.2.4 Dependence of phenotypes

Looking at the dynamics of these phenotypes, paw thickening was an acute event which peaked at day 1, started to recess, and returned to baseline at day 7 (**Figure 3.2A**). While paw swelling had decreased to normal levels by day 7, popLN cellularity was still in the growth phase, and began to decline after week 3 (**Figure 3.2B**). Chronologically, the paw phenotype occurred much earlier than the popLN phenotype, making the reaction in the paw likely to be a cause of the popLN phenotype. Their dynamics suggest that paw swelling and nodal expansion are either independent events with difference paces or that the latter depends on the former due to the order of occurrence. To test this, different

branches of the sciatic nerve were cut and the degree of paw swelling and level of cellularity increase in the popLNs were compared. Moreover, these two phenotypes seem not to be sustainable given they showed a trend of recession, suggesting the initiators of these phenotypes were acute and transient.

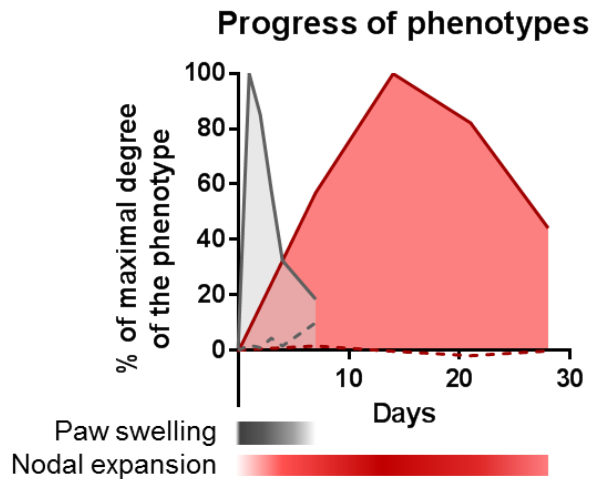


**Figure 4.2 Magnitude of paw swelling and nodal expansion during the time after denervation**

Data from **Figure 3.2** were re-scaled and merged into the same graph for comparison of dynamic of phenotypes. Peaks of mean measured values were set as 100% and the mean values of sham group at D0 were 0%. Grey line: paw thickness; red line: popLN cellularity. Solid line: the denervated side; dash line: the sham side.

#### 4.2.4.1 Paw swelling quantification

Continuous measurement of paw thickness creates a profile of pathology progression during a period of time. However, due to having 3 parameters – innervation status, time, and branch(es) cut – comparison between groups was difficult (**Figure 3.10**). By integrating the area between lines of intact and denervated over time, these two factors were compressed into one with the unit of area under the curve (AUC) for simpler comparisons (**Figure 3.11**). This method is also more intuitive visually. However, it sacrifices details of trends at specific times and can overlook important information (discussed in **4.2.4.4**).

#### *4.2.4.2 Single and dual denervation*

In the branch denervation dataset, nodal expansion reflected paw swelling levels in single denervation groups but not in dual denervation groups (**Figure 3.11** and **Figure 3.12**). Therefore, a simple model that nodal expansion represents size of denervation cannot explain cases of two branches denervation, and further suggests cross-talk or compensation between nerves once some nerves are cut and others are left intact. The idea of interactions between intact nerves and denervated tissues resembles the spared nerve injury (SNI) model designed to study peripheral pain by cutting two branches of the sciatic nerve. Denervation of the common peroneal nerve (CPN) and the tibial nerve (TN) affects mechanical sensitivity and thermal responsiveness of neighboring nerve territories [334], indicating that sensory changes in the areas remaining innervated to be driven by loss of innervation in the nearby areas. The principle of SNI can be a possible mechanism accounting for the relation between popLN cellularity and paw swelling levels in the dual denervation groups.

#### *4.2.4.3 Paw swelling levels, denervation degrees and popliteal lymph node cellularity*

In the branch denervation experiments, groups exhibited different denervation areas, paw swelling levels and popLN cellularity (**Figure 3.11** and **Figure 3.12**). Correspondence analyses showed subtle correlations between nodal cellularity and denervation degree or swelling level (**Figure 3.13AB**), but a substantial link between paw swelling levels and denervation degrees (**Figure 3.13C**). These results together with the chronological progression of nodal expansion and paw swelling (**Figure 3.2** and **Figure 3.13**) illustrate a plausible conclusion that denervation confers different paw swelling levels by size of the nerve, but this correlation only loosely transfers to nodal expansion. PopLN definitely reflects local immune status at some degrees but precise regulation of popLN cellularity might involve more complicated circuits. Therefore, the theory of SNI involving effects of neighboring denervated tissues might be a way to explain the observations here.

#### 4.2.4.4 A paw swelling resolution model

Looking at the paw thickness curve rather than the AUC of paw swelling in the branch denervation experiments, thickness of the denervated paws in groups All and CPN+SN had still not returned to basal level by day 7, graphically appearing like opened jaws (**Figure 3.10**). This pattern seems to relate to the popLN cellularity because these two subgroups had the highest popLN cellularity in the dataset and the CPN+SN group with the widest opened jaws also had the highest popLN cellularity (**Figure 3.12**). Based on this fact, the popLN cellularity might be influenced by the paw swelling at the last day (day 7), suggesting groups failing to resolve the swelling have greater nodal expansion. If this holds true, the factor controlling this process would be very important to predict nodal expansion.

The paws which had the sural nerve (SN) spared resolved the swelling at D4, quicker than those which had the SN cut (**Figure 3.10**). This observation renders the SN potentially a component of resolving paw swelling. Cutting only SN had very little impacts on paw swelling (**Figure 3.11**) and subsequent popLN cellularity (**Figure 3.12**). Cutting the CPN seems to be a driver of paw swelling and nodal expansion. This is compatible with the data of groups All, CPN, CPN+SN. In All and CPN+SN groups, losing resolution force (SN) and having pro-inflammatory power (CPN) together caused opened jaws and nodal expansion. The open jaw was not observed in the CPN group which still retained the SN innervation (**Figure 3.10** and **Figure 3.12**). In this assumption, loss of the CPN can drive paw swelling but has nothing to do with resolution. Loss of the SN can have little effects on initiation of swelling but plays the key role in resolution of swelling which then determines level of nodal expansion. This sounds reasonable and fits the data. However, the effects of cutting the TN are hard to define.

Cutting the TN alone caused paw swelling which was resolved early but still caused substantial nodal expansion (**Figure 3.10** and **Figure 3.12**), suggesting loss of the TN can lead to paw swelling. According to the previous theory, cutting the SN in addition to the TN should have sustained the paw swelling and led to nodal expansion. However, this did not occur in TN+SN group (**Figure 3.10** and **Figure 3.12**), suggesting that loss of the TN regained the resolution power. This can explain the phenomena in CPN+TN group having the TN cut and the SN with extra resolution power. If this is true, TN denervation imposes

two contradictory forces to paw swelling: one is positively driving it, and the other is facilitating resolution. When it comes to single denervation, the pro-inflammatory momentum is dominant and in the cases of dual denervation then it depends on the balance of swelling drivers and resolvers. Collectively, effects of sciatic branch denervation on paw swelling involves complex crosstalk between neural territories and different levels of immobility issues. According to the empirical data (**Figure 3.10**), a two-factor system consisting of swelling initiation and resolution is proposed (**Table 4.2**). It would be interesting to incorporate neurology to study contributions of each branch on peripheral swelling/edema in the future.

**Table 4.2 Proposed effects of sciatic branches on paw swelling**

Nerve	Denervation	
	Swelling initiation power	Resolution power loss
CPN	+++++	+
TN	+++ (single denervation)	+/-
SN	+	+++++

**Table 4.2 Proposed effects of sciatic branches on paw swelling**

In this model, paw swelling is taken as the outcome of two proposed contributors, swelling initiation and resolution, based on the empirical data (**Figure 3.10**).

This hypothesis of the resolution model takes the paw swelling at day 7 as the net result of the two forces and this outcome might decide the level of paw swelling and correlate with nodal expansion level. The feature of this model is instead of taking any single branch as either pro-swelling or anti-swelling, it divides the influence of branch denervation into two factors – driver and resolver. This model can explain the phenomena in the branch denervation dataset and using the net result at day 7 to link paw swelling and nodal expansion. This requires displaying paw thickness in a time-based plot to see how well the swelling resolved, which would not be seen if only the AUC compression method had been used. It also implies that the endpoint, rather than the process of paw swelling, is more relevant to nodal expansion. This hypothesis of how the paw and the popLN react to high level interactions between nerves and their territories might take another whole project to study.

#### 4.2.4.5 Targeting paw swelling

To further confirm if paw swelling and increased paw leukocyte numbers are required for popLN enlargement, CTZ was selected to treat mice before the denervation operation. CTZ treatment reduced tissue swelling by 40% (**Figure 3.14**) and leukocyte content from about 7% to 2.5% (**Figure 3.15**) in denervated paws. Although these effects were not statistically meaningful, nodal cellularity expansion was significantly suppressed by CTZ treatment (**Figure 3.16**). These data positively correlate leukocyte numbers in the drainage area and tissue swelling with popLN expansion. Given that CTZ treatment had more pronounced effects in the popLN than in its drainage area (**Figure 3.14**, **Figure 3.15** and **Figure 3.16**), this dataset points out the importance of histamine, H1R and H4R in denervation-induced LN responses.

How does histamine participate in immune responses, especially adaptive immunity in LNs and how does it relate to neural injury? Histamine in nerves has been known for more than 70 years decades [335]. The sources of histamine can be neurogenic (histaminergic nerves) or non-neural cells (mast cells and basophils). In the peripheral WD model, Olsson and Sjöstrand found endoneurial mast cells to start to proliferate in the distal end of the resected nerves 3 days after the operation [336]. Those mast cells degranulate to release histamine after Sx [337]. Mast cells are believed to facilitate DC activation and create a more permeable environment for leukocyte extravasation and cytokine diffusion by secreting not only histamine but SP, CGRP, interleukins, prostaglandins, interferons and chemokines [338, 339]. Degranulation of mast cells results in concurrent release of multiple soluble mediators including tumor necrosis factor alpha ( $\text{TNF}\alpha$ ) and histamine. These mediators control the magnitude and duration of immune responses. Specific to adaptive immunity,  $\text{TNF}\alpha$  but not histamine derived from mast cells in the infection condition promotes expression of vascular cell adhesion molecule 1 (VCAM1) which drives local recruitment of lymphocytes to the LN [314]. This finding links peripheral mast cells to expansion of LNs where the adaptive immunity develops. Notably, histamine injection together with bacterial infection to mast cell-deficient mice does not cause the nodal hypertrophy [314], but activation of histamine receptors, H1R and H4R, were required for denervation-induced nodal expansion (**Figure 3.16**). These results indicate

that histamine has different roles of facilitating adaptive immunity in the LN in infection and sterile injury models. Mast cells do not only affect lymph node and further adaptive immune responses via  $\text{TNF}\alpha$  but also closely collaborate with DCs for adaptive immunity [340]. Mast cells can transfer antigen-bound IgE to DCs, which then induces T cell proliferation [341]. *Vice versa*, DCs can equip mast cells with epitope-loaded MHCII via trogocytosis (a process in which immune cells, mostly lymphocytes, acquire surface molecules from antigen presenting cells by membrane conjugation) and MHCII-bearing mast cells preferably induce a type 1 immune response [342]. Given that MHCII is the key molecule for antigen presentation in the secondary lymphoid organs, mast cells might not only influence adaptive immune immunity via histamine but also MHCII. It is then important to understand what happens in the enlarged popLNs.

### 4.3 Reactions in the popliteal lymph node

Denervated popLNs exhibited significant enlargement. This expansion comprised substantial increase of the overall cellularity (**Figure 3.2B**), which was supported by a broad-range expansion of analyzed leukocyte subsets (**Figure 3.17A**). Vigorous expansion was observed specifically before the second post-surgical week followed by maintenance and recession phases (**Figure 3.2B** and **Figure 3.17A**). In a week after Sx, the denervated popLN contained 8~30 times more cells than the contralateral one (**Figure 3.3** and **Figure 3.17B**). Profiling immune subset progression by flow-cytometry on this stage revealed cell type-dependent multiphasic expansion behaviors (**Figure 3.17B**). There were a few key features: (1) numbers of all investigated cell types kept increasing within the week and reached relatively high levels at day 7; (2) expansion of T and B cells and resident DCs began slowly but grew quickly later; (3) CD169 macrophage numbers expanded stably; (4) Migratory DCs, NK cells and neutrophils were early peaking cell types, meaning their population grew quickly at the beginning and slowed down later (**Figure 3.17B**). These features show that the nodal expansion after Sx is a non-selective process, affecting all the cell types, but distinct cell types might play roles at different stages because their progression curves are different. Besides, the B cell population was the dominant cell type especially at day 7, covering about 50% of popLN cellularity (**Figure**

**3.17B**). This implies that a reaction involving B cells might be dominant after Sx. Stromal populations increased as well (**Figure 3.18A**). Compared to leukocytes, the stromal compartment showed less of an increase (<4-fold) (**Figure 3.18A**). This leukocyte-stromal cell non-proportional expansion was reflected by reduced density of High endothelial venules (HEVs), which serve as ports of entry of circulating leukocytes to LNs (**Figure 3.18B**). No matter what the reactions in denervated popLNs are, expansion of cells requires a change of migratory equilibrium and/or *in situ* proliferation and these rely on driver cells to initiate the scenario and a supportive microenvironment to sustain it.

#### 4.3.1 Migratory momentum

Intravenously injected cells from spleen and LNs preferably entered the denervated popLN rather than the intact one in the same animal (**Figure 3.24A**). This means leukocyte homing via blood is enhanced on the ipsilateral side after Sx. Homing seems to be critical for denervation-induced nodal expansion because blockade of adhesion molecules such as  $\alpha4/\alpha L$ -integrins, L-selectin and PNA<sub>d</sub> reduced the level of expansion (**Figure 3.24B**). These data render HEVs important compartments after Sx because HEVs are gates for leukocytes in the circulation to enter LNs [250]. Although LN vessels are well accepted to be innervated by several kinds of nerves [179, 181, 182], there is no literature directly linking HEV functions with nerves in LNs. However, vagal stimulation is reported to promote permeability of postcapillary and collective venules in the lung epithelium [343], so there are some precedents for nervous regulation of vascular permeability. Olivier et al. found that formation of tertiary lymphoid tissues in a colitis model requires innervation by the vagus nerve potentially supporting stromal organizer cells to seed [344]. This process seems critical for the development of tertiary lymphoid tissues but functions of the vagus nerve afterwards might still be influential given that vagal activation is able to control leukocyte trafficking via regulating venular junctions [343]. However, to link HEV functions with possibly vagal innervation requires verification of proximal innervation to the LN and characterization of the local vagal secretion because venules in the lung epithelium are controlled by vagal sensory axons [343].

Apart from homing, egress is the other force affecting leukocyte dwell time in LNs. Decline of cells in LNs in certain periods of time mirrors the egress rate. It was not different between intact and denervated popLNs at day 7 (**Figure 3.25**), but this might not be the case in the initiation phase. During immune responses, T cell receptor (TCR) activation triggers phosphorylation of Myosin IIA protein to slow down T cell motility [345]. This activation-associated response potentially increases the dwell time of T cells for better antigen recognition in the LNs during immune responses. Therefore, reduced egress after Sx might be present at earlier time points once antigen specific responses take place in denervated popLNs.

#### **4.3.2 B cell proliferation**

In addition to migratory factors, local proliferation can also contribute to the increase of cells. B cells but not T cells were found co-localized with the proliferation marker Ki67, in the denervated popLN (**Figure 3.29A**). Quantification of proliferating B cell clusters revealed that only denervated but not intact popLNs contained these clusters (**Figure 3.29B**). There are two possible reasons for B cell proliferation. One is due to the engagement of mitogenic neural substances such as nerve growth factor (NGF) which promotes B cell division and synergizes interleukin 2 (IL2) signaling [346]. The other is activation due to antigen exposure. This has been described in the central nervous system (CNS) injury models such as traumatic brain injury (TBI) and spinal cord injury (SCI) involving antigens such as neurofilaments and myelin basic proteins (MBPs) [347]. In the Sx model, these two can happen simultaneously. The example of NGF is positive regulation of cell division by neural substances [346], but neurotransmitters can also negatively control cell proliferation. Systemic sympathectomy by 6-hydroxydopamine (6-OHDA) treatment stimulates LN cell proliferation within a week [348]. In a neural resection model, peripheral tissues might suffer a storm of neural substances when the nerve is newly cut and then lose all the neural inputs later. By 7 days after Sx, denervated popLNs should no longer receive neural inputs. However, these responses are sometimes antigen- and cell type-dependent, for example, from sympathectomized animals, T cells divide less upon concanavalin A stimulation, but B cells proliferate more upon

lipopolysaccharide (LPS) challenge [349]. Sx-induced B cell proliferation was then found to be a T cell-dependent B cell response, which is discussed in **4.4**.

### **4.3.3 Driver cells**

B cell proliferation and leukocyte recruitment to denervated LNs are the mechanisms supporting a denervation-induced nodal expansion phenotype. However, these two events cannot occur independently by themselves but need specific triggers to initiate. Chronologically, the earlier cell types infiltrating the LN are more likely to be those pioneers. From the previous results, neutrophils, NK cells and migratory DCs are candidates (**Figure 3.17B**).

#### *4.3.3.1 Neutrophils*

Effective antibody-based neutrophil depletion was confirmed by surface Gr-1 staining (**Figure 3.19A**) and size-granularity characterization (**Figure 3.19B**) in spleen and blood. Although neutrophils were greatly reduced in the system, this did not attenuate denervation-induced nodal expansion (**Figure 3.20**). Although neutrophils are early peaking in denervated popLNs, they seem to be bystanders because a reduction of neutrophils by 90% in blood and 80% in spleen did not affect denervation-induced nodal expansion. In fact, neutrophils can be recruited to the lesion for myelin removal when neural resection takes place [47]. This reaction peaks in a day [47] which fits to its peaking time in denervated popLNs (**Figure 3.17**). Therefore, early recruitment of neutrophils might be a part of the neural injury reaction. This finding implies that nodal expansion after Sx might consist of several reactions.

#### *4.3.3.2 Natural killer cells*

Using NK1.1 antibody two thirds of NK cells were eliminated (**Figure 3.21A**). However, this did not change the denervation-induced nodal expansion level (**Figure 3.21B**). Expansion of NK cells, similar to neutrophils, is more likely to be an independent event to

the nodal expansion. NK cell infiltration is disposable for driving the non-selective expansion in all analyzed immune subsets in denervated popLNs. However, NK cells as well as neutrophils and T cells are infiltrating to the injured nerve [350]. A later paper from Davies et al. further defined the role of these NK cells upon neural injury as cleaners and neural regeneration promoters [351]. Like neutrophils, NK cells can be recruited by damage signals but not the immune reaction in denervated popLNs. However, given that they mediate clearance of neural debris and complement WD [351], should they be negatively correlated to denervation-induced nodal expansion? Regarding neutrophils and NK cells, they definitely have roles in neural injury responses but their functions in LN immune reactions require a non-injury approach to examine, given that sciatic resection, the surgical approach, might trigger both injury and immune responses.

#### 4.3.4 The microenvironment

To further understand the reaction in the popLN after denervation, expression of common chemokines and cytokines was profiled by quantitative PCR (qPCR). *Rpl32*, showing stability between sham and denervated operations, was selected as an internal reference gene (**Figure 3.26**). In denervated popLNs, *the chemokine (C-X-C motif) ligand 12 (Cxcl12)*, *Cxcl13*, *Il1a*, *Il1b*, *Il6*, *Il10*, *Il12* and *Il17f* increased after Sx (**Figure 3.27**). The same upregulation signature was found in denervated paws but without *Il12* and with *Il17a* and *Tnfa* (**Figure 3.28**). Putting these data together revealed that gene expression profiles in denervated popLNs and paws were well-aligned with each other (**Table 3.1**). This correlation suggests that reactions in paws and popLNs are likely associated with each other and it seems to have an acute inflammation at the beginning and a high IL17A and IL17F-driven reaction at the late stage.

##### 4.3.4.1 Pro-inflammatory cytokines

TNF $\alpha$  and IL6 producing cells are largely upregulated in the injured nerves during neural injury [350]. There are many cell types that can secrete these cytokines in that condition. Schwann cells release IL6 3 hours after Sx [64], TNF $\alpha$  and IL1 $\alpha$  at hour 5, and IL1 $\beta$  at

hour 24 [65]. Circulating monocytes infiltrate to the lesion and differentiate into macrophages roughly at day 4 [49], and then these cells release IL1 $\alpha$  to stimulate Schwann cells [50]. Therefore, these acute inflammatory cytokines form a pro-inflammatory environment in damaged nerves. However, these are occurring in the drainage area but how denervated popLNs establish a similar microenvironment is still unclear. Peripheral mast cells in an infection model can release TNF $\alpha$  to facilitate lymphocyte recruitment to the local LN [314], but this might not be the same in a neural injury model which is closer to sterile inflammation.

#### 4.3.4.2 *Anti-inflammatory cytokines*

IL10 in neural injury is interesting because of its anti-inflammatory activity, but it has been found in neural injury for a long time [352, 353]. In contrast to early induction of *Il10*, Dubový et al. found that Schwann cells produce pro- and anti-inflammatory cytokines – TNF $\alpha$ , IL1 $\beta$ , IL4 and IL10, simultaneously 7 days after lesion [354]. Therefore, IL10 might balance the inflammatory effects. However, this paper does not provide time-dependent data to see how the level changes. Peripheral neural injury in *Il10*<sup>-/-</sup> mice results in extensive macrophage infiltration to damaged nerves [355]. Besides, macrophages from these mice do not downregulate pro-inflammatory cytokines after myelin ingestion *in vitro*, meaning they are unlikely to turn into a repair mode [355]. This observation suggests that IL10 participates in the transition between acute inflammation and neural regeneration in neural injury.

#### 4.3.4.3 *Chemokines*

Chemokines CXCL12 and CXCL13 have not been well-connected to peripheral neural injury, but they are discussed intensively in the context of central nervous inflammation to attract T and B cells for CNS entry by upregulation [356]. In LNs, these chemokines are produced by follicular dendritic cells (FDCs) [205, 206] and the CXCL12-expressing population of reticular stroma (CRCs) [213]. They might upregulate CXCL12 and CXCL13 upon immune stimulation in this model. This can be the case after peripheral neural injury,

but the mechanism of upregulation of these two cytokines in denervated paws has remained unknown.

#### *4.3.4.4 Late expressed cytokines*

In another neural injury model of sciatic partial ligation, IL17 contributes to neurogenic pain, infiltration of T cells and macrophages to lesion sites and responsible dorsal root ganglia, and activation of neutrophils and DCs [357]. However, the expression of *Il17* during a period of time was not revealed in that study. In a multiple sclerosis model, TNF $\alpha$  and IL6 and induce CD4 T helper 17 (Th17) cells to produce IL17, contributing to chronic inflammation [358]. This occurs in the CNS and might also be the case in the periphery. It can account for the delayed expression of *Il17a* and *Il17f*. However, Th17 cells are not the only cell type producing IL17. Other local lymphoid cell types such as gamma-delta T ( $\gamma\delta$ T) cells and innate lymphoid cells (ILCs) can release IL17s as well. These cells are closely associated with nerves and related to allergic immunity (summarized in **1.8.5**). It is also possible that loss of neural tones activates their IL17 secretion, but this link seems to be indirect because delayed upregulation of *Il17* mismatched the standard time, 36-48 hours after injury, when a nerve begins to lose its integrity.

## **4.4 The immune response**

Immunostaining of a B cell germinal center marker – GL7, identified that the proliferating B cells in denervated popLNs were forming germinal centers (GCs) (**Figure 3.30**). GC formation is a signature step for T cell-dependent B cell response for affinity maturation and class switch of antibody production [136-138]. These processes require CD4 T helper cells to create a supportive microenvironment [130, 147] and involve follicular T helper (Tfh) cells [138, 142] and FDCs [165, 167] for antibody affinity maturation. At this stage, specific antigens are captured and presented by antigen presenting cells (APCs), cognate T and B cells interact and FDCs are decorated by the antigens with complements. Therefore, Sx can induce an antigen specific response in the popLN likely relying on CD4 T cells and antigen presenting cells.

#### 4.4.1 Upstream: T cell dependence, antigen presentation

Frequency of CD4 [359, 360] and CD8 [361] T cells in the system controls the quality of responses via affecting these T cells' division and cytokine secretion. Naïve CD4 T cell frequency is positively associated with the magnitude of the response [360]. Counts of germinal center B cells (GCBs) and Tfh cells highly correlate with each other and determine the magnitude of the response [143]. The size of this mutually sustaining unit is controlled by the amount of the antigen [143]. These studies provide quantitative insights on regulation of immune responsiveness by antigens and cognate CD4 T cells. To test whether cognate T cells are required, the OT-II system was selected. OT-II is a mouse line in which the predominant portion of CD4 T cells only recognize ovalbumin (OVA). This feature renders the OT-II system highly specific to OVA and thus compromises its reactivity to other antigens. Although Sx still caused 5 times LN cellularity expansion in OT-II mice, their expansion rate was significantly less than wildtype mice (**Figure 3.31**), possibly due to the lower frequency of cognate T cells. This result confirms the concept of T cell requirement for the B cell response.

To examine if denervation-induced nodal expansion relies on antigen presentation, a MHCII neutralizing antibody was utilized for prevention of engagement of MHCII and T cell receptor (TCR) for T cell activation. Blockade of MHCII substantially reduced the nodal expansion level after Sx (**Figure 3.32**). This suggests participation of antigen presentation in the denervation-induced nodal expansion. Although this method can also interfere with the interactions between Tfh cells and B cells in GC, this reaction requires Tfh cells to be primed by APCs first. It is very unlikely that MHCII blockade only masks B cells but not professional APCs.

Induction of adaptive immunity requires molecular or cellular transportation of antigens to the local LN. Soluble antigens can travel through lymphatics to LNs, reach B cell follicles [193] and local DCs in the T cell area [192] via conduits, and be captured by B cells or FDCs [362, 363]. Otherwise, professional APCs such as DCs [223] or their precursors – monocytes [364] – have to enter the LN with antigens. These pathways strongly rely on afferent lymphatic vessels bringing peripheral cells and antigens to the LNs [189, 223,

224, 365]. This route can be successfully blocked by cutting afferent lymphatics, which prevented lymph borne dye from entering the affected popLNs (**Figure 3.33**). Surgical ablation of afferent lymphatic inputs protected the popLN from expansion without affecting paw swelling after Sx (**Figure 3.34**). This suggested lymphatic inputs or their subsequent effects to be important mediators of denervation-driven nodal expansion. However, in rats, blockade of afferent lymphatics shrinks the LN reducing its size and number of follicles, gradually reaching the trough after 16 weeks, albeit this does not change cellular density in the parenchyma [366]. Hendriks et al. studied the effects of afferent lymphatic occlusion on LNs in rats chronologically and found that (1) subcapsular macrophages were reduced after a week and mostly gone after 6 weeks, (2) HEVs were flattened and possibly lost their integrity because lymphocyte recruitment was greatly reduced after 3 weeks, and (3) immune responsiveness declined and was completely lost after 8 weeks [367]. These early studies were based on histological methods. Quantitative analyses revealed that afferent lymphatic deprivation non-selectively reduces adherent lymphocytes on HEVs to 37.8% within a week [368] and this is likely due to loss of MECA-325 antigen [199]. Although this method has a flaw in that it gradually depletes immune cells and destabilizes HEVs, in fact the LN still retains some leukocytes after a week, so reduced level of nodal expansion was expected. However, it effectively abolished nodal expansion (**Figure 3.34**). Therefore, instead of having effects via affecting macrophages and lymphocyte entry, prevention of antigen access seems dominant and more likely.

#### **4.4.2 Downstream: antibody production and antigen specificity**

Given that B cells were forming GCs after Sx (**Figure 3.30**), those GCBs might differentiate into plasma cells (PCs) and produce antibody. Circulating immunoglobulins were dominated by IgG1 (**Figure 3.36A**). This indicates that the response is supported by a Th2 pathway due to the subclass of antibody. Total serum IgG was increased after Sx (**Figure 3.36B**). These results characterized the outcome of the denervation-driven nodal expansion. Therefore, neural injury involving a complete break of the sciatic nerve can trigger adaptive immune responses and antibody production.

The Hep2 slide is a commercial product with cells expressing several nuclear antigens commonly arousing autoimmunity in diseases. Sera after Sx were unable to stain the Hep2 slides (**Figure 3.37**), indicating those increased IgGs were not elicited by nuclear antigens. The Hep2 slides are used clinically to quickly evaluate auto-reactivity. It happens often when antinuclear antibodies are induced with other self-antigens. However, due to the complexity of autoimmune responses, it does not always involve nuclear antigens. Therefore, this test does not rule out the possibility of autoantibody generation. In the case of neural injury, other highly possible targets are neural components. It would be worthy to test the sera on mouse neural tissues. Potentially, these antibodies are polyclonal so that an examination platform with a wide spectrum will be favored.

Regarding the antigen specificity, another hypothesis is that commensal bacterial products drive a local immune response after breakdown of barrier function after Sx. This hypothesis requires a germ-free facility to address. Given that there is no immunization involved in the procedure, autoantigens and components from the microbial community are two reasonable types of antigens in this model. Otherwise, the antigen specificity can also be identified in an unbiased manner using mass-spectrometry-based proteomics analysis of MHCII-bound peptides [369, 370].

#### **4.4.3 Remote responses**

The LN response in this investigation was classified as a local response because it only took place on the ipsilateral but not contralateral side (**Figure 3.1**). Interestingly, the spleen was found to remotely respond to Sx with increased GCBs and PCs (**Figure 3.35**), indicating antigens generated in the trauma were transported to the spleen. Sx-caused antigens can potentially be released into blood and captured by splenic B cells and APCs that induce this remote response. CD11c<sup>lo</sup> phagocytic cells in blood (blood DCs) are capable of inducing a T cell-independent B cell response in the spleen [371]. Would these cells or monocytes acquire antigens in blood and induce a T cell-dependent B cell response in the spleen? Why do the remote responses in the model of Sx only trigger immune responses in the spleen but not in the contralateral LNs? These questions remain undefined here.

## 4.5 Neural involvement

Cross section of the sciatic nerve confirmed its possession of sympathetic nerves and SP- and CGRP-positive sensory nerves (**Figure 3.38**). Immunofluorescence mapped the sympathetic (**Figure 3.39**) and CGRP<sup>+</sup> (**Figure 3.40**) innervations in the popLN. Based on the results of staining and the fact that CGRP and SP are geographically close to each other in LNs [181, 182], the immune functions of these 3 nerves are discussed below.

### 4.5.1 Effects of sympathectomy

Systemic ablation of the SNS by 6-hydroxydopamine (6-OHDA) injection alone did not change popLN cellularity (**Figure 3.41A**). To avoid indirect effects of sympathectomy, superior cervical ganglionectomy (SCGx) was applied to locally sympathectomize superficial parotid lymph nodes (spLNs), but SCGx did not alter nodal cellularity either (**Figure 3.41B**). These results suggest sympathectomy alone does not substantially alter LN cellularity. However, sympathectomy has been reported to enhance recruitment of leukocytes to LNs [348] and kidneys [372] and tune the reactivity of lymphocytes [349]. Xiao et al. found that denervating the kidney by applying phenol on renal arteries reduced total leukocytes and T cell frequencies in the kidney, but this reduction was not observed when afferent fibers were selectively ablated by capsaicin [372]. This finding indicates that the spared nerves from capsaicin treatment – likely sympathetic nerves – favor leukocyte recruitment to kidneys. Interestingly, stimulation of beta 2 adrenergic receptors ( $\beta$ 2ARs) on lymphocytes retains lymphocytes in the LNs and shapes sympathetic input-mediated diurnal oscillation of lymphocyte trafficking to the LNs [248], indicating sympathectomy should enhance egress but not recruitment. In the same paper, treatment of 6-OHDA reduced cell counts in LNs of mice only during the night [248]. The later observation reflects the fact of temporal activation of the SNS and accounts for the lack of effects of sympathectomy in mice during the day.

Gene expression profiling revealed upregulation of *Il1a* and *Il4* in popLNs after 6-OHDA treatment (**Figure 3.42**). This result, together with the cellularity result shown previously,

indicated that sympathectomy does not change cellularity but the microenvironment, which might prime lymphocytes for subsequent responses. This finding agrees with the previous study showing altered responses of lymphocytes from 6-OHDA treated donors to *in vitro* stimulation [349].

A previous paper shows that recruitment of exogenous lymphocytes to LNs is promoted in sympathectomized recipient mice, but cells from sympathectomized mice do not home well to LNs [348], revealing different effects of sympathectomy on microenvironment and leukocytes in terms of cell recruitment to LNs. To examine how the microenvironment affects leukocyte trafficking behavior, adoptive transfer of exogenous cells to unilateral SCGx mice were conducted. Exogenous cells homed to sympathectomized and intact spLNs equally well (**Figure 3.43A**). Egress rate did not change either (**Figure 3.43B**). Therefore, local denervation did not alter leukocyte migratory behavior. This result does not agree with the previous paper from Madden et al. [348]. However, the study from Suzuki et al. showed  $\beta$ 2AR signaling of the donor cells but not of recipient mice determines LN cellularity [248], favoring a donor-determined mechanism which might explain the result observed in the present investigation (**Figure 3.43**). The effects of sympathectomy on LN cellularity is still not clearly defined, but the result here does not show alternation of cellular dynamics by sympathectomy. These observations show that nodal expansion at the level seen in the sciatic denervation model is insufficiently caused by loss of sympathetic innervation but rather that of other neural branches.

#### **4.5.2 Targeting substance P and calcitonin gene-related peptide**

Given that Sx induced nodal expansion (**Figure 3.3**), which neural tones result in this outcome was the next question to address. The sciatic nerve consists mostly of sensory nerves [278], and SP and CGRP released by nociceptive nerves are the most studied neural peptides from sensory nerves exhibiting immunomodulatory functions [373]. Nociceptive nerves are selectively decorated by specific voltage-gated ion channels such as  $\text{Na}_v1.7$ ,  $\text{Na}_v1.8$  and  $\text{Na}_v1.9$ . They are all well-established models for the study of nociception. Loss of  $\text{Na}_v1.8^+$  nerves – a subset of nociceptors – increases the cellularity in popLNs and potentiates stronger immune responses to *Staphylococcus aureus*

infection [79]. This paper shows that activation of Nav1.8+ nociceptors triggered by bacterial infection release CGRP which inhibits macrophages from secretion of inflammatory cytokines [79]. These findings leave SP and CGRP to be the key molecules for preventing denervation-induced nodal expansion. Therefore, results of agonizing or antagonizing these neural peptides with or without Sx are discussed below.

#### *4.5.2.1 Neuropeptide antagonism without sciatic denervation*

Neural resection results in loss of neural tones. To simulate the loss of specific neural tones, antagonists of CGRP or SP receptors were used to target specific efferent sensory neural tones. However, treatments of the SP antagonist (SR140333) and CGRP antagonist (BIBN4096), either separately or combined did not alter cellularity in blood and multiple hematopoietic organs including popLNs (**Figure 3.44**). Given that loss of sensory neural tones without any denervation surgery did not alter cellularity in these organs, nodal expansion could be driven by (1) inflammation/immune challenge and loss of neural tones – the “co-contribution” model or (2) “biphasic reaction” with acute neural substance storms at the beginning and loss of tones in the late phase (**Figure 4.3**). These two possibilities are not mutually exclusive because the release of neural substances when the nerve is resected can also cause inflammation mainly driven by SP and CGRP [373] (summarized in intro **1.4**).

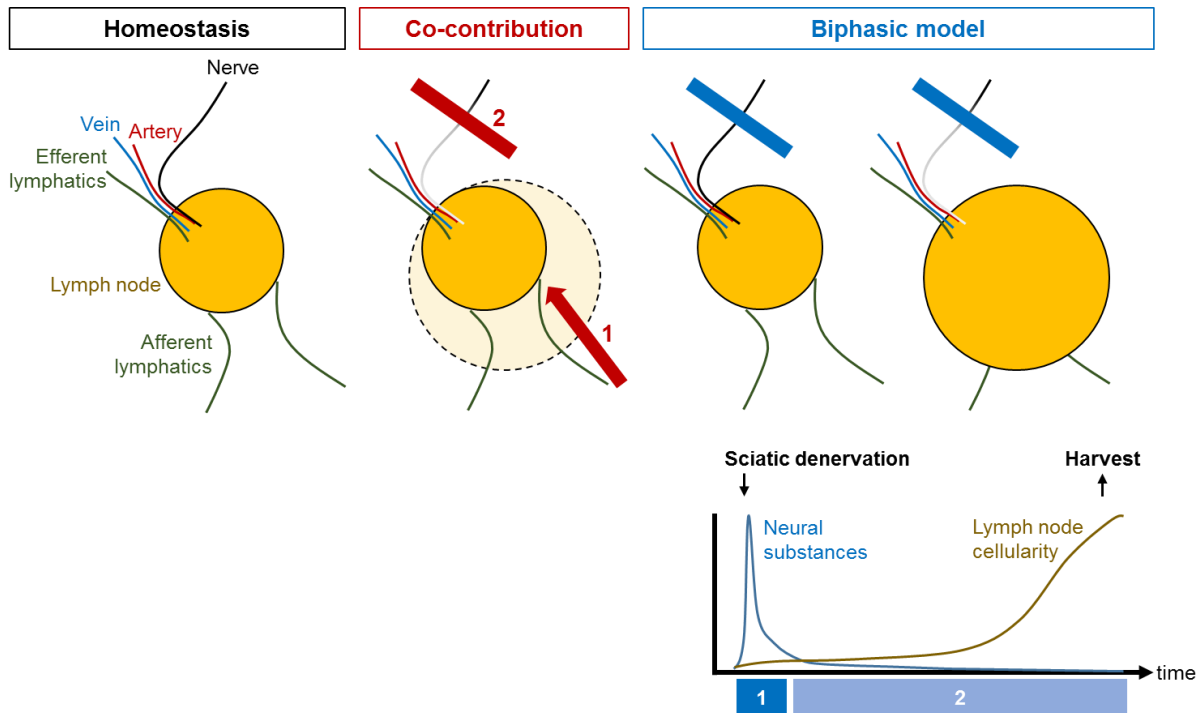


**Figure 4.3 Possible models of denervation-driven lymph node enlargement**

The lymph node is associated with blood vessels (artery and vein), lymphatics (afferent and efferent) and nerves. The network enables cell and molecule trafficking and modulates adaptive immunity developed in the lymph node. In a co-contribution model, inflammatory cues in the drainage area of the LN drive nodal expansion, and loss of innervation further exacerbates the level of nodal expansion. This can explain the comparison between ankle and sciatic denervation (3.7), indicating innervation control the responsiveness of the LN. Focusing more on “time”, the biphasic model describes two stages of neural substance actions. The first phase is a neural substance storm caused by loss of vesicle control after denervation (1.3.1.2). This wave of release leads to inflammation based on the theory of neurogenic inflammation (1.4). The second phase is deprivation of neural substances in the LN. This potentially alters the responsiveness of the LN. These models both consist two components, the trigger (inflammation) and development (lack of neural tones), and are compatible with each other.

Looking at the subsets in the popLN, only the neutrophil number was reduced by CGRP antagonism (Figure 3.45). However, neutrophils were shown to be unlikely to drive B cell responses in this model (Figure 3.20). Besides, this result contradicts previous findings. CGRP can suppress LPS-induced neutrophil recruitment via inhibiting secretion of  $TNF\alpha$  from macrophages [294]. The inhibitory function of CGRP to local inflammatory

macrophages has been confirmed in an infection model [79]. CGRP in these studies indirectly regulates neutrophils via macrophages. Pinho-Ribeiro et al. showed local direct effects of CGRP as inhibition of neutrophilic recruitment to the infection site and killing *Streptococcus pyogenes*. Therefore, the inhibitory action of CGRP to neutrophils can be unlocked by local administration of BIBN4096 (a CGRP receptor antagonist), or botulinum neurotoxin A, which ceases secretion of nerves [84]. These studies show direct and indirect inhibitory effects of CGRP on neutrophil functions, so antagonism of CGRP should enhance neutrophilic activities. Interestingly, BIBN4096 treatment alone for a week actually compromised neutrophil recruitment to the LN (**Figure 3.45**), potentially due to retention of neutrophils in the skin. In fact, these models are different in the way of external factors challenged, for example, bacterial infection or endotoxin was applied in previous publications, but this project did not involve external stimulus but only surgical denervation.

#### *4.5.2.2 Neuropeptide antagonism with sciatic denervation*

The biphasic reaction model hypothesizes that neural peptide storms when nerves are injured trigger neurogenic inflammation at the beginning and the inflammation is sustained or amplified because of lack of neural tones. Concurrent treatment of BIBN4069 and/or SR140333 with sciatic denervation did not rescue popLN expansion (**Figure 3.46**) or numbers of B cell subsets in spleens (**Figure 3.47**). This result questions the biphasic reaction hypothesis by showing the first phase – neurogenic inflammation, which is mainly induced by CGRP and SP, is redundant (**Figure 4.4**). In other words, CGRP or/and SP signaling are important to drive neurogenic inflammation, but blocking either one or the two of them combined does not prevent denervation-driven nodal expansion. It implies that either neurogenic inflammation is driven by other neural substances or other immunogenic cues should initiate the response.

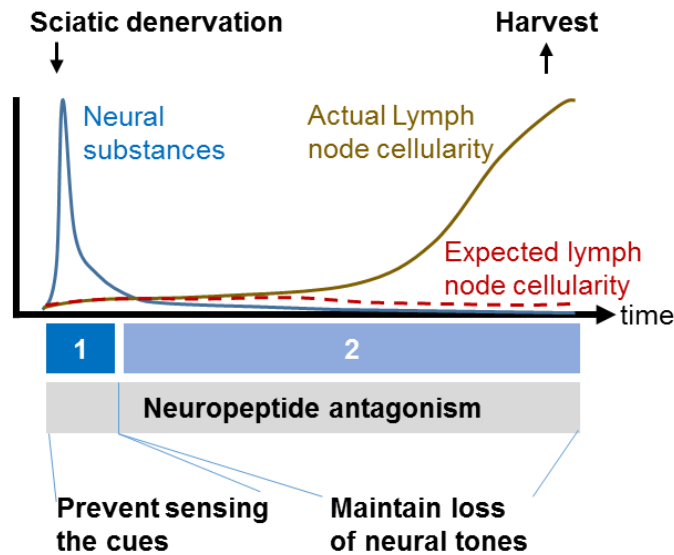


**Figure 4.4 Overlay of the biphasic model and neuropeptide antagonism regimen**

Consecutive treatments of SP and/or CGRP antagonist(s) before tissue harvest and analysis should block reception of neuropeptide signal and effects of neural substance storm. This was expected to prevent denervation-induced nodal expansion (red dash line). However, nodal expansion still took place (dark yellow line). This result suggested this biphasic model is wrong or other neural substances sufficiently induce inflammation at the early stage.

#### 4.5.2.3 Neuropeptide agonism with sciatic denervation

The co-contribution hypothesis consists of two arms. One is local immune perturbation and the other is amplification of the immune response due to the lack of neural tones. Whether loss of neural tone really exacerbates inflammation or enhances immune responses was tested by supplying SP and/or CGRP back to the unilaterally sciatic denervated mice. Combined treatment of CGRP and SP significantly suppressed expansion of CD11c and T cells in the popLN after Sx (**Figure 3.48**). Sx elicited lesser expansion of CD4 T and CD11c cells when SP was treated alone, and of CD8 T cells and neutrophils when CGRP was given (**Figure 3.48**). Remotely, the spleen also exhibited reduced GCBs and PCs when CGRP and SP were treated together (**Figure 3.49**), showing inhibitory effects of these neural peptides.

Mouse DCs [374] and T cells [375] express neurokinin 1 receptors (NK1Rs) to sense SP. Although SP exhibited inhibitory effects on CD11c and CD8 T cells here, SP is mostly reported to be an activator of DCs and T cells [106]. For example, in DCs, SP acts as a pro-survival signal as well as sustaining antigen presentation in the LN [376]. Besides, stimulation of NK1Rs on T cells promotes proliferation [377]. However, NK1R signaling skews DCs toward a Th1 response [378], which does not seem to be the case after Sx (**Figure 3.27**, **Figure 3.28** and **Table 3.1**). Therefore, SP might counteract the cytokine microenvironment shaped by denervation. Cell-type specific receptor knockouts will be helpful for identifying the target cells and narrow down the possible mechanisms. Notably, T cell can synthesize SP [377], so surgical denervation might not entirely remove the local SP. In rats, denervation by sciatic resection [379] or capsaicin treatment [380] does not deprive the ankle joint of SP and CGRP, suggesting production of SP and CGRP from non-neuronal cells. Information of the temporal and spatial distributions of SP will help to better delineate the role of SP in the denervation-induced adaptive immune responses.

Unlike SP, CGRP is mostly inhibitory to immune responses. It can inhibit macrophages from releasing  $\text{TNF}\alpha$  [79, 294] and promoting T cell proliferation upon viral immunization [381]. In T cells, CGRP suppresses IL2 production via cyclic adenosine monophosphate (cAMP) accumulation [382] and suppresses proliferation after specific antigen stimulation [383]. CGRP interferes with B cell development in the bone marrow via inhibiting IL7 signaling [384]. In the B cell line 70Z/3, CGRP suppresses LPS-induced surface immunoglobulin expression also via increasing cytosolic cAMP [385]. Stimulated mouse splenic cells exhibited a dose-dependent reduction of IL4 and interferon alpha ( $\text{IFN}\alpha$ ) production after CGRP treatment [386]. CGRP inhibits antigen presentation of Langerhans cells in human skin [82]. These findings show the inhibitory functions of CGRP in phagocytes, APCs and lymphocytes, and the results here point to a similar concept (**Figure 3.48** and **Figure 3.49**). Given that *Tnfa* was expressed more in paws after denervation (**Figure 3.28**) and peripheral mast cell-derived  $\text{TNF}\alpha$  is critical for immune responses in the LN after infection [314], injected CGRP might repress nodal expansion by interrupting  $\text{TNF}\alpha$  signaling. Nevertheless, CGRP is a potent vasodilator, which facilitates leukocyte extravasation via increasing vessel permeability [94, 95]. Therefore, it can also be pro-inflammatory. A good example for this is psoriasis, which is

associated with hyper-innervation of the skin by sensory nerves. In a mouse model of psoriasis, resection of thoracic cutaneous nerves results in effective disease remission accompanied by reduced CGRP and SP-dependent CD11c and CD4 cell infiltration [387]. With dual functions in opposite directions, CGRP's role is much more complicated. The data in this project suggests the inhibitory role is dominating in the model.

#### *4.5.2.4 Summary of effects of neuropeptides on denervation-induced nodal expansion*

Regarding denervation-induced nodal expansion, CGRP and/or SP antagonism had little effect but their agonism attenuated expansion of some subsets in popLNs and spleen (**Table 3.2**). This phenomenon reveals the repressor role of the neuropeptides in this model. Individual treatment of CGRP or SP shows cell type-specific effects, for example, SP in CD11c cells and CGRP in neutrophils in popLNs. Reasonably, these cell types inhibited by either CGRP or SP were all restricted from expansion when CGRP and SP were treated together (**Table 3.2**). This suggests CGRP and SP to unlikely counteract each other albeit functionally different indications were seen in immune responses in previous reports. The inhibited cell types in popLNs by combined treatment were CD11c cells and T cells (**Table 3.2**), suggesting that B cell responses might be compromised. However, numerically, B cells were unaffected locally in the popLN (**Table 3.2**). In contrast, GCBs and PCs were compromised while total B cell number remained the same in the spleen (**Table 3.2**). This result suggests that CGRP and SP agonism influences counts of T and CD11c cells, whereas in B cells, instead of affecting cell number, they might attenuate B cell differentiation.

## **4.6 Conclusion**

Sx causes popLN enlargement and paw swelling. These two major phenotypes seem to be acute events as there is a remission trend at the later stage of observation. Peripheral inflammation and/or the loss of neural tones are thought to co-contribute to the nodal expansion. This is supported by (1) requirement of losing direct innervation for nodal expansion because denervation bypassing the popLN such as Fx and ANKx does not

induce comparable effects, and (2) peripheral inflammation triggered by denervation. The second component can be compromised by blocking histamine sensing. Additionally, loose connections between three parameters – sizes of denervation area, degree of paw swelling and nodal expansion levels, also suggest nodal expansion might not be simply controlled by a single decisive factor but rather by multiple contributors. These observations fit a co-contribution model.

Even though paw swelling is not strictly connected to nodal expansion, these two tissues share common gene expression. Although *Tnfa*, *Il12* and *Il17a* are selectively expressed, *Cxcl12*, *Cxcl13*, *Il1a*, *Il1b*, *Il6*, *Il10* and *Il17f* are substantially increased in both tissues. Highly overlapping expression profiles strengthen the relations between the paw and the popLN. Besides, these cytokines and chemokines are supportive of a B cell response, acute inflammation, Th2 and Th17 responses. With this microenvironment, denervated popLNs attract exogenous cells to home well, mount T cell-dependent B cell responses ipsilaterally and boost IgG generation. Different immune subsets have distinct curves of expansion in denervated popLNs. Although NK cells, neutrophils and migratory DCs are three early peaking cell types, the inflammatory cascade described here does not rely on NK cells or neutrophils but on cognate CD4 T cells and requires antigen presentation.

The sciatic nerve is dominated by sensory and sympathetic fibers, which are also innervating the popLN. Mimicry of denervation by pharmacologically or surgically ablating either sympathetic signaling or CGRP and/or SP does not reproduce nodal expansion. Although sympathectomy has limited effects on popLN cellularity directly, it changes the local microenvironment with higher *Il1a* and *Il4* levels, possibly potentiating immune responses. Interestingly, compensation of losing CGRP and/or SP by intraperitoneal injection of CGRP and/or SP compromises denervation-induced nodal expansion. Specifically, CGRP and SP treatments individually in Sx exhibit cell type-specific effects. The combined treatment exerts an inclusive and stronger outcome affecting cell types responding to separate treatment of CGRP and SP.

These results reveal a pathway and consequences of an adaptive immune response aroused by neural injury, which deprives neural tone and causes inflammation. Neuropeptides CGRP and SP show inhibitory effects on the denervation-induced immune response indicating them to be potential agents for suppressing immune responses

caused by neural injury. This study sheds light on the dialog between the nervous and immune systems, albeit there are still many details to be investigated, for example, the specific cells sensing the change in neural tone. A better understanding here can identify the potential medical values of neural substances to avoid undesired acute immune outcomes and perturbation in long-term immune memory after injury. Moreover, the LN is an important organ to leverage systemic antigen-specific immune responses with great application potential [388]. This field merits further investigation to better illustrate how these systems interact to perturbations.



## 5 References

1. Constantinescu, C.S., et al., *Experimental autoimmune encephalomyelitis (EAE) as a model for multiple sclerosis (MS)*. Br J Pharmacol, 2011. **164**(4): p. 1079-106.
2. Lassmann, H. and M. Bradl, *Multiple sclerosis: experimental models and reality*. Acta Neuropathol, 2017. **133**(2): p. 223-244.
3. Langhorne, P., et al., *Medical complications after stroke: a multicenter study*. Stroke, 2000. **31**(6): p. 1223-9.
4. Garcia-Arguello, L.Y., et al., *Infections in the spinal cord-injured population: a systematic review*. Spinal Cord, 2017. **55**(6): p. 526-534.
5. Iversen, P.O., et al., *Depressed immunity and impaired proliferation of hematopoietic progenitor cells in patients with complete spinal cord injury*. Blood, 2000. **96**(6): p. 2081-3.
6. Soden, R.J., et al., *Causes of death after spinal cord injury*. Spinal Cord, 2000. **38**(10): p. 604-10.
7. DeVivo, M.J., et al., *Cause of death for patients with spinal cord injuries*. Arch Intern Med, 1989. **149**(8): p. 1761-6.
8. Dewan, M.C., et al., *Estimating the global incidence of traumatic brain injury*. J Neurosurg, 2018: p. 1-18.
9. Bickenbach, J., et al., *International perspectives on spinal cord injury*. 2013, World Health Organization.
10. Kawashima, Y., Sugimura M., Hwang Y-C., Kudo N., *The lymph system in mice*. Japanese Journal of Veterinary Research, 1964. **12**(4): p. 69-78.
11. Luscieti, P., et al., *Human lymph node morphology as a function of age and site*. J Clin Pathol, 1980. **33**(5): p. 454-61.
12. Ankeny, D.P. and P.G. Popovich, *Mechanisms and implications of adaptive immune responses after traumatic spinal cord injury*. Neuroscience, 2009. **158**(3): p. 1112-21.
13. Chamorro, A., X. Urra, and A.M. Planas, *Infection after acute ischemic stroke: a manifestation of brain-induced immunodepression*. Stroke, 2007. **38**(3): p. 1097-103.
14. Wong, C.H., et al., *Functional innervation of hepatic iNKT cells is immunosuppressive following stroke*. Science, 2011. **334**(6052): p. 101-5.
15. Cruse, J.M., et al., *Adhesion molecules and wound healing in spinal cord injury*. Pathobiology, 1996. **64**(4): p. 193-7.
16. Brommer, B., et al., *Spinal cord injury-induced immune deficiency syndrome enhances infection susceptibility dependent on lesion level*. Brain, 2016. **139**(Pt 3): p. 692-707.
17. Pruss, H., et al., *Spinal cord injury-induced immunodeficiency is mediated by a sympathetic-neuroendocrine adrenal reflex*. Nat Neurosci, 2017. **20**(11): p. 1549-1559.
18. Lucin, K.M., et al., *Impaired antibody synthesis after spinal cord injury is level dependent and is due to sympathetic nervous system dysregulation*. Exp Neurol, 2007. **207**(1): p. 75-84.
19. Meisel, C., et al., *Central nervous system injury-induced immune deficiency syndrome*. Nat Rev Neurosci, 2005. **6**(10): p. 775-86.

20. Held, K.S., et al., *Impaired immune responses following spinal cord injury lead to reduced ability to control viral infection*. *Exp Neurol*, 2010. **226**(1): p. 242-53.
21. Kerschensteiner, M., et al., *In vivo imaging of axonal degeneration and regeneration in the injured spinal cord*. *Nat Med*, 2005. **11**(5): p. 572-7.
22. Rotshenker, S., *Wallerian degeneration: the innate-immune response to traumatic nerve injury*. *J Neuroinflammation*, 2011. **8**: p. 109.
23. Lunn, E.R., et al., *Absence of Wallerian Degeneration does not Hinder Regeneration in Peripheral Nerve*. *Eur J Neurosci*, 1989. **1**(1): p. 27-33.
24. Sano, H., et al., *Critical role of galectin-3 in phagocytosis by macrophages*. *J Clin Invest*, 2003. **112**(3): p. 389-97.
25. Lubinska, L., *Early course of Wallerian degeneration in myelinated fibres of the rat phrenic nerve*. *Brain Res*, 1977. **130**(1): p. 47-63.
26. Tsao, J.W., et al., *Loss of the compound action potential: an electrophysiological, biochemical and morphological study of early events in axonal degeneration in the C57BL/Ola mouse*. *Eur J Neurosci*, 1994. **6**(4): p. 516-24.
27. Tsao, J.W., E.B. George, and J.W. Griffin, *Temperature modulation reveals three distinct stages of Wallerian degeneration*. *J Neurosci*, 1999. **19**(12): p. 4718-26.
28. Moldovan, M., S. Alvarez, and C. Krarup, *Motor axon excitability during Wallerian degeneration*. *Brain*, 2009. **132**(Pt 2): p. 511-23.
29. Glass, J.D., et al., *Very early activation of m-calpain in peripheral nerve during Wallerian degeneration*. *J Neurol Sci*, 2002. **196**(1-2): p. 9-20.
30. Stirling, D.P. and P.K. Stys, *Mechanisms of axonal injury: internodal nanocomplexes and calcium deregulation*. *Trends Mol Med*, 2010. **16**(4): p. 160-70.
31. Wang, J.T., Z.A. Medress, and B.A. Barres, *Axon degeneration: molecular mechanisms of a self-destruction pathway*. *J Cell Biol*, 2012. **196**(1): p. 7-18.
32. Ziv, N.E. and M.E. Spira, *Spatiotemporal distribution of Ca<sup>2+</sup> following axotomy and throughout the recovery process of cultured Aplysia neurons*. *Eur J Neurosci*, 1993. **5**(6): p. 657-68.
33. Beirowski, B., et al., *Quantitative and qualitative analysis of Wallerian degeneration using restricted axonal labelling in YFP-H mice*. *J Neurosci Methods*, 2004. **134**(1): p. 23-35.
34. Catenaccio, A., et al., *Molecular analysis of axonal-intrinsic and glial-associated co-regulation of axon degeneration*. *Cell Death Dis*, 2017. **8**(11): p. e3166.
35. Beirowski, B., et al., *The progressive nature of Wallerian degeneration in wild-type and slow Wallerian degeneration (WldS) nerves*. *BMC Neurosci*, 2005. **6**: p. 6.
36. Cullen, M.J., *Freeze-fracture analysis of myelin membrane changes in Wallerian degeneration*. *J Neurocytol*, 1988. **17**(1): p. 105-15.
37. Trapp, B.D., P. Hauer, and G. Lemke, *Axonal regulation of myelin protein mRNA levels in actively myelinating Schwann cells*. *J Neurosci*, 1988. **8**(9): p. 3515-21.
38. Jessen, K.R. and R. Mirsky, *The repair Schwann cell and its function in regenerating nerves*. *J Physiol*, 2016. **594**(13): p. 3521-31.
39. Tetzlaff, W., *Tight junction contact events and temporary gap junctions in the sciatic nerve fibres of the chicken during Wallerian degeneration and subsequent regeneration*. *J Neurocytol*, 1982. **11**(5): p. 839-58.
40. Beuche, W. and R.L. Friede, *The role of non-resident cells in Wallerian degeneration*. *J Neurocytol*, 1984. **13**(5): p. 767-96.

41. Fernandez-Valle, C., R.P. Bunge, and M.B. Bunge, *Schwann cells degrade myelin and proliferate in the absence of macrophages: evidence from in vitro studies of Wallerian degeneration*. J Neurocytol, 1995. **24**(9): p. 667-79.
42. Gray, M., et al., *Macrophage depletion alters the blood-nerve barrier without affecting Schwann cell function after neural injury*. J Neurosci Res, 2007. **85**(4): p. 766-77.
43. Huang, J.K., et al., *Glial membranes at the node of Ranvier prevent neurite outgrowth*. Science, 2005. **310**(5755): p. 1813-7.
44. Vargas, M.E., et al., *Endogenous antibodies promote rapid myelin clearance and effective axon regeneration after nerve injury*. Proc Natl Acad Sci U S A, 2010. **107**(26): p. 11993-8.
45. Bonnekoh, P.G., P. Scheidt, and R.L. Friede, *Myelin phagocytosis by peritoneal macrophages in organ cultures of mouse peripheral nerve. A new model for studying myelin phagocytosis in vitro*. J Neuropathol Exp Neurol, 1989. **48**(2): p. 140-53.
46. Mueller, M., et al., *Rapid response of identified resident endoneurial macrophages to nerve injury*. Am J Pathol, 2001. **159**(6): p. 2187-97.
47. Perkins, N.M. and D.J. Tracey, *Hyperalgesia due to nerve injury: role of neutrophils*. Neuroscience, 2000. **101**(3): p. 745-57.
48. Monaco, S., et al., *MHC-positive, ramified macrophages in the normal and injured rat peripheral nervous system*. J Neurocytol, 1992. **21**(9): p. 623-34.
49. Mueller, M., et al., *Macrophage response to peripheral nerve injury: the quantitative contribution of resident and hematogenous macrophages*. Lab Invest, 2003. **83**(2): p. 175-85.
50. La Fleur, M., et al., *Basement membrane and repair of injury to peripheral nerve: defining a potential role for macrophages, matrix metalloproteinases, and tissue inhibitor of metalloproteinases-1*. J Exp Med, 1996. **184**(6): p. 2311-26.
51. Heumann, R., et al., *Differential regulation of mRNA encoding nerve growth factor and its receptor in rat sciatic nerve during development, degeneration, and regeneration: role of macrophages*. Proc Natl Acad Sci U S A, 1987. **84**(23): p. 8735-9.
52. Lindborg, J.A., M. Mack, and R.E. Zigmond, *Neutrophils Are Critical for Myelin Removal in a Peripheral Nerve Injury Model of Wallerian Degeneration*. J Neurosci, 2017. **37**(43): p. 10258-10277.
53. Rosen, H. and S. Gordon, *Monoclonal antibody to the murine type 3 complement receptor inhibits adhesion of myelomonocytic cells in vitro and inflammatory cell recruitment in vivo*. J Exp Med, 1987. **166**(6): p. 1685-701.
54. Conforti, L., J. Gilley, and M.P. Coleman, *Wallerian degeneration: an emerging axon death pathway linking injury and disease*. Nat Rev Neurosci, 2014. **15**(6): p. 394-409.
55. Weerasuriya, A. and C.H. Hockman, *Perineurial permeability to sodium during Wallerian degeneration in rat sciatic nerve*. Brain Res, 1992. **581**(2): p. 327-33.
56. Mizisin, A.P. and A. Weerasuriya, *Homeostatic regulation of the endoneurial microenvironment during development, aging and in response to trauma, disease and toxic insult*. Acta Neuropathol, 2011. **121**(3): p. 291-312.
57. Moalem, G., K. Xu, and L. Yu, *T lymphocytes play a role in neuropathic pain following peripheral nerve injury in rats*. Neuroscience, 2004. **129**(3): p. 767-77.
58. Hendrix, S. and R. Nitsch, *The role of T helper cells in neuroprotection and regeneration*. J Neuroimmunol, 2007. **184**(1-2): p. 100-12.

59. Vidal, P.M., et al., *The role of "anti-inflammatory" cytokines in axon regeneration*. Cytokine Growth Factor Rev, 2013. **24**(1): p. 1-12.
60. Ishii, H., et al., *Adoptive transfer of Th1-conditioned lymphocytes promotes axonal remodeling and functional recovery after spinal cord injury*. Cell Death Dis, 2012. **3**: p. e363.
61. MacDonald, S.M., M. Mezei, and C. Mezei, *Effect of Wallerian degeneration on histamine concentration of the peripheral nerve*. J Neurochem, 1981. **36**(1): p. 9-16.
62. Ferreira, R., et al., *Histamine modulates microglia function*. J Neuroinflammation, 2012. **9**: p. 90.
63. Rocha, S.M., et al., *Histamine: a new immunomodulatory player in the neuron-glia crosstalk*. Front Cell Neurosci, 2014. **8**: p. 120.
64. Kurek, J.B., et al., *Up-regulation of leukaemia inhibitory factor and interleukin-6 in transected sciatic nerve and muscle following denervation*. Neuromuscul Disord, 1996. **6**(2): p. 105-14.
65. Shamash, S., F. Reichert, and S. Rotshenker, *The cytokine network of Wallerian degeneration: tumor necrosis factor-alpha, interleukin-1alpha, and interleukin-1beta*. J Neurosci, 2002. **22**(8): p. 3052-60.
66. Goethals, S., et al., *Toll-like receptor expression in the peripheral nerve*. Glia, 2010. **58**(14): p. 1701-9.
67. Boivin, A., et al., *Toll-like receptor signaling is critical for Wallerian degeneration and functional recovery after peripheral nerve injury*. J Neurosci, 2007. **27**(46): p. 12565-76.
68. Olsson, T., et al., *Facial nerve transection causes expansion of myelin autoreactive T cells in regional lymph nodes and T cell homing to the facial nucleus*. Autoimmunity, 1992. **13**(2): p. 117-26.
69. Kipnis, J., et al., *Neuroprotective autoimmunity: naturally occurring CD4+CD25+ regulatory T cells suppress the ability to withstand injury to the central nervous system*. Proc Natl Acad Sci U S A, 2002. **99**(24): p. 15620-5.
70. Cashman, C.R. and A. Hoke, *Deficiency of adaptive immunity does not interfere with Wallerian degeneration*. PLoS One, 2017. **12**(5): p. e0177070.
71. Bombeiro, A.L., et al., *Enhanced Immune Response in Immunodeficient Mice Improves Peripheral Nerve Regeneration Following Axotomy*. Front Cell Neurosci, 2016. **10**: p. 151.
72. Meyer zu Horste, G., et al., *The immunocompetence of Schwann cells*. Muscle Nerve, 2008. **37**(1): p. 3-13.
73. Wekerle, H., et al., *Antigen presentation in the peripheral nervous system: Schwann cells present endogenous myelin autoantigens to lymphocytes*. Eur J Immunol, 1986. **16**(12): p. 1551-7.
74. Kingston, A.E., et al., *Schwann cells co-cultured with stimulated T cells and antigen express major histocompatibility complex (MHC) class II determinants without interferon-gamma pretreatment: synergistic effects of interferon-gamma and tumor necrosis factor on MHC class II induction*. Eur J Immunol, 1989. **19**(1): p. 177-83.
75. Bourque, P.R., J.W. Chardon, and R. Massie, *Autoimmune peripheral neuropathies*. Clin Chim Acta, 2015. **449**: p. 37-42.
76. Barclay, A.N., *Signal regulatory protein alpha (SIRPalpha)/CD47 interaction and function*. Curr Opin Immunol, 2009. **21**(1): p. 47-52.

77. Gitik, M., et al., *Myelin down-regulates myelin phagocytosis by microglia and macrophages through interactions between CD47 on myelin and SIRPalpha (signal regulatory protein-alpha) on phagocytes*. J Neuroinflammation, 2011. **8**: p. 24.
78. Chiu, I.M., C.A. von Hehn, and C.J. Woolf, *Neurogenic inflammation and the peripheral nervous system's role in host defense and immunopathology*. Nat Neurosci, 2012. **15**(8): p. 1063-7.
79. Chiu, I.M., et al., *Bacteria activate sensory neurons that modulate pain and inflammation*. Nature, 2013. **501**(7465): p. 52-7.
80. Mikami, N., et al., *Calcitonin gene-related peptide is an important regulator of cutaneous immunity: effect on dendritic cell and T cell functions*. J Immunol, 2011. **186**(12): p. 6886-93.
81. Ding, W., et al., *Calcitonin gene-related peptide biases Langerhans cells toward Th2-type immunity*. J Immunol, 2008. **181**(9): p. 6020-6.
82. Hosoi, J., et al., *Regulation of Langerhans cell function by nerves containing calcitonin gene-related peptide*. Nature, 1993. **363**(6425): p. 159-63.
83. Ansel, J.C., et al., *Substance P selectively activates TNF-alpha gene expression in murine mast cells*. J Immunol, 1993. **150**(10): p. 4478-85.
84. Pinho-Ribeiro, F.A., et al., *Blocking Neuronal Signaling to Immune Cells Treats Streptococcal Invasive Infection*. Cell, 2018. **173**(5): p. 1083-1097 e22.
85. Baral, P., et al., *Nociceptor sensory neurons suppress neutrophil and gammadelta T cell responses in bacterial lung infections and lethal pneumonia*. Nat Med, 2018. **24**(4): p. 417-426.
86. Levite, M., *Neuropeptides, by direct interaction with T cells, induce cytokine secretion and break the commitment to a distinct T helper phenotype*. Proc Natl Acad Sci U S A, 1998. **95**(21): p. 12544-9.
87. Steinhoff, M., M. Schmelz, and J. Schaubert, *Facial Erythema of Rosacea - Aetiology, Different Pathophysiologies and Treatment Options*. Acta Derm Venereol, 2016. **96**(5): p. 579-86.
88. Amara, S.G., et al., *Alternative RNA processing in calcitonin gene expression generates mRNAs encoding different polypeptide products*. Nature, 1982. **298**(5871): p. 240-4.
89. McLatchie, L.M., et al., *RAMPs regulate the transport and ligand specificity of the calcitonin-receptor-like receptor*. Nature, 1998. **393**(6683): p. 333-9.
90. Donnerer, J. and C. Stein, *Evidence for an increase in the release of CGRP from sensory nerves during inflammation*. Ann N Y Acad Sci, 1992. **657**: p. 505-6.
91. Vriens, J., G. Appendino, and B. Nilius, *Pharmacology of vanilloid transient receptor potential cation channels*. Mol Pharmacol, 2009. **75**(6): p. 1262-79.
92. Supowit, S.C., H. Zhao, and D.J. DiPette, *Nerve growth factor enhances calcitonin gene-related peptide expression in the spontaneously hypertensive rat*. Hypertension, 2001. **37**(2 Pt 2): p. 728-32.
93. Supowit, S.C., et al., *Alpha 2-adrenergic receptor activation inhibits calcitonin gene-related peptide expression in cultured dorsal root ganglia neurons*. Brain Res, 1998. **782**(1-2): p. 184-93.
94. Brain, S.D., et al., *Potent vasodilator activity of calcitonin gene-related peptide in human skin*. J Invest Dermatol, 1986. **87**(4): p. 533-6.
95. Brain, S.D., et al., *Calcitonin gene-related peptide is a potent vasodilator*. Nature, 1985. **313**(5997): p. 54-6.

96. Gray, D.W. and I. Marshall, *Human alpha-calcitonin gene-related peptide stimulates adenylate cyclase and guanylate cyclase and relaxes rat thoracic aorta by releasing nitric oxide*. Br J Pharmacol, 1992. **107**(3): p. 691-6.
97. Crossman, D.C., et al., *Action of calcitonin gene-related peptide upon bovine vascular endothelial and smooth muscle cells grown in isolation and co-culture*. Br J Pharmacol, 1990. **99**(1): p. 71-6.
98. Russell, F.A., et al., *Calcitonin gene-related peptide: physiology and pathophysiology*. Physiol Rev, 2014. **94**(4): p. 1099-142.
99. De Camilli, P. and R. Jahn, *Pathways to regulated exocytosis in neurons*. Annu Rev Physiol, 1990. **52**: p. 625-45.
100. McConalogue, K., et al., *Substance P-induced trafficking of beta-arrestins. The role of beta-arrestins in endocytosis of the neurokinin-1 receptor*. J Biol Chem, 1999. **274**(23): p. 16257-68.
101. Steinhoff, M.S., et al., *Tachykinins and their receptors: contributions to physiological control and the mechanisms of disease*. Physiol Rev, 2014. **94**(1): p. 265-301.
102. Lundberg, J.M., et al., *Co-existence of substance P and calcitonin gene-related peptide-like immunoreactivities in sensory nerves in relation to cardiovascular and bronchoconstrictor effects of capsaicin*. Eur J Pharmacol, 1985. **108**(3): p. 315-9.
103. Bull, H.A., et al., *Neuropeptides induce release of nitric oxide from human dermal microvascular endothelial cells*. J Invest Dermatol, 1996. **106**(4): p. 655-60.
104. Ziche, M., et al., *Nitric oxide mediates angiogenesis in vivo and endothelial cell growth and migration in vitro promoted by substance P*. J Clin Invest, 1994. **94**(5): p. 2036-44.
105. Hong, H.S., et al., *A new role of substance P as an injury-inducible messenger for mobilization of CD29(+) stromal-like cells*. Nat Med, 2009. **15**(4): p. 425-35.
106. Suvas, S., *Role of Substance P Neuropeptide in Inflammation, Wound Healing, and Tissue Homeostasis*. J Immunol, 2017. **199**(5): p. 1543-1552.
107. Covenas, R. and M. Munoz, *Cancer progression and substance P*. Histol Histopathol, 2014. **29**(7): p. 881-90.
108. Holzer, P., *Neurogenic vasodilatation and plasma leakage in the skin*. Gen Pharmacol, 1998. **30**(1): p. 5-11.
109. Brain, S.D. and T.J. Williams, *Substance P regulates the vasodilator activity of calcitonin gene-related peptide*. Nature, 1988. **335**(6185): p. 73-5.
110. Paus, R., et al., *Substance P stimulates murine epidermal keratinocyte proliferation and dermal mast cell degranulation in situ*. Arch Dermatol Res, 1995. **287**(5): p. 500-2.
111. Sternberg, G.M., *Explanation of Acquired Immunity from Infectious Diseases*. Science, 1895. **1**(13): p. 346-9.
112. Bonilla, F.A. and H.C. Oettgen, *Adaptive immunity*. J Allergy Clin Immunol, 2010. **125**(2 Suppl 2): p. S33-40.
113. Parish, C.R., *Immune response to chemically modified flagellin. II. Evidence for a fundamental relationship between humoral and cell-mediated immunity*. J Exp Med, 1971. **134**(1): p. 21-47.
114. Spellberg, B. and J.E. Edwards, Jr., *Type 1/Type 2 immunity in infectious diseases*. Clin Infect Dis, 2001. **32**(1): p. 76-102.
115. Luckheeram, R.V., et al., *CD4(+)T cells: differentiation and functions*. Clin Dev Immunol, 2012. **2012**: p. 925135.

116. Azuma, M., et al., *B70 antigen is a second ligand for CTLA-4 and CD28*. Nature, 1993. **366**(6450): p. 76-9.
117. Baroja, M.L., et al., *The anti-T cell monoclonal antibody 9.3 (anti-CD28) provides a helper signal and bypasses the need for accessory cells in T cell activation with immobilized anti-CD3 and mitogens*. Cell Immunol, 1989. **120**(1): p. 205-17.
118. Starbeck-Miller, G.R., H.H. Xue, and J.T. Harty, *IL-12 and type I interferon prolong the division of activated CD8 T cells by maintaining high-affinity IL-2 signaling in vivo*. J Exp Med, 2014. **211**(1): p. 105-20.
119. Zhang, N. and M.J. Bevan, *CD8(+) T cells: foot soldiers of the immune system*. Immunity, 2011. **35**(2): p. 161-8.
120. Bevan, M.J., *Helping the CD8(+) T-cell response*. Nat Rev Immunol, 2004. **4**(8): p. 595-602.
121. Nakanishi, Y., et al., *CD8(+) T lymphocyte mobilization to virus-infected tissue requires CD4(+) T-cell help*. Nature, 2009. **462**(7272): p. 510-3.
122. Hwang, E.S., et al., *T helper cell fate specified by kinase-mediated interaction of T-bet with GATA-3*. Science, 2005. **307**(5708): p. 430-3.
123. Sullivan, B.M., et al., *Antigen-driven effector CD8 T cell function regulated by T-bet*. Proc Natl Acad Sci U S A, 2003. **100**(26): p. 15818-23.
124. Intlekofer, A.M., et al., *Effector and memory CD8+ T cell fate coupled by T-bet and eomesodermin*. Nat Immunol, 2005. **6**(12): p. 1236-44.
125. Pipkin, M.E., et al., *Interleukin-2 and inflammation induce distinct transcriptional programs that promote the differentiation of effector cytolytic T cells*. Immunity, 2010. **32**(1): p. 79-90.
126. Williams, M.A., A.J. Tyznik, and M.J. Bevan, *Interleukin-2 signals during priming are required for secondary expansion of CD8+ memory T cells*. Nature, 2006. **441**(7095): p. 890-3.
127. Feau, S., et al., *Autocrine IL-2 is required for secondary population expansion of CD8(+) memory T cells*. Nat Immunol, 2011. **12**(9): p. 908-13.
128. Kurosaki, T., K. Kometani, and W. Ise, *Memory B cells*. Nat Rev Immunol, 2015. **15**(3): p. 149-59.
129. Nutt, S.L., et al., *The generation of antibody-secreting plasma cells*. Nat Rev Immunol, 2015. **15**(3): p. 160-71.
130. Pieper, K., B. Grimbacher, and H. Eibel, *B-cell biology and development*. J Allergy Clin Immunol, 2013. **131**(4): p. 959-71.
131. Davidson, H.W., M.A. West, and C. Watts, *Endocytosis, intracellular trafficking, and processing of membrane IgG and monovalent antigen/membrane IgG complexes in B lymphocytes*. J Immunol, 1990. **144**(11): p. 4101-9.
132. West, M.A., J.M. Lucocq, and C. Watts, *Antigen processing and class II MHC peptide-loading compartments in human B-lymphoblastoid cells*. Nature, 1994. **369**(6476): p. 147-51.
133. Jones, B. and C.A. Janeway, Jr., *Cooperative interaction of B lymphocytes with antigen-specific helper T lymphocytes is MHC restricted*. Nature, 1981. **292**(5823): p. 547-9.
134. Kawabe, T., et al., *The immune responses in CD40-deficient mice: impaired immunoglobulin class switching and germinal center formation*. Immunity, 1994. **1**(3): p. 167-78.

135. Howard, M., et al., *Identification of a T cell-derived b cell growth factor distinct from interleukin 2*. J Exp Med, 1982. **155**(3): p. 914-23.
136. Allen, C.D., T. Okada, and J.G. Cyster, *Germinal-center organization and cellular dynamics*. Immunity, 2007. **27**(2): p. 190-202.
137. Breitfeld, D., et al., *Follicular B helper T cells express CXC chemokine receptor 5, localize to B cell follicles, and support immunoglobulin production*. J Exp Med, 2000. **192**(11): p. 1545-52.
138. De Silva, N.S. and U. Klein, *Dynamics of B cells in germinal centres*. Nat Rev Immunol, 2015. **15**(3): p. 137-48.
139. Hoshi, H., et al., *Lymph follicles and germinal centers in popliteal lymph nodes and other lymphoid tissues of germ-free and conventional rats*. Tohoku J Exp Med, 1992. **166**(3): p. 297-307.
140. Olson, G.B. and B.S. Wostmann, *Cellular and humoral immune response of germfree mice stimulated with 7S HGG or Salmonella typhimurium*. J Immunol, 1966. **97**(2): p. 275-86.
141. Ohwaki, M., et al., *A comparative study on the humoral immune responses in germ-free and conventional mice*. Immunology, 1977. **32**(1): p. 43-8.
142. Gitlin, A.D., Z. Shulman, and M.C. Nussenzweig, *Clonal selection in the germinal centre by regulated proliferation and hypermutation*. Nature, 2014. **509**(7502): p. 637-40.
143. Baumjohann, D., et al., *Persistent antigen and germinal center B cells sustain T follicular helper cell responses and phenotype*. Immunity, 2013. **38**(3): p. 596-605.
144. Wang, Y., et al., *Germinal-center development of memory B cells driven by IL-9 from follicular helper T cells*. Nat Immunol, 2017. **18**(8): p. 921-930.
145. Slifka, M.K., et al., *Humoral immunity due to long-lived plasma cells*. Immunity, 1998. **8**(3): p. 363-72.
146. Bortnick, A. and D. Allman, *What is and what should always have been: long-lived plasma cells induced by T cell-independent antigens*. J Immunol, 2013. **190**(12): p. 5913-8.
147. Walker, J.A. and A.N.J. McKenzie, *TH2 cell development and function*. Nat Rev Immunol, 2018. **18**(2): p. 121-133.
148. Min, B., et al., *Basophils produce IL-4 and accumulate in tissues after infection with a Th2-inducing parasite*. J Exp Med, 2004. **200**(4): p. 507-17.
149. Williams, J.W., et al., *Transcription factor IRF4 drives dendritic cells to promote Th2 differentiation*. Nat Commun, 2013. **4**: p. 2990.
150. Gao, Y., et al., *Control of T helper 2 responses by transcription factor IRF4-dependent dendritic cells*. Immunity, 2013. **39**(4): p. 722-32.
151. Tussiwand, R., et al., *Klf4 expression in conventional dendritic cells is required for T helper 2 cell responses*. Immunity, 2015. **42**(5): p. 916-28.
152. Kumamoto, Y., et al., *CD301b(+) dermal dendritic cells drive T helper 2 cell-mediated immunity*. Immunity, 2013. **39**(4): p. 733-43.
153. Le Gros, G., et al., *Generation of interleukin 4 (IL-4)-producing cells in vivo and in vitro: IL-2 and IL-4 are required for in vitro generation of IL-4-producing cells*. J Exp Med, 1990. **172**(3): p. 921-9.
154. Iezzi, G., et al., *The interplay between the duration of TCR and cytokine signaling determines T cell polarization*. Eur J Immunol, 1999. **29**(12): p. 4092-101.

155. Yamane, H., J. Zhu, and W.E. Paul, *Independent roles for IL-2 and GATA-3 in stimulating naive CD4+ T cells to generate a Th2-inducing cytokine environment.* J Exp Med, 2005. **202**(6): p. 793-804.
156. Coutinho, A., et al., *Mechanism of thymus-independent immunocyte triggering. Mitogenic activation of B cells results in specific immune responses.* J Exp Med, 1974. **139**(1): p. 74-92.
157. Vos, Q., et al., *B-cell activation by T-cell-independent type 2 antigens as an integral part of the humoral immune response to pathogenic microorganisms.* Immunol Rev, 2000. **176**: p. 154-70.
158. Rawlings, D.J., et al., *Integration of B cell responses through Toll-like receptors and antigen receptors.* Nat Rev Immunol, 2012. **12**(4): p. 282-94.
159. Fagarasan, S. and T. Honjo, *T-Independent immune response: new aspects of B cell biology.* Science, 2000. **290**(5489): p. 89-92.
160. Martin, F., A.M. Oliver, and J.F. Kearney, *Marginal zone and B1 B cells unite in the early response against T-independent blood-borne particulate antigens.* Immunity, 2001. **14**(5): p. 617-29.
161. Taillardet, M., et al., *The thymus-independent immunity conferred by a pneumococcal polysaccharide is mediated by long-lived plasma cells.* Blood, 2009. **114**(20): p. 4432-40.
162. Bortnick, A., et al., *Long-lived bone marrow plasma cells are induced early in response to T cell-independent or T cell-dependent antigens.* J Immunol, 2012. **188**(11): p. 5389-96.
163. Maul, R.W. and P.J. Gearhart, *AID and somatic hypermutation.* Adv Immunol, 2010. **105**: p. 159-91.
164. Muramatsu, M., et al., *Class switch recombination and hypermutation require activation-induced cytidine deaminase (AID), a potential RNA editing enzyme.* Cell, 2000. **102**(5): p. 553-63.
165. Kranich, J. and N.J. Krautler, *How Follicular Dendritic Cells Shape the B-Cell Antigenome.* Front Immunol, 2016. **7**: p. 225.
166. Jarjour, M., et al., *Fate mapping reveals origin and dynamics of lymph node follicular dendritic cells.* J Exp Med, 2014. **211**(6): p. 1109-22.
167. Park, C.S. and Y.S. Choi, *How do follicular dendritic cells interact intimately with B cells in the germinal centre?* Immunology, 2005. **114**(1): p. 2-10.
168. Dedeoglu, F., et al., *Induction of activation-induced cytidine deaminase gene expression by IL-4 and CD40 ligation is dependent on STAT6 and NFkappaB.* Int Immunol, 2004. **16**(3): p. 395-404.
169. Muramatsu, M., et al., *Specific expression of activation-induced cytidine deaminase (AID), a novel member of the RNA-editing deaminase family in germinal center B cells.* J Biol Chem, 1999. **274**(26): p. 18470-6.
170. Castigli, E., et al., *TACI and BAFF-R mediate isotype switching in B cells.* J Exp Med, 2005. **201**(1): p. 35-9.
171. He, B., et al., *The transmembrane activator TACI triggers immunoglobulin class switching by activating B cells through the adaptor MyD88.* Nat Immunol, 2010. **11**(9): p. 836-45.
172. Pasare, C. and R. Medzhitov, *Control of B-cell responses by Toll-like receptors.* Nature, 2005. **438**(7066): p. 364-8.

173. Miyasaka, M. and T. Tanaka, *Lymphocyte trafficking across high endothelial venules: dogmas and enigmas*. Nat Rev Immunol, 2004. **4**(5): p. 360-70.
174. von Andrian, U.H., *Intravital microscopy of the peripheral lymph node microcirculation in mice*. Microcirculation, 1996. **3**(3): p. 287-300.
175. Moussion, C. and J.P. Girard, *Dendritic cells control lymphocyte entry to lymph nodes through high endothelial venules*. Nature, 2011. **479**(7374): p. 542-6.
176. Felten, D.L., et al., *Noradrenergic and peptidergic innervation of lymphoid tissue*. J Immunol, 1985. **135**(2 Suppl): p. 755s-765s.
177. Felten, D.L., et al., *Sympathetic innervation of lymph nodes in mice*. Brain Res Bull, 1984. **13**(6): p. 693-9.
178. Giron, L.T., Jr., K.A. Crutcher, and J.N. Davis, *Lymph nodes--a possible site for sympathetic neuronal regulation of immune responses*. Ann Neurol, 1980. **8**(5): p. 520-5.
179. Panuncio, A.L., et al., *Adrenergic innervation in reactive human lymph nodes*. J Anat, 1999. **194** ( Pt 1): p. 143-6.
180. Huang, J., et al., *S100+ cells: a new neuro-immune cross-talkers in lymph organs*. Sci Rep, 2013. **3**: p. 1114.
181. Fink, T. and E. Weihe, *Multiple neuropeptides in nerves supplying mammalian lymph nodes: messenger candidates for sensory and autonomic neuroimmunomodulation?* Neurosci Lett, 1988. **90**(1-2): p. 39-44.
182. Kurkowski, R., W. Kummer, and C. Heym, *Substance P-immunoreactive nerve fibers in tracheobronchial lymph nodes of the guinea pig: origin, ultrastructure and coexistence with other peptides*. Peptides, 1990. **11**(1): p. 13-20.
183. Weihe, E., et al., *Molecular anatomy of the neuro-immune connection*. Int J Neurosci, 1991. **59**(1-3): p. 1-23.
184. Junt, T., et al., *Subcapsular sinus macrophages in lymph nodes clear lymph-borne viruses and present them to antiviral B cells*. Nature, 2007. **450**(7166): p. 110-4.
185. Ngo, V.N., et al., *Lymphotoxin alpha/beta and tumor necrosis factor are required for stromal cell expression of homing chemokines in B and T cell areas of the spleen*. J Exp Med, 1999. **189**(2): p. 403-12.
186. Bajenoff, M., et al., *Stromal cell networks regulate lymphocyte entry, migration, and territoriality in lymph nodes*. Immunity, 2006. **25**(6): p. 989-1001.
187. Willard-Mack, C.L., *Normal structure, function, and histology of lymph nodes*. Toxicol Pathol, 2006. **34**(5): p. 409-24.
188. Schudel, A.F., D. M., and Thomas, S. N. , *Material design for lymph node drug delivery*. Nat Rev Materials, 2019. **4**: p. 415–428.
189. Trevaskis, N.L., L.M. Kaminskis, and C.J. Porter, *From sewer to saviour - targeting the lymphatic system to promote drug exposure and activity*. Nat Rev Drug Discov, 2015. **14**(11): p. 781-803.
190. Thomas, S.N. and A. Schudel, *Overcoming transport barriers for interstitial-, lymphatic-, and lymph node-targeted drug delivery*. Curr Opin Chem Eng, 2015. **7**: p. 65-74.
191. Ikomi, F., Y. Kawai, and T. Ohhashi, *Recent advance in lymph dynamic analysis in lymphatics and lymph nodes*. Ann Vasc Dis, 2012. **5**(3): p. 258-68.
192. Sixt, M., et al., *The conduit system transports soluble antigens from the afferent lymph to resident dendritic cells in the T cell area of the lymph node*. Immunity, 2005. **22**(1): p. 19-29.

193. Roozendaal, R., et al., *Conduits mediate transport of low-molecular-weight antigen to lymph node follicles*. *Immunity*, 2009. **30**(2): p. 264-76.
194. Gretz, J.E., et al., *Lymph-borne chemokines and other low molecular weight molecules reach high endothelial venules via specialized conduits while a functional barrier limits access to the lymphocyte microenvironments in lymph node cortex*. *J Exp Med*, 2000. **192**(10): p. 1425-40.
195. Phan, T.G., et al., *Subcapsular encounter and complement-dependent transport of immune complexes by lymph node B cells*. *Nat Immunol*, 2007. **8**(9): p. 992-1000.
196. Carrasco, Y.R. and F.D. Batista, *B cells acquire particulate antigen in a macrophage-rich area at the boundary between the follicle and the subcapsular sinus of the lymph node*. *Immunity*, 2007. **27**(1): p. 160-71.
197. Drinker, C.K., M.E. Field, and H.K. Ward, *The Filtering Capacity of Lymph Nodes*. *J Exp Med*, 1934. **59**(4): p. 393-405.
198. Iannacone, M., et al., *Subcapsular sinus macrophages prevent CNS invasion on peripheral infection with a neurotropic virus*. *Nature*, 2010. **465**(7301): p. 1079-83.
199. Mebius, R.E., et al., *The influence of afferent lymphatic vessel interruption on vascular addressin expression*. *J Cell Biol*, 1991. **115**(1): p. 85-95.
200. Hoshi, H., K. Kamiya, and E. Endo, *Cortical structure of the lymph node. I. Effect of blockage of the afferent lymph flow to mouse popliteal nodes for protracted periods*. *J Anat*, 1981. **133**(Pt 4): p. 593-606.
201. Banchereau, J. and R.M. Steinman, *Dendritic cells and the control of immunity*. *Nature*, 1998. **392**(6673): p. 245-52.
202. Chang, J.E. and S.J. Turley, *Stromal infrastructure of the lymph node and coordination of immunity*. *Trends Immunol*, 2015. **36**(1): p. 30-9.
203. Luther, S.A., et al., *Coexpression of the chemokines ELC and SLC by T zone stromal cells and deletion of the ELC gene in the *plt/plt* mouse*. *Proc Natl Acad Sci U S A*, 2000. **97**(23): p. 12694-9.
204. Cyster, J.G., et al., *Follicular stromal cells and lymphocyte homing to follicles*. *Immunol Rev*, 2000. **176**: p. 181-93.
205. Wang, X., et al., *Follicular dendritic cells help establish follicle identity and promote B cell retention in germinal centers*. *J Exp Med*, 2011. **208**(12): p. 2497-510.
206. Gunn, M.D., et al., *A B-cell-homing chemokine made in lymphoid follicles activates Burkitt's lymphoma receptor-1*. *Nature*, 1998. **391**(6669): p. 799-803.
207. Katakai, T., *Marginal reticular cells: a stromal subset directly descended from the lymphoid tissue organizer*. *Front Immunol*, 2012. **3**: p. 200.
208. Mionnet, C., et al., *Identification of a new stromal cell type involved in the regulation of inflamed B cell follicles*. *PLoS Biol*, 2013. **11**(10): p. e1001672.
209. Legler, D.F., et al., *B cell-attracting chemokine 1, a human CXC chemokine expressed in lymphoid tissues, selectively attracts B lymphocytes via BLR1/CXCR5*. *J Exp Med*, 1998. **187**(4): p. 655-60.
210. Ansel, K.M., et al., *In vivo-activated CD4 T cells upregulate CXC chemokine receptor 5 and reprogram their response to lymphoid chemokines*. *J Exp Med*, 1999. **190**(8): p. 1123-34.
211. Okada, T., et al., *Chemokine requirements for B cell entry to lymph nodes and Peyer's patches*. *J Exp Med*, 2002. **196**(1): p. 65-75.
212. Fleige, H., et al., *IL-17-induced CXCL12 recruits B cells and induces follicle formation in BALT in the absence of differentiated FDCs*. *J Exp Med*, 2014. **211**(4): p. 643-51.

213. Bannard, O., et al., *Germinal center centroblasts transition to a centrocyte phenotype according to a timed program and depend on the dark zone for effective selection.* Immunity, 2013. **39**(5): p. 912-24.
214. Bleul, C.C., et al., *The lymphocyte chemoattractant SDF-1 is a ligand for LESTR/fusin and blocks HIV-1 entry.* Nature, 1996. **382**(6594): p. 829-33.
215. Oberlin, E., et al., *The CXC chemokine SDF-1 is the ligand for LESTR/fusin and prevents infection by T-cell-line-adapted HIV-1.* Nature, 1996. **382**(6594): p. 833-5.
216. Griffith, J.W., C.L. Sokol, and A.D. Luster, *Chemokines and chemokine receptors: positioning cells for host defense and immunity.* Annu Rev Immunol, 2014. **32**: p. 659-702.
217. He, W., et al., *Circadian Expression of Migratory Factors Establishes Lineage-Specific Signatures that Guide the Homing of Leukocyte Subsets to Tissues.* Immunity, 2018. **49**(6): p. 1175-1190 e7.
218. Olson, T.S. and K. Ley, *Chemokines and chemokine receptors in leukocyte trafficking.* Am J Physiol Regul Integr Comp Physiol, 2002. **283**(1): p. R7-28.
219. Burns, J.M., et al., *A novel chemokine receptor for SDF-1 and I-TAC involved in cell survival, cell adhesion, and tumor development.* J Exp Med, 2006. **203**(9): p. 2201-13.
220. Infantino, S., B. Moepps, and M. Thelen, *Expression and regulation of the orphan receptor RDC1 and its putative ligand in human dendritic and B cells.* J Immunol, 2006. **176**(4): p. 2197-207.
221. Balabanian, K., et al., *The chemokine SDF-1/CXCL12 binds to and signals through the orphan receptor RDC1 in T lymphocytes.* J Biol Chem, 2005. **280**(42): p. 35760-6.
222. Cruz-Orengo, L., et al., *CXCR7 influences leukocyte entry into the CNS parenchyma by controlling abluminal CXCL12 abundance during autoimmunity.* J Exp Med, 2011. **208**(2): p. 327-39.
223. Randolph, G.J., V. Angeli, and M.A. Swartz, *Dendritic-cell trafficking to lymph nodes through lymphatic vessels.* Nat Rev Immunol, 2005. **5**(8): p. 617-28.
224. Bao, X., et al., *Endothelial heparan sulfate controls chemokine presentation in recruitment of lymphocytes and dendritic cells to lymph nodes.* Immunity, 2010. **33**(5): p. 817-29.
225. Yoshida, R., et al., *Secondary lymphoid-tissue chemokine is a functional ligand for the CC chemokine receptor CCR7.* J Biol Chem, 1998. **273**(12): p. 7118-22.
226. Forster, R., et al., *CCR7 coordinates the primary immune response by establishing functional microenvironments in secondary lymphoid organs.* Cell, 1999. **99**(1): p. 23-33.
227. Schumann, K., et al., *Immobilized chemokine fields and soluble chemokine gradients cooperatively shape migration patterns of dendritic cells.* Immunity, 2010. **32**(5): p. 703-13.
228. de Paz, J.L., et al., *Profiling heparin-chemokine interactions using synthetic tools.* ACS Chem Biol, 2007. **2**(11): p. 735-44.
229. Baekkevold, E.S., et al., *The CCR7 ligand elc (CCL19) is transcytosed in high endothelial venules and mediates T cell recruitment.* J Exp Med, 2001. **193**(9): p. 1105-12.
230. Nakano, H., et al., *Genetic defect in T lymphocyte-specific homing into peripheral lymph nodes.* Eur J Immunol, 1997. **27**(1): p. 215-21.

231. Nakano, H., et al., *A novel mutant gene involved in T-lymphocyte-specific homing into peripheral lymphoid organs on mouse chromosome 4*. *Blood*, 1998. **91**(8): p. 2886-95.
232. Mori, S., et al., *Mice lacking expression of the chemokines CCL21-ser and CCL19 (plt mice) demonstrate delayed but enhanced T cell immune responses*. *J Exp Med*, 2001. **193**(2): p. 207-18.
233. Nakano, H., et al., *Blood-derived inflammatory dendritic cells in lymph nodes stimulate acute T helper type 1 immune responses*. *Nat Immunol*, 2009. **10**(4): p. 394-402.
234. Allende, M.L., et al., *Expression of the sphingosine 1-phosphate receptor, S1P1, on T-cells controls thymic emigration*. *J Biol Chem*, 2004. **279**(15): p. 15396-401.
235. Matloubian, M., et al., *Lymphocyte egress from thymus and peripheral lymphoid organs is dependent on S1P receptor 1*. *Nature*, 2004. **427**(6972): p. 355-60.
236. Chaffin, K.E. and R.M. Perlmutter, *A pertussis toxin-sensitive process controls thymocyte emigration*. *Eur J Immunol*, 1991. **21**(10): p. 2565-73.
237. Lo, C.G., et al., *Cyclical modulation of sphingosine-1-phosphate receptor 1 surface expression during lymphocyte recirculation and relationship to lymphoid organ transit*. *J Exp Med*, 2005. **201**(2): p. 291-301.
238. Spiegel, S. and S. Milstien, *Sphingosine-1-phosphate: an enigmatic signalling lipid*. *Nat Rev Mol Cell Biol*, 2003. **4**(5): p. 397-407.
239. Mandala, S., et al., *Alteration of lymphocyte trafficking by sphingosine-1-phosphate receptor agonists*. *Science*, 2002. **296**(5566): p. 346-9.
240. Kappos, L., et al., *A placebo-controlled trial of oral fingolimod in relapsing multiple sclerosis*. *N Engl J Med*, 2010. **362**(5): p. 387-401.
241. Sanford, M., *Fingolimod: a review of its use in relapsing-remitting multiple sclerosis*. *Drugs*, 2014. **74**(12): p. 1411-33.
242. Kabashima, K., et al., *Plasma cell S1P1 expression determines secondary lymphoid organ retention versus bone marrow tropism*. *J Exp Med*, 2006. **203**(12): p. 2683-90.
243. Pham, T.H., et al., *S1P1 receptor signaling overrides retention mediated by G alpha i-coupled receptors to promote T cell egress*. *Immunity*, 2008. **28**(1): p. 122-33.
244. Hall, J.G. and B. Morris, *The immediate effect of antigens on the cell output of a lymph node*. *Br J Exp Pathol*, 1965. **46**(4): p. 450-4.
245. Bankovich, A.J., L.R. Shiow, and J.G. Cyster, *CD69 suppresses sphingosine 1-phosphate receptor-1 (S1P1) function through interaction with membrane helix 4*. *J Biol Chem*, 2010. **285**(29): p. 22328-37.
246. Shiow, L.R., et al., *CD69 acts downstream of interferon-alpha/beta to inhibit S1P1 and lymphocyte egress from lymphoid organs*. *Nature*, 2006. **440**(7083): p. 540-4.
247. Tomura, M., et al., *Activated regulatory T cells are the major T cell type emigrating from the skin during a cutaneous immune response in mice*. *J Clin Invest*, 2010. **120**(3): p. 883-93.
248. Suzuki, K., et al., *Adrenergic control of the adaptive immune response by diurnal lymphocyte recirculation through lymph nodes*. *J Exp Med*, 2016. **213**(12): p. 2567-2574.
249. Druzd, D., et al., *Lymphocyte Circadian Clocks Control Lymph Node Trafficking and Adaptive Immune Responses*. *Immunity*, 2017. **46**(1): p. 120-132.
250. Girard, J.P., C. Mousson, and R. Forster, *HEVs, lymphatics and homeostatic immune cell trafficking in lymph nodes*. *Nat Rev Immunol*, 2012. **12**(11): p. 762-73.

251. Schnoor, M., et al., *Crossing the Vascular Wall: Common and Unique Mechanisms Exploited by Different Leukocyte Subsets during Extravasation*. *Mediators Inflamm*, 2015. **2015**: p. 946509.
252. Pick, R., et al., *Time-of-Day-Dependent Trafficking and Function of Leukocyte Subsets*. *Trends Immunol*, 2019. **40**(6): p. 524-537.
253. Liu, K., et al., *In vivo analysis of dendritic cell development and homeostasis*. *Science*, 2009. **324**(5925): p. 392-7.
254. Chen, S., et al., *Suppression of tumor formation in lymph nodes by L-selectin-mediated natural killer cell recruitment*. *J Exp Med*, 2005. **202**(12): p. 1679-89.
255. Herzog, B.H., et al., *Podoplanin maintains high endothelial venule integrity by interacting with platelet CLEC-2*. *Nature*, 2013. **502**(7469): p. 105-9.
256. Romero-Ortega, M., *Peripheral Nerves, Anatomy and Physiology of*. *Encyclopedia of Computational Neuroscience*, 2014.
257. McCorry, L.K., *Physiology of the autonomic nervous system*. *Am J Pharm Educ*, 2007. **71**(4): p. 78.
258. Ernsberger, U. and H. Rohrer, *Sympathetic tales: subdivisions of the autonomic nervous system and the impact of developmental studies*. *Neural Dev*, 2018. **13**(1): p. 20.
259. McLachlan, E.M. and R.L. Meckler, *Characteristics of synaptic input to three classes of sympathetic neurone in the coeliac ganglion of the guinea-pig*. *J Physiol*, 1989. **415**: p. 109-29.
260. Baron, R., W. Janig, and E.M. McLachlan, *The afferent and sympathetic components of the lumbar spinal outflow to the colon and pelvic organs in the cat. III. The colonic nerves, incorporating an analysis of all components of the lumbar prevertebral outflow*. *J Comp Neurol*, 1985. **238**(2): p. 158-68.
261. Benninger, B. and J. McNeil, *Transitional Nerve: A New and Original Classification of a Peripheral Nerve Supported by the Nature of the Accessory Nerve (CN XI)*. *Neurol Res Int*, 2010. **2010**: p. 476018.
262. Berthoud, H.R. and W.L. Neuhuber, *Functional and chemical anatomy of the afferent vagal system*. *Auton Neurosci*, 2000. **85**(1-3): p. 1-17.
263. Espinosa-Medina, I., et al., *The "sacral parasympathetic": ontogeny and anatomy of a myth*. *Clin Auton Res*, 2018. **28**(1): p. 13-21.
264. Dail, W.G., G. Walton, and M.P. Olmsted, *Penile erection in the rat: stimulation of the hypogastric nerve elicits increases in penile pressure after chronic interruption of the sacral parasympathetic outflow*. *J Auton Nerv Syst*, 1989. **28**(3): p. 251-7.
265. de Groat, W.C. and M. Kawatani, *Reorganization of sympathetic preganglionic connections in cat bladder ganglia following parasympathetic denervation*. *J Physiol*, 1989. **409**: p. 431-49.
266. Taylor, D.C., H.W. Korf, and F.K. Pierau, *Distribution of sensory neurons of the pudendal nerve in the dorsal root ganglia and their projection to the spinal cord. Horseradish-peroxidase studies in the rat*. *Cell Tissue Res*, 1982. **226**(3): p. 555-64.
267. Zeisel, A., et al., *Molecular Architecture of the Mouse Nervous System*. *Cell*, 2018. **174**(4): p. 999-1014 e22.
268. Tayo, E.K. and R.G. Williams, *Catecholaminergic parasympathetic efferents within the dorsal motor nucleus of the vagus in the rat: a quantitative analysis*. *Neurosci Lett*, 1988. **90**(1-2): p. 1-5.

269. Baral, P., S. Udit, and I.M. Chiu, *Pain and immunity: implications for host defence*. Nat Rev Immunol, 2019.
270. Kabata, H. and D. Artis, *Neuro-immune crosstalk and allergic inflammation*. J Clin Invest, 2019. **130**: p. 1475-1482.
271. Souza-Moreira, L., et al., *Neuropeptides as pleiotropic modulators of the immune response*. Neuroendocrinology, 2011. **94**(2): p. 89-100.
272. Assas, B.M., J.I. Pennock, and J.A. Miyan, *Calcitonin gene-related peptide is a key neurotransmitter in the neuro-immune axis*. Front Neurosci, 2014. **8**: p. 23.
273. Bellinger, D.L., et al., *Sympathetic modulation of immunity: relevance to disease*. Cell Immunol, 2008. **252**(1-2): p. 27-56.
274. Elenkov, I.J., et al., *The sympathetic nerve--an integrative interface between two supersystems: the brain and the immune system*. Pharmacol Rev, 2000. **52**(4): p. 595-638.
275. Kenney, M.J. and C.K. Ganta, *Autonomic nervous system and immune system interactions*. Compr Physiol, 2014. **4**(3): p. 1177-200.
276. Tracey, K.J., *Reflex control of immunity*. Nat Rev Immunol, 2009. **9**(6): p. 418-28.
277. Olofsson, P.S., et al., *Rethinking inflammation: neural circuits in the regulation of immunity*. Immunol Rev, 2012. **248**(1): p. 188-204.
278. Savastano, L.E., et al., *Sciatic nerve injury: a simple and subtle model for investigating many aspects of nervous system damage and recovery*. J Neurosci Methods, 2014. **227**: p. 166-80.
279. Schmalbruch, H., *Fiber composition of the rat sciatic nerve*. Anat Rec, 1986. **215**(1): p. 71-81.
280. Dimitrijevic, M. and S. Stanojevic, *The intriguing mission of neuropeptide Y in the immune system*. Amino Acids, 2013. **45**(1): p. 41-53.
281. Rosas-Ballina, M., et al., *Acetylcholine-synthesizing T cells relay neural signals in a vagus nerve circuit*. Science, 2011. **334**(6052): p. 98-101.
282. Mashaghi, A., et al., *Neuropeptide substance P and the immune response*. Cell Mol Life Sci, 2016. **73**(22): p. 4249-4264.
283. Lorton, D. and D.L. Bellinger, *Molecular mechanisms underlying beta-adrenergic receptor-mediated cross-talk between sympathetic neurons and immune cells*. Int J Mol Sci, 2015. **16**(3): p. 5635-65.
284. Bartik, M.M., et al., *Costimulatory signals modulate the antiproliferative effects of agents that elevate cAMP in T cells*. Cell Immunol, 1994. **158**(1): p. 116-30.
285. Ramer-Quinn, D.S., R.A. Baker, and V.M. Sanders, *Activated T helper 1 and T helper 2 cells differentially express the beta-2-adrenergic receptor: a mechanism for selective modulation of T helper 1 cell cytokine production*. J Immunol, 1997. **159**(10): p. 4857-67.
286. Kanemi, O., et al., *Acute stress reduces intraparenchymal lung natural killer cells via beta-adrenergic stimulation*. Clin Exp Immunol, 2005. **139**(1): p. 25-34.
287. Shakhar, G. and S. Ben-Eliyahu, *In vivo beta-adrenergic stimulation suppresses natural killer activity and compromises resistance to tumor metastasis in rats*. J Immunol, 1998. **160**(7): p. 3251-8.
288. Xiao, J., et al., *Modulation of natural killer cell function by alpha-adrenoreceptor-coupled signalling*. Neuro Endocrinol Lett, 2010. **31**(5): p. 635-44.

289. Ding, W., et al., *Calcitonin Gene-Related Peptide-Exposed Endothelial Cells Bias Antigen Presentation to CD4+ T Cells toward a Th17 Response*. J Immunol, 2016. **196**(5): p. 2181-94.
290. Tsujikawa, K., et al., *Hypertension and dysregulated proinflammatory cytokine production in receptor activity-modifying protein 1-deficient mice*. Proc Natl Acad Sci U S A, 2007. **104**(42): p. 16702-7.
291. Zimmerman, B.J., D.C. Anderson, and D.N. Granger, *Neuropeptides promote neutrophil adherence to endothelial cell monolayers*. Am J Physiol, 1992. **263**(5 Pt 1): p. G678-82.
292. Sung, C.P., et al., *CGRP stimulates the adhesion of leukocytes to vascular endothelial cells*. Peptides, 1992. **13**(3): p. 429-34.
293. Huang, J., et al., *Calcitonin gene-related peptide inhibits chemokine production by human dermal microvascular endothelial cells*. Brain Behav Immun, 2011. **25**(4): p. 787-99.
294. Gomes, R.N., et al., *Calcitonin gene-related peptide inhibits local acute inflammation and protects mice against lethal endotoxemia*. Shock, 2005. **24**(6): p. 590-4.
295. Paunicka, K.J., et al., *Severing corneal nerves in one eye induces sympathetic loss of immune privilege and promotes rejection of future corneal allografts placed in either eye*. Am J Transplant, 2015. **15**(6): p. 1490-501.
296. Arima, Y., et al., *Regional neural activation defines a gateway for autoreactive T cells to cross the blood-brain barrier*. Cell, 2012. **148**(3): p. 447-57.
297. Mendez-Ferrer, S., et al., *Haematopoietic stem cell release is regulated by circadian oscillations*. Nature, 2008. **452**(7186): p. 442-7.
298. Garcia-Garcia, A., et al., *Dual cholinergic signals regulate daily migration of hematopoietic stem cells and leukocytes*. Blood, 2019. **133**(3): p. 224-236.
299. Borovikova, L.V., et al., *Vagus nerve stimulation attenuates the systemic inflammatory response to endotoxin*. Nature, 2000. **405**(6785): p. 458-62.
300. Rosas-Ballina, M., et al., *Splenic nerve is required for cholinergic antiinflammatory pathway control of TNF in endotoxemia*. Proc Natl Acad Sci U S A, 2008. **105**(31): p. 11008-13.
301. Wang, H., et al., *Nicotinic acetylcholine receptor alpha7 subunit is an essential regulator of inflammation*. Nature, 2003. **421**(6921): p. 384-8.
302. Parrish, W.R., et al., *Modulation of TNF release by choline requires alpha7 subunit nicotinic acetylcholine receptor-mediated signaling*. Mol Med, 2008. **14**(9-10): p. 567-74.
303. Koopman, F.A., et al., *Vagus nerve stimulation inhibits cytokine production and attenuates disease severity in rheumatoid arthritis*. Proc Natl Acad Sci U S A, 2016. **113**(29): p. 8284-9.
304. Gabanyi, I., et al., *Neuro-immune Interactions Drive Tissue Programming in Intestinal Macrophages*. Cell, 2016. **164**(3): p. 378-91.
305. Moriyama, S., et al., *beta2-adrenergic receptor-mediated negative regulation of group 2 innate lymphoid cell responses*. Science, 2018. **359**(6379): p. 1056-1061.
306. Klose, C.S.N., et al., *The neuropeptide neuromedin U stimulates innate lymphoid cells and type 2 inflammation*. Nature, 2017. **549**(7671): p. 282-286.
307. Wallrapp, A., et al., *The neuropeptide NMU amplifies ILC2-driven allergic lung inflammation*. Nature, 2017. **549**(7672): p. 351-356.

308. Sui, P., et al., *Pulmonary neuroendocrine cells amplify allergic asthma responses*. Science, 2018. **360**(6393).
309. Branchfield, K., et al., *Pulmonary neuroendocrine cells function as airway sensors to control lung immune response*. Science, 2016. **351**(6274): p. 707-10.
310. Sloan, E.K., et al., *Social stress enhances sympathetic innervation of primate lymph nodes: mechanisms and implications for viral pathogenesis*. J Neurosci, 2007. **27**(33): p. 8857-65.
311. Straub, R.H., et al., *Increased density of sympathetic nerve fibers in metabolically activated fat tissue surrounding human synovium and mouse lymph nodes in arthritis*. Arthritis Rheum, 2011. **63**(11): p. 3234-42.
312. Helme, R.D., et al., *The effect of substance P on the regional lymph node antibody response to antigenic stimulation in capsaicin-pretreated rats*. J Immunol, 1987. **139**(10): p. 3470-3.
313. Shepherd, A.J., et al., *Mobilisation of specific T cells from lymph nodes in contact sensitivity requires substance P*. J Neuroimmunol, 2005. **164**(1-2): p. 115-23.
314. McLachlan, J.B., et al., *Mast cell-derived tumor necrosis factor induces hypertrophy of draining lymph nodes during infection*. Nat Immunol, 2003. **4**(12): p. 1199-205.
315. Kochi, T., et al., *Characterization of the arterial anatomy of the murine hindlimb: functional role in the design and understanding of ischemia models*. PLoS One, 2013. **8**(12): p. e84047.
316. Hendriks, H.R., *Occlusion of the lymph flow to rat popliteal lymph nodes for protracted periods*. Z Versuchstierkd, 1978. **20**(3): p. 105-12.
317. Savastano, L.E., et al., *A standardized surgical technique for rat superior cervical ganglionectomy*. J Neurosci Methods, 2010. **192**(1): p. 22-33.
318. Lucas, D., et al., *Chemotherapy-induced bone marrow nerve injury impairs hematopoietic regeneration*. Nat Med, 2013. **19**(6): p. 695-703.
319. Petersilge, C.A., et al., *Denervation hypertrophy of muscle: MR features*. J Comput Assist Tomogr, 1995. **19**(4): p. 596-600.
320. Gubser, C., et al., *Monoclonal regulatory T cells provide insights into T cell suppression*. Sci Rep, 2016. **6**: p. 25758.
321. Guermonprez, P., et al., *Antigen presentation and T cell stimulation by dendritic cells*. Annu Rev Immunol, 2002. **20**: p. 621-67.
322. Buchner, C., et al., *Anti-nuclear antibody screening using HEp-2 cells*. J Vis Exp, 2014(88): p. e51211.
323. Glinka, Y., M. Gassen, and M.B. Youdim, *Mechanism of 6-hydroxydopamine neurotoxicity*. J Neural Transm Suppl, 1997. **50**: p. 55-66.
324. Pinho-Ribeiro, F.A., W.A. Verri, Jr., and I.M. Chiu, *Nociceptor Sensory Neuron-Immune Interactions in Pain and Inflammation*. Trends Immunol, 2017. **38**(1): p. 5-19.
325. Kubera, M., et al., *Effect of sciatic denervation on cell-mediated immunity*. Int J Immunopharmacol, 1997. **19**(1): p. 25-9.
326. Thangam, E.B., et al., *The Role of Histamine and Histamine Receptors in Mast Cell-Mediated Allergy and Inflammation: The Hunt for New Therapeutic Targets*. Front Immunol, 2018. **9**: p. 1873.
327. Criado, P.R., et al., *Histamine, histamine receptors and antihistamines: new concepts*. An Bras Dermatol, 2010. **85**(2): p. 195-210.

328. Thurmond, R.L., E.W. Gelfand, and P.J. Dunford, *The role of histamine H1 and H4 receptors in allergic inflammation: the search for new antihistamines*. Nat Rev Drug Discov, 2008. **7**(1): p. 41-53.
329. Kimura, L.F., et al., *Mast cells and histamine play an important role in edema and leukocyte recruitment induced by Potamotrygon motoro stingray venom in mice*. Toxicon, 2015. **103**: p. 65-73.
330. Branco, A., et al., *Role of Histamine in Modulating the Immune Response and Inflammation*. Mediators Inflamm, 2018. **2018**: p. 9524075.
331. O'Mahony, L., M. Akdis, and C.A. Akdis, *Regulation of the immune response and inflammation by histamine and histamine receptors*. J Allergy Clin Immunol, 2011. **128**(6): p. 1153-62.
332. Rosa, A.C. and R. Fantozzi, *The role of histamine in neurogenic inflammation*. Br J Pharmacol, 2013. **170**(1): p. 38-45.
333. Dunford, P.J., et al., *Histamine H4 receptor antagonists are superior to traditional antihistamines in the attenuation of experimental pruritus*. J Allergy Clin Immunol, 2007. **119**(1): p. 176-83.
334. Decosterd, I. and C.J. Woolf, *Spared nerve injury: an animal model of persistent peripheral neuropathic pain*. Pain, 2000. **87**(2): p. 149-58.
335. Kwiatkowski, H., *Histamine in nervous tissue*. J Physiol, 1943. **102**(1): p. 32-41.
336. Olsson, Y. and J. Sjostrand, *Proliferation of mast cells in peripheral nerves during Wallerian degeneration. A radioautographic study*. Acta Neuropathol, 1969. **13**(2): p. 111-21.
337. Olsson, Y., *Degranulation of mast cells in peripheral nerve injuries*. Acta Neurol Scand, 1967. **43**(3): p. 365-74.
338. Galli, S.J., S. Nakae, and M. Tsai, *Mast cells in the development of adaptive immune responses*. Nat Immunol, 2005. **6**(2): p. 135-42.
339. Krystel-Whittemore, M., K.N. Dileepan, and J.G. Wood, *Mast Cell: A Multi-Functional Master Cell*. Front Immunol, 2015. **6**: p. 620.
340. Sumpter, T.L., S.C. Balmert, and D.H. Kaplan, *Cutaneous immune responses mediated by dendritic cells and mast cells*. JCI Insight, 2019. **4**(1).
341. Carroll-Portillo, A., et al., *Mast cells and dendritic cells form synapses that facilitate antigen transfer for T cell activation*. J Cell Biol, 2015. **210**(5): p. 851-64.
342. Dudeck, J., et al., *Mast cells acquire MHCII from dendritic cells during skin inflammation*. J Exp Med, 2017. **214**(12): p. 3791-3811.
343. McDonald, D.M., *Neurogenic inflammation in the rat trachea. I. Changes in venules, leucocytes and epithelial cells*. J Neurocytol, 1988. **17**(5): p. 583-603.
344. Olivier, B.J., et al., *Vagal innervation is required for the formation of tertiary lymphoid tissue in colitis*. Eur J Immunol, 2016. **46**(10): p. 2467-2480.
345. Jacobelli, J., et al., *A single class II myosin modulates T cell motility and stopping, but not synapse formation*. Nat Immunol, 2004. **5**(5): p. 531-8.
346. Brodie, C. and E.W. Gelfand, *Functional nerve growth factor receptors on human B lymphocytes. Interaction with IL-2*. J Immunol, 1992. **148**(11): p. 3492-7.
347. Ankeny, D.P. and P.G. Popovich, *B cells and autoantibodies: complex roles in CNS injury*. Trends Immunol, 2010. **31**(9): p. 332-8.
348. Madden, K.S., et al., *Sympathetic nervous system modulation of the immune system. II. Induction of lymphocyte proliferation and migration in vivo by chemical sympathectomy*. J Neuroimmunol, 1994. **49**(1-2): p. 67-75.

349. Madden, K.S., et al., *Sympathetic nervous system modulation of the immune system. III. Alterations in T and B cell proliferation and differentiation in vitro following chemical sympathectomy*. J Neuroimmunol, 1994. **49**(1-2): p. 77-87.
350. Cui, J.G., et al., *Possible role of inflammatory mediators in tactile hypersensitivity in rat models of mononeuropathy*. Pain, 2000. **88**(3): p. 239-48.
351. Davies, A.J., et al., *Natural Killer Cells Degenerate Intact Sensory Afferents following Nerve Injury*. Cell, 2019. **176**(4): p. 716-728 e18.
352. Be'eri, H., et al., *The cytokine network of wallerian degeneration: IL-10 and GM-CSF*. Eur J Neurosci, 1998. **10**(8): p. 2707-13.
353. Sawada, T., et al., *Spatiotemporal quantification of tumor necrosis factor-alpha and interleukin-10 after crush injury in rat sciatic nerve utilizing immunohistochemistry*. Neurosci Lett, 2007. **417**(1): p. 55-60.
354. Dubovy, P., I. Klusakova, and I. Hradilova Svizenska, *Inflammatory profiling of Schwann cells in contact with growing axons distal to nerve injury*. Biomed Res Int, 2014. **2014**: p. 691041.
355. Siqueira Mietto, B., et al., *Role of IL-10 in Resolution of Inflammation and Functional Recovery after Peripheral Nerve Injury*. J Neurosci, 2015. **35**(50): p. 16431-42.
356. Krumbholz, M., et al., *Chemokines in multiple sclerosis: CXCL12 and CXCL13 up-regulation is differentially linked to CNS immune cell recruitment*. Brain, 2006. **129**(Pt 1): p. 200-11.
357. Kim, C.F. and G. Moalem-Taylor, *Interleukin-17 contributes to neuroinflammation and neuropathic pain following peripheral nerve injury in mice*. J Pain, 2011. **12**(3): p. 370-83.
358. Kuwabara, T., et al., *The Role of IL-17 and Related Cytokines in Inflammatory Autoimmune Diseases*. Mediators Inflamm, 2017. **2017**: p. 3908061.
359. Foulds, K.E. and H. Shen, *Clonal competition inhibits the proliferation and differentiation of adoptively transferred TCR transgenic CD4 T cells in response to infection*. J Immunol, 2006. **176**(5): p. 3037-43.
360. Moon, J.J., et al., *Naive CD4(+) T cell frequency varies for different epitopes and predicts repertoire diversity and response magnitude*. Immunity, 2007. **27**(2): p. 203-13.
361. Ford, M.L., et al., *Antigen-specific precursor frequency impacts T cell proliferation, differentiation, and requirement for costimulation*. J Exp Med, 2007. **204**(2): p. 299-309.
362. Batista, F.D. and N.E. Harwood, *The who, how and where of antigen presentation to B cells*. Nat Rev Immunol, 2009. **9**(1): p. 15-27.
363. Heesters, B.A., et al., *Antigen Presentation to B Cells*. Trends Immunol, 2016. **37**(12): p. 844-854.
364. Jakubzick, C., et al., *Minimal differentiation of classical monocytes as they survey steady-state tissues and transport antigen to lymph nodes*. Immunity, 2013. **39**(3): p. 599-610.
365. Thomas, S.N., et al., *Impaired humoral immunity and tolerance in K14-VEGFR-3-Ig mice that lack dermal lymphatic drainage*. J Immunol, 2012. **189**(5): p. 2181-90.
366. Hoshi, H., et al., *Histological observations on rat popliteal lymph nodes after blockage of their afferent lymphatics*. Arch Histol Jpn, 1985. **48**(2): p. 135-48.

367. Hendriks, H.R., I.L. Eestermans, and E.C. Hoefsmit, *Depletion of macrophages and disappearance of postcapillary high endothelial venules in lymph nodes deprived of afferent lymphatic vessels*. Cell Tissue Res, 1980. **211**(3): p. 375-89.
368. Hendriks, H.R., A.M. Duijvestijn, and G. Kraal, *Rapid decrease in lymphocyte adherence to high endothelial venules in lymph nodes deprived of afferent lymphatic vessels*. Eur J Immunol, 1987. **17**(12): p. 1691-5.
369. Bozzacco, L. and H. Yu, *Identification and quantitation of MHC class II-bound peptides from mouse spleen dendritic cells by immunoprecipitation and mass spectrometry analysis*. Methods Mol Biol, 2013. **1061**: p. 231-43.
370. Graham, D.B., et al., *Antigen discovery and specification of immunodominance hierarchies for MHCII-restricted epitopes*. Nat Med, 2018. **24**(11): p. 1762-1772.
371. Balazs, M., et al., *Blood dendritic cells interact with splenic marginal zone B cells to initiate T-independent immune responses*. Immunity, 2002. **17**(3): p. 341-52.
372. Xiao, L., et al., *Renal Denervation Prevents Immune Cell Activation and Renal Inflammation in Angiotensin II-Induced Hypertension*. Circ Res, 2015. **117**(6): p. 547-57.
373. Chiu, I.M., C.A. von Hehn, and C.J. Woolf, *Neurogenic inflammation and the peripheral nervous system in host defense and immunopathology*. Nat Neurosci, 2012. **15**(8): p. 1063-7.
374. Marriott, I. and K.L. Bost, *Expression of authentic substance P receptors in murine and human dendritic cells*. J Neuroimmunol, 2001. **114**(1-2): p. 131-41.
375. Stanisz, A.M., et al., *Distribution of substance P receptors on murine spleen and Peyer's patch T and B cells*. J Immunol, 1987. **139**(3): p. 749-54.
376. Janelins, B.M., et al., *Proinflammatory tachykinins that signal through the neurokinin 1 receptor promote survival of dendritic cells and potent cellular immunity*. Blood, 2009. **113**(13): p. 3017-26.
377. Lambrecht, B.N., et al., *Endogenously produced substance P contributes to lymphocyte proliferation induced by dendritic cells and direct TCR ligation*. Eur J Immunol, 1999. **29**(12): p. 3815-25.
378. Janelins, B.M., et al., *Neurokinin-1 receptor agonists bias therapeutic dendritic cells to induce type 1 immunity by licensing host dendritic cells to produce IL-12*. Blood, 2013. **121**(15): p. 2923-33.
379. Ahmed, M., et al., *Effects of surgical denervation on substance P and calcitonin gene-related peptide in adjuvant arthritis*. Peptides, 1995. **16**(4): p. 569-79.
380. Ahmed, M., et al., *Capsaicin effects on substance P and CGRP in rat adjuvant arthritis*. Regul Pept, 1995. **55**(1): p. 85-102.
381. Yaraee, R., et al., *Effect of neuropeptides (SP and CGRP) on antigen presentation by macrophages*. Immunopharmacol Immunotoxicol, 2005. **27**(3): p. 395-404.
382. Wang, F., et al., *Calcitonin gene-related peptide inhibits interleukin 2 production by murine T lymphocytes*. J Biol Chem, 1992. **267**(29): p. 21052-7.
383. Bulloch, K., et al., *Selective regulation of T-cell development and function by calcitonin gene-related peptide in thymus and spleen. An example of differential regional regulation of immunity by the neuroendocrine system*. Ann N Y Acad Sci, 1998. **840**: p. 551-62.
384. Schlomer, J.J., et al., *Calcitonin gene-related peptide inhibits early B cell development in vivo*. J Leukoc Biol, 2007. **81**(3): p. 802-8.

385. McGillis, J.P., et al., *Modulation of B lymphocyte differentiation by calcitonin gene-related peptide (CGRP). II. Inhibition of LPS-induced kappa light chain expression by CGRP.* Cell Immunol, 1993. **150**(2): p. 405-16.
386. Kawamura, N., et al., *Differential effects of neuropeptides on cytokine production by mouse helper T cell subsets.* Neuroimmunomodulation, 1998. **5**(1-2): p. 9-15.
387. Ostrowski, S.M., et al., *Cutaneous denervation of psoriasiform mouse skin improves acanthosis and inflammation in a sensory neuropeptide-dependent manner.* J Invest Dermatol, 2011. **131**(7): p. 1530-8.
388. Tostanoski, L.H., et al., *Reprogramming the Local Lymph Node Microenvironment Promotes Tolerance that Is Systemic and Antigen Specific.* Cell Rep, 2016. **16**(11): p. 2940-2952.



## 6 Appendices

### 6.1 Appendix 1 – flow cytometry configuration

#### Flow cytometry configuration

Excitation laser (nm)	Fluorescence channel	Default filter	Filter range (nm)
405	9	450/50	425-475
	10	550/40	530-570
488	1	525BP	xxx-550
	2	575BP/26	562-588
	3	620/30	606-635
	4	695/30	680-710
	5	755LP	>755
633	6	660BP	650-670
	7	725/20	715-735
	8	755/LP	>755

## 6.2 Appendix 2 – antibody list

### Antibodies for Flow-Cytometry

Purpose	Target	Fluorochrome	Clone	Amount	Product #	Manufacturer	Panels
blocking	CD16/32		93	1:50	101302	Biolegend	2, 4
staining (flow)	CD3	PE/Dazzle™	17A2	1:200	100246	Biolegend	1, 2
staining (flow)	CD4	BV570	RM4-5	1:200	100542	Biolegend	2
staining (flow)	CD4	APC	GK1.5	1:400	100412	Biolegend	2
staining (flow)	CD8	PE	53-6.7	1:200	100707	Biolegend	1
staining (flow)	CD8	PE/Cy7	53-6.7	1:400	100722	Biolegend	2
staining (flow)	CD11b	PE	M1/70	1:400	101208	Biolegend	2
staining (flow)	CD11b	Alexa 700	M1/70	1:200	101222	Biolegend	4
staining (flow)	CD11c	APC/Cy7	N418	1:200	117323	Biolegend	1, 2, 4
staining (flow)	CD31	APC	MEC13.3	1:200	102509	Biolegend	5
staining (flow)	CD45	PE/Dazzle™	30-F11	1:200	103145	Biolegend	4
staining (flow)	CD45	FITC	30-F11	1:200	103107	Biolegend	5
staining (flow)	CD45R/B220	PE/Cy7	RA3-6B2	1:200	103222	Biolegend	1, 3
staining (flow)	CD49b	PE/Cy7	DX5	1:200	108922	Biolegend	
staining (flow)	CD103	FITC	2E7	1:200	121419	Biolegend	4
staining (flow)	CD138	PE	281-2	1:200	142504	Biolegend	3
staining (flow)	CD169	Alexa 647	3D6.112	1:200	142408	Biolegend	1
staining (flow)	EpCAM	Alexa 647	G8.8	1:200	118212	Biolegend	4
staining (flow)	FAS	PE-CF594	Jo2	1:200	562499	BD Bioscience	3
staining (flow)	GL7	Alexa 647	GL7	1:200	144606	Biolegend	3
staining (flow)	Gr-1	PerCP/Cy5.5	RB6-8C5	1:200	108428	Biolegend	1
staining (flow)	Gr-1	FITC	RB6-8C5	1:400	108406	Biolegend	2, 3
staining (flow)	Ly6C	PE	HK1.4	1:200	128007	Biolegend	4
staining (flow)	Ly6G	PerCP/Cy5.5	1A8	1:200	127615	Biolegend	4
staining (flow)	MHCII	PE/Cy5	M5/114.15.2	1:1000	107611	Biolegend	2
staining (flow)	MHCII	PE/Cy7	M5/114.15.2	1:200	107629	Biolegend	3
staining (flow)	NK1.1	Alexa 700	PK136	1:200	56-5941-82	eBioscience	1
staining (flow)	podoplanin	PE	8.1.1.	1:200	127407	Biolegend	5

1. general immune subsets in the popliteal lymph node
2. dendritic cells in the popliteal lymph node
3. B cell differentiation subsets
4. immune subsets in paws
5. stromal cells in the popliteal lymph node

Continued on the next page

## Antibodies for Immunofluorescence

Purpose	Target	Fluorochrome	Clone	Amount	Product #	Manufacturer	Note
staining (IF)	TH		poly	1:1000	AB152	Merck Millipore	1
staining (IF)	CD31	Alexa 647	MEC13.3	1:100	102516	Biolegend	1
staining (IF)	CD4	APC	GK1.5	1:100	100412	Biolegend	1
staining (IF)	CD8	Alexa 647	53-6.7	1:100	100724	Biolegend	1
staining (IF)	B220	Alexa 488	RA3-6B2	1:100	103225	Biolegend	1
staining (IF)	Ki67	PE	SoIA15	1:100	12-5698-82	eBioscience	1
staining (IF)	GL7	Alexa 647	GL7	1:100	144606	Biolegend	1
staining (IF)	CGRP		poly	1:1000	24112	Immunostar	1
staining (IF)	$\beta$ 3-tubulin	Alexa 488	2G10-TB3	1:200	54-4510-82	eBioscience	1
staining (IF)	NF-H		poly	1:200	AB5539	Merck Millipore	1
staining (IF)	NF-M		poly	1:200	AB5735	Merck Millipore	1
staining (IF)	SP		poly	1:1000	20064	Immunostar	1
staining (IF)	G anti-Rb IgG	biotin	poly	1:500	BP-9100	Vector Laboratories	2
staining (IF)	G anti-Ch IgY	Alexa 488	poly	1:500	A-11039	Thermo Fisher Scientific	2

1. primary antibodies

2. secondary antibodies

## Antibodies for *in vivo* treatments

Purpose	Target	Clone	Amount	Product #	Manufacturer	Pairs
depletion	Ly6G	1A8	200 $\mu$ g/mouse (D0, D4)	BE0075	BioXCell	1
depletion	NK1.1	PK136	200 $\mu$ g/mouse (D-1, D4)	BE0036	BioXCell	2
blocking	integrin $\alpha$ 4	PS/2	100 $\mu$ g/mouse (D1, D4)	BE0071	BioXCell	3
blocking	integrin $\alpha$ L	M17/4	100 $\mu$ g/mouse (D1, D4)	BE0006	BioXCell	4
blocking	CD62L	Mel-14	200 $\mu$ g/mouse (D1, D4)	BE0021	BioXCell	5
blocking	PNA <sub>D</sub>	MECA-79	200 $\mu$ g/mouse (D1, D4)	120802	Biolegend	6
blocking	MHCII	Y3P	500 $\mu$ g/mouse (D0, D4)	BE0178	BioXCell	7
Purpose	Isotype	Clone	Amount	Product #	Manufacturer	Pairs
isotype	Rat IgG2b, $\kappa$	LTF-2	200 $\mu$ g/mouse (D0, D4)	BE0090	BioXCell	1
isotype	Mouse IgG2a, $\kappa$	C1.18.4	200 $\mu$ g/mouse (D-1, D4)	BE0085	BioXCell	2
isotype	Rat IgG2b, $\kappa$	LTF-2	100 $\mu$ g/mouse (D1, D4)	BE0090	BioXCell	3
isotype	Rat IgG2a, $\kappa$	2A3	100 $\mu$ g/mouse (D1, D4)	BE0089	BioXCell	4
isotype	Rat IgG2a, $\kappa$	2A3	200 $\mu$ g/mouse (D1, D4)	BE0089	BioXCell	5
isotype	Rat IgM, $\kappa$	RTK2118	200 $\mu$ g/mouse (D1, D4)	400802	Biolegend	6
isotype	Mouse IgG2a, $\kappa$	C1.18.4	500 $\mu$ g/mouse (D-1, D4)	BE0085	BioXCell	7

### 6.3 Appendix 3 – primer list

#### Primers for qPCR

Primer name	Species	Sequence (5' to 3')	Annealing (°C)
Rpl32-F	mouse	ACAATGTCAAGGAGCTGGAG	60
Rpl32-R	mouse	TTGGGATTGGTGACTIONCTGATG	60
CCL19-F	mouse	ATGTGAATCACTCTGGCCCAGGAA	60
CCL19-R	mouse	AAGCGGCTTTATTGGAAGCTCTGC	60
CCL21-F	mouse	TGAACAGACACAGCCCTCAAGA	60
CCL21-R	mouse	CCTCTTTGCCTGTGAGTTGGA	60
CXCL12-F	mouse	CAGAGCCAACGTCAAGCA	60
CXCL12-R	mouse	AGGTACTCTTGGATCCAC	60
CXCL13-F	mouse	CATAGATCGGATTCAAGTTACGCC	60
CXCL13-R	mouse	TCTTGGTCCAGATCACAACCTCA	60
TNFa-F	mouse	GCCTCTTCTCATTCTGCTTG	60
TNFa-R	mouse	CTGATGAGAGGGAGGCCATT	60
TGFb-F	mouse	TAAAATCGACATGCCGTCCC	60
TGFb-R	mouse	GAGACATCAAAGCGGACGAT	60
IFNg-F	mouse	TCAAGTGGCATAGATGTGGAAGAA	60
IFNg-R	mouse	TGGCTCTGCAGGATTTTCATG	60
IL1A-F	mouse	TTGGTTAAATGACCTGCAACA	62
IL1A-R	mouse	GAGCGCTCACGAACAGTTG	62
IL1B-F	mouse	TGTAATGAAAGACGGCACACC	62
IL1B-R	mouse	TCTTCTTTGGGTATTGCTTGG	62
IL2-F	mouse	AACCTGAAACTCCCCAGGAT	60
IL2-R	mouse	CGCAGAGGTCCAAGTTCATC	60
IL4-F	mouse	GGCATTGTTGAACGAGGTCACA	60
IL4-R	mouse	GACGTTTGGCACATCCATCTC	60
IL6-F	mouse	ACAAGTCGGAGGCTTAATTACACAT	60
IL6-R	mouse	TTGCCATTGCACAACCTCTTTTC	60
IL7-F	mouse	GTGCCACATTAAGACAAAGAAG	60
IL7-R	mouse	GTTTATTTCGGGCAATTACTATC	60
IL10-F	mouse	CCCATTCTCGTCACGATCTC	60
IL10-R	mouse	TCAGACTGGTTTGGGATAGGTTT	60
IL12 p35-F	mouse	TACTAGAGAGACTTCTTCCACAACAAGAG	60
IL12 p35-R	mouse	TCTGGTACATCTTCAAGTCCTCATAGA	60
IL13-F	mouse	CAGCAGCTTGAGCACATTTTC	60
IL13-R	mouse	CGGGATACTGACAGACTCATTTC	60
IL17A-F	mouse	GGACTCTCCACCGCAATGA	60
IL17A-R	mouse	GGCACTGAGCTTCCCAGATC	60
IL17F-F	mouse	CCCCATGGGATTACAACATCAC	60
IL17F-R	mouse	CATTGATGCAGCCTGAGTGTCT	60



LUDWIG-  
MAXIMILIANS-  
UNIVERSITÄT  
MÜNCHEN

Dean's Office  
Medical Faculty



## Affidavit

**Chen, Chien-Sin**

Surname, first name

Street

**Munich**

Zip code, town

**Germany**

Country

I hereby declare, that the submitted thesis entitled

**Neural Regulation of Lymph Node Immune Responses**

is my own work. I have only used the sources indicated and have not made unauthorised use of services of a third party. Where the work of others has been quoted or reproduced, the source is always given.

I further declare that the submitted thesis or parts thereof have not been presented as part of an examination degree to any other university.

**Munich, 12,12,2019**

Place, date

**Chien-Sin Chen**

Signature doctoral candidate